UNIVERSITY OF VERONA

Department of Medicine

Life and Health Sciences PhD School

Biomolecular Medicine PhD Course

XXXI cycle

Aromatic amino acids decarboxylase and histidine decarboxylase: deep functional investigations give insights into pathophysiological mechanisms with possible therapeutic implications

S.S.D. BIO/10

Coordinator: Prof. Lucia De Franceschi

Tutor: Prof. Mariarita Bertoldi

PhD candidate: Giada Rossignoli

This work is licensed under a Creative Commons Attribution-NonCommercial-
NoDerivs 3.0 Unported License, Italy. To read a copy of the licence, visit the web page:

http://creativecommons.org/licenses/by-nc-nd/3.0/

Attribution — You must give appropriate credit, provide a link to the license, and indicate if changes were made. You may do so in any reasonable manner, but not in any way that suggests the licensor endorses you or your use.

NonCommercial — You may not use the material for commercial purposes.

NoDerivatives — If you remix, transform, or build upon the material, you may not distribute the modified material.

"Aromatic amino acids decarboxylase
and histidine decarboxylase:
deep functional investigations give insights into pathophysiological mechanisms
with possible therapeutic implications"

Giada Rossignoli

PhD thesis
Verona, 28 April 2019

Abstract

Aromatic amino acids decarboxylase and histidine decarboxylase (AADC and HDC) are two homologous enzymes responsible for the synthesis of dopamine/serotonin and histamine, respectively, and other minor signalling aromatic amines. All these molecules are main protagonists or regulators of several physiological pathways, which are fundamental both in central nervous system and in peripheral tissues. Alterations of their homeostasis, indeed, as well as of AADC and HDC functioning or expression, cause and/or participate in the development and progression of several often severe and disabling pathological conditions, such as AADC Deficiency and cholangiocarcinoma. Consequently, AADC and HDC characterization might be useful in the pathophysiological understanding of several diseases and in improving/developing new therapeutic strategies. However, the knowledge of the biochemical features of these two crucial enzymes is still rather limited. Thus, the aim of this thesis is to biochemically characterise human HDC, mostly unknown, and to individuate some possible regulative mechanisms for both HDC and AADC. In addition, a neuronal AADC Deficiency cell model, derived from patient induced pluripotent stem cells (iPSCs), was used to evaluate endogenous AADC features, as well as to research further alterations in dopaminergic pathway.

Investigations on human recombinant HDC allowed to discover that, surprisingly, its conformation and catalytic efficiency are influenced by redox state: increasing oxidizing conditions, indeed, favour a more stable and active form of the dimeric enzyme, due to the presence of an intermolecular reversible disulphide bridge involving residue Cys180 of both subunits. Then, in solution analyses of a possible phosphorylation of AADC identified Ser193 as protein kinase A target site, and allowed the detection of an effect on enzyme kinetic parameters, in particular an increased affinity for its substrates. Finally, endogenous AADC levels analyses in dopaminergic neurons derived from AADC Deficiency patients suggested a possible positive feedback mechanism that could tend to increase AADC expression, and the same cell model showed alterations in other cell types besides neurons, in particular glia cells, suggesting that variations in neurons-glia cells

interplay could participate in the pathophysiology mechanisms of AADC Deficiency. Altogether, data and information obtained from the performed experiments have increased AADC and HDC knowledge, as well as paved the way for new hypothesis regarding possible efforts in the development of new disease treatments.

Table of contents

List of Abbreviations

5-HIAA	5-hydroxyindoleacetic acid
5-HTR	L-5-hydroxytryptophan receptor
AADC	aromatic amino acids decarboxylase
AC	adenylate cyclase
AD	Alzheimer's disease
ADHD	attention deficit hyperactivity disorder
ALDH	aldehyde dehydrogenase
ATP	adenosine triphosphate
BBB	blood-brain barrier
β-ME	β-mercaptoethanol
BSA	bovine serum albumin
cAMP	cyclic adenosine monophosphate
CarbiDOPA	L-α-methyl-α-hydrazino-3,4-2,3,4-trihydroxyphenylpropionic acid
CNS	central nervous system
CSAD	cysteine sulfinic acid decarboxylase
CSF	cerebrospinal fluid
DA	dopamine
DA neurons	dopaminergic neurons
DAPT	difluorophenyl acetyamino propanoylamino 2-phenylacetate
db-cAMP	dibutyryl-cyclic adenosine monophosphate
DAPI	4′,6-diamidino-2-phenylindole
DME	L-3,4-dihydroxyphenylalanine methyl ester
DMEM	Dulbecco's modified eagle medium
DPBS	Dulbecco's phosphate-buffered saline
DR	dopamine receptor
DTT	1,4-dithiothreitol
EAE	experimental autoimmune encephalomyelitis
EDTA	ethylenediaminetetraacetic acid
ESC	embryonic stem cell
FCS	foetal calf serum
FN/Lam	Fibronectin/Laminin
FP	floor plate
GABA	γ-aminobutyric acid
GAD65/67	glutamate decarboxylase

GAPDH	Glyceraldehyde 3-phosphate dehydrogenase
GSH	reduced glutathione
H_2O_2	hydrogen peroxide
HDC	histidine decarboxylase
HME	histidine methyl ester
HRP	horseradish peroxidase
HVA	homovanillic acid
iPSC	induced pluripotent stem cell
IsO	isthmic organizer
KOSR	KnockOut serum replacement medium
L-5HTP	L-5-hydroxytryptophan
L-DOPA	L-3,4-dihydroxyphenylalanine
MAO-A/B	monoamine oxidase
MHB	midbrain-hindbrain boundary
MS	multiple sclerosis
PBS	phosphate-buffered saline
PD	Parkinson's disease
PKA	cAMP-dependent protein kinase
PKC	protein kinase C
PLP	pyridoxal 5'-phosphate
PO	Poly-L-ornithine
P/S	Penicillin/Streptomycin
PSC	pluripotent stem cell
RIPA	radioimmunoprecipitation assay buffer
SB	sample buffer
TBS	tris-buffered saline
TH	tyrosine hydroxylase
TMN	tuberomammillary nucleus
TS	Tourette syndrome

Thesis overview

The main topic of this thesis deals with AADC and HDC, two homologues pyridoxal 5'-phosphate (PLP)-dependent decarboxylases, with the aim to characterise some of their peculiar features, as described in *Chapter 4*. This thesis, indeed, is divided into several chapters.

The introduction part starts with an overall picture of PLP-dependent α-decarboxylases features, reported in *Chapter 1*, followed by a focus on the thesis experimental investigation subjects of this family, AADC and HDC. A comprehensive overview of their physiological role and pathological implications in several diseases are proposed in *Chapter 2*. *Chapter 3* exhaustively describes the highly innovative dopaminergic neuronal model derived from induced pluripotent stem cells, as well as its choice for the proposed research.

The three results chapters are focused on the various identified features of AADC and HDC: *Chapter 6* highlights a redox modulation of HDC activity, *Chapter 7* mainly focuses on AADC phosphorylation, and, lastly, *Chapter 8* reports investigations on endogenous AADC, as well as other dopaminergic pathway enzymes, in neurons of AADC Deficiency patients. Partial conclusions are reported at the end of each results chapter, and a comprehensive discussion is proposed in *Chapter 9*. Complete bibliography, as *Chapter 10*, and a list of attached publications, as *Chapter 11*, complete the thesis.

Chapters 7 and 8 experiments were performed during two research periods in other Institutes, hosted by University of Georgia at Athens (USA) and University College of London Institute of Child Health (UK), respectively.

Chapter 1

AADC and HDC are two homologous enzymes of human group II PLP-dependent α-decarboxylases family

1.1. Human group II PLP-dependent α-decarboxylases

The observations outlined in this chapter led to the drafting of attached Publication 2 (*Chapter 11*).

1.1.1. PLP is a versatile cofactor

PLP-dependent enzymes are found in all organisms, from prokaryotes to higher eukaryotes [1], and catalyse many essential reactions, mainly linked to amino acids and amines metabolism, like transamination, racemization, β- and α-decarboxylation, β- and γ-elimination and β- and γ-substitution. This wide variety of reactions is possible due to the strongly electron withdrawing capability of PLP pyridinium ring, that stabilises β- or α- carbanions on the amine or amino acid portion of substrates, as proposed since the 1950s from Metzler and Snell [2- 4] and Braunstein and colleagues [5-7]. Thus, the general reaction chemistry is controlled by PLP, due to its ability to perform these reactions at a slow rate in solution, but protein environment is responsible for the reaction specificity towards different substrates and for the enormous acceleration rates typical of these enzymes.

1.1.2. Human group II PLP-dependent α-decarboxylases

The wide catalytic versatility of PLP-enzymes is accompanied by a limited structural diversity. On the basis of amino acid sequence comparisons, predicted secondary structures and published three-dimensional configurations since then, in

1995 PLP-enzymes were distributed into five different fold-types (from I to V) [8], followed by later updates with new structures information [9]. The most common fold type, i.e. fold-type I, is typical of aminotransferases, almost all α-decarboxylases, and also enzymes which catalyse α- or γ-eliminations. Enzymes that catalyse β-elimination reactions belong to fold-type II, while alanine racemase and a minor subset of decarboxylases to fold-type III and D-alanine aminotransferase together with few other enzymes to fold-type IV. Lastly, fold-type V group comprises glycogen and starch phosphorylases.

Regarding PLP-dependent α-decarboxylases only, another classification, based on evolutionary relationships derived by amino acid sequence comparisons [10], divides them into 4 groups. In particular, group II comprises AADC, HDC, glutamate decarboxylase (GAD65/67) and cysteine sulfinic acid decarboxylase (CSAD), from prokaryotic and eukaryotic organisms, sharing the PLP-binding motif of fold-type I. The hallmarks of these decarboxylases mainly include a glycine-rich motif upstream from the PLP-bound lysine residue and an invariant aspartate interacting with the cofactor pyridine nitrogen [9,10].

1.1.3. Group II PLP-dependent α-decarboxylases show major structural similarities and slight differences

The considerable increase in the knowledge of the structural features of group II PLP-dependent α-decarboxylases started in 2001, when the first crystal structure of a member of this family was solved, i.e. *Sus scrofa* AADC [11], sharing an about 90% sequence identity with the human homologous enzyme. Since then, extensive research focused on the characterisation of their structure-function relationships has driven a substantial progress toward the understanding of their similar enzymatic activities, highlighting, at the same time, key differences responsible for substrate specificity, and, most importantly, of detailed pathological states phenotypes/molecular alterations associations regarding these enzymes [12].

The overall topology

Decarboxylase domains of AADC, HDC, GDC65/67 and CSAD share a number of structural features that remained invariant upon the long evolutionary history of this superfamily (***Figure 1.1***), as they maintained the structurally conserved region of the decarboxylase domain and the positioning of key residues for PLP binding (***Figure 1.2***) [13].

Figure 1.1. Schematic representation of protein sequences of human group II PLP-dependent α-decarboxylases [14].
The length of each sequence is indicated on the right of each bar. The position of the decarboxylase domain (PFAM ID: PF00282 [15]) relative to each sequence is also shown.

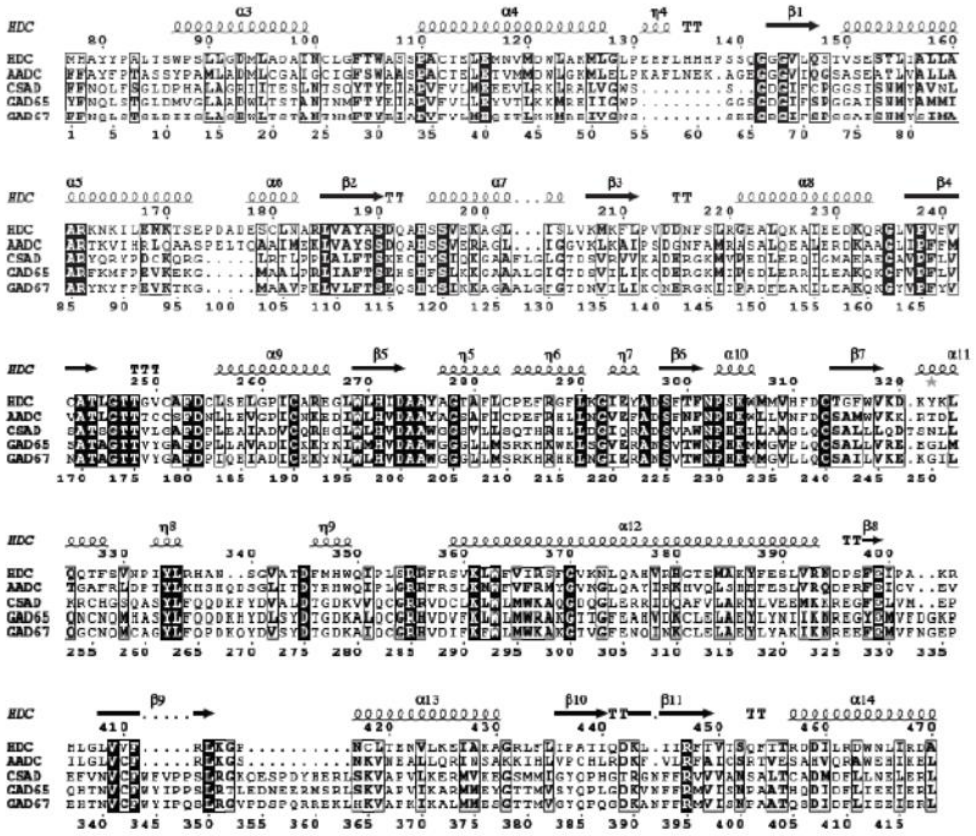

Figure 1.2. Multiple sequence alignment of human group II PLP-dependent α-decarboxylases [14].

Amino acid one-letter code is used. Dashes represent insertions and deletions. Invariant positions are boxed in black. The secondary structures of human HDC (PDB code 4E1O) are reported in the first line of each block: α-helices and β-strands are rendered as squiggles and arrows, respectively. ESPript (http://espript.ibcp.fr; [16]) was used to render this figure.

In particular, native PLP-dependent α-decarboxylases share a dimeric quaternary structure, which is necessarily required to generate a functional enzyme [17]. Each of the two monomers is composed of three distinct domains (***Figure 1.3***).

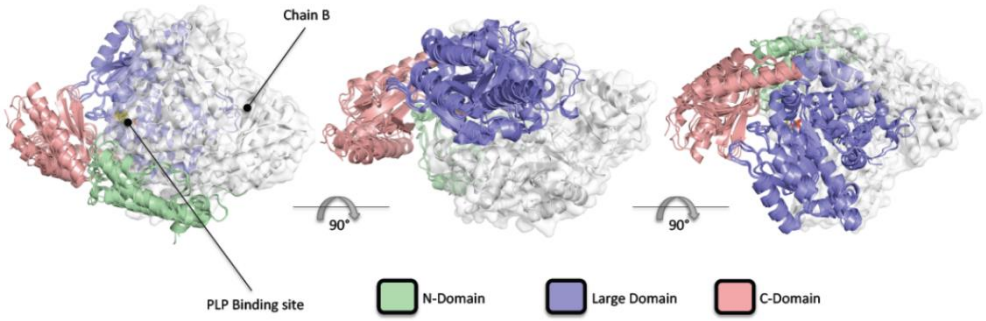

Figure 1.3. Structural superposition of human group II PLP-dependent α-decarboxylases [14].
The N-terminal, large and C-terminal domains are represented in green, cyan and pink, respectively. Chain B is represented as grey cartoons and surface.

The "large" domain, which displays the α/β rearrangement typical of fold-type I enzymes and hosts the cofactor, consists of seven buried β-strands forming a β-sheet surrounded by eight α-helices. The "large" domains are the main responsible for the dimeric interface that involves both electrostatic and hydrophobic interactions between the two monomers. The "C-terminal", or "small" domain, positioned externally in the native structure, is composed by a four-stranded antiparallel β-sheet and three α-helices. Lastly, the "N-terminal" domain, composed by two helices linked by an extended strand, forms a clamp to the neighbouring subunit, with the first helix of one subunit aligning antiparallel to the equivalent helix of the other subunit, suggesting that the main function of this domain would be to extend and/or stabilise the interface between the two monomers.

Active site residues interacting with cofactor

The active sites, one for each monomer, are located at the dimer interface, and each of them is partially composed by residues belonging to the other monomer. PLP-interacting residues, in particular, are highly conserved among the four considered enzymes (***Figure 1.4***).

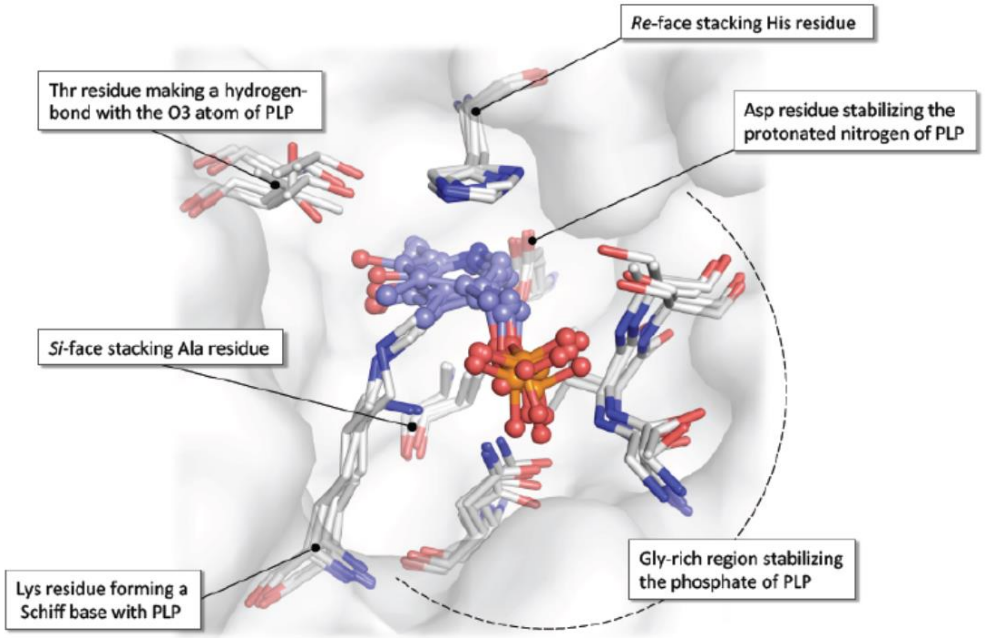

Figure 1.4. Homologous residues of human group II PLP-dependent α-decarboxylases interacting with cofactor [14].
Protein residues are represented as white sticks, PLP is represented as cyan balls and sticks.

The cofactor binds to an evolutionarily invariant ε-amino group of a lysine residue through a Schiff base linkage. A conserved aspartate electrostatically interacts, through its carboxylate group, with the protonated pyridine nitrogen of PLP, providing stabilization of the carbanionic intermediates during enzymatic catalysis, while the 3-oxygen atom of the cofactor ring is stabilized via a hydrogen bond with a threonine residue. In addition, PLP pyridine is positioned between a base-stacking with a histidine on the *re* face and a hydrophobic interaction with a conserved alanine residue on the *si* face. Lastly, the negative phosphate moiety interacts with the enzymes through an extended hydrogen bond network, as well as dipole interactions with the "large" domain α5-helix.

Active sites residues interacting with substrates

While AADC and HDC have been both crystallized in complex with their inhibitors L-α-methyl-α-hydrazino-3,4-2,3,4-trihydroxyphenylpropionic acid (carbiDOPA, MK485) [11] and histidine methyl ester (HME) [18], the structures of GAD65 and GAD67 have been determined with their reaction product γ-

aminobutyric acid (GABA) [19]. The complexes data give therefore precious insights into the binding mode of inhibitors and substrates of human group II PLP-dependent α-decarboxylases, suggesting, meanwhile, the reaction specificity and substrate selectivity determinants of each enzyme.

The binding cleft is deeply buried into the active site cavity and extends beneath the *si* face of the PLP pyridine ring for all decarboxylases. In the case of GAD65/GAD67/CSAD, the need to bind and select an aliphatic chain instead of an aromatic one imposes a narrower binding cleft compared to AADC and HDC, achieved by a structural modification of the loop region connecting the N-terminal with the large domain. In particular, an aromatic residue in AADC and HDC (Phe80 and Tyr81, respectively) twists the loop by making a stacking interaction with another Tyr residue of the large domain (Tyr274 and Tyr276, respectively) and creates the necessary space to bind aromatic ligands (***Figure 1.5***).

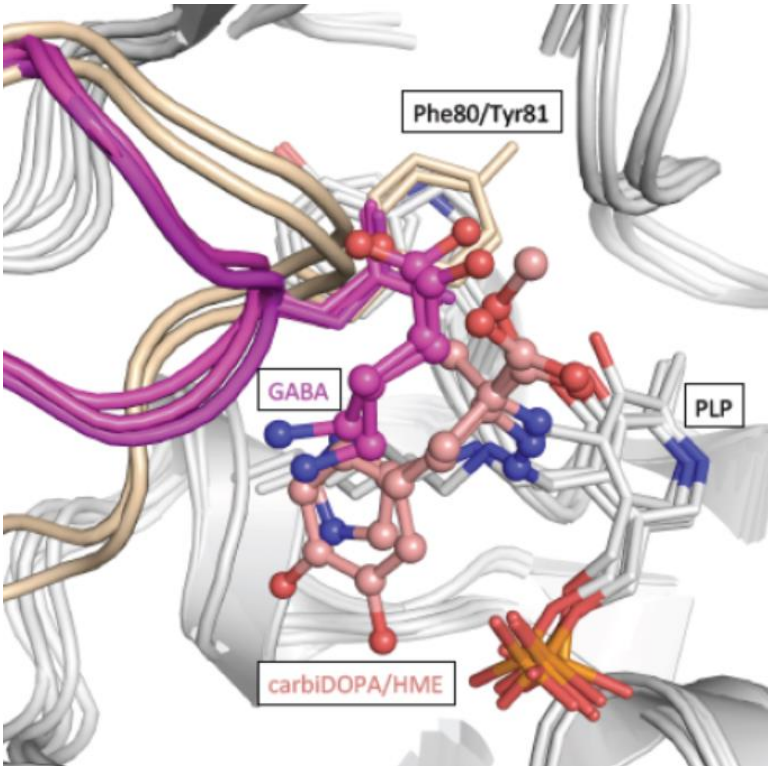

Figure 1.5. Comparison of the substrate-specificity loop of human group II PLP-dependent α-decarboxylases [14].
The loops of AADC and HDC with PLP bound to carbiDOPA or HME, respectively, are colored in beige, while the loops of GAD65, GAD67 and CSAD are depicted in magenta. Residues are labelled according to PDB numbering and shown as sticks. CarbiDOPA (pink), HME (pink) and GABA (magenta) are shown as balls and sticks.

The mobile catalytic loop

Human group II PLP-dependent α-decarboxylases are all characterized by the presence of a highly flexible loop for monomer, essential for the catalytic mechanism, that extends towards the active site of the other monomer in a "closed" conformation [17,18,20]. The loop "closed" conformation is well ordered and clearly assigned in HDC, CSAD and GAD67 [18,19] structures, whereas it was found mostly disordered, lacking electron density map, in AADC and GAD65 [11,19] (***Figure 1.6***).

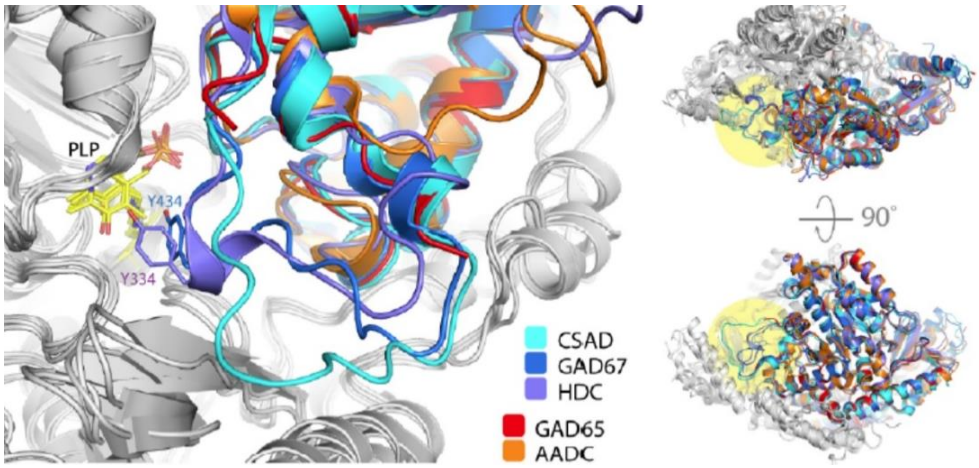

Figure 1.6. Comparison of the mobile catalytic loop of group II PLP-dependent α-decarboxylases [14].
The loop is located at the dimer interface and extends towards the active site of the other monomer. The coordinates of the loops of AADC and GAD65 are missing due to the high flexibility of this region. Tyr334 and Tyr434 of HDC and GAD67, respectively, are shown as sticks.

Structural and mechanistic data strongly suggest that, before substrate binding, the loop adopts an "open" conformation that is more solvent-exposed and prone to proteases cleavage respect to the "close" conformation [21], while after substrate binding and during catalysis, it could occlude the active site cleft and act as a lid for solvent shielding, assisting the conversion of carboxylate to the more hydrophobic CO_2 product [20]. Moreover, this loop is also known as "the catalytic loop", as it has been demonstrated that some loop residues take part in catalytic mechanism: Tyr to Phe substitution, indeed, in AADC, HDC and GAD (Tyr332, 334 and 434, respectively) resulted in an enzyme unable to produce amines, clearly

assigning to this residue a crucial role for decarboxylase activity, and identifying it as the putative proton donor to the negatively charged Cα atom of the carboanionic quinonoid reaction intermediate [18,19,20]. In addition, although the conserved Tyr residue of the loop is crucial for catalysis, other residues composing the loop have been demonstrated to be important for proper positioning of catalytic loop, since enzymatic studies on AADC and HDC have shown that also the alteration of the surrounding loop region affects the catalytic activity [22,23].

The open and close conformations

An interesting aspect of group II PLP-dependent α-decarboxylases regulation recently emerged, forcing the reconsideration of PLP addiction mechanism and preferential degradation of the apo-decarboxylases (i.e. without cofactor bound to the active site). Human apo-AADC crystal structure determination [24] showed that the apo-enzyme presents an unexpected "open" conformation in which, compared with the holo-enzyme (i.e. with PLP bound to the active site), the dimer subunits move up to 20 Å apart through a rigid body quaternary rearrangement of the dimer around the N-terminal domain interface (***Figure 1.7***).

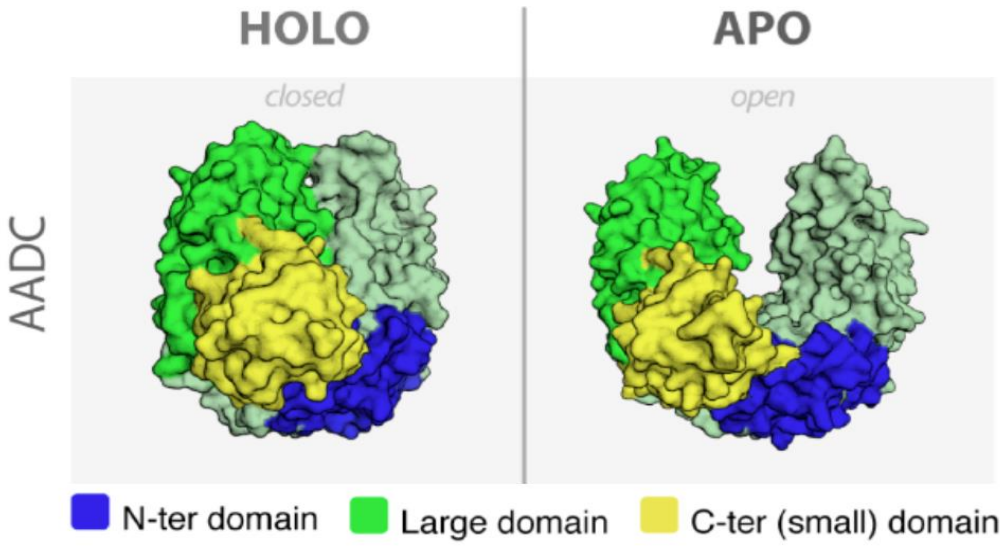

Figure 1.7. Molecular surface representation of the closed and open dimers of AADC [14]. *Protein is rendered as surface representation. The N-terminal, large and C-terminal domains are represented in blue, green and yellow, respectively. Chain B is represented as cyan cartoon.*

The apo-AADC "open" conformation implies that a large part of the dimer interface, comprising the two active sites, is solvent-exposed, with the mobile catalytic loop of the active site even more flexible and unstructured. Considering that ubiquitin-ligases recognise unstructured regions of target protein or newly exposed surfaces, this "open bivalve shell" structure could explain why apo-AADC is degraded at least 20-fold faster than the holo-enzyme in rat brain cells [25]. Recently, using molecular dynamics simulations and normal mode analyses coupled with small-angle X-ray scattering and fluorescence spectroscopy, a similar conformational opening was also described for holo-GAD65 [26], enabling regulation of GABA synthesis based on PLP availability.

1.1.4. Human group II PLP-dependent α-decarboxylases share a common catalytic mechanism

The Schiff base linkage between the cofactor and the ε-amino group of a lysine residue located in the active site characterises all the active forms of PLP-enzymes. This structure, known as internal aldimine, converts, through transaldimination and a geminal diamine intermediate step with both enzyme and substrate amino groups bound to PLP-C4', in an external aldimine, in which the α-amino group of the incoming amino acidic substrate has replaced the lysine ε-amino group in the linkage with the cofactor (***Figure 1.8***).

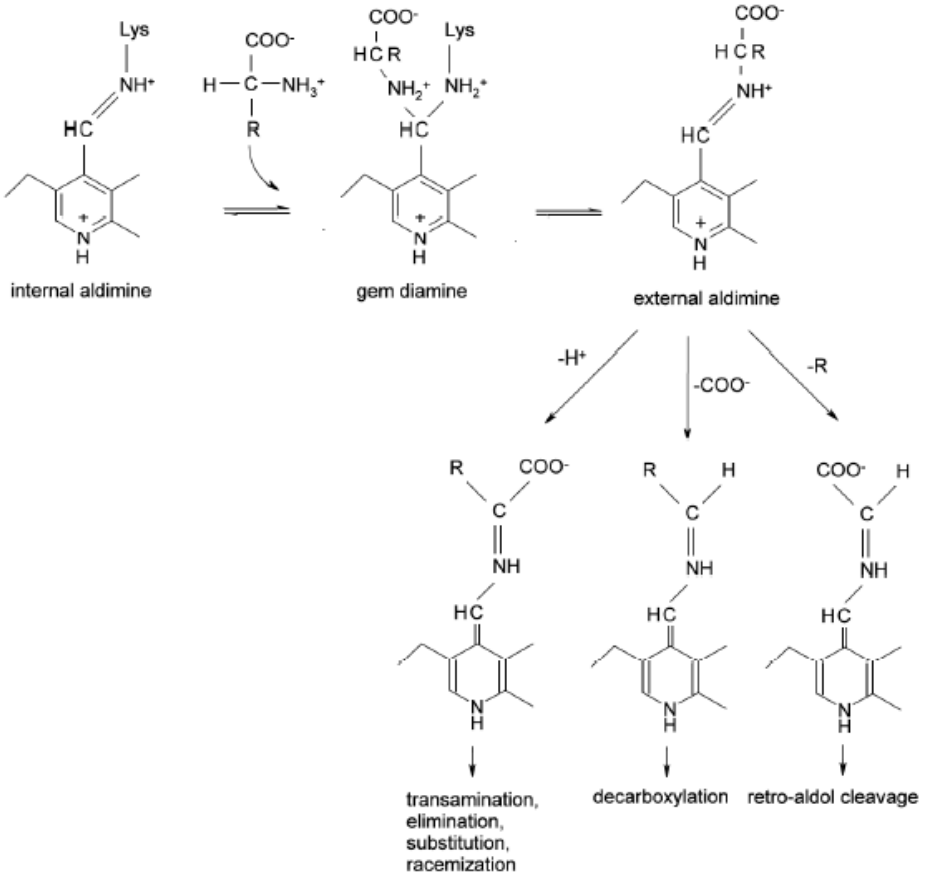

Figure 1.8. Catalytic intermediates and versatility of PLP-catalysed reactions [14].

The different type of reaction catalysed by a PLP-enzyme depends on which of the substrate α-substituents is lost: according to Dunathan's hypothesis [27], the leaving group is the one that is positioned perpendicular to the coenzyme-imine π system by interactions between enzyme and substrate. This fundamental concept explains how reaction specificity is controlled and points on the role of the polypeptide chain in directing coenzyme intrinsic catalytic properties: the reaction catalysed, indeed, depends on which of the three bonds of the α-carbon is held in a correct position to be broken by the specific enzyme catalytic site structure interacting with the substrate. In any case, this event results in the formation of a quinonoid intermediate in which the substrate and the cofactor generate a coplanar structure. The only exception to this common catalytic mechanism is represented by PLP-dependent phosphorylases, where PLP phosphate group participates in proton transfer acid-base reactions [28].

In group II PLP-dependent α-decarboxylases, the carboanionic quinonoid intermediate is subsequently re-protonated at the α-carbon to form the amine product, that, through a second transaldimination reaction, is released from the active site, with the concomitant reconstitution of the internal aldimine enzymatic form. ***Figure 1.9*** shows substrates and reaction products of the considered enzymes.

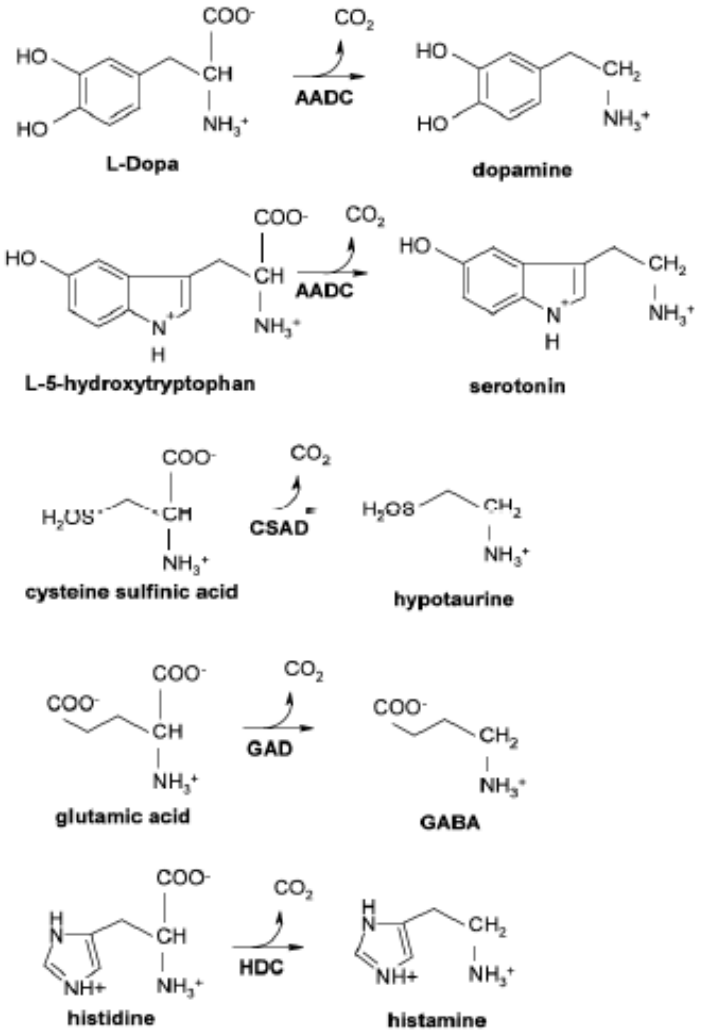

Figure 1.9. Substrates and products of the human group II PLP-dependent α-decarboxylases [14].

The most effective drugs targeting members of this family, mainly developed for active site interaction, are still lacking specificity, probably due to the common catalytic mechanism and the high active site homology between group II PLP-dependent α-decarboxylases. In light of this, structural information gained on this sub-family in recent years provided us with a detailed description of key similarities

and differences that could be exploited for new therapeutic strategies. Indeed, the elucidation, from a molecular point of view, of their similar structural traits and of those underlying their individual substrate preference could help in facing the different diseases in which these decarboxylases are key players. In fact, residues of the mobile loop as well as those involved in the apo-to-holo transition could be envisaged as preferential targets for planning an oriented drug-design for finding more suitable drugs with therapeutic promise or for developing a pharmacological chaperone approach.

1.2. AADC and HDC are highly homologous

1.2.1. AADC and HDC form a subgroup in their family

A detailed comparison of the available sequences and structures of decarboxylase domains of AADC, HDC, GAD65, GAD67 and CSAD suggests that this group of enzymes can be further clustered into two different evolutionary subgroups, comprising AADC and HDC in first subgroup (root mean-square deviation, RMSD ≈ 0.8 Å), and GAD65/GAD67/CSAD in the second one (mean RMSD ≈ 0.5 Å) [10]. Considering their mature forms, AADC and HDC, indeed, share a 52.1% identity and an up to 82.6% sequence similarity [29], classifying them as highly homologous enzymes (***Figure 1.10***).

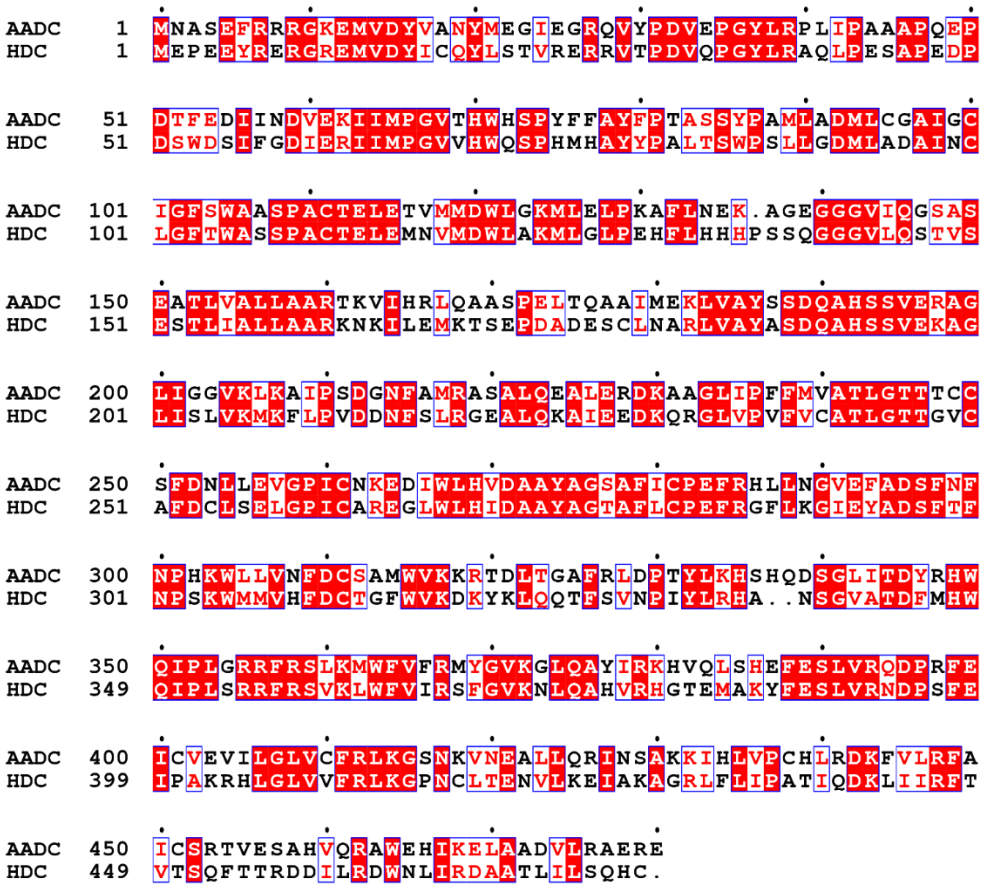

Figure 1.10. Multiple sequence alignment of human AADC and HDC.
Sequences were taken from the NCBI website (https://www.ncbi.nlm.nih.gov/). Amino acid one-letter code is used. Dashes represent insertions and deletions. Invariant positions are boxed in red and similar residues are written in red. ESPript (http://espript.ibcp.fr) was used to render this figure starting from a Clustal Omega alignment (http://www.ebi.ac.uk/Tools/msa/clustalo/).

1.2.2. Actual enzyme-targeting compounds bind AADC and HDC active sites

Many compounds have been already identified as possible AADC and HDC inhibitors, and almost all of them bind to enzymes active sites, which is the most conserved region between the two proteins. A structural comparison of the substrate-binding pocket of AADC and HDC, both crystallised in complex with one of their inhibitors, carbiDOPA [11] and HME [18], respectively, highlights, indeed, a highly similar conformation of the external aldimine (***Figure 1.11***).

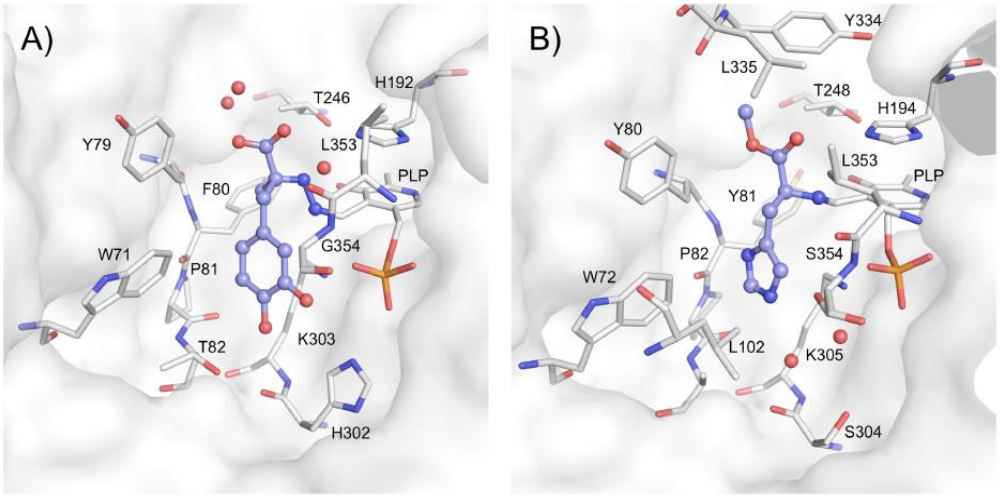

Figure 1.11. Comparison of the active sites of A) AADC and B) HDC [14].
Residues are labelled according to PDB numbering and shown as white sticks. CarbiDOPA and HME are shown as cyan ball-and-sticks.

The catechol hydroxyl groups of carbiDOPA make hydrogen bonds with the side chain of Thr82, and with the phosphate moiety of PLP and imidazole ring of His302, while HME imidazole ring makes two hydrogen-bonds with the main-chain of Tyr81 and a structural water molecule. Interestingly, the latter and a second water molecule in the substrate binding pocket of HDC occupy the same position of the two hydroxyl groups of the catechol ring of carbiDOPA in AADC.

The crucial, and distinctive, difference between the two substrate binding pockets is represented by the presence in HDC of a serine residue (Ser354) that is replaced by a glycine in AADC. The HME imidazole ring positioning at hydrogen bonding distance from Ser354 suggests that the latter could be a key residue for substrate specificity. The S354G mutation, indeed, resulted in a decreased affinity of HDC for its natural substrate, histidine, and an acquired ability to catalyze the decarboxylation of L-3,4-dihydroxyphenylalanine (L-DOPA), the AADC preferred substrate, suggesting that the mutation allows the binding of a six-membered ring enlarging the size of HDC substrate-binding pocket [14].

CarbiDOPA together with benserazide (N-(DL-seryl)N'-2,3,4-trihydroxybenzyl-hydrazine; Ro-4-4602), are the only two AADC inhibitors actually used as drugs, classically administrated in Parkinson's disease therapy to prevent L-DOPA degradation by peripheric AADC and thus increasing its bioavailability for central nervous system (CNS) uptake. While carbiDOPA is a *per*

se AADC powerful irreversible inhibitor [30], benserazide behaves as a poor inhibitor [31], but is rapidly bioactivated to 2,3,4-triydroxybenzylhydrazine [32] (***Figure 1.12***).

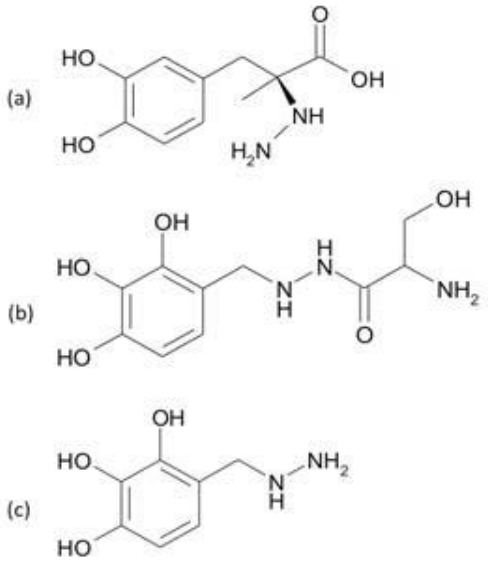

Figure 1.12. AADC inhibitors currently used in therapy [33].
Chemical structure of (a) carbiDOPA, (b) benserazide and (c) 2,3,4-trhydroxybenzylhydrazine

However, both these inhibitors are not AADC selective and are able to react with free PLP, generating pyridoxal kinase hydrazone-derivatives inhibitors [34], but also with many other PLP-dependent enzymes, as showed for kynureninase and kynurenine aminotransferase [35].

HME, a L-histidine analog, is the first discovered HDC inhibitor [36], identified through screening of substrate-derived compounds. Even if it is an efficient inhibitor, it is not actually used in therapy due to its fast degradation by plasmatic enzymes [37] that dramatically decrease its bioavailability. This is a common feature of methylated substrate analogues that could be potentially used as drugs, as for DOPA methyl ester (DME), the corresponding methyl analog of L-DOPA, although in more recent years other delivering formulation were considered, like nasal powder preparations [38] and trans buccal delivery [39] that are expected to increase its bioavailability and be capable of maintaining better plasma levels of the drug, allowing DME to currently being in Phase III clinical trials with expected low adverse effects [40] (***Figure 1.13***).

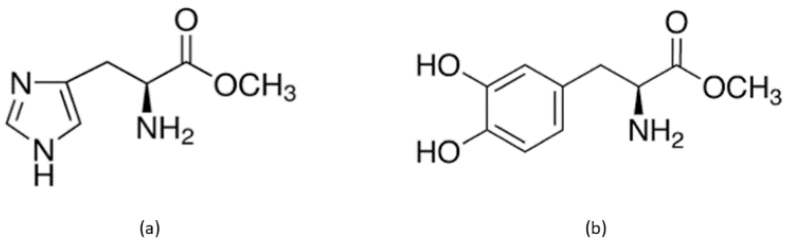

Figure 1.13. Chemical structures of (a) HME and (b) DME.

The substrate-analogues inhibitors group is, for both enzymes, more extensive, comprising also α-fluoromethyl derivatives like α-fluoromethylDOPA (2-(Fluoromethyl)-3-(3,4-dihydroxyphenyl)alanine, FMD) [41], and α-fluoromethylhistidine (FMH) [42], both powerful irreversible inhibitors of the corresponding enzyme, acting by suicide mechanism through covalent linking to the active site following decarboxylation reaction. Even if fluorinated drugs and fluorine-containing compounds are already widely applied in medicine, like general anaesthetics, antibiotics, antiviral and antimalarial agents, anti-inflammatory drugs, antidepressants and antipsychotics, many epidemiological studies published during the last 50 years present a number of reasons for the serious assessment of the risks of fluoride to human body [43]. In particular, fluoride has been found to inhibit the activity of many important enzymes, both directly and/or through fluorinated metabolites, e.g. fluoroacetate [44], and to form aluminofluoride complexes able to simulate phosphate groups in many biochemical reactions [45], representing a strong potential danger for living organisms [46].

Natural compounds, like (-)-epigallocatechin-3-O-gallate (EGCG) and (-)-epigallocatechin (ECG), show significant irreversible inhibition of AADC with a Ki in the micromolar range [47], but they lack of specificity since they were found to inhibit also HDC with the same affinity [48] (***Figure 1.14***).

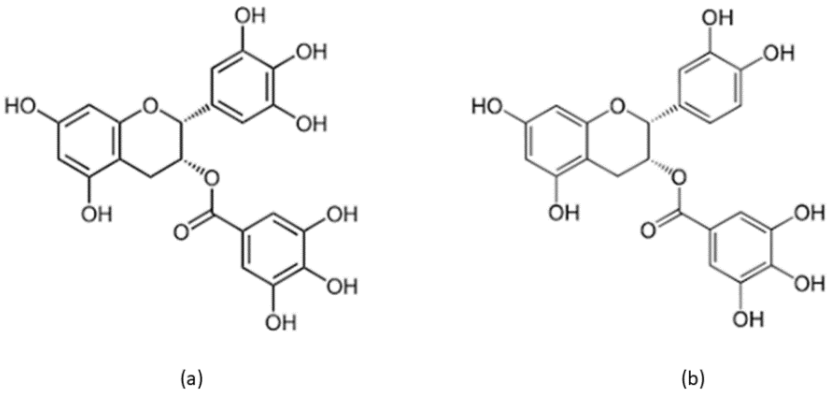

Figure 1.14. Chemical structures of (a) EGCG and (b) ECG.

Many other naturally occurring compounds, in particular plant-derived compounds, were found to have inhibitory activity on both enzymes: dimeric diarylpropanes from *Euonymus glabra Roxb* (*E. glabra*) active extract act on AADC [49], ellagitannins extract from *Filipendula ulmaria* petal show Ki values nearly equal to that of HME for HDC [50], and flower buds extracts from *Lonicera japonica Thunb* have inhibitory activity against HDC expression and histamine production [51]. However, no information is available about which kind of inhibition they exert and/or their inhibition mechanism.

The resolution of AADC and HDC structures in complex with inhibitors [11,18] paved the way for bioinformatic screening and rational based drug design, using structural information to find higher selective and powerful inhibitors. This method recently led to the identification of a class of compounds with inhibitory activity toward AADC [52], and to the synthesis of an aminooxy analog of L-histidine, i.e. 4(5)-aminooxymethylimidazole (O-IMHA) capable to form a PLP-inhibitor complex (oxime) in HDC active site [53]. However, no investigation regarding their pharmacokinetic or toxicological properties has been carried out until now, implying that they are interesting candidates that need further optimization and *in vivo* validation.

The highly AADC/HDC homology grade, in particular at the active site, together with the advantage of more generally modulation of their activity for clinical application, not only through inhibition, but in some cases also activation, of these two enzymes, suggest the need to focus on other enzymatic features rather than the only active site-directed inhibition. Based on this necessity, it would be

particularly interesting to identify and analyse enzymatic features like post-translational modifications and cellular proteins equilibria, with the aim to explore other possible mechanisms for AADC and HDC modulation.

1.3. Knowledge of AADC and HDC regulation mechanisms is incomplete and fragmented

A great deal of information about AADC has accumulated since its first identification in extracts from mammalian kidney in 1938, thus 80 years ago. However, major questions remain regarding functional aspects of this important enzyme: despite its complex kinetics, indeed, which suggests that enzyme regulation could be useful, many evidences for the control of AADC reaction have been described, but they are, till now, fragmented, partial and/or not mechanistically detailed. On the other side, few studies were focused on HDC post-translational regulation mechanisms, with conflicting results as well.

1.3.1. HDC is post-translational processed through proteolytic cleavage

Comparisons between mature homologous amino acid decarboxylases indicate that the C-terminal 20-kDa region of HDC is deleted. The enzyme, indeed, is translated as a ~74 kDa form, which is subsequently subjected to a C-terminal proteolytic cleavage. Analysis of the recombinant 74-kDa species expressed in a baculoviral-insect cell expression system revealed that the mouse 74-kDa form is distributed in the insoluble fraction and exhibits lower enzyme activity in comparison with the C-terminal deleted 54-kDa form, which is localized in the cytosol [54]. In contrast to mouse HDC, human recombinant 74-kDa species exhibited comparable enzyme activity to its C-terminal deleted 54-kDa species [55]. These results suggested that the C-terminal 20-kDa region of HDC could be involved in regulation of both intracellular localization and enzymatic activity.

In a rat basophilic/mast cell line, RBL2H3, the 74-kDa form showed to be very unstable and degraded through the ubiquitin–proteasome pathway [56], and found

to be localized in the cytosol, whereas the 54-kDa form was in the granule fraction upon sucrose density gradient fractionation [57]. In elicited mouse peritoneal neutrophils, granular localization of the 54-kDa form was also observed, but both fractions contained enzymatic activity of HDC, indicating that the post-translational cleavage determines the intracellular localization of HDC, rather than its enzymatic activation, in this cell line [58]. Transient expression of rat HDC in COS-7 cells indicated that recombinant HDC is associated to the endoplasmic reticulum (ER) through a 20 amino acid sequence (residues 588-607) at C-terminus [59], suggesting that HDC could be targeted to the ER in a singular manner, i.e. post-translational targeting, the details of which remain unknown.

Recently, caspase-9 was identified as one of the possible processing proteins responsible for enzymatic activation of mouse HDC in P-815 cells [60], and Caspase-9-mediated cleavage of HDC was accompanied by formation of the 54-kDa species with a concomitant drastic increase in its enzymatic activity. In addition, in another type of cells, i.e. Sf9 cells, proteolytic cleavage of the recombinant 74-kDa protein, resulting in its enzymatic activation, was found to be mediated by elastase [61].

These contradictory data about proteolytic activation of HDC show that it remains still unknown how the post-translational processing of this enzyme is regulated and what the physiological roles of the cleavage are.

1.3.2. Evidence suggests that AADC could be regulated by phosphorylation

AADC has classically been regarded as a post-translational unregulated enzyme. However, the first indication that this enzyme may be subjected to this type of regulation was provided around 30 years ago from an investigation in rat retina [62]: when light is turned off AADC activity drops rapidly at first and then more slowly, suggesting that at least two processes are responsible for the fall of enzyme activity, while exposure to short periods of dark followed by light results in a rapid increase of AADC activity. In addition, this effect is similar to that of dopamine receptor (DR) antagonists [63] or adrenergic receptor antagonists [64]. Interestingly, similar effects have also been shown to occur in several brain regions

in both rats and mice, and a number of DR1 and DR2 antagonists have been shown to increase AADC activity in rat and mouse striatum [65,66], and rat nucleus accumbens and olfactory tubercles [67]. On the contrary, DR agonists have been shown to result in a decreased enzymatic activity [66,67]. In addition, changes in AADC activity induced by DR antagonists have been shown to possess a biphasic time course: an early, short lasting (1 hour) activation, indeed, is followed by a second, later onset (3 hours) and longer lasting activation [65,66]. Moreover, the initial activation has been shown to be not sensitive to protein synthesis inhibitors, suggesting a post-translational activation mechanism [65], whereas the later onset activation is sensitive to protein synthesis inhibitors [66], suggesting that new protein synthesis is required.

A likely mechanism by which this post-translational regulation of AADC could occur is phosphorylation. This hypothesis is supported by a number of observations. AADC primary structure contains a number of recognition motifs for phosphorylation by cyclic adenosine monophosphate (cAMP)-dependent protein kinase (PKA), protein kinase C (PKC), calcium/calmodulin-dependent protein kinase II (Ca-CM PKII), and proline-directed protein kinase [68]. Further, a number of treatments that tend to increase protein phosphorylation has been shown to increase AADC activity: intracerebroventricular injection of forskolin or 8-bromo cyclic AMP (8Br-cAMP) [69], which increase PKA mediated phosphorylation, phorbol 12-myristate-13-acetate (PMA) [66], a PKC activator, and okadaic acid [70], a protein phosphatase inhibitor, all result in an increase in AADC activity. There is therefore good evidence for a regulation of AADC at least by PKA and PKC.

At present, few data are available concerning the effects of phosphorylation on purified AADC activity, and few papers have been published reporting that both recombinant and immunoprecipitated (from brain homogenates) AADC could be phosphorylated by the catalytic subunits of PKA, and that the enzymatic activity increases in both cases (70% for the recombinant and 20% for the immunoprecipitated enzyme) [71]. Moreover, interaction with α-synuclein, implicated in Parkinson's disease, has been reported to reduce phosphorylation levels of AADC (by 1.5-fold), probably by activation of a phosphatase such as

protein phosphatase 2 (PP2A), and, concomitantly, α-synuclein leads to inhibition of AADC activity, suggesting another possible compromised mechanism of dopamine homeostasis in Parkinson's disease pathogenesis [72].

The above described regulation of AADC though PKA-dependent mechanisms may well underlie the regulation of AADC activity following changes in DR activation. The predominant DR in pre-synapsis, where AADC is localised, is DR2 type family [73], that is mainly coupled to an inhibition of adenylate cyclase (AC), resulting in a decrease in cAMP production [74]. Compounds which block DR2 activation will therefore disinhibit AC, increasing cAMP production and subsequent PKA activation. Activated PKA could then phosphorylate AADC, resulting in an increase in activity. Whilst the above hypothesis is an attractive explanation for many of the observed effects, there is evidence that the situation could be somehow more complex. As previously described, PMA administration, which increases PKC activity, has also been shown to regulate AADC activity [70]. Thus, DR2-AC-PKA pathway might represent only one of several possible post-translational regulatory mechanisms for AADC, since AADC regulation by PKC-dependent mechanisms was showed to be independent from DRs [75], suggesting that AADC might be regulated by at least one stimulus other than DR-dependent signalling.

At present, no data are available concerning the effects of phosphorylation on AADC activity towards any substrate other than L-DOPA. Further, studies have rarely focused on brain regions other than those considered primarily dopaminergic. It would be interesting to unravel, therefore, whether different results can be obtained, for example, in primarily serotonergic brain regions, such as pineal gland, using L-5-hydroxytryptophan (L-5HTP) as substrate. Further, L-5HTP receptors are known to utilize the PKC pathway [76,77], and therefore it would be interesting to understand whether these receptors can modulate AADC activity similar to DRs, and whether any such effect involves a PKC-dependent processes.

1.3.3. Only hypothalamic HDC seems to be regulated by phosphorylation

Few studies suggest that HDC, in particular the hypothalamic one, could be regulated through phosphorylation.

Crude preparation of mouse mastocytoma HDC incubated with PKA showed a decreased activity, but this effect was not detectable for purified preparations, tested for radioactive phosphate incorporation during PKA and adenosine triphosphate (ATP) incubation [78]. Rat hypothalamic HDC seemed to be almost completely inhibited after homogenate incubation under phosphorylating conditions (ATP, cAMP, and Mg^{2+}) in presence of PKA [79], and PKA-dependent inhibition of rat hypothalamic HDC was also showed to be reversed by addition of PKA inhibitors, as well as by stimulation of phosphoprotein phosphatases and incubation with calmodulin in presence of calcium ions [80].

However, incubation of rat gastric mucosal supernatant with various combinations of ATP, Mg^{2+}, cAMP and PKA and endogenous phosphatases blocking compounds did not show to significantly alter HDC activity. In addition, a similar result was also achieved with the purified enzyme [81].

These conflicting results, obtained starting from different preparations, i.e. hypothalamic or gastric HDC, are still waiting further research aimed to understand if and how this protein can be regulated by phosphorylation.

1.3.4. AADC and HDC post-translational regulation mechanisms understanding can help diseases treatment

It is now apparent that, contrary to classical view, AADC might be a post-translational regulated enzyme, potentially involved in a constant temporal balancing of monoaminergic neurotransmission, although the importance of this regulation is at present not well understood, as well as the factors and elements controlling this activation/inhibition. On the other side, HDC regulation is almost unknown, with only few, and contradictory, results suggesting a phosphorylation-based modulation.

Identification of these mechanisms may not only elucidate the physiological regulation of AADC and HDC, but also be of importance for understanding, managing and/or developing new therapies for many pathological conditions regarding dopamine and histamine homeostasis impairments.

Chapter 2

AADC and HDC play a fundamental role in human physiology

2.1. AADC: physiological role and implication in diseases

2.1.1. AADC synthetises fundamental neurotransmitters

AADC converts L-DOPA and L-5HTP to neurotransmitters dopamine (DA) and serotonin, respectively, which are also precursors of adrenaline/noradrenaline and melatonin, accordingly. Enzyme name derives from its ability to decarboxylate, although much less efficiently, also other aromatic amino acids such as tyrosine, tryptophan and phenylalanine to the corresponding amines (tyramine, tryptamine and phenethylamine, respectively), known as trace aromatic amines. Thus, as expected, AADC is found in catecholamine- and serotonin-producing neurons and in other tissues of neuronal origin, such as adrenal and pineal glands and glial cells [82]. Interestingly, this enzyme is also present in non-neuronal tissues, mainly in liver, kidneys, lung, spleen and pancreas, even if its function in these organs is not yet completely clarified [82].

DA exerts its functions through DRs binding, triggering the signalling cascade in target cells. There are at least five subtypes of DRs, which are divided into two families: the DR1-like family comprises DR1 and DR5 receptors, whereas the DR2, DR3 and DR4 receptors are members of the DR2-like family. The first family stimulate AC to produce cAMP, downstream increasing intracellular calcium among other cAMP mediated processes, while DR2 class exerts the opposite effect. In CNS, DR1-2 receptor subtypes are found at 10-100 times the levels of DR3-5 subtypes [83], but DR1 is also present in smooth muscles of blood vessels in most major organs, as well as in juxtaglomerular apparatus and

renal tubules, while DR2 in glomeruli, zona glomerulosa cells of adrenal cortex, renal tubules, and postganglionic sympathetic nerve terminals [84]. Pulmonary artery expresses DR1, DR2, DR4, and DR5 [85], which are also been discovered in epicardium, myocardium, and endocardium of heart [86].

The fourteen known serotonin receptors (5-HTR) are divided into 7 classes of G protein-coupled receptors, except for 5-HTR3, which is a ligand-gated Na^+ and K^+ cation channel. In particular, they can activate an intracellular second messenger cascade to produce an excitatory (5-HTR2 through inositol trisphosphate and diacylglycerol, and 5-HTR4, 5-HTR6 and 5-HTR7 through cAMP) or inhibitory (5-HTR1 and 5-HTR5 through cAMP) response. Notably, all classes are expressed in CNS, while some of them are also expressed in other tissues: 5-HTR3 and 5-HTR4 in peripheral nervous system and gastrointestinal tract, 5-HTR1 in blood vessels, 5-HTR7 in blood vessels and gastrointestinal tract, while 5-HTR2 is widely expressed in all above mentioned tissues, and platelets and smooth muscle as well [87].

DA, serotonin and their derivative compounds are all metabolized by the same set of enzymes, i.e. both forms of monoamine oxidase (MAO-A/B), catechol-O-methyl transferase (COMT) and aldehyde dehydrogenase (ALDH), which act in different sequential breakdown pathways, but producing some main end-products [88], i.e. homovanillic acid (HVA) from DA and 5-hydroxyindoleacetic acid (5-HIAA) from serotonin (***Figure 2.1***). In clinical research, measurements of these metabolites in plasma are commonly used to estimate levels of AADC activity in brain [89].

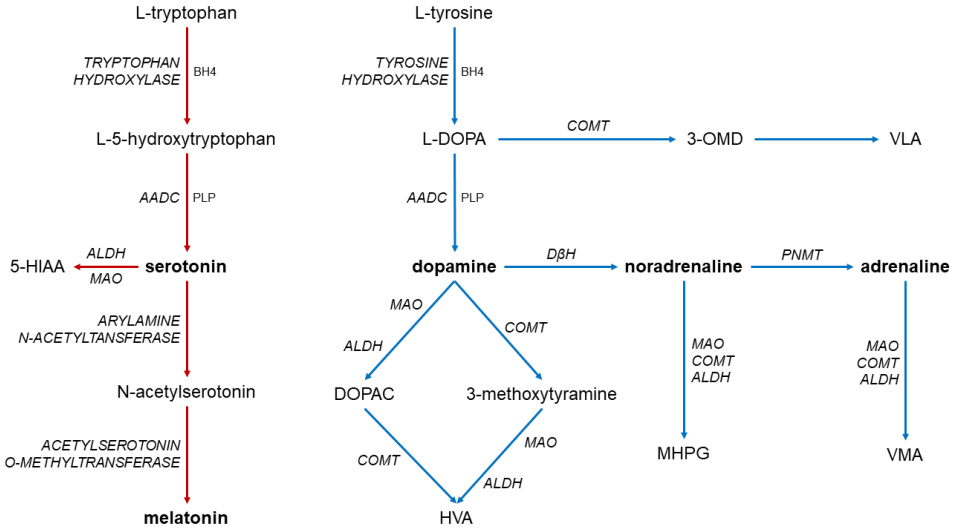

Figure 2.1. Synthetic and metabolic pathways of serotonin and DA in neurons.
BH4: tetrahydrobiopterin, ALDH: aldehyde dehydrogenase, MAO: monoamine oxidase, 5-HIAA: 5-hydroxyindoleacetic acid, 3-OMD: 3-orthomethyldopa, VLA: Vanillylactic acid, DβH: dopamine β-hydroxylase, PNMT: phenolethanolamine N-methyltransferase, MHPG: 3-methoxy 4-hydroxyphenylglycol, VMA: Vanillylmandelic acid, DOPAC: 3,4-dihydroxyphenylacetic acid, COMT: Catechol O-methyltransferase, HVA: Homovanillic acid.

In addition, DA is susceptible to oxidation by direct reaction with oxygen [90], producing quinones and free radicals that cause cell toxicity and may contribute to cell death that occurs in some pathological conditions [91].

2.1.2. Dopamine is one of the main neurotransmitters but also a signal molecule outside central nervous system

Dopaminergic neurons (DA neurons) are comparatively few in number [92], and their cell bodies are confined in groups to a few relatively small brain areas [93]. However, their axons project to many other brain areas, playing important roles in executive functions, motor control, motivation, arousal, reinforcement, and reward, as well as lower-level functions including lactation and sexual gratification.

DA neurons are arranged in different nuclei: retrorubral field (RrF, group A8), *substantia nigra pars compacta* (SNc, group A9), ventral tegmental area (VTA, group A10), posterior hypothalamus (group A11), arcuate nucleus (group A12), *zona incerta* (group A13), and periventricular nucleus (group A14) [94], each of them projects to distinct CNS areas, and thus controls specific functions. In

particular, the midbrain area hosts nuclei that form the two major DA pathways: SNc neurons, which project to dorsolateral striatum, constituting the so-called nigrostriatal pathway and regulating motor function and learning of new motor skills, and VTA and RrF neurons, which project to ventromedial striatum (*nucleus accumbens*) and to parts of limbic system and prefrontal cortex, forming the meso-limbic and the meso-cortical systems, respectively, and regulating emotional behaviour and cognitive function (***Figure 2.2***) [95].

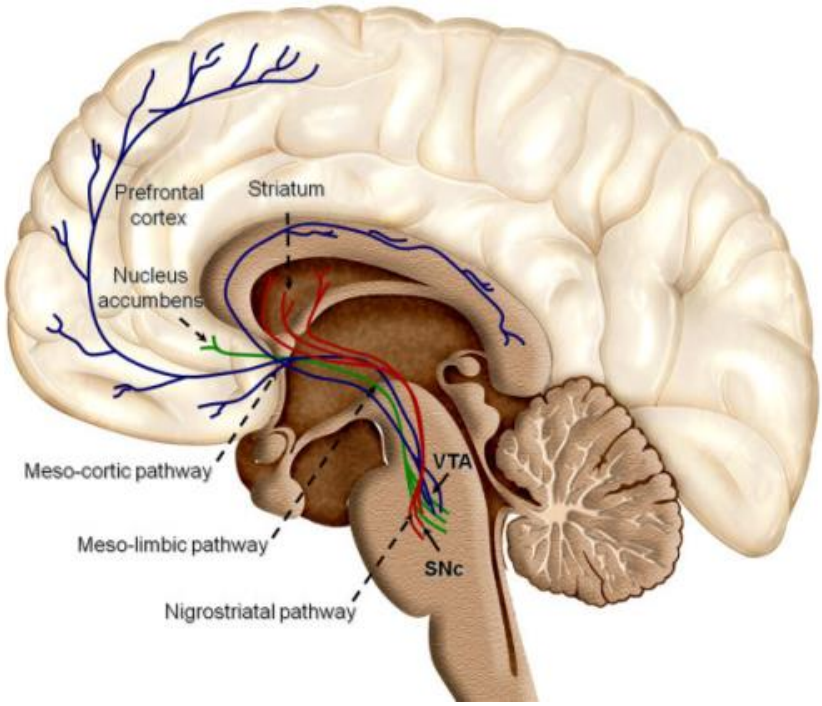

Figure 2.2. Representation of midbrain DA neurons organization and projections in CNS.
Red: nigrostriatal pathway; Green: meso-limbic pathway; Blue: meso-cortical pathway.

The other DA neurons groups project to other nervous system areas, exerting specific functions: A11 group project to spinal cord, but its function is still not well established [96]; groups A12 and A14 form an important projection, the tuberoinfundibular pathway, which goes to pituitary gland, influencing the secretion of the prolactin hormone [97]; lastly, A13 group projects to several areas of hypothalamus, participating in the control of gonadotropin-releasing hormone, which is necessary to activate the development of male and female reproductive systems after puberty [97].

DA does not cross the blood–brain barrier, so its synthesis and functions in peripheral areas are to a large degree independent of those in CNS. It is found in bloodstream, even if over 95% of DA in plasma is in form of dopamine sulphate, a conjugate with unknown biological functions, produced in the digestive system and thought to be the result of a mechanism for detoxifying DA that is ingested with food or produced by the digestive process [88]. The relatively small quantity of unconjugated DA in bloodstream may be produced by sympathetic nervous system, digestive system, or possibly other organs, and acts as a vasodilator through DRs located in arteries walls [98].

Several peripheral systems use DA as exocrine or paracrine factor that exerts its function in a limited area and/or specialized tissues. The renal dopaminergic system, for example, composed by tubule DA-synthetizing cells that release the molecule into the tubular fluid, is the main responsible for the increasing in blood supply to kidneys, in glomerular filtration rate and in excretion of sodium in the urine [84]. Furthermore, the exocrine pancreatic part secretes DA into small intestine, where its function is not clearly established, but probably linked to intestinal mucosa protection and gastrointestinal motility reduction [99], while DRs were also found in beta cells of endocrine pancreas, where DA acts to reduce the amount of insulin they release [99], even if the source of modulator is still unknown. Lastly, not only DRs were found on immune cells, especially lymphocytes, but immune cells themselves were found to synthetise and release DA [100], reducing lymphocytes activation level [101].

2.1.3. Serotonin mainly acts outside central nervous system as modulator in many physiological processes

Serotonergic neurons project from nine nuclei (designated B1-B9), located along the midline of the brainstem and centred on the reticular formation [102,103], to almost every part of the CNS: axons of neurons in lower raphe nuclei terminate in spinal cord, while axons of higher nuclei spread out in cerebellum and entire brain (***Figure 2.3***).

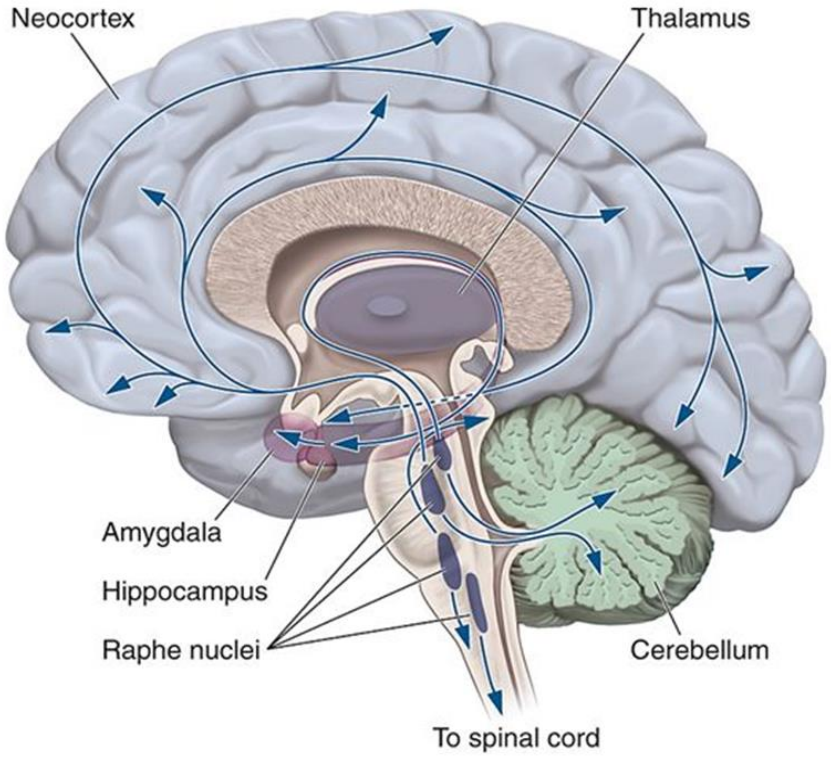

Figure 2.3. Representation of serotoninergic neurons organization and projections in CNS.

Serotonergic neurons have been supposed regulating various functions, including appetite and sleep, but also cognitive ones, like memory and learning, mood, anxiety and psychosis, even if strong clarity has not been achieved [104,105].

However, approximately 90% of the human body's total serotonin is secreted by enterochromaffin-like cells in gastrointestinal tract, where it regulates intestinal movements and motility through stimulation of myenteric neurons [106,107]. Serotonin is released in response to food intake in gut lumen but its secretion is even faster and quantitatively higher in presence of noxious substance or toxins, thus activating receptors in chemoreceptor trigger zone that stimulate vomiting [108]. In bloodstream, serotonin is actively taken up and stored by platelets, which release it during coagulation as a vasoconstrictor that directly or indirectly contracts endothelial smooth muscle cells [109], but also as a fibrocyte mitotic growth factor, aiding healing [110]. Serotonin, indeed, can also act as growth factor, stimulating, for example, cellular growth to repair liver damage [111] and regulating bone mass [112,113].

2.1.4. Trace amines regulate neurotransmission

Trace amines are monoaminergic neuromodulators [114], structurally and metabolically related to classical monoamine neurotransmitters [115], but present in trace concentrations compared to classical monoamines. They are found both in central and in peripheral nervous tissues, and play significant roles in regulating monoamine neurotransmitters quantity in synaptic clefts of monoaminergic neurons, preventing neurotransmitters reuptake as well as inhibiting neuronal firing [116]. Although trace amines can be synthesized within parent monoamine neurotransmitter systems, there is evidence that some of them might comprise their own independent neurotransmitter systems [114].

2.1.5. Impaired dopamine homeostasis is linked to several neurological diseases

Dopaminergic system plays a central role in several significant medical conditions, thus many drugs are used in order to regulate different aspects of DA physiology, for medical or recreational purposes [117].

A number of studies have reported a physiological age-related decline in both DA synthesis and DRs density in brain [118], mainly in striatum [119], probably linked to changes in cognitive flexibility and increased movement rigidity during aging [120]. One of the most studied age-related and chronic progressive neurological disorder, Parkinson's disease (PD), is caused by low levels of DA due to DA neurons degeneration and death in *substantia nigra* (A9 DA neurons group). The reasons of this cell lost, also accompanied by astrocytes death and significant increase in number of microglia [121], is poorly understood, and there is speculation of several mechanisms by which neurons could be damaged [122]. They include proteasomal and lysosomal system dysfunction, as well as reduced mitochondrial activity, even if the most reliable one seems to be an abnormal accumulation of protein α-synuclein, those insoluble aggregates form inclusions called Lewy bodies [123], also detected in many of the remaining neurons (***Figure 2.4***).

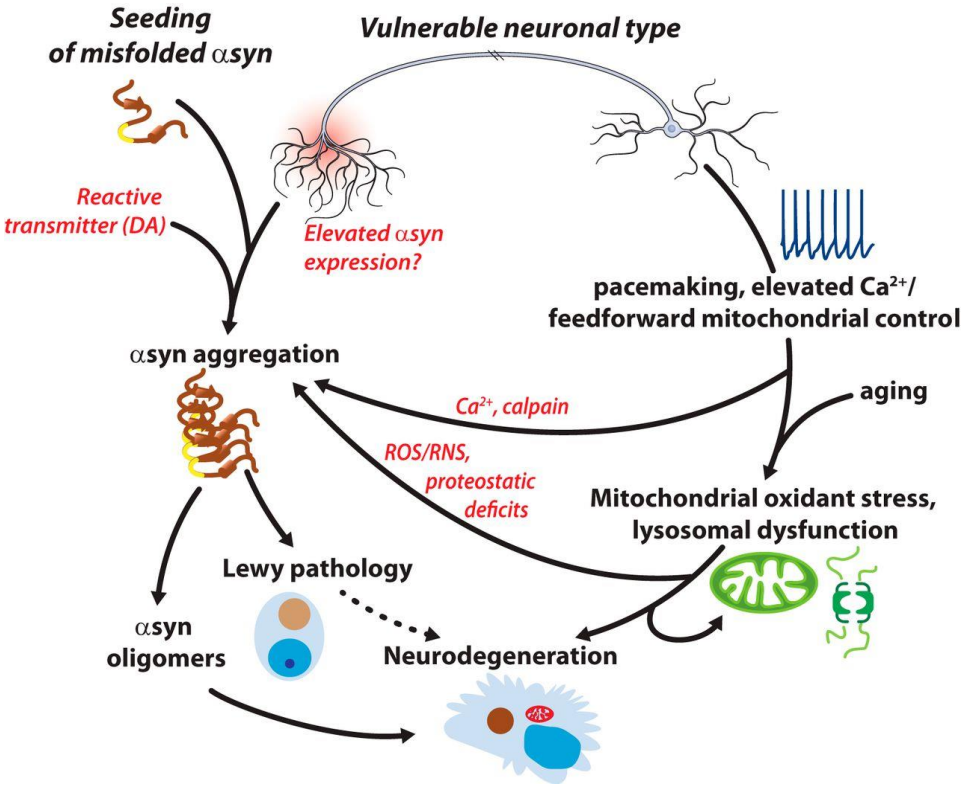

Figure 2.4. Overview of putative mechanisms involved in A9 DA neurons cell death and PD pathophysiology.

Since A9 DA neurons form the nigrostriatal pathway, the most evident, and early-developed, symptoms mainly regard impaired motor functions, like tremors, slowness of movement, rigidity, difficulty with walking and postural instability [124], that worsen with disease progression. However, also cognitive disturbances can occur from the early stages of PD and can increase in prevalence with the duration of the disease [125], including, among the most commons, executive dysfunction, like problems on planning, cognitive flexibility, abstract thinking, inhibiting inappropriate actions, initiating appropriate actions, working memory, and control of attention [125], but also dementia [126] and mood alterations, like depression, apathy, and anxiety [124]. Research indicates that PD is the product of a complex interaction of both genetic and environmental factors [127], with 5–10% of cases linked to mutation in one of several specific genes ("sporadic" or non-familial PD) [128], and in 15% of cases a first-degree relative already presented the disease [129]. The incomplete knowledge of PD pathophysiology, together with the complex factors interconnection in disease possible causes and

low rate of genetic established background, have prevented, till now, the development of a PD definitive cure, but different medications, surgery, and physical therapy are used as treatments directed at improving symptoms [129]. Initial treatment typically aims to find an optimal balancing between symptoms control and side-effects. L-DOPA, indeed, is the most effective treatment for the motor symptoms, as it can pass through blood-brain barrier (BBB) and be readily converted to DA, but its prolongated use leads to development of involuntary movements complications, called dyskinesias, together with fluctuations in medication response and long-term decreased effectiveness [130]. In addition, only a small amount of L-DOPA crosses BBB because it is rapidly metabolized to DA by extra-neuronal AADC, causing side effects including nausea, vomiting and orthostatic hypotension [131]. Thus, carbiDOPA or benserazide, two AADC inhibitors which do not cross the BBB, are usually administrated in combination with L-DOPA, improving the availability of the latter to brain passage. On the other side, L-DOPA therapy is often postponed in less severe cases and replaced by other medications, mainly dopamine agonists, to mimic DA function [132], in order to delay the onset of complications linked to L-DOPA use (***Figure 2.5***).

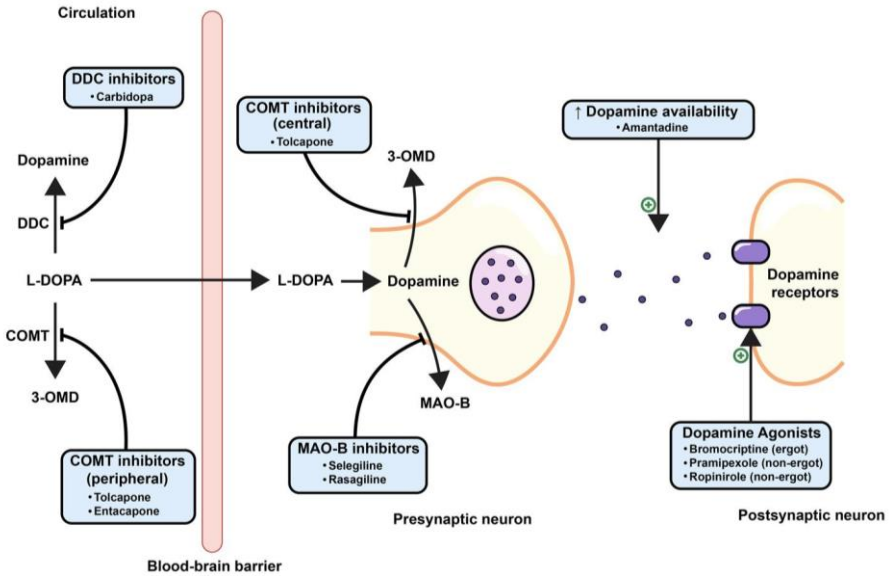

Figure 2.5. Overview of PD standard therapy.

As the disease progresses and neurons continue to be lost, all these medications become ineffective and surgery, deep brain stimulation (DBS), subcutaneous apomorphine infusion and enteral L-DOPA pumps are used [133], until final stages of the disease, during which palliative care is provided to improve quality of life [134]. Since PD is the second most common neurodegenerative disorder [135], over recent years an active research was focused on finding and testing new and hopefully definitive therapies. Among these, investigations about neuroprotection lead to the proposal of several molecules, including anti-apoptotics (omigapil, CEP-1347), anti-glutamatergics, monoamine oxidase inhibitors (selegiline, rasagiline), pro-mitochondrials (coenzyme Q10, creatine), calcium channel blockers (isradipine) and growth factors, even if none of them conclusively demonstrated, so far, a reducing degeneration tendency [122]. Moreover, a promising α-synuclein vaccine that primes human immune system to destroy α-synuclein, PD01A, has entered clinical trials in humans [136]. Stem cell technology, lastly, is at the forefront of PD research, as stem cells transplanted into rodents' and monkeys' brains have been found not only to survive but also to reduce motor and behavioural abnormalities [137-139]. However, use of foetal stem cells is controversial, and particular efforts are nowadays put in the developing effective treatments using induced pluripotent stem cells derived from adult cells [140].

Altered dopaminergic neurotransmission is implicated in other neurological diseases, like for example the attention deficit hyperactivity disorder (ADHD), a condition associated with impaired cognitive control, mainly in regulating attention, inhibiting behaviours, and forgetting things or missing details. Alteration in neurotransmission regards genetic variants in DRs and DA transporter, but also in other neurotransmitter receptors and transporters [141], and is usually treated with psychostimulants, like methylphenidate (Ritalin, Concerta) and amphetamine (Adderall, Dexedrine), which increase both DA and norepinephrine levels in brain through indirect activation of DRs and norepinephrine receptors [142], in particular in prefrontal cortex [143].

In addition, DA plays a role in pain processing in CNS and its decreased levels and/or abnormalities in dopaminergic neurotransmission have been

associated with painful symptoms that frequently occur in several clinical conditions [144]. Moreover, nausea and vomiting are largely determined by activity in area postrema in medulla of brainstem, in a region known as chemoreceptor trigger zone, which contains a large population of DR2 type. Consequently, drugs that activate DR2 receptors, like agonists such as apomorphine, have a high potential to cause nausea [145], while, on the contrary, DR2 antagonists, such as metoclopramide, are useful anti-nausea drugs [146].

2.1.6. Impaired serotonin homeostasis is linked to both central nervous system and peripheral diseases

Serotonin implication in mood and psychosis led to development of drugs that increase the low concentrations of neurotransmitter linked to depression and generalized anxiety disorder. These drugs, like tricyclic antidepressants (TCAs), inhibit the re-uptake of serotonin, making it stay in the synaptic cleft longer and allowing an increased neurotransmission signal, but they act also on norepinephrine receptors. Newer selective serotonin reuptake inhibitors (SSRIs) have been shown to induce fewer side-effects and to not interact with other drugs [147].

Considering serotonin role in in digestive tract, other drugs are already applied as antiemetics. Enterochromaffin-like cells, indeed, not only react to toxic food but are also very sensitive to irradiation and cancer chemotherapy. Drugs that block serotonin receptors are very effective in controlling nausea and vomiting caused by cancer treatment, and are considered the gold standard for this purpose [148].

2.1.7. AADC deficiency is a genetic disease caused by mutations in AADC gene

Mutations in AADC gene, both homozygous and compound heterozygous, lead to the synthesis of pathogenic variants with an impaired enzymatic activity and consequently to a rare autosomal recessive neurometabolic disorder called Aromatic Amino Acids Decarboxylase Deficiency (AADC Deficiency) (OMIM

608643). This deficiency typically manifests from earliest years through a multisystemic impairment, with severe delay in reaching milestones such as walking and talking (developmental delay), but also weak muscle tone (hypotonia), muscle stiffness, involuntary writhing movements of limbs (athetosis), and with autonomic dysfunctions, like inappropriate sweating, nasal congestion, drooling and gastroesophageal reflux, reduced ability to control body temperature, low blood pressure (hypotension) and blood sugar levels (hypoglycaemia), sometimes leading to fainting (syncope) and cardiac arrest. Many patients experience peculiar episode crises, called oculogyric crises, characterized by abnormal rotation of eyeballs, extreme irritability and agitation, pain, muscle spasms, and uncontrolled movements in particular of head and neck. Complications linked to many different aspects of this disease may lead, in some cases, to vegetative state and death [149]. AADC Deficiency is typically detected through detailed clinical assessment and a number of diagnostic tests, starting from the most common symptoms identification. When the diagnosis is clinically suspected, cerebrospinal fluid (CSF) analysis of neurotransmitters should be undertaken, in order to detect the characteristic HVA, 5-HIAA and 3-methoxy 4-hydroxyphenylglycol (MHPG) reduction together with L-DOPA, 5-HTP and 3-orthomethyldopa (3-OMD) increasing (***Figure 2.6***).

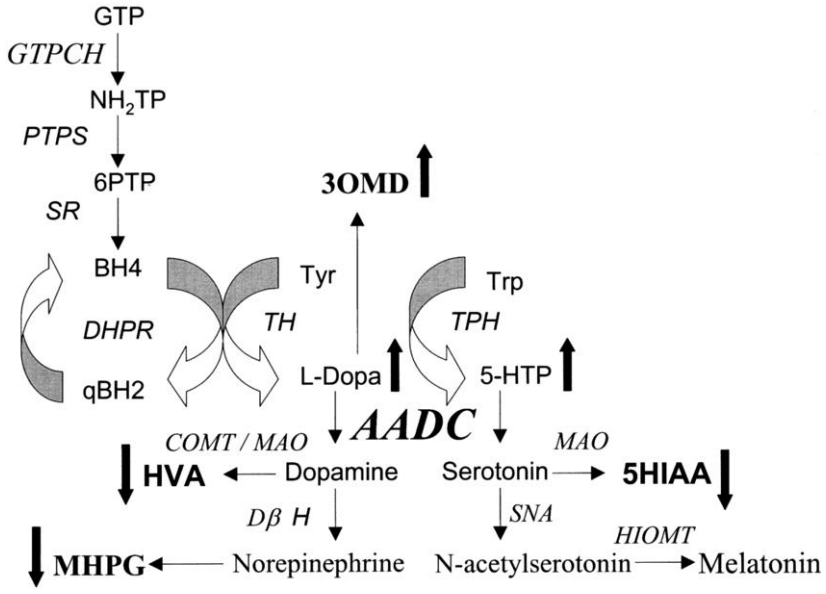

Figure 2.6. Alteration of neurotransmitters levels in AADC Deficiency detected through CSF analysis [150].

Furthermore, AADC activity can be measured in plasma, confirming a decreased or lost enzymatic activity, and finally, *AADC* genetic sequencing can be performed to definitely confirm the diagnosis [149]. Since the first case of AADC Deficiency has been published [151], only about other 100 people with this condition have been described in medical literature worldwide, and about 20% of these individuals are from Taiwan. However, new cases and new mutations are continuously detecting, both in homozygous and compound heterozygous states, mainly thanks to increase disease knowledge and use of CSF analyses and genetic screenings. In a recent paper many of the pathogenic homozygous mutations were characterized in purified recombinant form [152], revealing that structural changes of most of these variants are linearly related to catalytic changes. In particular, almost the totality of these mutations concerns residues belonging to relevant structural elements for the transition from the apo "open" to the holo "closed" and active form of the enzyme. More recently, *in vitro* biochemical characterizations and molecular investigations of enzymatic phenotypes of heterozygous variant were also started, revealing that some mutations can lead to interallelic complementation [153]. Different types of mutations, indeed, show different effects on AADC enzyme: while frameshifts, often resulting in premature stop codon codification, and nonsense mutations are more likely to lead to nonsense-mediated decay, missense mutations more likely result in an altered gene product, those features are linked to the specific position of the mutation in the protein, leading to decreased affinity for PLP and/or for L-DOPA, altered stability and/or impossibility to acquire the proper three-dimensional structure. These different biochemical features could be linked not only to the disease phenotype, as patients affected by AADC Deficiency show variable symptoms severity, but also to the choice of the better treatment, as patients present different treatments response. Indeed, there is currently no cure for AADC Deficiency, and different medications are used to help treating signs and symptoms of the disease, including by default pyridoxine (vitamin B6), dopamine receptor agonists, MAO inhibitors and calcium folinate (***Figure 2.7***), with a combination of other compounds depending on the symptoms of each individual (α-adrenergic agonists,

anticholinergic agents, selective serotonin reuptake inhibitors, gastrointestinal medications, melatonin) [149].

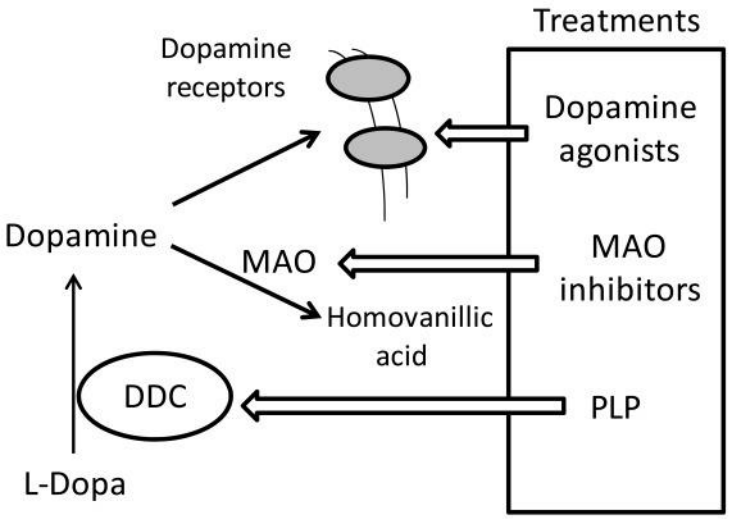

Figure 2.7. Current treatment options for AADC Deficiency.

Due to the variable, and in many cases low, response to available treatments, current studies and researches are trying to find alternative, and hopefully definitive, therapies. After previous not successful attempts to develop an *AADC*-knock out mouse model, as foetal mice died in utero, in 2013 Lee *et al*. published a model with the common Taiwanese mutation IVS6+4A>T [154]. They subsequently rescued the phenotype of the *AADC*-knock in mouse with gene therapy, using an AAV9-CMV-h*AADC* vector by intracerebroventricular injection [155], a method already used in PD gene therapy trails [156]. In 2015, Lee, Muramatsu *et al*. used an yfAAV9/3-Syn-I-m*AADC* vector via intraperitoneal injection, with better results in neuronal transduction, possibly because the used promoter (synapsin) was better targeted for neuronal expression [157]. The first AADC Deficiency gene therapy trial started in 2012, one year before the *AADC*-knock in mouse model was published, and was based on an adeno-associated viral vector-mediated gene transfer of human gene injected bilaterally into the putamen of four patients, all with the common mutation IVS6+4A>T [158]: motor improvements were observed, as well as AADC activity increase through 6-[(18)F]fluorodopa imaging for substrate uptake evaluation and DA and serotonin

levels measurements in CSF; in addition, patients showed fewer oculogyric crises and improvement of emotional stability and sleep. More AADC gene therapy trials have been started recently, in Taiwan and USA in particular [159,160], and preliminary analyses show motor improvements with no severe side effects. Nevertheless, progress in motor functions are limited, and no amelioration of all the other disease symptoms is detected, possibly due to AADC wide diffusion outside CNS.

2.2. HDC: physiological role and implication in diseases

2.2.1. HDC is the only histamine synthetizing enzyme

HDC is the enzyme responsible for histamine biosynthesis from L-histidine through decarboxylation. Even if the most well-known function of this biological amine is to be a key immune response modulator, histamine is also an important neurotransmitter and a modulator of cell growth. Thus, it is produced and released not only by basophils and mast cells, but also by histaminergic neurons and other specialised cells, in which histamine exerts specific functions.

There are four different histamine receptors, named H1R through H4R according to the order in which they were discovered, all belonging to the G-protein coupled receptors family [161]. They trigger different signalling pathways that specifically depend on both the receptor and the cell type expressing them. H1R leads to phospholipase C activation, producing inositol triphosphate and calcium mobilization, and, although it has been traditionally related to allergic response, it is also expressed in nerve cells, vascular smooth and endothelial cells among others. H2R is expressed in many immune cell types, parietal cells and nerve cells, and mediates its effects stimulating AC and increasing intracellular cAMP levels. H3R is mainly located in the presynaptic membrane of histaminergic neurons, where regulates the production of histamine in CNS, but it also regulates the release of many neurotransmitters, acting as a presynaptic heteroreceptor, since it inhibits cAMP accumulation. H4R inhibits cAMP

formation as well, but it is expressed in CNS and immune cells of haematopoietic origin.

Once formed, histamine is either stored or rapidly inactivated by its primary degradative enzymes, histamine-N-methyltransferase (HNMT) or diamine oxidase (DAO). In CNS, histamine released into synaptic cleft is primarily metabolised by HNMT, while in other tissues both enzymes may play a role. Several other enzymes, including MAO and ALDH, further process the immediate metabolites of histamine for excretion or recycling (***Figure 2.8***).

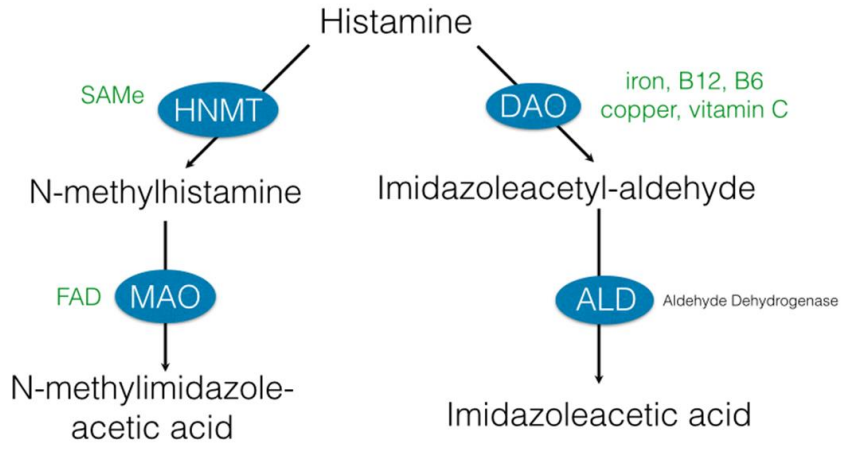

Figure 2.8. Metabolic pathways of histamine.
DAO: diamine oxidase; FAD: flavin adenine dinucleotide; HNMT: histamine-N-methyltransferase; MAO: monoamine oxidase; SAMe: S-Adenosyl methionine.

A deeper knowledge of the multiple roles played by histamine has been achieved thanks to knock out animal models [162].

2.2.2. Histamine is a fundamental signalling molecule inside and outside central nervous system

Histaminergic neurons cell bodies are located in a portion of the posterior hypothalamus known as tuberomammillary nucleus (TMN) and project widely throughout CNS, including cerebral cortex, hippocampus, neostriatum, *nucleus accumbens*, amygdala, and other parts of hypothalamus, as well as spinal cord (***Figure 2.9***).

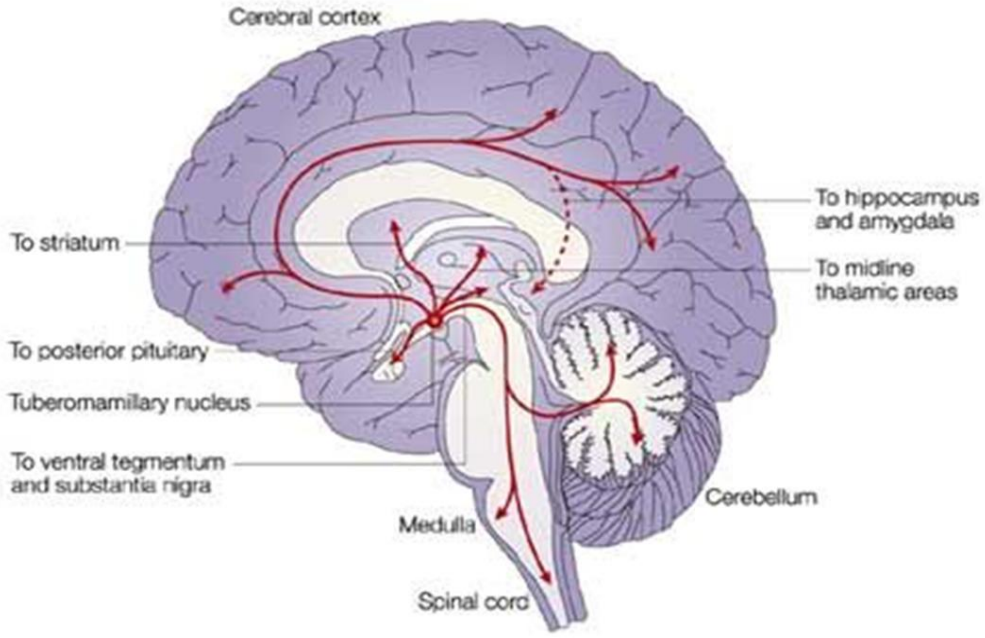

Figure 2.9. Representation of histaminergic neurons organization and projections in CNS.

The main role of histaminergic neurons is regulation of circadian rhythm and promotion of arousal when activated [163], especially in cortex region, as neural firing rate is strongly positively correlated with the individual's state of arousal, i.e. rapid firing during wakefulness periods and slow firing during periods of relaxation/tiredness, up to a state of no firing during REM and NREM (non-REM) sleep. Histaminergic neurons network, in particular through projections to basal forebrain and dorsal pons, is involved in control of learning and memory [164].

Outside CNS, enterochromaffin-like cells in gastric glands of stomach release histamine that stimulates nearby parietal cells: they uptake carbon dioxide, and water, from the blood converting it to carbonic acid that readily dissociates into hydrogen and bicarbonate ions, and extrude hydrogen ions into the stomach lumen, linking histamine release to decrease in stomach pH [165].

Histamine, stored in granules and released by mast cells and basophils in connective tissue, is clearly involved in inflammatory response, stimulating vasodilatation and permeabilization of vessels [166], which results in net distribution of blood plasma from vessel into tissue space, allowing the transfer of white cells and inflammation mediators such as complement, lysozyme, antibodies, and the consequent inflammatory response development. Another

relevant biological function of histamine, both secreted by mast cells [167] and in its unstored diffusible form [168] appear to include tissue repair and angiogenesis stimulation. This hypothesis is supported by interesting observation about the induction of histamine synthesis in tissues undergoing repair or growth, since HDC high expression level was detected in rapidly proliferating sites, such as wound healing [169,170], embryonic tissues [171] and regenerating liver [172]. Although histamine association with cell growth regulation has been addressed as a potentially important role of this modulator, the underlying mechanism is not yet clear and still remains controversial.

2.2.3. Impaired histamine homeostasis is linked to neurological as well as peripheral diseases

Histaminergic neurons network is involved in maintaining vigilance and it is a key controller of memory and learning. Thus, it is not surprising that impairments in these functions are linked not only to sedating sides effects of antihistaminergic developed as allergic reactions medications, but also to inhibition of histamine biosynthesis or loss (i.e. degeneration or destruction) of histamine-releasing neurons.

Cognitive impairments of Alzheimer's disease (AD) are traditionally attributed to neurodegeneration of cholinergic system induced by extracellular Aβ plaque deposits and intracellular neurofibrillary tangle accumulation in learning and memories brain regions [173] (***Figure 2.10***).

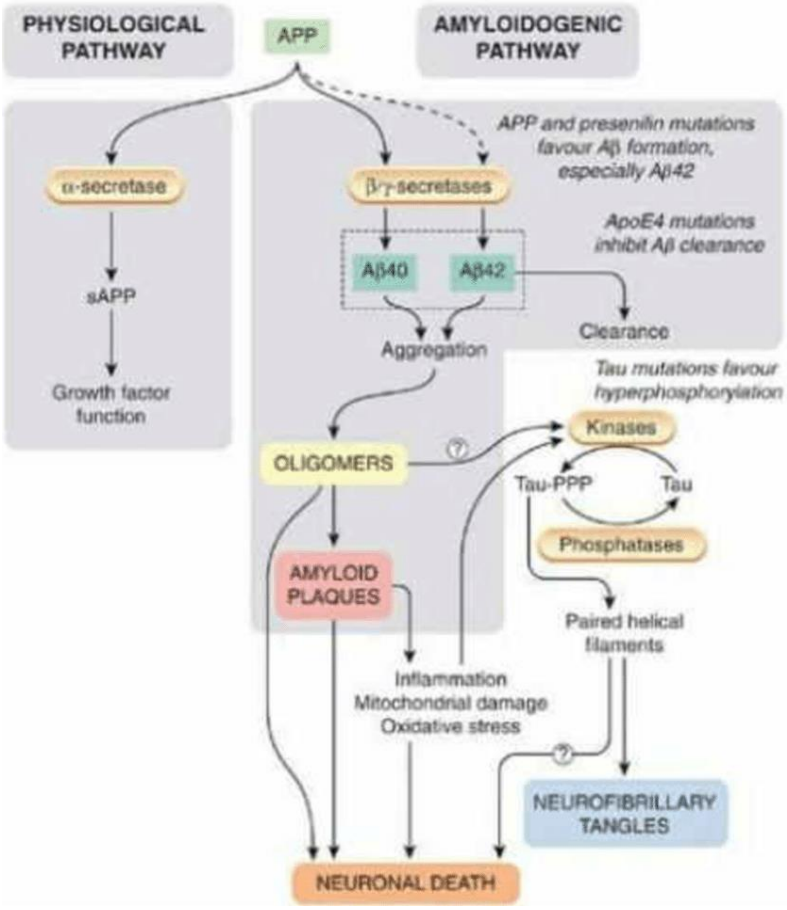

Figure 2.10. Representation of pathophysiology mechanisms of AD [174].

The central hallmark of this progressive disabling disease, indeed, is the deterioration of learning and memory as well as other cognitive symptoms like problems with language, disorientation, mood swings, loss of motivation, not managing self-care, and behavioural issues [175], and it accounts for about 50-75% of dementia cases, representing the most common cause of dementia among elderly [176], even if its exact cause is not still completely understood. Monogenetic causes of AD, indeed, represent only 5% of cases, usually early-onset ones, while most of cases do not exhibit autosomal-dominant inheritance and are termed sporadic AD, in which many environmental and genetic differences may act as risk factors [177]. Current treatments, based on glutamatergic (NMDA-receptors antagonists) and acetyilcholinergic (acetylcholine esterase inhibitors) systems alterations, are limited, with several side-effects and/or only partially effectiveness in ameliorating cognitive

symptoms, mainly during early stages of the disease [178], while rescue attempts aimed to reduce amyloid load and/or to immunize against Aβ accumulation yielded so far mixed and essentially ineffectively results [178,179]. It is now increasingly recognized that alterations in neuronal histaminergic system contribute to cognitive impairments displayed by these patients [180-182]. AD patients, indeed, show alterations of histamine concentrations in brain and degeneration of histamine TMN neurons [183-185], as well as decreased quantity of H1R in frontal cortex and temporal cortex, which correlates with the severity of cognitive symptoms [186]. Given that H1R-deficient mice exhibits a dementia-like behavioural phenotype [187], with many common human symptoms [188,189], cognitive deficits seen in AD patients may be linked to changes in H1R function and it is possible that histamine-related drugs might ameliorate cognitive symptoms. In addition, it has been shown that histamine can stimulate neurogenesis *in vitro* and *in vivo* [190,191] increasing the expression of fibroblast growth factor receptor 1, known to be involved in proliferation and differentiation of neural precursor cells, probably through activation of H1R [192], findings in line with the reduced adult neurogenesis in hippocampus of H1R-deficient mice [189]: thus, stimulation of adult neurogenesis with histamine-related drugs would be a possible strategy to counteract the progressive and irreversible global brain atrophy linked to neurogenesis alterations, already recognized as integral part of AD [193].

As fundamental mediator of immune system, histamine is involved in many immune system disorders and allergies caused by hypersensitivity of immune system to typically harmless substances in the environment. Activated mast cells and basophils undergo degranulation, releasing inflammatory chemical mediators, including histamine, and thus causing several systemic effects, such as vasodilation, mucous secretion, nerve stimulation, and smooth muscle contraction, leading to rhinorrhoea, itchiness, dyspnoea, and in some cases anaphylaxis. Depending on the individual, allergen, and mode of introduction, symptoms can be system-wide or localized to particular body systems, but they are all commonly treated with medications that block allergic mediators action or prevent activation of cells and degranulation processes, including, among others, generic anti-

histaminergics. Inflammatory features of histamine in immune reactions have made it an important factor in pathogenesis of not only allergic reactions but also various autoimmune diseases. For example, it has been shown that histamine is implicated, even if with contrasting results, in pathophysiology of multiple sclerosis (MS) and its experimental model, experimental autoimmune encephalomyelitis (EAE). MS is the principal chronic inflammatory demyelinating disease of CNS with an immunopathological aetiology, depending on genetic as well as environmental factors [194], and consisting of BBB leakage, destruction of myelin sheaths, oligodendrocyte damage and cell death, axonal damage, glial scar formation and presence of inflammatory infiltrates that mainly consist of lymphocytes and macrophages (***Figure 2.11***).

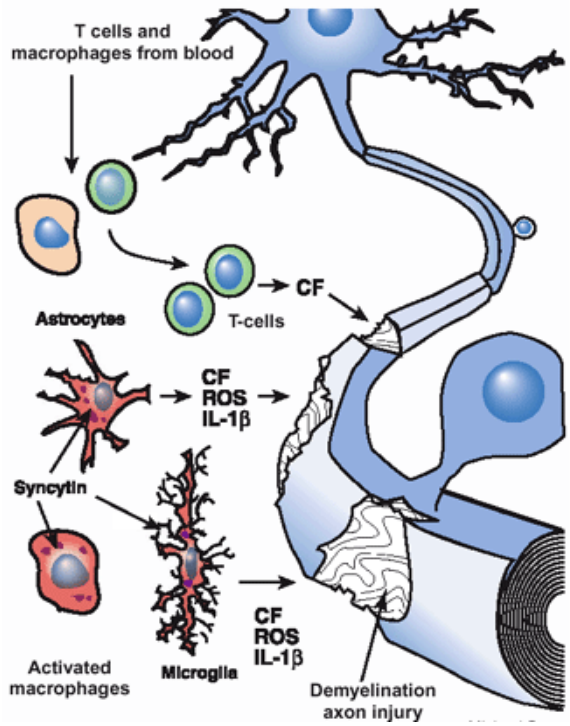

Figure 2.11. Representation of pathophysiology mechanisms of MS [195].

It has been shown that histamine can change the permeability of BBB, which leads to elevation of infiltrated cells in CNS and neuroinflammation, and that its level is associated with the onset of EAE [167,196]. On the contrary, it was also reported that EAE is significantly more severe in *HDC*$^{-/-}$ mice, with diffuse inflammatory infiltrates, including a prevalent granulocytic component, in brain

and cerebellum, and endogenous histamine appears to regulate the autoimmune response against myelin in EAE model, and to limit immune damage in CNS [197].

It is an old clinical/pathological observation that areas of long-standing inflammation have an increased risk of development of cancerous processes, linking abnormal and persistent inflammatory responses to tumour development promotion. It has been demonstrated that inflammatory mediators, which under normal circumstances are activated only for a short time and then are rapidly down-regulated, can, when improperly regulated, support the development, invasiveness or angiogenic activity of some tumours. Large amount of data is now available regarding the effects of histamine on cell proliferation, together with observations that histamine can be induced and made available in an unstored diffusible form, and increased histamine content and HDC overexpression have been detected in a wide range of different carcinoma types and neuroendocrine tumours, in particular gastrointestinal cancers [198]. Recent information suggests that there are two main phases in the development of clinically manifested tumours, that are the malignant transformation of normal cells, and the subsequent tumorous progression of the transformed clones. In fact, the major driving forces of this process are the random mutations that cells accumulate during their individual life, modifying their genome, as well as constantly leading to the formation of newer mutant variants among the already cancerous cells, and the continuous clone selection, which sorts out from the numerous competing tumour cell variants the most resistant clones, which are able to escape from anti-tumour mechanisms activated against them, gradually independent from mechanisms controlling cellular growth, tissue integrity and homeostasis. In addition, tumour invasion and metastasis are closely dependent on cancer cells acquired capability to induce angiogenesis. Histamine derived from cells other than mast cells, like tumour-associates macrophages, was showed to play a significant role in angiogenesis through miming a “constant tissue inflammation” state [199], and many types of tumour cells can release histamine inducing HDC expression to increase angiogenesis and sustain its own growth and survival [200].

This aspect was studied in detail in recent years for cholangiocarcinoma, a relatively rare neoplasia, with an annual incidence rate of 1–2 cases per 100,000 in the Western world [201] but an increasing rising rate worldwide over the past few decades [202], regarding cholangiocytes, i.e. epithelial cells of the bile duct [203]. Cholangiocarcinoma is thought to progress from early hyperplasia and metaplasia, through dysplasia, to development of carcinoma [204], and chronic inflammation, together with obstruction of the bile ducts, resulting in an impaired bile flow, are thought to play a role in this progression. Even if a number of risk factors for development of cholangiocarcinoma have been described, indeed, the most common one is primary sclerosing cholangitis (PSC), an inflammatory disease of bile ducts [205,206], that also share its general symptoms with the neoplasia, like abnormal liver function, jaundice (yellowing of the eyes and skin), abdominal pain, generalized itching, weight loss and fever. Cholangiocarcinoma is considered to be an incurable and rapidly lethal cancer, with 5-year survival rate of 0% when disease is inoperable because distal lymph nodes show metastases [207], and less than 5% in general [208], unless both primary tumour and any metastases can be fully removed by surgery. No potentially curative treatment exists except surgery, indeed, and most people have advanced stage disease and are inoperable at the time of diagnosis, in particular for patients with PCS who develop cholangiocarcinoma [209]. Even if they are minor components of liver epithelia (3 to 5% of the endogenous liver cells) respect to the most common hepatocytes (70% of the nucleated liver population) [210], cholangiocytes coat intrahepatic and extrahepatic bile ducts, participating in several tissue processes and playing a key role in bile secretion via net release of bicarbonate and water, i.e. bile-acid independent bile flow driven by active transport of electrolytes (***Figure 2.12***).

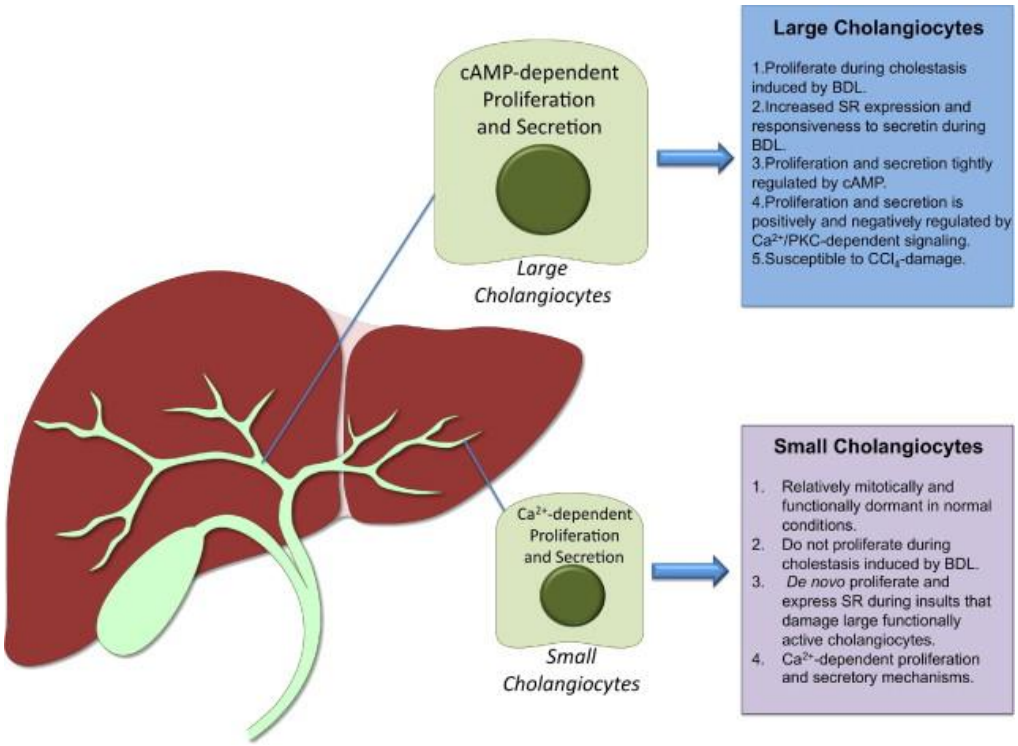

Figure 2.12. Schematic representation of cholangiocytes localisation and features [211].

Cholangiocytes proliferation is critical for homeostatic maintenance of biliary tree and secretory function during the pathogenesis of chronic cholestatic liver diseases and after liver injury, and is regulated by a variety of neuroendocrine factors [212], both stimulatory or inhibitory, through autocrine and paracrine mechanisms, including gastrointestinal hormones (secretin, somatostatin, and gastrin), neuropeptides, and neurotransmitters [213] (***Figure 2.13***).

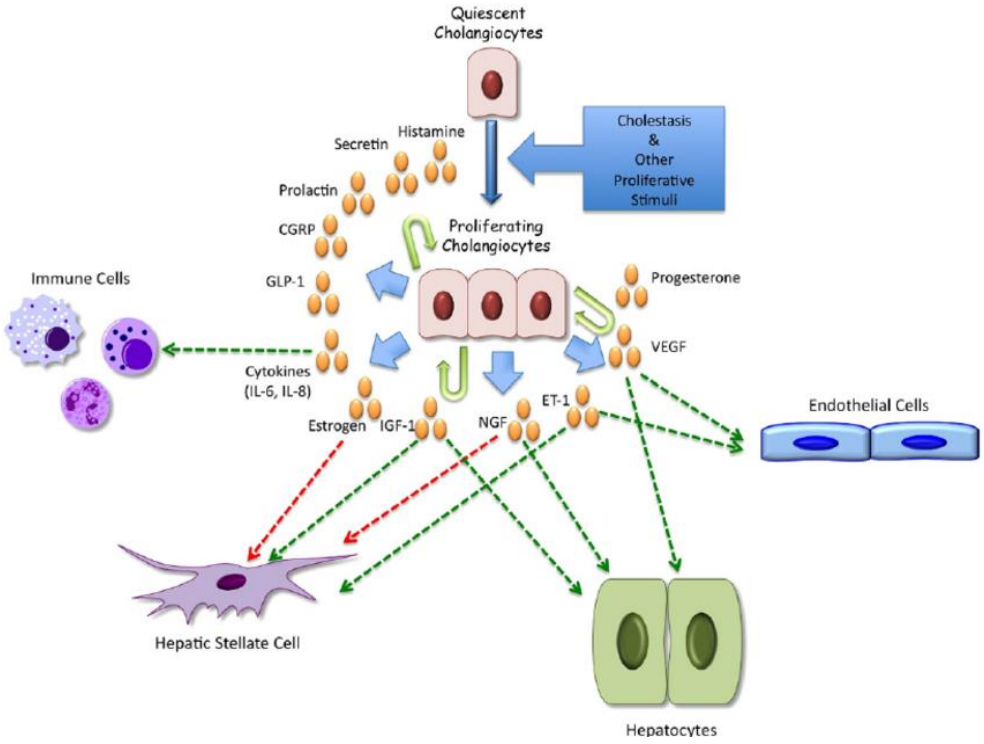

Figure 2.13. Illustration of the neuroendocrine factors secreted by cholangiocytes that regulate their proliferation, secretory function, and known and/or postulated interactions with other cell types [211].

Cholangiocytes have low mitotic activity in normal state and also display a heterogeneous profile regarding proliferative/apoptotic responses to liver injury [214,215]: usually large but not small cholangiocytes proliferate in response to activation of cAMP-dependent signalling, leading to increased intrahepatic bile duct mass [216], but small cholangiocytes proliferate in response to HR1 stimulation [217], and in pathologic conditions of damage of large cholangiocytes small ducts replenish the damaged biliary tree by de novo acquisition of large cholangiocyte phenotypes [218]. In cholangiocarcinoma, it has been detected an increased histamine content *in vitro*, due to enhanced HDC expression, and histamine behaves as a trophic factor increasing tumour growth through an autocrine mechanism via vascular endothelial growth factor (VEGF) expression stimulation [219]. Furthermore, the *in vivo* loss of HDC by pharmacological or genetic modification inhibits tumour growth, suggesting the potential therapeutic value of blocking histamine production by HDC targeting [220].

2.2.4. Premature termination of HDC is associated with Tourette syndrome

In 9 affected members of a 2-generation family with Gilles de la Tourette syndrome (TS), Ercan-Sencicek *et al*. identified a heterozygous 951G-A transition in exon 9 of the HDC gene, resulting in a Trp317-to-ter (W317X) substitution, and consequently in a truncated protein lacking key segments of the active domain [221]. Even if HDC W317X mutation is considerably rare, two subsequent genetic studies support the possibility that histamine dysregulation contributes to TS more broadly [221,222]. TS is a neurobehavioural disorder characterized by chronic, sudden, brief, intermittent, involuntary or semi-voluntary motor tics, and/or phonic or vocal tics, sometimes associated with behavioural abnormalities. In general, tics are common, occurring in mild forms in approximately 20% of young people, and clinically significant cases occur in about 5%. Interestingly, approximately 75% of children with a clinically significant tic disorder improve to the point that they no longer have clinically significant tics by young adulthood [223]. Thus, TS usually begins in childhood and persists for at least a year, affecting around 1% of the population [224], more commonly males, with a sex ratio of about 3:1 [225]. However, 'pure' TS is uncommon, with up to 90% of cases carrying at least one additional diagnosis, most commonly autism spectrum disorder (ASD) [226], obsessive-compulsive disorder (OCD) or ADHD [227]. Given this high level of comorbidity, the pathophysiology of tics can be expected to overlap with that of some of these other conditions, all associated with dysregulation of cortico-basal ganglia circuitry. The first evidence is that TS patients show elevated DA tone in striatum [228,229], thus explaining why DR2 blockers, besides numerous side effects, are the most efficacious pharmacotherapy for tics [230], while psychostimulant drugs and DR agonists can trigger stereotypic behaviours that have been interpreted as tic-like [231], supporting the idea that elevated DA levels may explain, or at least contribute to, the development of tics. To confirm that, the proposed pathophysiological process was investigated in *HDC*-knock out mouse model, focusing on DA modulation of striatum. In knock out animals, baseline striatal DA level is elevated [232], and also accentuated in animal dark phase, when histamine is normally elevated in

mice, consistent with negative regulation of DA by histamine, while intracerebroventricular histamine infusion reduces striatal DA levels [233]. Even if mechanistic work focusing on disease-relevant abnormalities in *HDC*-knock out model has just begun, like DA dysregulation and abnormalities in DA receptors [233] and abnormalities in histamine receptors, especially in H3R [234], the now clear association of histamine dysregulation with TS and related conditions emerged only recently, and many questions remain, in particular regarding histamine-DA interactions in basal ganglia as an important locus of pathology.

Chapter 3

Induced pluripotent stem cells as model for investigation of physiological and pathological mechanisms

Since first human embryonic stem cells (ESCs) were isolated in 1998 [235], pluripotent stem cells (PSCs) became a new reality in the study of human diseases. However, isolation and use of ESCs lines harbour ethical issues, and are strictly governed by laws in many countries due to the fact that their generation involve manipulation and destruction of pre-implantation stage embryo. It is with the discovery of cellular reprogramming that a fundamental step toward the *in vitro* modelling of human diseases has been done, theoretically allowing the study of all diseases starting from patient cells. Induced PSCs (iPSCs) generated from somatic cells share most of human ESCs characteristics, such as the ability to indefinitely proliferate and to potentially develop into all types of differentiated cells, providing a new source of patients-derived cells. Thus, iPSCs technology is, currently, the most faithful and closest to reality cell model available to study patient-specific phenotypes and investigate pathophysiological mechanisms of human diseases, in particular for those disorders affecting tissues of difficult sampling, such as CNS.

3.1. Overview of iPSCs technology development

iPSCs reprogramming was performed for the first time in 2006 by Takahashi and Yamanaka [236], awarded the 2012 Nobel Prize. Starting from the hypothesis that genes fundamental for ESCs function might be able to induce an embryonic state in adult cells, they chose twenty-four genes previously identified as important for PSCs phenotype and used retroviruses to deliver these genes into mouse fibroblasts. The produced ESCs-like colonies showed reactivation of *FBX15*, a

pluripotent stem cell-specific gene, and capacity of indefinite propagation. Sequential removal of factors from the original pool allowed the identification of four factors as necessary and together sufficient to generate ESCs-like colonies: these factors are OCT3/4, SOX2, KLF4 and cMYC, also known as Yamanaka factors. Even if these iPSCs were similar to ESCs in unlimited self-renewal and pluripotency, their molecular characterisation revealed that gene expression and epigenetic marks were somewhere between those of fibroblasts and ESCs, and, in addition, cells failed to produce viable chimeras when injected into developing embryos. A second-generation mouse iPSCs were developed in 2007 by three different research groups (Yamanaka's, together with a Harvard and a Massachusetts Institute of Technology group) [237-239]. These cells, which produced viable chimeric mice, were derived from mouse fibroblasts expressing the same four transcription factors but selected for *NANOG*, an ESCs functionally important gene.

Human iPSCs were derived for the first time in 2007 by two independent research groups (Yamanaka of Kyoto University, Japan, and James Thomson of University of Wisconsin-Madison). While Yamanaka reprogrammed human fibroblasts with the same four genes set previously used in mouse through a retroviral system [240], Thomson employed a different set (*OCT3/4, SOX2*, *NANOG* and *LIN28*) using a lentiviral system [241]. After these first fibroblasts reprogramming, human iPSCs were successfully derived also from keratinocytes [242, 243], peripheral blood cells [244,245] and renal epithelial cells from urine [246].

3.1.1. Factors used for iPSCs generation are linked to pluripotency state

Both Yamanaka and Thomson transcription factors sets include OCT3/4 and SOX2. OCT3/4 (octamer-binding transcription factor), a protein encoded by *POU5F1* gene [247], is a homeodomain transcription factor critically involved in ESCs self-renewal [248] through a fine regulation of its expression level [249]. OCT3/4 is therefore a master regulator of pluripotency and it is often used as a marker of stemness, while differentiated cells show a reduced expression.

Changes in OCT3/4 levels do not independently promote differentiation, but are also controlled by levels of SOX2, a member of the Sox family of transcription factors, which have been shown to play key roles in many stages of mammalian development and in maintenance of embryonic and neural stem cells. SOX2 binds to DNA cooperatively with OCT3/4, with the primary role of controlling OCT3/4 expression in ESCs, and they both perpetuate their own expression when concurrently present [250].

Yamanaka transcription factors set is completed with KLF4 and cMYC. KLF4 (gut-enriched Krüppel-like factor), a zinc-finger transcription factor [251], has been garnering attention in recent years because some of its functions are apparently contradicting. It is, indeed, highly expressed in non-dividing cells and its overexpression induces cell cycle arrest, in particular preventing cell division when DNA is damaged [252-256]. However, KLF4 has been shown to play multiple and different functions, that switch between pro-cell survival to pro-cell death factor [257-260]. cMYC, the first discovered member of *MYC* genes and proto-oncogenes family, regulates the expression of several target genes, resulting in numerous biological effects, like cell proliferation promotion, cell growth regulation, apoptosis inhibition and stem cell self-renewal stimulation. Since cMYC amplification occurs in several cancer types, including breast, colorectal, pancreatic, gastric, and uterine cancers [261], possible cMYC-induced iPSCs development of lethal teratomas leaded researchers to select other types of transcription factors for reprogramming.

Thomson factors replace KLF4 and cMYC with NANOG and LIN28. NANOG is a transcription factor critically involved in self-renewal of undifferentiated ESCs [262]. It is thought to function in concert with OCT3/4 and SOX2, in a complex regulatory network in which OCT3/4 and SOX2 are capable of directly regulating NANOG by binding to its promoter, maintaining the self-renewing undifferentiated state of the inner cell mass of blastocyst, as well as of ESCs and iPSCs cells [263]. While differential up- and down-regulation of OCT3/4 and SOX2 has been shown to promote differentiation toward divergent developmental programs, down-regulation of NANOG must occur for differentiation to proceed [264]. LIN28 is an RNA-binding protein that binds to and enhances the translation of IGF-2 (insulin-

like growth factor 2) mRNA [265], and is thought to regulate self-renewal of stem cells, since it is highly expressed during early embryogenesis [266].

3.1.2. Different approaches for iPSCs generation can avoid insertional problems

Methods pioneered by Yamanaka and others demonstrated that adult cells can be reprogrammed to iPSCs, but there are still many challenges associated with this technology, mainly linked to low reprogramming efficiency and risk of insertions into target cells genome due to integration of transcription factors delivering system. During the years that followed Yamanaka's and Thomson's demonstration of iPSCs reprogramming from somatic cells, other strategies and techniques were developed in order to avoid, or at least to limit, these two main problems.

Alternate vectors

One of the key strategies for avoiding problems like low efficiency and tumorigenesis has been the use of alternate vectors. In 2008, Hochedlinger *et al*. produced cells identical to ESCs using an adenovirus to transport transcription factors genes into skin and liver cells of mice. Adenovirus, contrary to other vectors like lentiviruses and retroviruses, does not incorporate any of its own genes into the targeted host, avoiding, therefore, the potential for insertional mutagenesis [267]. One year later, Freed *et al*. used the same technology to successfully reprogram human fibroblasts into iPSCs [268].

Another method of delivering is based on plasmids: transfection with two plasmid constructs carrying reprogramming factors, the first plasmid codifying for *c-MYC*, while the second one for the other three Yamanaka factors, successfully reprogrammed mouse cells [269]. Although plasmid delivering avoids viruses, it still requires cancer-promoting genes, and, in addition, it is much less efficient compared to retroviral methods.

Chemical compounds

Another strategy to improve low efficiency of reprogramming and avoid insertional problems is based on molecules and compounds that can mimic the effects of transcription factors, compensating for reprogramming factors that do not effectively target the genome and meantime avoiding genomic integration. Key studies using this strategy, based on histone deacetylase (HDAC) inhibitor valproic acid [270] and histone methyl transferase (HMT) inhibitor BIX-0129 [271], were conducted from 2008. In 2013 Deng *at al*. first created iPSCs without any genetic modification, using a cocktail of seven small compounds to induce mouse somatic cells into stem cells (CiPSCs) [272]. Although CiPSCs contributed to all major cells types when transferred into developing mouse embryos, proving their pluripotency, the reprogramming efficiency (about 0.2%) was comparable to those of standard iPSCs production techniques.

MicroRNA

Several mechanisms have been proposed about the addition of microRNAs to enhance iPSCs potential. ESCs-specific microRNA molecules have been demonstrated to enhance efficiency of induced pluripotency by acting upstream of OCT3/4, SOX2 and KLF4, but downstream of c-MYC [273]. In addition, microRNAs can induce reprogramming even without added transcription factors, and predict iPSCs differentiation potential [274].

3.2. iPSCs differentiation into dopaminergic midbrain neurons mimics neuronal development

PSCs have the remarkable property of long-term self-renewal, and at the same time they can potentially give rise to any type of differentiate cells. To induce lineage differentiation from iPSCs, investigators use insights gained from development: therefore, in the majority of cases, differentiation protocols are based

on initial generation of embryoid bodies and subsequent step-wise addition of growth factors or their inhibitors and/or cytokines, known to play a role during certain steps of the particular cellular development, combined with monolayer culture systems. This has enabled the generation of a number of cell types, such as, for example, neural subpopulations, like glutamatergic cortical neurons [275], cholinergic neurons [276], DA neurons [277], oligodendrocytes [278], and astrocytes [279], but also cardiac muscle cells [280-283], and hepatocytes [284-286], among many others.

3.2.1. Neurodevelopment is a multi-step process

Even though not fully understood, many knowledges have been collected to describe the mechanisms involved in differentiation of PSCs. Based on acquired information, it is now possible to induce stem cells to differentiate into different cells types *in vitro* by changing physical and/or chemical conditions of growth, reproducing the development process leading to a fully differentiated phenotype. Neurodevelopment, based on a spatiotemporally regulation and a sequential, progressive restrictions in cell fate, is therefore retraced *in vitro* through development-based protocols that recapitulate the *in vivo* action of morphogens and signal molecules identified as key players during nervous system development.

Following implantation of blastomere and during gastrulation, 3 distinct germ layers are formed: endoderm, which develops to internal organs, mesoderm, which gives rise to bone, muscle, and vasculature, and ectoderm, from which results in skins and nervous system specification (***Figure 3.1***).

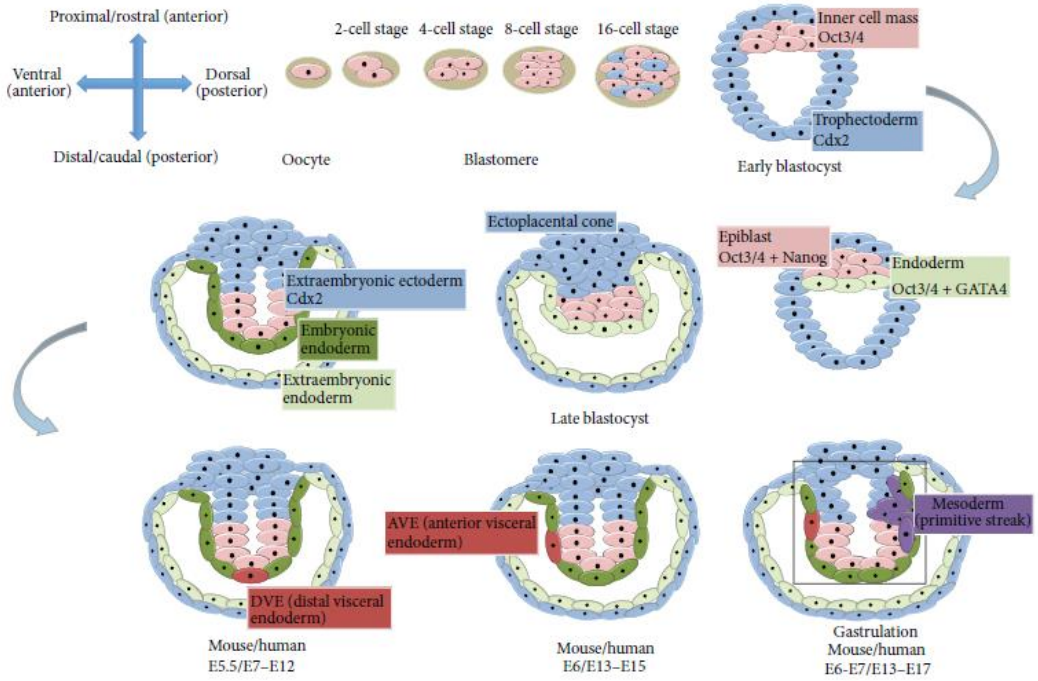

Figure 3.1. Developmental stages of mouse and human embryos [287].
Timelines are given for mouse and human embryonic development.

This 3-layered structure undergoes progressive morphological transformations, in which mesoderm and endoderm invaginate, and ectoderm forms an epithelial sheet [287]. Subsequently, neurodevelopment has been described to proceeds in three principal consecutive steps (***Figure 3.2***).

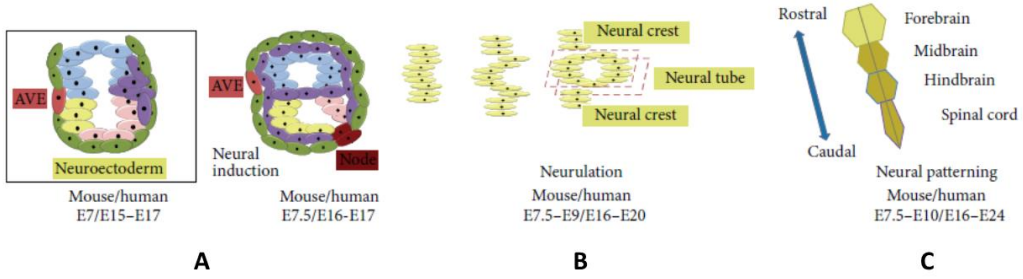

Figure 3.2. Neural induction (A), neurulation (B), and neural patterning (C) overview [287].
Timelines are given for mouse and human embryonic development.

Firstly, embryonic ectoderm forms a ticker layer on the dorsal axis: the neural plate (***Figure 3.2A***). Subsequently, neurulation of neural plate occurs through a set of morphological transformations, including changes in cells shape and cell-cell adhesion (***Figure 3.2B***), giving rise to the development of neural tube (***Figure***

3.2C). During early development of neural tube, two main signalling centres are formed: the isthmic organizer (IsO), which defines the midbrain-hindbrain boundary (MHB), and the floor plate (FP), which controls ventral identities. IsO and FP are the main responsible for the final neural patterning because they release transcription factors and morphogens that drive the expression of specific genes responsible for regional identity, specification and proliferation of progenitors. Such insights from developmental neurobiology provide a conceptual framework for the directed differentiation of iPSCs [288].

3.2.2. Dopaminergic neurons development is subjected to a complex spatiotemporal transcriptional regulation

The ability to recreate human midbrain DA neurons *in vitro* is linked to the growing knowledge of how these cells develop *in vivo*. Understanding the spatiotemporal interdependence of molecular signalling pathways acting during *in vivo* neural development is essential in order to set up, and further refine, current protocols for generation of midbrain DA neurons.

The formation of IsO starts through the coordinated expression and mutual repression of transcription factors OTX2 (orthodenticle homolog 2) in the midbrain and GBX2 (gastrulation brain homeobox 2) in the hindbrain (***Figure 3.3A***), which in turn regulate the cross-repression of two morphogens, WNT1 (wingless-int1) and FGF8 (fibroblast growth factor 8) (***Figure 3.3B***), respectively.

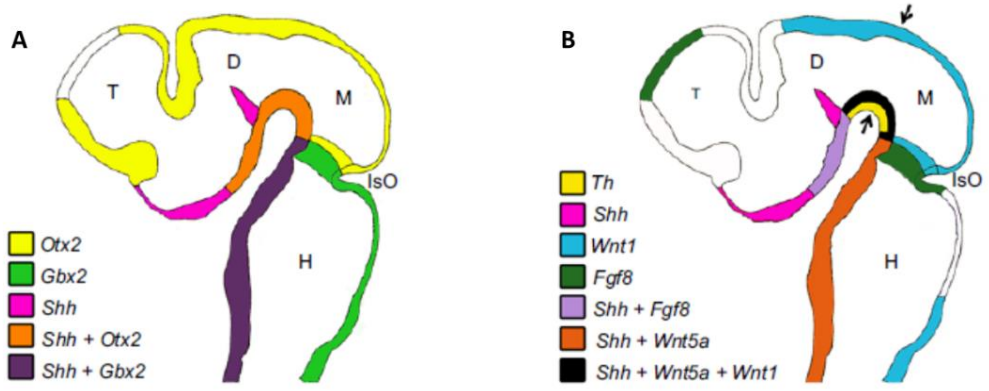

Figure 3.3. Expression patterns of genes important for DA neurons development [288]. *Sagittal view of an E11.5 mouse embryo, showing the expression of transcription factors and morphogens important for VM patterning in relation to Th expression.*

WNT1 expression in the midbrain plays a crucial role in specification and differentiation of midbrain DA neurons progenitors, while FGF8 was demonstrated to be required [289] and sufficient [290] for the induction of IsO. Cells at the MHB are responsive to the concentration gradient generated by secretion of FGF8 in the IsO: high concentrations of FGF8 drive a hindbrain cell fate, while lower concentrations in the anterior tissue ensure that cells adopt a midbrain identity [291-292] (***Figure 3.3A***).

FP development is driven by FOXA2 (forkhead box protein A2), whose expression is initially induced by SHH (sonic hedgehog), secreted by the notochord (***Figure 3.3A***). When the FP itself starts expressing SHH, it becomes the secondary organizer of the neural tube, responsible for ventral/dorsal patterning: higher levels of SHH define a ventral stem cells phenotype (with expression of FOXA1/2), in contrast to lower levels which are essential to specify the dorsal area (***Figure 3.3B***). Consequently, information from both signalling centres, IsO and FP, are integrated in midbrain DA neurons progenitors development.

Further to this initial patterning, FOXA1/2 [294] and OTX2 [295] regulate the expression of LMX1A and LMX1B, two LIM homeobox transcription factors. LMX1A is required for DA neurons specification in the FP, suppressing also the emergence of lateral fates [296-298], and LMX1B is necessary for DA neurons progenitors differentiation [299]. Therefore, the combined and coordinated action of SHH-FOXA2 and OTX2-WNT1-LMX1A networks is essential for the specification of midbrain DA neurons progenitors in FP and, concomitantly, for the suppression of alternative neural fates.

Midbrain dopaminergic neurogenesis takes place in the ventricular zone (VZ) of the FP (***Figure 3.4A and 3.4B)***), where radial glial DA neurons progenitors, expressing MASH1 (mouse achaete-schute homolog 1) and NGN2 (neurogenin 2) (***Figure 4C***), divide to generate postmitotic cells, or neuroblasts.

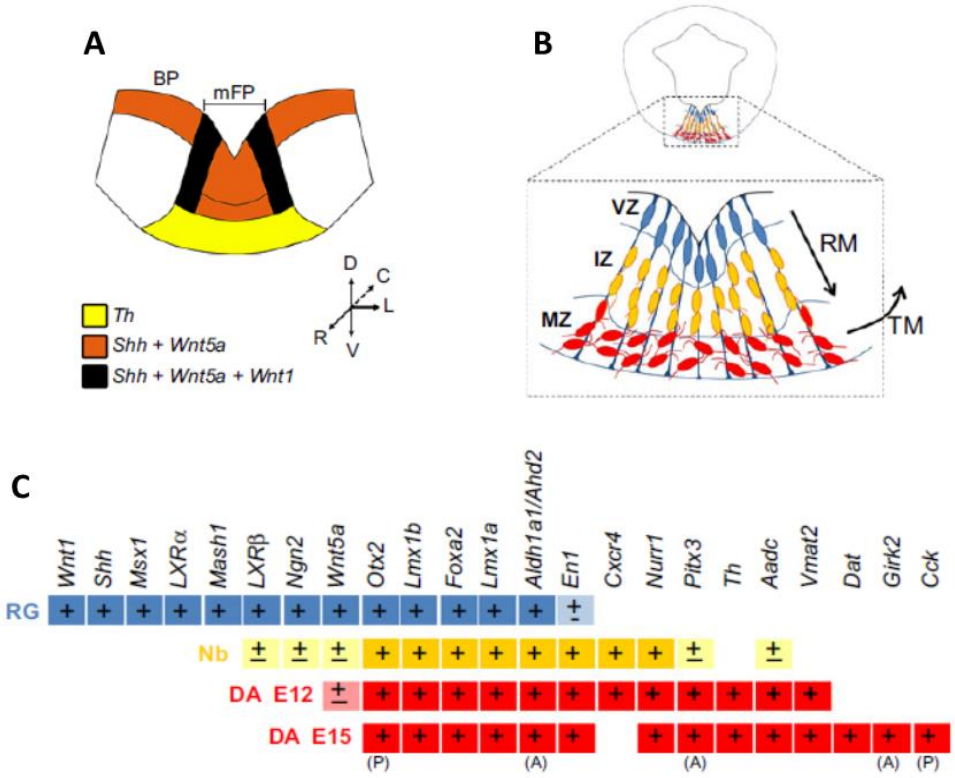

Figure 3.4. Coronal view of midbrain FP (A and B) and gene expression profile of midbrain DA lineage (C) [288].

The expression of MASH1 and NGN2 is directly or indirectly regulated by SHH-FOXA2 and OTX2-WNT1-LMX1A networks: FOXA2 dose-dependently controls dopaminergic neurogenesis [300,301] by directly regulating LMX1A, that increases the expression of NGN2 via MSX1 [296]. Moreover, FOXA2 increases the expression of FERD3l (Fer3-like), which in turn represses HES1 (hairy and enhancer of Split1), a suppressor of pro-neural genes MASH1 and NGN2. In addition, also WNT1 controls the expression of these genes in the midbrain FP, by undirected and directed regulation of LMX1A [302].

Subsequently, neuroblasts migrate toward the intermediate zone (IZ) of midbrain FP (***Figure 3.4B***), where they progressively acquire DA neurons phenotype (***Figure 3.4C***), and express later transcription factors, such as NURR1 (nuclear receptor related 1 protein) and PITX3 (pituitary homeobox 3). Expression of PITX3 is indirectly sustained by WNT1 [303], while LMX1A/B directly regulates NURR1 and PITX3 [302]. Migration, and differentiation, of DA neurons progresses from IZ to mantle zone (MZ) of midbrain FP (***Figure 3.4B***), where

neuroblasts mature and start to express the enzyme tyrosine hydroxylase (TH), involved in DA synthesis (***Figure 3.4C***). This process is regulated by some of the early factors described above, such as OTX2, LMX1A/B and FOXA1/2, together with the homeobox genes EN1/2 (engrailed 1/2), and late transcription factors, such as NURR1 and PITX3, which all remain expressed in postmitotic DA neurons (***Figure 3.4C***). Thus, the morphogen-controlled gene networks in the midbrain FP WNT1-LMX1A and SHH-FOXA2 cooperatively regulate not only DA neurons specification and neurogenesis, but also differentiation and survival. For example, FOXA1/2 are required for the expression of NURR1, EN1 and AADC in DA neuroblasts and neurons, as well as the expression of TH in DA neurons [300,301]. NURR1 regulates the expression of several genes that define a mature DA neuron, including *TH, SLC18A2/VMAT2* (solute carrier family-18 member-2/vesicular monoamine transporter-2), *SLC6A3/DAT* (solute carrier family-6 member-3/dopamine transporter), *AADC, BDNF* (brain-derived neurotrophic factor) [304-311]. PITX3 upregulates *TH, DRD2* (dopamine receptor 2), *VMAT* and *DAT* [312,313]. In addition, NURR1 and PITX3 regulate each other [314,315], and are required for the maintenance of adult DA neurons [316,317], whereas EN1/2 promotes the survival of adult DA neurons [318], together with BDNF [319,320] and glial cell-line derived neurotrophic factor (GDNF) [321-329].

3.2.3. Dopaminergic neurons differentiation protocols have improved during last ten years

These aforementioned developmental studies provide a conceptual framework to rationalise neural induction strategies for differentiation of human iPSCs into midbrain DA neurons. Numerous protocols describing differentiation of DA neurons from iPSCs, indeed, have been developed during the last decade.

Initial approaches were adapted from mouse ESCs protocols, based on generation of embryoid bodies, use of stromal cells or astrocytes as feeders, and activation of a few key signalling pathways (SHH, FGF8, NURR1) to recapitulate some aspects of mouse embryonic development [330-333]. These ESCs differentiation protocols applied to human cells produced TH-positive neurons, but

none of them generated cells co-expressing the two transcription factors required for proper midbrain DA neuron specification, i.e. FOXA2 and LMX1A. In addition, they presented other problems, like incorrectly specified TH-positive cells [334], poor survival rate after transplantation [335] and overgrow with undesirable progeny [336,337]. The first attempt to overcome these limitations and derive human DA neurons from human ESCs was based on forced expression of LMX1A treating cells with SHH and FGF8 [338].

Since then, a more rigorous temporal implementation and recapitulation of morphogenic signals important for midbrain DA neuron development improved differentiation protocols. Use of dual SMAD inhibitors (SB431542 and NOGGIN or LDN-193189) at the beginning of differentiation protocol, to inhibit transforming growth factor beta (TGF-β) and bone morphogenetic protein (BMP) signalling pathways, improved neural induction, suppressing non-neuronal fates, and eliminated the need for feeder layers [339]. Moreover, high levels of SHH, as observed during neural induction, was showed to be crucial for midbrain specification [340], together with WNT signalling [302,303,341,342,343-346], implemented using GSK3β inhibitors (CHIR99021) [339]. Further improvements introduced the formation of embryoid bodies [347], followed by cell adhesion on laminin or differentiation as floating spheres [348].

These researches emphasise the importance of understanding the precise effects and time exposure to different signalling molecules in order to continuously refine current protocols.

3.3. iPSC differentiation into dopaminergic neurons still needs improvements

Differentiation methods quality is assessed through several criteria, including the simplicity of procedure, the efficiency of differentiation and the versatility across animal species. These methods are mainly based on chemically defined media and on ready-to-use products, whose compositions have been kept confidential, preventing the possibility to prepare and optimize them in individual

laboratories. In addition, these commercially available media widely vary in their ability to support neurons in culture [349], requiring cell- and procedure-specific analyses to monitor optimum conditions for differentiation results. Moreover, standard culture conditions constitute a major barrier in lineage differentiation: while they try to recreate the *in vivo* continuous and gradual changing in chemical factors concentrations, they do not provide all necessary environmental factors, in particular cell–cell and cell–extracellular matrix (ECM)-mediated signals, precluding the influence of neighbouring cells simultaneous maturation and interplay.

To date, most emphasis has been put on forcing stem cells to a neural fate and then differentiating them into specific neuronal and glial types [350]. However, a common problem with these protocols is the difficulty in maintaining neural precursors in an immature, undifferentiated state, avoiding the spontaneous and premature differentiation that commonly occurs in these cultures. Whereas in embryo, proliferative, undifferentiated neural precursors can be maintained, it is rare to see this kind of cells in cultures. At the same time, the duration of many differentiation protocols does not reflect human development, showing a differentiated progeny that, not surprisingly, resembles foetal tissue more than adult tissue, and fails to show mature phenotype. In addition, the purity of neuronal cell population remains problematic [351], and it is still linked to protocol and cell line used for neural induction, together with experimental practice [352-354]. Strategies to improve protocols might involve cell sorting, incorporation of novel developmental factors to current differentiation protocols, as well as achieving the right signalling level or balance between different factors and pathways.

3.4. iPSCs technology is particularly useful in neurological monogenic diseases modelling

Human ESCs provide not only an effective tool to improve biological knowledge related to processes of cell differentiation but are as well a stable source of cells for cell-based therapies in the field of regenerative medicine. Their

indefinite propagation ability, as well as the possibility to differentiate into every other cell type, represent a source of cells that could be used to replace those lost due to damage or disease. Despite these biological advantages, the use of ESCs and their derivates involves enormous ethical and legal issues due to destruction of human embryos. The establishment of human iPSCs cells has overcome these ethical problems, as well as increased the applications of PSCs, since unlimited supplies of autologous cells could be used to generate transplants without any risk of immune rejection. Moreover, iPSCs are already used in personalized drug discovery efforts and understanding of patient-specific bases of diseases (***Figure 3.5***).

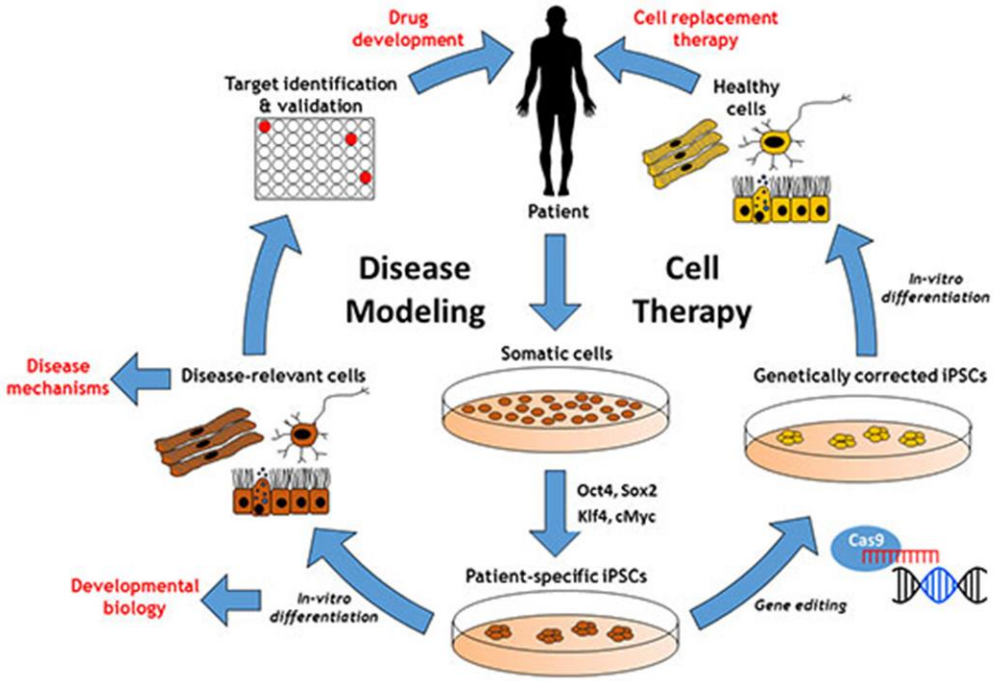

Figure 3.5. Overview of iPSCs technology applications.

iPSCs derived from a patient, indeed, can be used to analyse the development/progression of the disease [238,243], capturing early stages which might be crucial for the development of therapies aimed at preventing, for example, neurodegenerative pathologies. Moreover, polygenic diseases result from the additive inheritance of multiple polymorphisms that culminate in an affected phenotype. Therefore, it is increasingly important to understand how specific risk variants functionally contribute to underlying pathogenesis, making the creation of

iPSCs libraries with defined polymorphisms and phenotypic data a useful resource to validate the effects of each identified gene variant and to facilitate mechanistic understanding of human physiological and pathological conditions.

The maximum expression of iPSCs technology is probably into the field of monogenic diseases, caused by inheritance of a single defective gene. The number of diseases with known causal genetic loci has doubled in the last 10 years, as seen in Online Mendelian Inheritance in Man (OMIM) entry statistics, mainly thanks to improvements in genetic diagnostics and implementation of screening programs. As a result, rare genetic diseases affect 350 million people worldwide and the global prevalence of all single gene diseases at birth is approximately 1/100. Due to iPSCs features, it is not surprising that there has been an extraordinary expectation to utilise these cells to model human "diseases in a dish" [255,256]. Many studies have already shown that iPSCs derived from a variety of monogenic disorders can remarkably recapitulate disease phenotypes *in vitro* when differentiated into disease-relevant cell types. Even if in human monogenic disorders a single gene mutation is predominantly responsible for the phenotype of the disease, allowing the prediction of the consequences of a specific mutation on a particular protein function, not all clinical symptoms severity, therapies responsiveness and/or disease onset of patients correlate with biochemical protein alteration. iPSCs technology, indeed, represents a promising technology to identify patient-specific genetic background and possible non-genetic factors that influence disease-causing mutations, like alterations in other genes, haplotypes or polymorphisms associated with and/or influencing the development of the particular disease, together with epigenetic and/or environmental modulation. Therefore, iPSCs can be an useful tool for discovering and validating newly proposed disease mechanisms, but also for screening environmental factors/small compounds for disease phenotypes modulation, allowing researchers to conduct mechanistic studies and directly use these cells for patient-personalized drug screening.

Chapter 4

Aims of the thesis

The still incomplete knowledge of AADC and HDC biochemical features has driven the experimental work of this thesis, with the aim to:

1. Produce and characterise human HDC wild-type, as well as artificial mutants, using in solution biochemical techniques, to detect structural/functional features and measure the kinetic parameters of the purified enzyme;
2. Analyse a possible phosphorylation modification of AADC, using an in vitro phosphorylation assay, and identify the involved residue(s) as well as its functional effect;
3. Use induced pluripotent stem cells-derived neurons from healthy control and AADC Deficiency patients as an innovative cell model to evaluate AADC features, as well as wider cellular effects of dopamine homeostasis alteration.

Chapter 5

Materials and methods

5.1. Materials

All chemicals and reagents were purchased from international established companies and were of the highest purity available.

5.2. Bioinformatic analyses

5.2.1. Multiple sequence alignments

For human group II PLP-dependent α-decarboxylases alignment, used sequences were taken from NCBI website (https://www.ncbi.nlm.nih.gov/) and are, in order, HDC, AADC, GAD65/67 and CSAD.

For HDCs alignment, used sequences were taken from the NCBI website (https://www.ncbi.nlm.nih.gov/) and are, in order: *Homo sapiens*, *Mus musculus*, *Rattus norvegicus*, *Bos taurus*, *Gallus gallus*, *Danio rerio*, *Drosophila melanogaster*, *Morganella morganii*, *Klebsiella aerogenes* and *Raoultella planticola*. Secondary structures of human HDC (PDB code 4E1O) are reported in the first line of each block: α-helices and β-strands are rendered as squiggles and arrows, respectively.

In both cases amino acid one-letter code is used and ESPript (http://espript.ibcp.fr) was used to render this figure starting from a Clustal Omega alignment (http://www.ebi.ac.uk/Tools/msa/clustalo/).

5.2.2. Phosphorylation sites prediction

Bioinformatic analyses of AADC and HDC possible phosphorylation sites were performed using NetPhos 3.1 free online server (http://www.cbs.dtu.dk/services/NetPhos) using the corresponding amino acid sequences of cloned genes.

5.3. In solution materials and methods

5.3.1. HDC and AADC plasmid constructs

The gene encoding human HDC, carried in mammalian expression vector pCMV6, was purchased from ORIGENE and amplified in order to obtain the gene sequence codifying for amino acid sequence Met2-Cys479, corresponding to the proteolyzed active form of the enzyme, followed by thrombin protease cleavage site. In addition, restriction sites for enzymes NdeI and XhoI were inserted upstream and downstream, respectively, for subcloning the modified HDC gene sequence upstream of a 6xHis tag into the bacterial expression plasmid pET28a. The designed and synthetized (Eurofins Genomics) primers were 5'-AGGGACCATGGGCATGGAGCCTGAGGAGTACAGA-3' for primer forward and 5'-ATTTACTCGAGGGATCCACGCGGAACCAGACAGTGCTGACTCAGGAT-3' for primer reverse (NdeI and XhoI restriction sites are underlined with a solid line in forward and reverse primer, respectively, while thrombin cleavage site is underlined with dotted line). Moreover, as the purchased gene was detected to correspond to a non-pathological minor isoform of HDC, harbouring a methionine residue at position 30, the gene was correcting introducing the more common threonine at this position. The modification was introduced in the construct described above by QuikChange site-directed mutagenesis kit (Agilent Technologies) using the oligonucleotide 5' -

GAGAGACGTGTGACGCCAGACGTGCAGC - 3' and its complement (the mutated codon is underlined) (Eurofins Genomics).

C180S and C418S mutations of HDC were introduced in the construct described above using the same kit and oligonucleotides 5' - GCTGATGAGTCCAGCCTAAATGCCCGA - 3' and its complement and GGGTCCTAATAGTCTCACAGAAAATGTG and its complement for C180S and C418S, respectively (mutated codons are underlined) (Eurofins Genomics).

AADC was produced starting from pDDChis construct that contains the complete open reading frame of thuman AADC including a C-terminal 6xHis tag into a pTrcHis2A expression vector [12].

All corrected nucleotide sequences of constructs were confirmed by DNA sequencing (BMR Genomics).

5.3.2. AADC and HDC expression and purification

E. coli BL21(DE3) chemical competent cells were transformed by heat shock at 42°C with the desired construct and grown in 4.5 L of Luria–Bertani (LB) broth supplemented with kanamycin (35 mg/mL) for HDC or with ampicillin (100 mg/mL) for AADC. Cultures were grown at 37°C to an OD_{600nm} of 0.4-0.6, and expression was induced with isopropyl β-D-1-thiogalactopyranoside (IPTG) 0.4 mM for HDC and 0.1 mM for AADC, for 15 h at 30°C. Cells were harvested and resuspended in 20 mM sodium phosphate buffer pH 7.4, containing 0.5 M NaCl, 20 mM imidazole, 50 μM PLP, 0.5 mM phenylmethylsulfonyl fluoride (PMSF), and protease inhibitor cocktail, with the addition of 10 mM β-mercaptoethanol (β-ME) for HDC. Lysozyme was then added to a concentration of 0.2 mg/mL and incubated for 20 min at room temperature. After a freeze-thaw cycle, leupeptin and pepstatin (1μg/mL) were added and the suspension was centrifuged at 30,000 g for 30 min. The cleared lysate was diluted to about 30 mg/mL and loaded on a HisPrep FF 16/10 column (GE Healthcare) equilibrated with 20 mM sodium phosphate buffer pH 7.4, containing 0.5 M NaCl and 20 mM imidazole, with the addition of 10 mM β-ME for HDC. A linear gradient was then inserted (0-100% in 200 mL) with the same buffer containing 350 mM imidazole for HDC and 500 mM

imidazole for AADC. Run was performed at 2 mL/min flow rate with detection at 280 nm. Soluble HDC or AADC elutes as a single symmetrical peak. After addition of 50 μM PLP, protein solution was concentrated, and imidazole and unbound coenzyme were removed by extensive washing with 0.1 M potassium phosphate buffer pH 7.4, with the addition of 10 mM β-ME for HDC (RedHDC), using Amicon Ultra 10 concentrators (Millipore). Enzymes concentration was determined by using an ε_M of $1.57x10^5$ $M^{-1}cm^{-1}$ for HDC and $1.42x10^5$ $M^{-1}cm^{-1}$ for AADC. PLP content was determined by releasing the coenzyme in 0.1 M NaOH using ε_M of 6600 $M^{-1}cm^{-1}$ at 388 nm.

5.3.3. Denaturing, semi-denaturing and native polyacrylamide gel electrophoresis

Purification procedure was evaluated by 12% denaturing Sodium Dodecyl Sulphate - Polyacrylamide Gel Electrophoresis (SDS-PAGE) loading 3 μL of cell lysate and column flowthrought and 12 μL of column wash and eluted fractions during imidazole gradient, with the addition of 4X denaturing and reducing Sample Buffer (SB). After proteins concentration, their purity was detected by a single band corresponding to a molecular weight of about 55 kDa in denaturing SDS-PAGE loading 8 μg of protein with the addition of 4X denaturing and reducing SB.

Semi-denaturing 8% SDS-PAGE was used to evaluate the presence of intermolecular disulfide bridges of 5 μg OxHDC (HDC in the fully oxidized form, see below) incubated with increasing concentrations of β-ME, 1,4-dithiothreitol (DTT) or reduced glutathione (GSH) for one hour and loaded with the addition of 4X denaturing non-reducing SB.

Native PAGE analysis was performed in the same sample conditions of semi-denaturing SDS-PAGE but samples were loaded with the addition of 2X non-denaturing non-reducing SB.

5.3.4. Size-exclusion liquid chromatography

Size-exclusion liquid chromatography was use to prepared OxHDC starting from the reduced one (RedHDC) purified in presence of 10 mM β-ME (see *above*).

RedHDC was loaded on a Sephacryl H-200 (16/60) (GE Healtcare) column equilibrated with 0.1 M potassium phosphate buffer pH 7.4 and 0.15 M NaCl on an Akta FPLC system (GE Healthcare). Run was performed using the same buffer at 0.5 mL/min flow rate with detection at 280 nm. Soluble OxHDC elutes as a single symmetrical peak and was incubated with 100 μM PLP. Unbound coenzyme was removed by extensive washing with 0.1 M potassium phosphate buffer pH 7.4 and protein solution was concentrated in the same buffer using Amicon Ultra 10 concentrators (Millipore). Enzyme concentration was determined by using an ε_M of $1.57x10^5$ $M^{-1}cm^{-1}$ at 280 nm and PLP content was determined by releasing the coenzyme in 0.1 M NaOH using ε_M of 6600 $M^{-1}cm^{-1}$ at 388 nm.

Size-exclusion liquid chromatography was used to determine the molecular dimensions of HDC holoenzymes (300 μg) in both oxidized and reduced forms. Samples were loaded on a Sephacryl H-200 (16/60) (GE Healtcare) column equilibrated with 0.1 M potassium phosphate buffer pH 7.4, with the addition of 10 mM β-ME for RedHDC, on an Akta FPLC system (GE Healthcare). Run was performed using the same buffer at 0.5 mL/min flow rate with detection at 280 nm. Three chromatography experiments were run per sample, and software Unicorn 5.01 (GE Healthcare) was used to calculate the elution volume of each peak. Apparent molecular dimensions of eluting species were calculated as kDa using the linear equation:

$$x = \frac{y - t}{m}$$

where y represents the peak elution volume, and t and m refer to intercept and slope, respectively, of the linear fitting calibration curve extrapolated from a set of molecular weight standards under the same experimental conditions.

Curves fitting was performed using Origin® 8 Pro (OriginLab).

5.3.5. Coenzyme binding affinity measurements

Apoenzyme was prepared by incubating 10 μM enzyme with 50 mM phenyl hydrazine for HDC or 10 mM hydroxylamine for AADC at 25°C for 2 hours in 0.5

M potassium phosphate buffer pH 6.8, with the addition of 20 mM GSH for RedHDC. The solution was then loaded on a Desalting 26/10 column (GE Healtcare) preequilibrated with the same buffer without phenyl hydrazine or hydroxylamine. Eluted enzyme was then concentrated using Amicon Ultra 10 concentrators (Millipore) and washed with 0.1 M potassium phosphate buffer pH 7.4, with the addition of 20 mM GSH for apo-RedHDC.

Equilibrium apparent dissociation constant for PLP, K_D(PLP), was determined by measuring the quenching of intrinsic fluorescence of 0.03 µM HDC or 0.15 µM AADC apoenzyme in presence of PLP at concentrations ranging from 0.005 to 20 µM in 0.1 M potassium phosphate buffer pH 7.4, with the addition of 1 mM GSH for apo-RedHDC.

Data were fitted to the following equation:

$$\boldsymbol{Y = Y_{max}} \frac{[\boldsymbol{E}]_t + [\boldsymbol{PLP}]_t + \boldsymbol{K_{D(PLP)}} - \sqrt{\left([\boldsymbol{E}]_t + [\boldsymbol{PLP}]_t + \boldsymbol{K_{D(PLP)}}\right)^2 - \mathbf{4}[\boldsymbol{E}]_t[\boldsymbol{PLP}]_t}}{\mathbf{2}[\boldsymbol{E}]_t}$$

where $[E]_t$ and $[PLP]_t$ represents the total concentrations of the enzyme and PLP, respectively, Y refers to the intrinsic quenching changes at a PLP concentration, and Y_{max} refers to the fluorescence changes when all enzyme molecules are complexed with coenzyme.

Curves fitting was performed using Origin® 8 Pro (OriginLab).

5.3.6. Spectroscopic measurements

Absorption measurements were performed using Jasco V-550 spectrophotometer at protein concentration of 1 mg/mL. Circular dichroism measurements were made with Jasco J-710 spectropolarimeter at protein concentration of 1 mg/mL for near-UV and visible spectra or 0.1 mg/mL for far-UV spectra and denaturation curves. Fluorescence spectra were recorded using a FP-750 Jasco spectrofluorimeter with 5 nm excitation and emission bandwidths, following excitation at different wavelengths.

All the spectroscopic measurements were carried out in 0.1 M potassium phosphate buffer pH 7.4 at 25 °C, with the addition of 10 mM β-ME or 10 to 20 mM GSH for RedHDC.

5.3.7. Dynamic light scattering analyses

The dynamic light scattering (DLS) analyses were performed using Zetasizer Nano S (ZEN1600) instrument (Malvern Instruments) with a constant 90° scattering angle and a 633 nm wavelength laser at 25 °C. Sample volume was 0.8 mL at 2 μM enzyme concentration in 0.1 M potassium phosphate buffer (pH 7.4), with the addition of 10 mM β-ME for RedHDC. A total of 100 scans were obtained for each sample, after an equilibration time of 10 min, and all samples were analysed in triplicate.

5.3.8. Enzyme activity assays

The decarboxylase activity of enzymes was measured by a stopped spectrophotometric assay [12,357]. Enzyme was incubated for an appropriate incubation time (a time within which a linear product formation is observed) with different L-histidine, L-DOPA, L-5HTP or L-phenylalanine concentrations and 10 μM PLP in a final volume of 250 μL of 0.1 M potassium phosphate buffer pH 7.4., with the addition of 1 mM GSH for RedHDC. The reaction was then stopped by boiling at 100 °C for 2 minutes. 2,4,6-Trinitrobenzenesulfonic acid (TNB) (1 mL of a 4.3 mM solution) and toluene (1.5 mL) were added and the extraction of trinitrophenyl-derivative was carried out at 42 °C for 45 minutes with continuous shaking. Concentration of trinitrophenyl-derivative in toluene layer was quantified using a calibration curve of absorbance at 340 nm as a function of trinitrophenyl-derivative concentration. Kinetic parameters were determined by incubating enzymes in presence of different substrate concentrations under saturating PLP concentration.

Concentrations of HDC and its variants were 0.3 μM and reaction times were 10 min for both forms and all variants. Inhibitors, when present, were used at 1 or

100 µM. Concentrations of AADC were 0.1 µM for activity measurement using L-DOPA, 0.3 µM using L-5HTP and 0.5 µM using L-phenylalanine, while reaction times were 6 minutes with L-DOPA and 10 minutes with L-5HTP and L-phenylalanine.

Obtained data were fitted to the Michaelis-Menten equation for kinetic parameters determination using Origin® 8 Pro (OriginLab).

5.3.9. Glutathionylation assay and western blotting

OxHDCwt and OxHDCC180S (25 ng/µL) were incubated at room temperature for 30 minutes in 50 mM HEPES pH 7.5 with 125 µM GSH alone. Moreover, combined treatments with 100 µM hydrogen peroxide (H_2O_2) or 100 µM diamide incubation for 30 minutes, followed by incubation of 125 µM GSH, were performed. Reaction was blocked adding denaturing non-reducing 4X SB and samples were run in an 8% SDS-PAGE. After electrophoresis, proteins were transferred to a PVDF membrane (Immobilon P, Millipore, Bedford, MA) and non-specific binding was blocked by incubation in 5% bovine serum albumin (BSA) in Tris-buffered saline with 0.1% Tween 20 (TBS-T) at room temperature for 1 hour. Membranes were then probed with mouse primary monoclonal antibody against GSH-protein complexes (ViroGen), diluted 1:1000 in 5% BSA in TBS-T, overnight at 4 °C and, after 3 washing steps with TBS-T, blots were incubated with anti-mouse horseradish peroxidase-conjugated antibody (Cell Signaling Technology), diluted 1:2000 in 5% Skim Milk Powder, at room temperature for 1 hour. After 3 washing steps with TBS-T, S-glutathionylated proteins were detected with chemiluminescent detection system (Immun-Star™ WesternC™ Kit, Bio-Rad) using ChemiDoc XRS Imaging System (Bio Rad).

5.3.10. Stopped-flow kinetic analyses

Stopped-flow kinetics experiments were performed on an RSM-1000 instrument from OLIS, Inc. (Bogart, GA), equipped with a stopped-flow cell compartment. This instrument has a dead time of 2 ms and can collect UV-visible

scans at speeds up to 1000 Hz. Stopped-flow experiments were performed at 25 °C in 0.1 M potassium phosphate buffer pH 7.4 with the addition of 10 mM GSH for RedHDC. Scans were collected from 250 to 800 nm for various periods of time and scanning rates after mixing an equal amount of 1 mg/mL HDC and 2 mM L-histidine. Stopped-flow data were analyzed using Global Works software provided by OLIS, Inc. Data were fitted to models of either one or two exponentials as necessary to obtain reasonable fits.

5.3.11. Phosphorylation assay

Phosphorylation assay was performed at 37 °C for 30 minutes. Standard phosphorylation mix was composed by 50 mM Tris-HCl pH 7.5, 1 mM $MgCl_2$, 1 mM ATP and 1:10 ration between AADC or HDC and PKA (produced in the host laboratory), if not otherwise specified. Kinetic parameters of AADC and HDC were then calculated as previously described using aliquots from the phosphorylation mix.

5.4. Cellular material and methods

5.4.1. Cell lines

For this study an age-matched control iPSCs, derived from an ICH Dubowitz Biobank (London) fibroblasts sample, and 2 iPSCs lines (Patient 1 and Patient 2) from 2 AADC Deficiency patients, that provided written informed consent for this study (REC reference 13/LO/0171), were used. A clinical and genetic summary of both patients are provided in ***Table 1***.

Patient	Clinical Phenotype	Location of Mutation	Type of Mutation	Predicted protein
1	Hypotonia Neurodevelopmental delay Oculogyric crises Complex movement disorder Autonomic disfunctions	Exon 11	Missense (homozygosis)	R347G
2	Hypotonia Neurodevelopmental delay Oculogyric crises Complex movement disorder Autonomic disfunctions	Exon 2 Exon 3	Non-sense Missense (compound heterozygosis)	Stop codon C100S

Table 1. Clinical and genetic data of the two AADC Deficiency patients.

5.4.2. iPSCs in culture

iPSCs were cultured in sterile 6-wells plates on Corning® Matrigel®, prepared in KnockOut Serum Replacement (KOSR) full medium (1 vial in 25 total mL of KnockOut Dulbecco Modified Eagle Medium, i.e. DMEM, 1:5 KnockOut Serum Replacement, 1% L-Glutamine, 0.1% β-ME, 1% Non-Essential Amino Acids 100X, 1:100 Basic Fibroblast Growth Factor 10 ng/mL), using mTeSR™1 complete media (mTeSR basal media plus 5X mTeSR supplements, 1:100 Penicillin/Streptomycin, i.e. P/S, 10,000 U/mL) with daily media change (2 mL/well), and incubation at 37° C at 5% CO_2.

5.4.3. iPSCs passaging

iPSC cells were passaged at 80-90% confluence with ethylenediaminetetraacetic acid (EDTA). Each well was washed with 2 mL of 1X Dulbecco's phosphate-buffered saline (DPBS) and then incubated with 1 mL EDTA 0.02% solution for 3 to 5 minutes, checking cells detaching at bright field (BF) microscope. After complete aspiration of EDTA solution, cells were flushed and collected in 4 mL of mTeSR™1 complete media with 10 µM Thiazovivin, a Rho-associated protein kinase (ROCK) inhibitor that blocks apoptosis of dissociated cultured human iPSCs, increasing their survival without affecting their

pluripotency. The 4 mL were plated in 2 new wells previously coated for at least 1 hour with Corning® Matrigel® prepared as described *above*.

5.4.4. iPSC spontaneous differentiation cleaning

Spontaneous differentiation was removed taking advantage of different sedimentation velocity between iPSCs and differentiated cells. Each well that showed spontaneous differentiation spots was allowed to become confluent, washed once with 2 mL of 1X DPBS and incubated with 1 mL of 1X TrypLE™ Select for 3 to 5 minutes at 37° C, checking cells detaching at BF microscope. Reaction time was stopped through sample transfer in 8 ml of mTeSR™1 complete media, followed by centrifugation at 300 g for 5 minutes. Medium was aspirate, cells were resuspended in 2 mL of mTeSR™1 complete media with 10 µM Thiazovivin, and plated in a well previously coated with gelatine (from porcine skin, 0.1% in water). Cells were incubated for 20-30 minutes and then transferred to a new well precoated with Corning® Matrigel® without washing of any cell attached to gelatine, i.e. differentiated cells.

5.4.5. iPSCs differentiation into midbrain DA neurons

iPSCs were differentiated following Kirkeby protocol [347] with minor modifications. A visual representation of time plan, with media and factors used, is presented in ***Figure 5.1***.

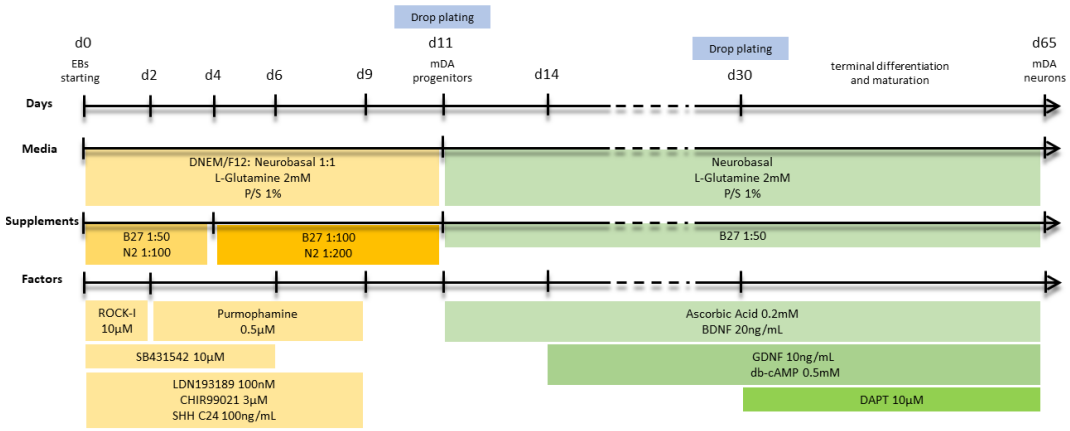

Figure 5.1. Timeline and media composition of differentiation protocol for midbrain DA neurons, adapted from the original protocol [347].

At day 0 confluent iPSCs (4 wells of a 6-wells plate) were washed once with 2 mL/well of 1X DPBS and incubated with 1 mL/well of 1X TrypLE™ Select for 3 to 5 minutes at 37° C, checking cells detaching at BF microscope. When detaching was complete, cells were harvested with 8 mL of mTeSR™1 complete media followed by centrifugation at 300 g for 5 minutes. Cells were resuspended in 11 mL of embryonic bodies (EBs) medium (DMEM/F12:Neurobasal 1:1, L-Glutamine 2 mM, P/S 1%, B27 supplements 1:50, N2 supplements 1:100, LDN193189 100 nM, CHIR99021 3 µM, SHH C24 100 ng/mL, SB431542 10 µM and Thiazovivin 10 µM) and plated on a 11 cm diameter non-adherent bacterial dish.

At day 2 EBs were collected through centrifugation at 300g for 1 minute, resuspended in 11 mL of freshly prepared EBs medium with Purmophamine 0.5µM in place of Thiazovivin, and re-plated on the same non-adherent bacterial dish.

At day 4 EBs were collected through centrifugation at 300g for 1 minute, resuspended in 6 mL of freshly prepared neural differentiation (ND) medium (DMEM/F12:Neurobasal 1:1, L-Glutamine 2 mM, P/S 1%, B27 supplements 1:100, N2 supplements 1:200, LDN193189 100 nM, CHIR99021 3 µM, SHH C24 100 ng/mL, SB431542 10 µM and Purmophamine 0.5 µM) and plated in 6 wells of a Poly-L-ornithine (PO), Fibronectin/Laminine (FN/Lam) pre-coated 12-wells plate. Plate was previously prepared: 0.75 ml/well of PO 15 µg/mL in 1X DPBS was leaved in incubation at 37° C for 2 days, then washed with 1 mL of 1X DPBS

before incubation with 0.75 ml/well of FN/Lam 5 µg/mL each in 1X DPBS for other 2 days at 37 °C; plate is ready to use after final washing with 1 mL of 1x DPBS.

Media was changed every 2 days. From day 6 ND medium without SB431542 was used, while from day 9 also LDN193189, CHIR99021, SHH and Purmophamine were removed.

At day 11 DA neurons progenitors were re-plated via drop plating for final differentiation. Cells were washed once with 1X DPBS and incubated with 500 µL/well of Accumax™ solution at 37°C checking cells detaching at BF microscope. Enzymatic reaction was stopped harvesting cells with 6 mL of KOSR full medium and centrifugation at 300 g for 5 minutes. DA neurons progenitors were resuspended at 30.000 cells/µL concentration in Final Differentiation (FD) medium (Neurobasal, L-Glutamine 2mM, P/S 1%, B27 supplements 1:50, Ascorbic Acid 0.2 mM and BDNF 20 ng/mL) and plated drop-by-drop in the centre of 6 wells of an air-dried PO-FN/Lam pre-coated 12-wells plate (see *above* for plate preparation). Cell drops were incubated at 37°C and 1 mL/well of FD medium was added after cells adhesion to the plate.

Medium change was performed every 2 days, switching to FD medium with the addition of GDNF 10ng/mL and dibutyryl-cyclic adenosine monophosphate (db-cAMP) 0.5 mM from day 14.

At day 30 drop plating were reperformed with the already described procedure using final FD medium including Tert-butyl difluorophenyl acetyamino propanoylamino 2-phenylacetate (DAPT) 10 µM. Cells were plated drop-by-drop in the centre of 5 wells of an air-dried PO-FN/Lam pre-coated 12-wells plate (see *above* for plate preparation) but also in the centre of 4 wells of a Lab-Tek™ slide previously PO-FN/Lam pre-coated and air-dried like plates (0.5 mL PO and FN/Lam solutions/well). Medium change was performed every 2 days till day 65, when Lab-Tek™ slide was fixed for immunocytochemistry analysis (see *below*) and cell on plate were detached through medium flushing and collected in a sterile 1.5 mL tube/well through centrifugation at 300g for 10 minutes. Medium was aspirated and samples were kept at -80 °C for further analyses.

5.4.6. Immunocytochemistry

At day 65 cells grown on Lab-Tek™ slides were washed 3 times with 1X DPBS and then fixed with 300 µL/well of 4% paraformaldehyde (PFA) in 1X DPSB at room temperature for 10 minutes. After 3 washings with 1X DPBS, cells were incubated in Blocking Solution (10% Fetal Calf Serum, i.e. FCS, and 0.3% Triton X-100 in 1X PBS) at room temperature for 30 minutes. Cells were then incubated in 300 µL/well of primary antibody solution, prepared as reported in ***Table 2*** in Blocking Solution, overnight at 4 °C.

Primary Ab	Company	Type	Dilution	Secondary Ab
TH	Aves	chicken	1:400	Anti-chicken 594nm
MAP2	Sigma	mouse	1:400	Anti-mouse 488nm
AADC	Invitrogen	rabbit	1:400	Anti-rabbit 488 nm
GFAP	Millipore	mouse	1:400	Anti-mouse 594 nm
MAO-A	Abcam	rabbit	1:200	Anti-rabbit 488nm
MAO-B	Abcam	rabbit	1:400	Anti-rabbit 488nm

Table 2. Primary and secondary antibodies used for immunocytochemistry analyses of midbrain DA neurons at day 65.

After 3 washings with 1X DPBS, cells were incubated in 300 µL/well of Alexa Fluor® secondary antibody solution (1:400 antibody dilution in Blocking Solution) at room temperature for 45 minutes. After 3 washings with 1X DPBS, nuclei were stained with 4′,6-diamidino-2-phenylindole (DAPI, 1:1000 in 1x PBS) at room temperature in the dark for 5 minutes. Cells were then washed 3 times with 1X DPBS, polystyrene chamber walls were removed from the bottom glass slide, which was then covered with cover slip using ProLong® Gold Antifade Mountant.

Images were acquired using an Inverted Zeiss LSM 710 Confocal Microscope and counting was carried out examining three randomly-selected fields from each differentiation using ImageJ. 1800 nuclei were manually counted blind within each field and cells were marked positive for MAP2 and double positive for MAP2 and TH. For quantification plots three independent differentiations data for each cell line were plotted using GraphPad Prism and statistically analysed using unpaired t test.

5.4.7. Bicinchoninic acid (BCA) assay

Total proteins amount was measured for each sample. Frozen samples pellets from -80 °C were dissolved in 200 µL of radioimmunoprecipitation assay (RIPA) buffer with the addition of 2:10 Proteases Inhibitors Cocktail and 2X Phosphatases Inhibitors Cocktail. Pellet were resuspended, vortexed for 1 minute, incubated on ice for 30 minutes and centrifuged at 13,000 g for 15 minutes. Supernatant was collected and total proteins were quantified using Pierce™ BCA Protein Assay Kit. In a 96-wells plate 10 µL of sample, 10 µL of water and 10 µL of each protein standard were incubated with reagent mix (A+B, B:A 1:50) at 37 °C for 30 minutes. Absorbances were measured with a Tecan plate reader at 555 nm. Protein concentration was determined as µg/mL using the following equation:

$$x = \frac{\mathbf{y} - \mathbf{t}}{\mathbf{m}}$$

where y represents the sample absorbance, and t and m refer to intercept and slope, respectively, of the linear fitting calibration curve extrapolated from standards absorbances.

Curves fitting was performed using Origin® 8 Pro (OriginLab).

5.4.8. Immunoprecipitation

100 µL of 1 mg/mL cells lysate samples, prepared and quantified as already descripted, were pre-incubated with 10 µL of Protein G Agarose beads, already cleaned through 4 steps of washings with 1X DPBS and centrifugations, through incubation on a rotary mixer at 4 °C for 30 minutes. Samples were centrifugated at 14,000 g at 4°C for 1 minute and supernatant was transferred in a new tube. Primary antibodies were added to aliquoted pre-cleaned lysates, i.e. 1:50 rabbit anti-AADC (Cell Signaling Technology) (IP), 1:50 Normal Rabbit IgG (Cell Signaling Technology) for Isotype Control (IC) and no antibody for Negative Control (NC), and samples were incubated on a rotary mixer at 4° C overnight. 10 µL Protein G agarose beads/sample, previously washed as described *above*, were added to each

sample and were incubated on a rotary mixer at 4 °C for 3 hours. Samples were washed 5 times through centrifugation and 500 µL of fresh RIPA buffer with the addition of 2:10 Proteases Inhibitors Cocktail and 2X Phosphatases Inhibitors Cocktail, discarding the supernatant. After last washing step, pellets were resuspended in 20 µL of 4X Laemmli SB, heated at 100 °C for 5 minutes and centrifugated at 14,000 g for 1 minute. 2 µL of pre-cleaned lysate, 10 µL of each washing step and 2 µl of IP, IC and NC were directly loaded on gel for western blotting analysis (see *below*).

5.4.9. Western Blotting

10 µg of total proteins with 2.5 µL of 4X Laemmli SB and 2 µL DTT 0.5 M were heated at 100 °C for 5 minutes and loaded per gel well. Precision Plus Protein™ Dual Color Standards marker and samples ran on a Mini-Protean (4-20%) TGX Stain-Free pre-casted gel in Tris-glycine SDS (TGS) Buffer 1X. Proteins were transferred to a Trans-Blot® Turbo™ Transfer Pack membrane using the Trans-Blot® Turbo™ Transfer System (Bio-Rad). Blot was blocked in 5% Skim Milk Powder in TBS-T at room temperature for 1 hour and then incubated overnight at 4 °C with the diluted monoclonal primary antibody (***Table 3***) in TBS-T.

Primary Ab	Company	Type	Dilution	Secondary Ab
AADC	Cell Signaling Technology	Rabbit	1:1000	Yes
MAO-A	Abcam	Rabbit HRP-conjugated	1:5000	No
MAO-B	Abcam	Rabbit	1:1000	Yes

Table 3. Primary antibodies used for western blotting analyses.

Membrane was washed 3 times with TBS-T and then incubated, when necessary, at room temperature for 1 hour with 1:3000 dilution of anti-rabbit horseradish peroxidase (HRP)-conjugated antibody (Cell Signaling Technology) in 5% Skim Milk Powder in TBS-T. After 3 washing steps with TBS-T, membrane was visualised using SuperSignal™ West Pico Chemiluminescent Substrate using ChemiDoc XRS Imaging System (Bio Rad).

Glyceraldehyde 3-phosphate dehydrogenase (GAPDH) was used as housekeeping gene loading control. After first visualisation, membrane was stripped through incubation with Restore™ Stripping Buffer at room temperature for 20 minutes. Membrane was washed 3 times with TBS-T and then blocked in 5% Skim Milk Powder in TBS-T at room temperature for 1 hour. After incubation with GAPDH HRP-conjugated antibody (Cell Signalling Technology) 1:5000 in TBS-T at room temperature for 1 hour, membrane was washed 3 times for 10 minutes with TBS-T and blot was visualised as above.

Images were acquired using ChemiDoc MP (BioRad) and quantifications were carried out using ImageJ Gel Analysis method. Five values obtained from as many independent images for different control-Patien1-Patient2 sets were plotted using GraphPad Prism and statistically analysed using unpaired t test.

Chapter 6

Cysteine 180 is a redox sensor modulating activity of human HDC

Part of data presented in this chapter led to the drafting of attached Publication 4 (*Chapter 11*).

6.1. Cys180 is the only not conserved cysteine residue among HDCs

Multiple sequence alignment of group II PLP-dependent α-decarboxylases sequences reveals that 6 out of 11 cysteine residues of human HDC are shared among them, while the remaining 4 are typical of HDC. In particular, Cys180 and Cys418, the cysteine residues mutated in serine in the crystallization paper by Komori *et al*. [18], belong to these, as highlighted by black arrows in ***Figure 6.1***.

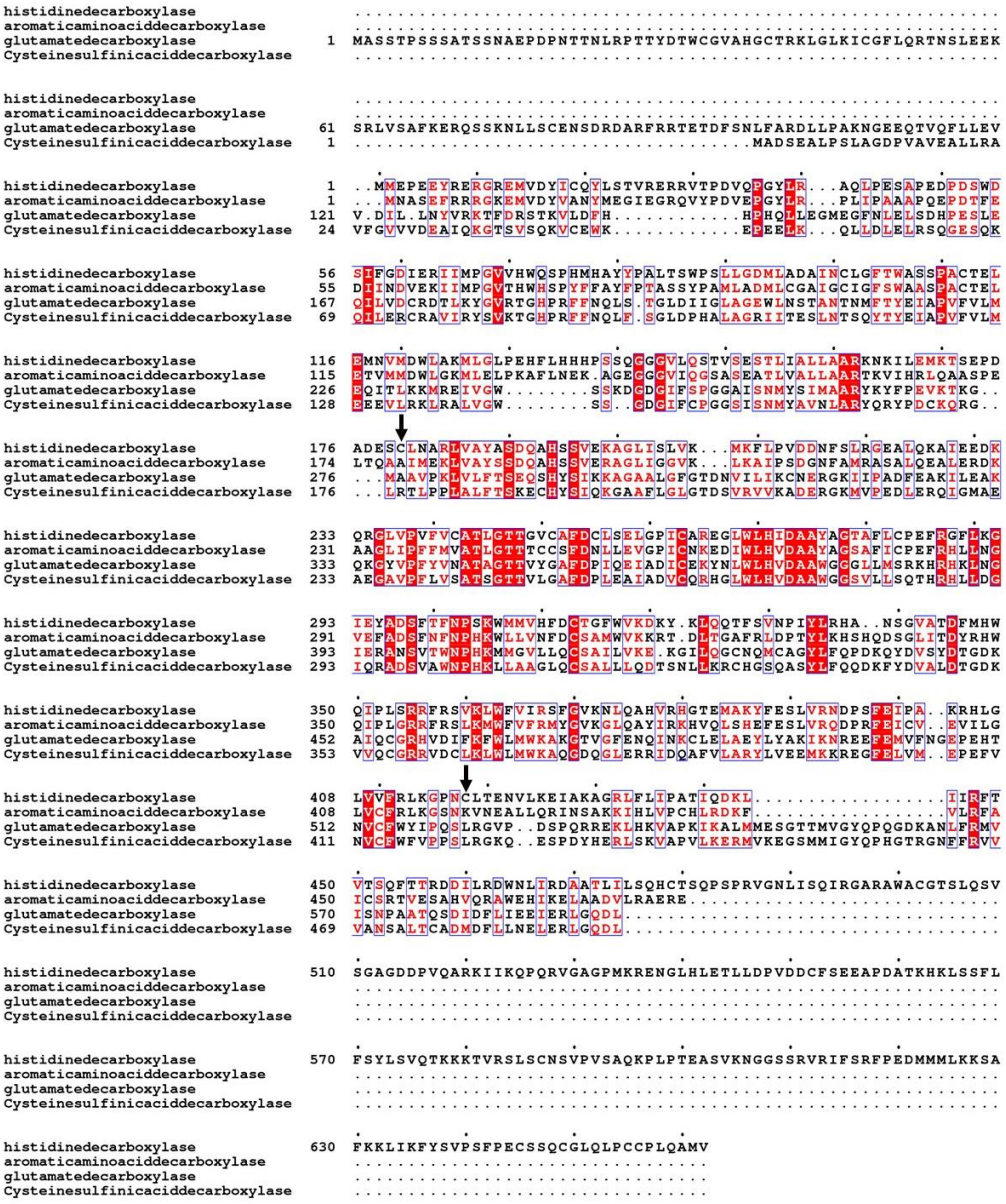

Figure 6.1. Multiple sequence alignment of human group II PLP-dependent α-decarboxylases. *Used sequences were taken from the NCBI website (https://www.ncbi.nlm.nih.gov/) and are, in order: HDC, AADC, GAD and CSAD.*
Positions of C180 and C418 are indicated with two black arrows. Amino acid one-letter code is used. Dashes represent insertions and deletions. Invariant positions are boxed in red and similar residues are written in red. ESPript (http://espript.ibcp.fr) was used to render this figure starting from a Clustal Omega alignment (http://www.ebi.ac.uk/Tools/msa/clustalo/).

In addition, a multiple sequence alignment of HDCs from different origin, mammalians as well as other organisms, shows that Cys180 is the only one that is peculiar to human HDC (***Figure 6.2***).

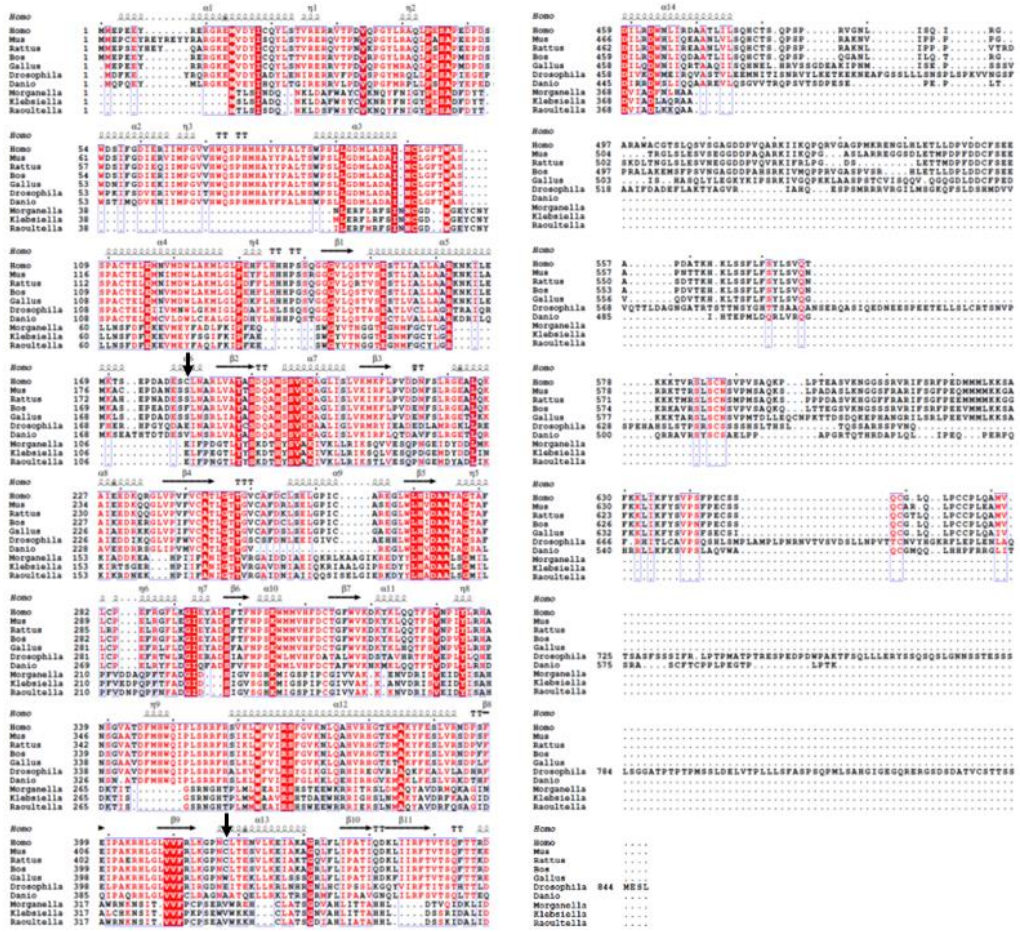

Figure 6.2. Multiple sequence alignment of HDCs.

Used sequences were taken from the NCBI website (https://www.ncbi.nlm.nih.gov/) and are, in order: Homo sapiens, Mus musculus, Rattus norvegicus, Bos taurus, Gallus gallus, Danio rerio, Drosophila melanogaster, Morganella morganii, Klebsiella aerogenes and Raoultella planticola. Positions of C180 and C418 are indicated with two black arrows.

Amino acid one-letter code is used. Dashes represent insertions and deletions. Invariant positions are boxed in red and similar residues are written in red. The secondary structures of human HDC (PDB code 4E1O) are reported in the first line of each block: α-helices and β-strands are rendered as squiggles and arrows, respectively. ESPript (http://espript.ibcp.fr) was used to render this figure starting from a Clustal Omega alignment (http://www.ebi.ac.uk/Tools/msa/clustalo/).

The consideration that Cys180 is not conserved and, together with Cys-418, was supposed to contribute to protein stability [1,2] raises questions about the role it could play.

6.2. Human wild-type HDC exists in an equilibrium between a reduced and an oxidized form

The gene encoding amino acid sequence Met2-Cys479 of human wild-type HDC (HDCwt) has been cloned in pET28a, transformed in BL21 *E. coli*, expressed, and purified through affinity chromatography as reported in *Chapter 5*. It has been immediately noted that the protein formed a yellow precipitate during purification and later washing steps, thus, considering the suggested aggregation tendency possibly due to exposed cysteine residues [358], reducing agent was added during the whole protocol. In these conditions, HDCwt (RedHDCwt) yield is 2.5 mg/L, the enzyme binds two moles of PLP per dimer, and is pure as evidenced by a single band in SDS-PAGE analysis (***Figure 6.3, lane 5***), at around 55 kDa.

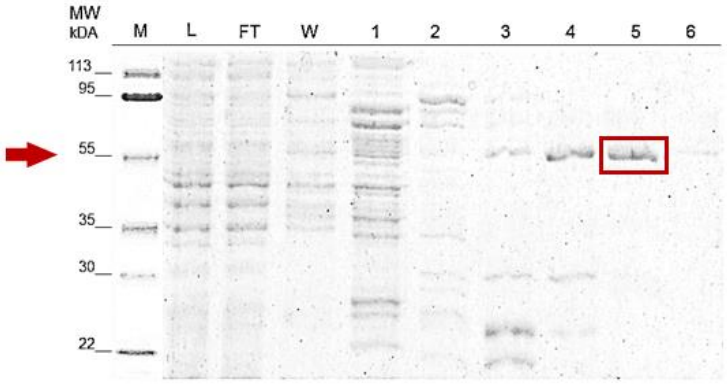

Figure 6.3. 12% SDS-PAGE analysis of RedHDCwt purification.
M, Molecular Weight Marker; L, cellular lysate loaded onto the column; FT, flow through the column during the loading; W, column wash after loading; from 1 to 6, collected fractions during elution gradient. Red squared highlights the band corresponding to eluted HDC, while red arrow indicates its corresponding molecular weight.

Even if reducing agent addition is necessary during purification procedure in order to avoid protein loss as aggregates, it can be removed through gel filtration and extensive washings (see *Chapter 5*), and protein does not aggregate if maintained at low concentrations, i.e. lower than 2.5 mg/mL (OxHDCwt).

It has been immediately noted that, incubating again OxHDCwt with increasing reducing agent concentrations followed by semi-denaturing SDS-PAGE (i.e. denaturing but non-reducing conditions), the enzyme presents one or two bands on gel depending on reductant concentration (***Figure 6.4***). β-ME, DTT, or GSH has

been used as reducing agents, showing in every case the same behaviour, as evident from ***Figure 6.4(a), 6.4(b) and 6.4(c)***, respectively.

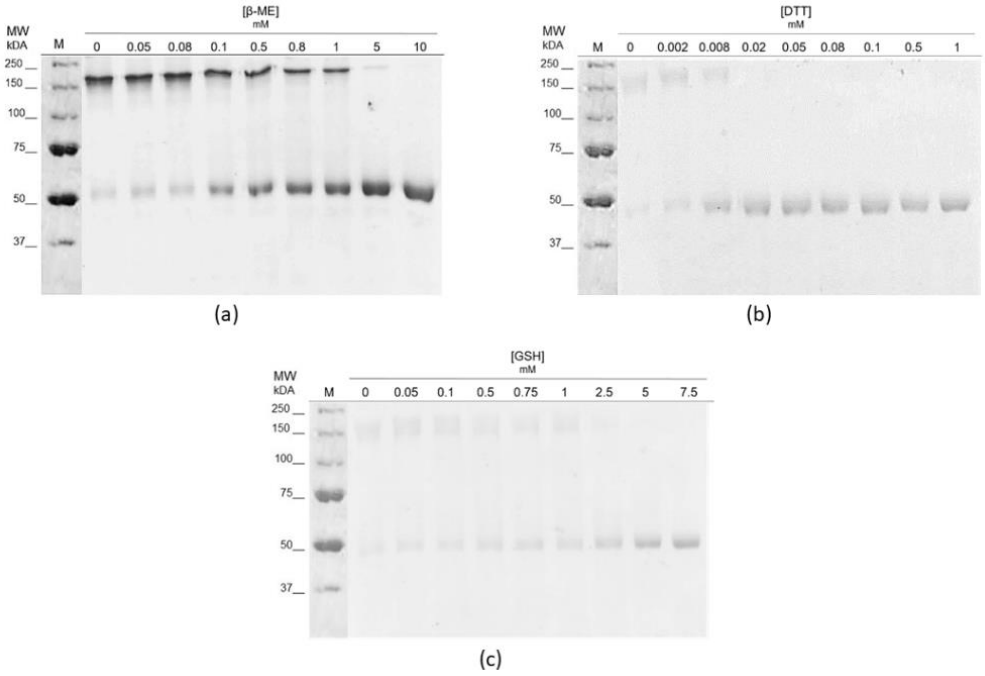

Figure 6.4. 10% semi-denaturing SDS-PAGE analysis of OxHDCwt with increasing reducing agent concentrations.
5 µg OxHDCwt was incubated for 1 hour at room temperature with the corresponding reducing agent concentration in KP 0.1 M pH 7.4. (a) β-ME; (b) DTT; (c) GSH.
Reducing agent concentrations used for each sample are indicated above each panel lane.
M, Molecular Weight Marker.

To obtain a fully reduced species, reductant to protein ratio should be at least 2000-fold molar excess. The molecular weight of the fastest band, at about 55 kDa, corresponds to the completely reduced monomeric form (RedHDCwt), which amount increases in presence of increasing reducing agent concentration. However, at null or low reductant concentrations a low mobility band (OxHDCwt), at around 160 kDa, is detected, suggesting that the higher molecular weight form with slower protein running mobility is characterised by the presence of one or more reversible disulphide bridge(s) between monomers.

Interestingly, the two forms exhibit a nearly same elution volume in size-exclusion chromatography (62.6 ± 0.1 and 61.8 ± 0.2 mL for RedHDCwt and OxHDCwt, respectively) (***Figure 6.5(a)***), as well as the same electrophoretic mobility on a native PAGE gel, even in the same conditions used for semi-

denaturing analysis, i.e. in presence of increasing reducing agent concentrations (***Figure 6.5(b)***).

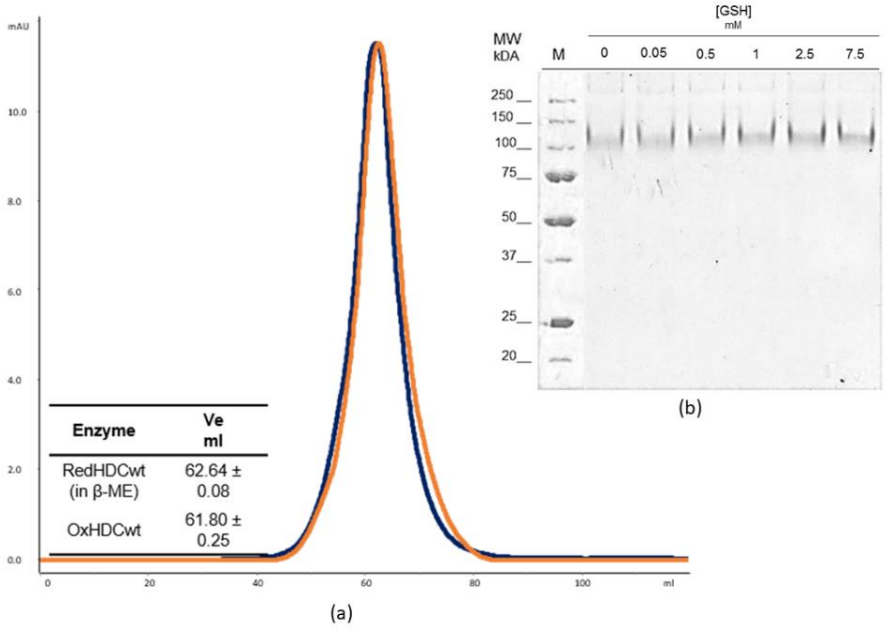

Figure 6.5. Analyses of HDCwt oligomeric state.
(a): Size-exclusion liquid chromatography analysis of HDCwt forms. Chromatograms were recorded at 300 µg enzyme in 0.1 M KP buffer pH 7.4 without or with reducing agent.
Blue: OxHDCwt; Orange: RedHDCwt in 20 mM GSH.
Inset(a): Elution volume of the corresponding form.
(b): 10% native PAGE analysis of OxHDCwt with increasing GSH concentrations. M, Molecular Weight Marker; from 1 to 6, 3 µg OxHDCwt incubate for 1 hour at room temperature with the corresponding GSH concentrations in KP 0.1 M pH 7.4.

Even if at zero and low reducing agent concentration, a slight band with a higher molecular weight can also be detected on native PAGE, suggesting a propensity to aggregation of OxHDCwt, these analyses show that both HDCwt forms are present in solution as dimers, thus suggesting that one or more suggested disulphide bridge(s) are located at dimer interface. However, OxHDCwt elutes about 1 mL earlier than RedHDCwt (***Figure 6.5(a)Inset***).

In addition, dynamic light scattering analysis reveals that RedHDCwt has a smaller hydrodynamic radius than the oxidized form (***Table 6.1***).

Enzyme	size d*nm
RedHDCwt	9.90 ± 0.08
OxHDCwt	11.60 ± 0.04

Table 6.1. Hydrodynamic radius of HDCwt forms.
Data were recorded at 2 μM enzyme in 0.1 M KP buffer pH 7.4 without or with 10 mM β-ME.

It should be pointed out that the theoretical diameter [359] is predicted to be 8 nm calculated on the basis of determined structure, a value closer to that measured for RedHDCwt.

The slightly earlier elution volume and greater hydrodynamic radius of OxHDCwt suggest that the conformational rearrangement RedHDCwt→OxHDCwt results in a less compact dimeric structure.

6.3. HDC reduced and oxidized forms display slight structural changes

Absorbance spectra of RedHDCwt and OxHDCwt show, in addition to the 280 nm band that is attributed to aromatic amino acids, the presence of two bands in visible region with maxima at 339 and 415 nm for RedHDCwt and at 333 and 414 nm for OxHDCwt (***Figure 6.6***), attributable to the enoliminic and ketoenaminic tautomer of the internal aldimine between PLP and Lys304, respectively.

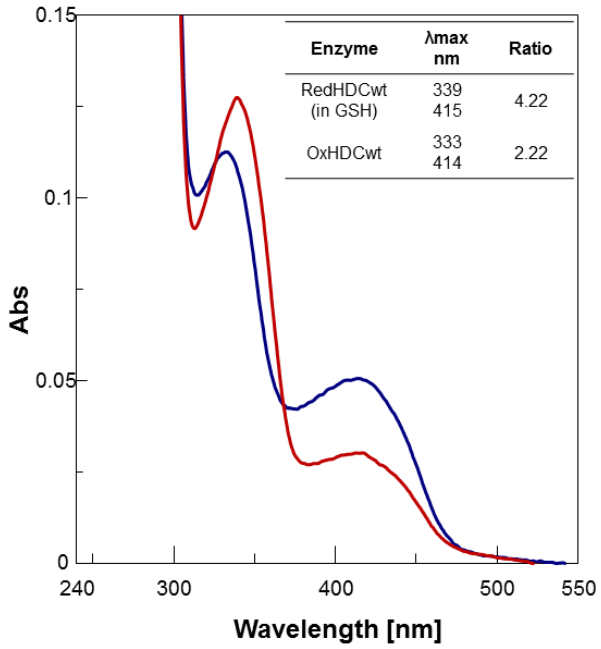

Figure 6.6. Absorbance spectra of HDCwt forms.
Red: RedHDCwt; Blue: OxHDCwt.
Spectra were recorded at 1 mg/mL in 0.1 M potassium phosphate buffer pH 7.4 without or with 20 mM GSH.
Inset: absorbance maxima wavelengths of both forms.

Besides the slight differences in wavelength maxima, the equilibrium between these two tautomeric species is different, with 339 nm/415 nm and 333 nm/414 nm ratios of 4.22 and 2.22, respectively (***Figure 6.6 Inset***), thus indicating an altered PLP microenvironment in the two states of the enzyme.

While far-UV circular dichroism spectra are superimposable (***Figure 6.7 Inset***), indicative of a similar secondary structure content, dichroic signals in visible region reflect a similar coenzyme behaviour already displayed in absorbance, with the addition of a slight difference between RedHDCwt and OxHDCwt in near-UV (***Figure 6.7***).

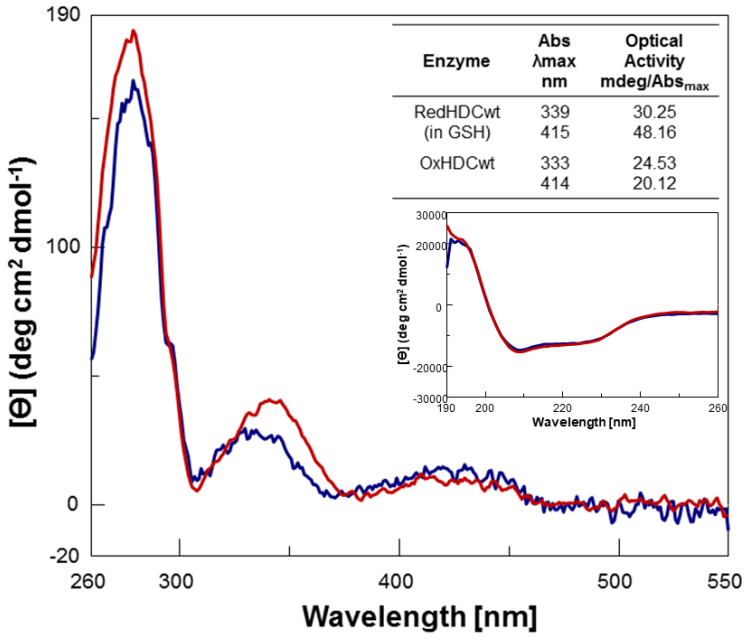

Figure 6.7. Circular dichroism spectra of HDCwt forms.
Red: RedHDCwt; Blue: OxHDCwt.
Near-UV and visible circular dichroism spectra were recorded at 1 mg/mL in 0.1 M potassium phosphate buffer pH 7.4 without or with 20 mM GSH.
Insets: optical activities and far-UV spectra measured at 0.1 mg/mL in 0.1 M potassium phosphate buffer pH 7.4 without or with 20 mM GSH.

Optical activities (millidegrees per absorbance unit at a fixed wavelength at the same protein concentration) for the enolimine and ketoenamine are 30.25 and 48.16 for RedHDCwt and 24.53 and 20.12 for OxHDCwt, respectively, supporting the presence of a different PLP microenvironment.

Fluorescence data essentially provide the same information of that from spectrophotometric and spectropolarimetric experiments. Intrinsic fluorescence spectra recorded upon excitation at 280 nm show an emission band centred at 335 nm for RedHDCwt and 333 nm for OxHDCwt with slightly different relative intensities (***Figure 6.8(a)***). Interestingly, a red-shifted broad shoulder is more pronounced in OxHDCwt, emitting at 494 nm (***Figure 6.8(a) Inset***), suggesting an energy transfer and thus a different positioning of PLP with respect to aromatic amino acids.

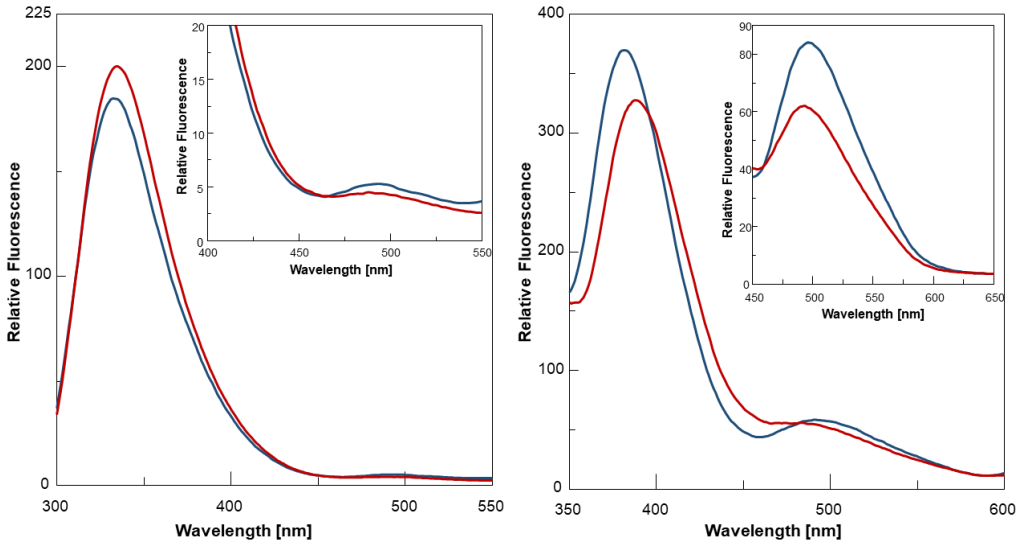

Figure 6.8. Emission fluorescence spectra of HDCwt forms.
Red: RedHDCwt; Blue: OxHDCwt.
(a): Intrinsic fluorescence emission spectra of HDCwt forms after excitation at 280 nm. Spectra were recorded at 0.1 mg/mL in 0.1 M potassium phosphate buffer pH 7.4 without or with 20 mM GSH.
Inset: close-up of the fluorescence emission maximum in the 490 nm region.
(b): Cofactor fluorescence emission spectra HDCwt forms after excitation at 339 and 333 nm of RedHDCwt and OxHDCwt, respectively, at 1 mg/mL in 0.1 M potassium phosphate buffer pH 7.4 without or with 20 mM GSH.
Inset: cofactor fluorescence emission spectra after excitation at 415 and 414 nm for RedHDCwt and OxHDCwt, respectively.

Cofactor emission fluorescence upon excitation of the enolimine tautomer at 339 and 333 nm for RedHDCwt and OxHDCwt, respectively, shows emissions at 386 and 485 nm for RedHDCwt and 381 and 491 nm for OxHDCwt, with the latter one slightly more pronounced (***Figure 6.8(b)***), while when the ketoenamine tautomer of the two species was excited at 415 nm (RedHDCwt) and 414 nm (OxHDCwt), a band centred at 485 nm and at 496 nm was recorded (***Figure 6.8(b) Inset***). Altogether, fluorescence results witness a modest change in cofactor microenvironment and in interconnections among PLP and surrounding residues in the two HDC forms.

6.4. HDC in oxidized form is more stable and active than HDC reduced form

Thermostability (Tm) of the two enzymatic forms has been assessed by monitoring the dichroic signal at 222 nm with an increase in temperature from 25 to 90 °C at a rate of 1.5 °C/min (***Table 6.2***).

Enzyme	**Tm** °C
RedHDCwt	62.78 ± 0.06
OxHDCwt	65.97 ± 0.02

Table 6.2. Melting temperatures of HDCwt forms.
Tm were calculated starting from the denaturation curves of enzyme recorded at 0.1 mg/mL concentration in 0.1 M potassium phosphate buffer pH 7.4 without or with 10 mM β-ME monitoring the dichroic signal at 222 nm with an increase in temperature from 25 to 90 °C at a rate of 1.5 °C/min.

While Tm of RedHDCwt is 62.78 ± 0.06 °C, that of OxHDCwt is 65.97 ± 0.02 °C, thus suggesting that the oxidized form of HDC is slightly more stable than the reduced form, possible due to the presence of intermolecular disulphide bridge(s).

Kinetic parameters of RedHDCwt and OxHDCwt (***Table 6.3***) show that the catalytic efficiency of the oxidized form is 3-fold higher than that of the reduced form, and this is driven by the combination of both 1.6-fold increase in k_{cat} and 2-fold decrease in K_M.

Enzyme	**k_{cat}** s^{-1}	**K_M** mM	**k_{cat}/K_M** s^{-1}/mM^{-1}
RedHDCwt	0.70 ± 0.02	0.064 ± 0.008	10.9 ± 1.4
OxHDCwt	1.10 ± 0.05	0.033 ± 0.006	33.3 ± 6.2

Table 6.3. Kinetic parameter of HDCwt forms.
Kinetic parameters were calculated incubating 0.075 nmol HDCwt with 0.05 to 2 mM L-histidine in 0.1 M potassium phosphate buffer pH 7.4 without or with 1 mM GSH.

The presence of an altered PLP positioning/orientation at HDC active site between the two forms does not seem to affect the apparent equilibrium dissociation constant for the coenzyme: differences in calculated values, indeed, are negligible, i.e. 32.8 ± 0.4 mM for RedHDCwt and 44.0 ± 0.3 nM for OxHDCwt, indicating a quite similar affinity for the cofactor.

These data indicate that, interestingly, oxidized HDCwt is more active and more stable than the reduced form.

6.5. C180S behaves like RedHDCwt, while C418S is sensitive to reductants as OxHDCwt

The three-dimensional structure of active human HDC (residues 2−477) in complex with the inhibitory substrate analogue HME was determined in 2012 using an enzymatic form bearing a double-amino acid substitution (C180S and C418S), to increase protein stability and prevent nonspecific aggregation [18,357]. In functionally active dimeric arrangement, Cys180 belongs to the large domain that is responsible for dimeric interface formation, and faces near to the corresponding Cys180 of the other monomer, while Cys418 is located at the surface of the C-terminal small domain, far from the other subunit (***Figure 6.9***).

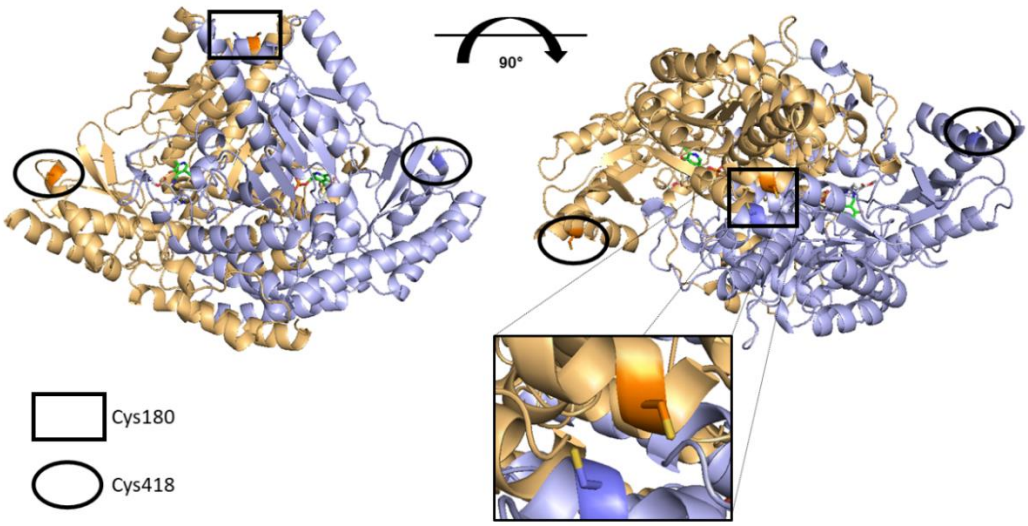

Figure 6.9. Representation of HDCwt.
Human HDC structure [18] was taken from PDB (PDB code 4E1O) and rendered with PyMol. The two monomers are represented in orange and light blue cartoons, while PLP and HME were represented as sticks, coloured in green and grey, respectively.
Ser180 and Ser418 were replace with the original cysteine residues, represented as sticks, and highlighted with squares and circles, respectively.

Thus, HDCC180S and HDCC418S variants have been cloned, expressed and purified following the same wild-type protocol (RedHDCC180S and

RedHDCC418S, respectively). The yields are similar to that of wild-type enzyme, their homogeneity was assessed as a single band on an SDS-PAGE gel, and both of them bind 2 moles of PLP/dimer (data not shown). In addition, oxidized forms where produced for both variants (OxHDCC180S and OxHDCC418S) as already specified for wild-type.

Semi-denaturing SDS-PAGE analyses, performed under the same conditions as the wild-type (see *before*), show that HDCC180S appears as a monomer at any β-ME concentration (***Figure 6.10(a)***), while C418S exists as oxidized/reduced species in equilibrium depending on the concentration of the reducing agent (***Figure 6.10(b)***), a behaviour resembling that of HDCwt.

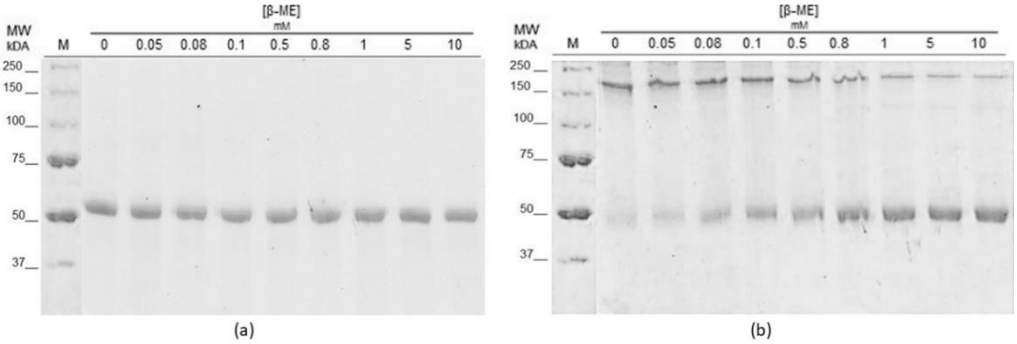

Figure 6.10. 10% semi-denaturing SDS-PAGE analyses of (a) OxHDCC180S and (b) OxHDCC418S with increasing reducing agent concentrations.
5 µg OxHDC variants were incubated for 1 hour at room temperature with the corresponding reducing agent concentration in KP 0.1 M pH 7.4.
The reducing agent concentrations are indicated above each panel.
M, Molecular Weight Marker.

Thus, OxHDCC180S is not sensitive to reducing or oxidizing conditions, revealing that Cys180 is the residue responsible for the reversible disulfide bridge.

In addition, calculated Tm and hydrodynamic radius for both variant show that OxHDCC180S features strongly resembles those of RedHDCwt, while OxHDCC418S behaves as OxHDCwt (***Table 6.4***).

Enzyme	Tm °C	size d*nm
RedHDCwt	62.78 ± 0.06	9.90 ± 0.08
OxHDCwt	65.97 ± 0.02	11.60 ± 0.04
OxHDCC180S	62.68 ± 0.04	10.65 ± 0.05
OxHDCC418S	65.49 ± 0.02	11.56 ± 0.06

Table 6.4. Melting Temperatures and hydrodynamic radius of HDCwt forms and variants.
Tm were calculated starting from the denaturation curves of enzyme recorded at 0.1 mg/mL concentration in 0.1 M potassium phosphate buffer pH 7.4 without or with 10 mM β-ME monitoring the dichroic signal at 222 nm with an increase in temperature from 25 to 90 °C at a rate of 1.5 °C/min.
Hydrodynamic radius was calculated at 2 µM enzyme in 0.1 M KP buffer pH 7.4 without or with 10 mM β-ME.

Analyses of absorbance, dichroic, and fluorescence properties of HDCC180S and HDCC418S variants show that these species exhibit slight structural changes, in particular in PLP microenvironment, and no alterations in cofactor binding, as detected for wild-type (data not shown). Interestingly, functional characterisation shows that catalytic efficiencies of both RedHDCC180S and OxHDCC180S are almost identical to that of RedHDCwt, while those of RedHDCC418S and OxHDCC418S are similar to those of RedHDCwt and OxHDCwt, respectively (***Table 6.5***).

Enzyme	k_{cat} s^{-1}	K_M mM	K_{cat}/K_M s^{-1}/mM^{-1}
RedHDCwt	0.70 ± 0.02	0.064 ± 0.008	10.9 ± 1.4
OxHDCwt	1.10 ± 0.05	0.033 ± 0.006	33.3 ± 6.2
RedHDCC180S	0.60 ± 0.02	0.057 ± 0.008	10.5 ± 1.5
OxHDCC180S	0.72 ± 0.02	0.062 ± 0.007	11.6 ± 1.3
RedHDCC418S	0.74 ± 0.04	0.060 ± 0.010	12.3 ± 2.2
OxHDCC418S	1.05 ± 0.03	0.042 ± 0.007	25.0 ± 4.2

Table 6.5. Kinetic parameter of HDCwt forms and variants.
Kinetic parameters were calculated incubating 0.075 nmol HDC with 0.05 to 2 mM L-histidine in 0.1 M potassium phosphate buffer pH 7.4 without or with 1 mM GSH.

Taken together, these data indicate that HDCC180S is insensitive to reducing agent presence, as its structural and biochemical features resemble those of

RedHDCwt in any condition, individuating Cys180 as the residue responsible for the formation of the intermolecular disulphide bridge in HDCwt.

6.6. Cys180 is not a S-glutathionylation target

Since HDC seems to be regulated by oxidative environment and this latter condition may induce also other reversible modifications, such as S-glutathionylation of cysteine residues, analyses were carried out in order to investigate if HDC can be subjected to this type of post-translational modification in response to intracellular redox state.

In particular, to determine the effect of oxidative stress on possible glutathionylation of this enzyme, OxHDCwt and OxHDCC1800S (500 ng) were incubated with different thiol-specific oxidants for 30 min, GSH was added to the oxidized protein and further analyzed with anti-α-SSG antibody under denaturing but non-reducing conditions (***Figure 6.11***), as described in *Chapter 5*.

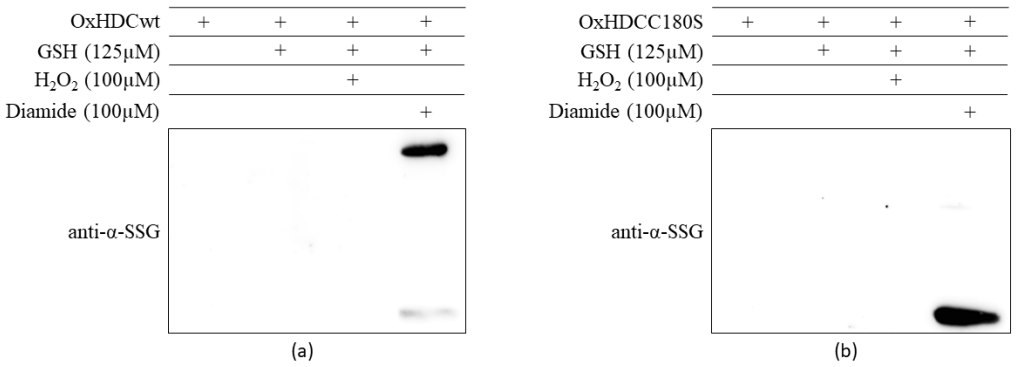

Figure 6.11. Effect of oxidant/GSH treatment on S-glutathionylation of (a) OxHDCwt and (b) OxHDCC180S.
500 ng of enzymes were incubated at room temperature with the indicated concentration of GSH or oxidant agent followed by GSH addition for 30 minutes in 50 mM HEPES pH 7.5. Reaction was blocked adding non-reducing 4X SB and samples were run in an 8% SDS-PAGE followed by western blot analysis with an anti-α-SSG antibody.
The images are representative of 4 independent experiments.

Treatment of both OxHDCwt and OxHDCC180S with GSH and H_2O_2 followed by GSH did not cause significant modification of proteins. However, when both of them underwent a combined treatment with 100 μM diamide and 125 μM GSH, S-glutathionylation of protein was rapidly observed. S-glutathionylation signal was

intense for OxHDCwt dimer (***Figure 6.11(a)***) and for OxHDCC180S monomer (***Figure 6.11(b)***): since the signal is present in the dimeric form, where Cys180 is involved in the disulphide bridge between monomers, it can be assumed that the detected signal is not due to GSH linkage at this residue, as also confirmed by its detection in monomeric C180S mutant. Thus, Cys180 does not undergo to this type of post-translational modification.

6.7. Cys418 seems to be responsible for HDC aggregation tendency

Because it has been claimed that HDC tends to aggregate [358] and for this reason the structure of the enzyme has been determined in C180S/C418S double-mutant form [18], and no aggregation was detected in presence of reducing agent (see *before*), this hypothesis was further investigated by concentrating 500 µL of 10 µM OxHDCwt, OxHDCC180S, and OxHDCC418S to 25 µL in an Amicon ultra devices. Supernatants and pellets (if present) were then ran on an SDS-PAGE gel under denaturing reducing and non-reducing conditions.

Interestingly, a yellow pellet was present in OxHDCwt and OxHDCC180S samples, with no PLP release in solution, while no precipitation occurs with the OxHDCC418S variant. Even if the SDS-PAGE analyses of pellets were impossible, due to the too high molecular weight of aggregates, not able to enter gel pores, from previous considerations follows that Cys418 concurs in structural stability, although the molecular reason for the aggregation of OxHDCwt needs to be further investigated.

6.8. Preliminary data:

Stopped-flow kinetic analyses of HDC

Previous kinetic experiments suggested that there could be differences in catalytic mechanism between the two forms of HDC (RedHDCwt and OxHDCwt). In particular, spectroscopic analyses in presence of the substrate (data not shown) reveal that, for both enzymes, the external aldimine signal at around 427-428 nm can clearly be seen after substrate addition, but its formation proceeds slower for

RedHDCwt respect to the oxidized form, in line with calculated catalytic parameters. On the other hand, at the end of the reaction the initial spectrum of the enzyme, with two absorption maxima in the visible region at around 333 and 418 nm can be detected only for RedHDCwt, while OxHDCwt presents instead a 333 nm and a 387 nm bands. Thus, stopped-flow analyses of the two forms of HDCwt were performed in order to deeper investigate the different kinetic behaviour between them.

RedHDCwt stopped-flow analysis shows a small amplitude fast increase followed by a slow increase at 422 nm, concomitantly with a slow decrease at 332 nm (***Figure 6.12***).

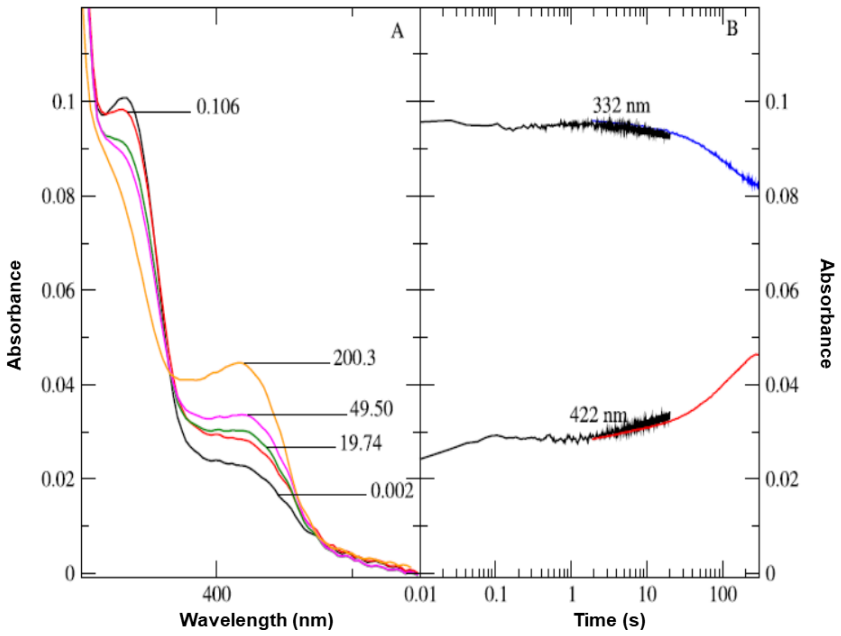

Figure 6.12. Stopped-flow analysis of the first-phase of RedHDCwt decarboxylation reaction.
The experiment was performed at 25 °C in 0.1 M potassium phosphate buffer pH 7.4 with the addition of 10 mM GSH.
Scans were collected from 250 to 800 nm for various periods of time and scanning rates after mixing an equal amount of 1 mg/mL RedHDCwt and 2 mM L-histidine.

The 422 nm peak subsequently decays back to the 332 nm peak when substrate is consumed (***Figure 6.13***).

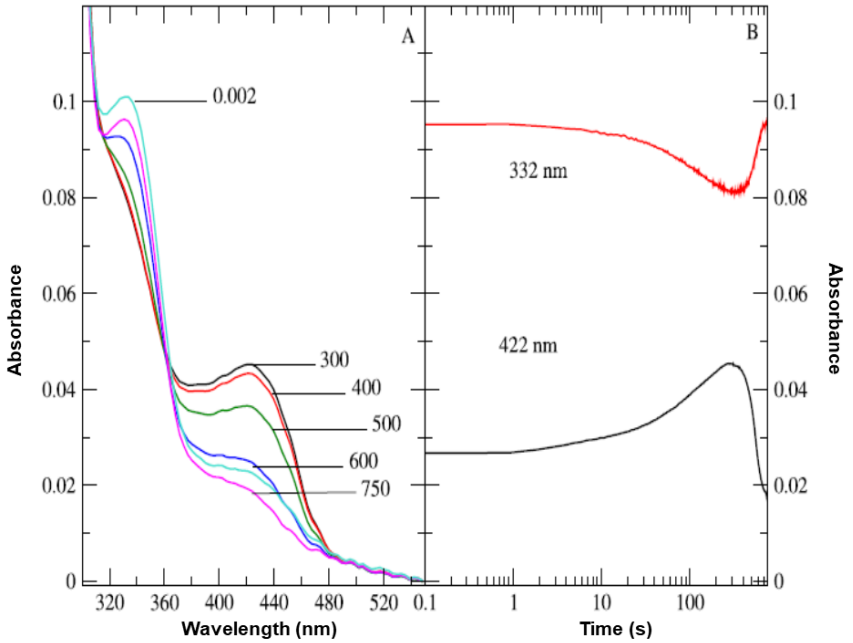

Figure 6.13. Stopped-flow analysis of the second-phase of RedHDCwt decarboxylation reaction.
The experiment was performed at 25 °C in 0.1 M potassium phosphate buffer pH 7.4 with the addition of 10 mM GSH.
Scans were collected from 250 to 800 nm for various periods of time and scanning rates after mixing an equal amount of 1 mg/mL RedHDCwt and 2 mM L-histidine.

The behaviour of OxHDCwt is different from the reduced form. In fact, a fast reaction (90 s^{-1}) of the 415 nm peak to form an external aldimine with a maximum at about 430 nm was detected, with a further decay to a peak at around 380 nm, with a velocity of 1.6 s^{-1} (***Figure 6.14***), probably attributable to the decarboxylation reaction.

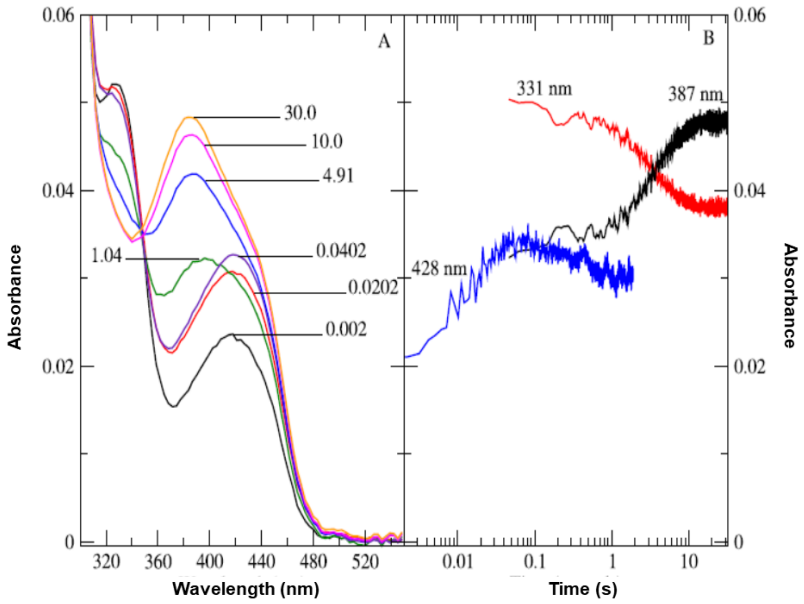

Figure 6.14. Stopped-flow analysis of the fast-phase of OxHDCwt decarboxylation reaction.
The experiment was performed at 25 °C in 0.1 M potassium phosphate buffer pH 7.4. Scans were collected from 250 to 800 nm for various periods of time and scanning rates after mixing an equal amount of 1 mg/mL OxHDCwt and 2 mM L-histidine.

In addition, an independent slower reaction of the 332 nm peak at about 0.1 s^{-1} to form a 388 nm peak, which predominates during the steady state, was also seen, presumably corresponding to the absorbance analysis end state (***Figure 6.15***).

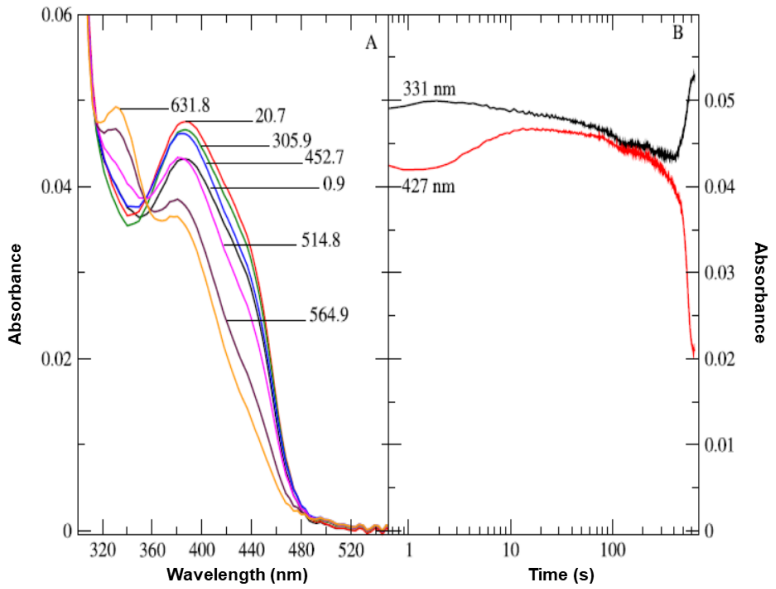

Figure 6.15. Stopped-flow analysis of the slow-phase of OxHDCwt decarboxylation reaction.
The experiment was performed at 25 °C in 0.1 M potassium phosphate buffer pH 7.4. Scans were collected from 250 to 800 nm for various periods of time and scanning rates after mixing an equal amount of 1 mg/mL OxHDCwt and 2 mM L-histidine.

Finally, the 388 nm peak decays at about 0.03 s^{-1} to give the initial enzyme spectrum (data not shown).

These preliminary analyses suggest that the different catalytic efficiency (see *above*) between reduced and oxidized form of HDC can be due to differences/alterations in reaction steps, even if further analyses have to be performed in order to deeply characterize the different catalytical behaviour between the two HDC forms.

6.9. Preliminary data:

First screening of possible HDC inhibitors

Since HDC was found to be overexpressed and/or histamine content was quantified as higher than in physiological conditions in many diseases, a bioinformatic screening, performed as part of a collaboration at University of Roma "La Sapienza", was implemented in order to identify some possible enzyme inhibitors. ***Figure 6.16*** shows the structures of the resulting molecules.

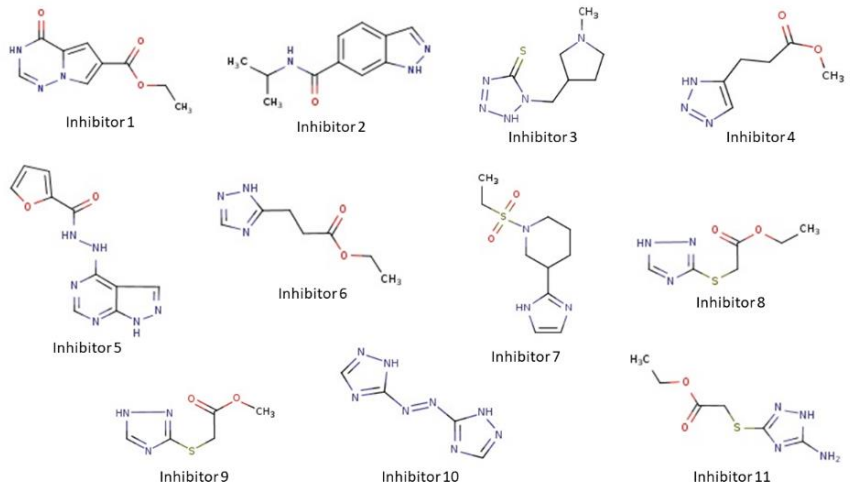

Figure 6.16. Representation of the structures of bioinformatic screening-identified possible inhibitors of HDC.

Structures were taken from the producing company (MolPort) website.
Inhibitor 1: Ethyl 4-oxo-3H,4H- pyrrole[2,1-f][1,2,4]triazin-6-carboxylate; Inhibitor 2: N-(propan-2-yl)-1H-indazol-6-carboxyamide; Inhibitor 3: 1-[(1-methylpirrolydin-3-il)methil]-2,5-dihidro-1H-1,2,3,4-tetrazol-5-thion; Inhibitor 4: methyl 3-(1H-1,2,3-triazol-5-il)propanoate; Inhibitor 5: N'-{1H-pyrazol[3,4-d]pirimidine-4-il}furan-2-carboxrhydrazide; Inhibitor 6: ethyl 3-(1H-1,2,4-triazol-5-il)propanoate; Inhibitor 7: 1-(ethan sulphonyl)-3-(1H-imidazol-2-il)piperidine; Inhibitor 8: ethyl 2-(1H-1,2,4-triazol-3-sulphonil)acetate; Inhibitor 9: methyl 2-(1H-1,2,4-triazol-3-ilsulfanil)acetate; Inhibitor 10: 5-[(E)-2-(1H-1,2,4-triazol-5-yl)diazen-1-il]-1H-1,2,4-triazol; Inhibitor 11: ethyl 2-[(5-amino-1H-1,2,4-triazol-3-il)sulphonyl]acetate.

A preliminary analysis to monitor their effects as non-competitive inhibitors was performed and the majority of identified compounds was tested *in vitro* at 1 and 100 µM in presence of saturating concentrations of L-histidine (***Figure 6.17***). Moreover, compounds where tested using the oxidized form of HDC, demonstrated to be more active (see *above*).

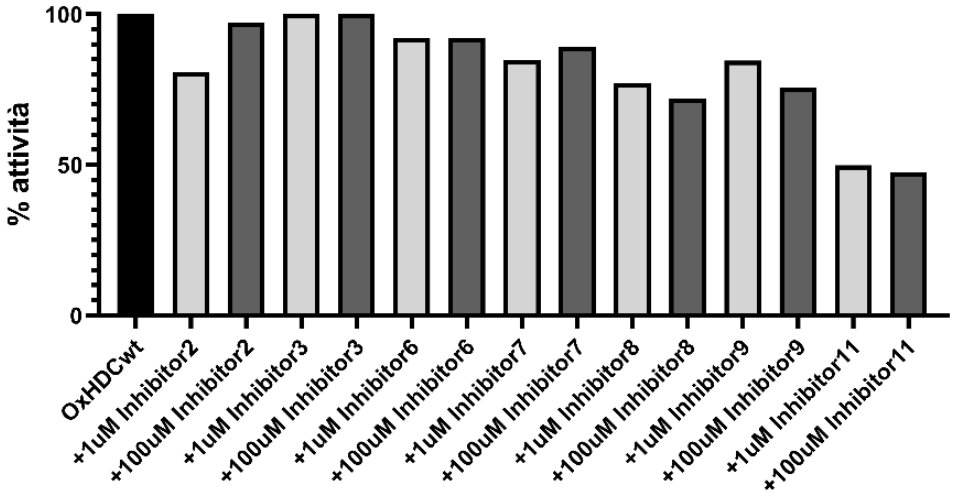

Figure 6.17. Residual activity percentage of OxHDCwt in presence of bioinformatic screening-identified possible inhibitors.
Residual activities were calculated incubating 0.075 nmol HDCwt with 1 or 100 µM inhibitor followed by activity assay under saturating concentration of L-histidine in 0.1 M potassium phosphate buffer pH 7.4.
OxHDCwt: 100% activity.

Although some compounds did not show any effect or only a modest one, such as Inhibitor 3 and 6, some of them seem to considerably decrease the activity of OxHDCwt, in particular Inhibitor 8 and, even more, Inhibitor 11, of about 25 and 50% respectively. Interestingly, these two inhibitors, share some structural features (***Figure 6.18***).

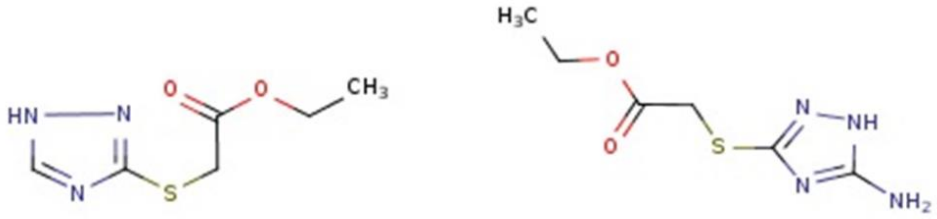

Inhibitor 8 Inhibitor 11

Figure 6.18. Representation of the structures of the two most active compounds among those bioinformatic screening-identified as possible inhibitors of HDC.
Structures were taken from the producing company (MolPort) website.
Inhibitor 8: ethyl 2-(1H-1,2,4-triazol-3-sulphonil)acetate; Inhibitor 11: ethyl 2-[(5-amino-1H-1,2,4-triazol-3-il)sulphonyl]acetate.

Both compounds are centred on a sulphur atom, linked to an imidazole ring and an esterified chain, containing also a double bond with an oxygen atom. The main difference between them regard an additional ammine group linked to the imidazole ring in Inhibitor 11. Thus, can be reasonably assumed that these two compounds skeletons could be used as lead-compounds for a second bioinformatic screening.

6.10. Partial conclusions and future prospects

Besides its role in histamine production, HDC is now attracting attention because of its involvement in cell proliferation and link with many tumours, in particular gastrointestinal ones [198]. Among them, cholangiocarcinoma is difficult to diagnose and has limited treatments: surgical resection, the treatment of choice in such a case, is not always feasible given frequently late diagnosis. Recently, it has been demonstrated that HDC expression is enhanced in cholangiocarcinoma, and the increased level of histamine secretion is related to tumour growth [219]. Treatment with HME, an inhibitor of HDC, slows cancer progression [360]. Few inhibitors of HDC have been further explored, but none of them is used in clinical practice. The discovery of HDC inhibitors has been especially hindered by the poor characterisation of mammalian HDC until now, mainly due to its small quantities in the cell types where it is expressed [361], together with the post-translational proteolytic activation [60] and the extremely low stability of this enzyme [358].

The only determined structure, indeed, is that of the human protein engineered with two cysteine-for-serine substitutions (C180S and C418S), supposed to increase its stability [18]. Notably, these two cysteine residues are not conserved in group II PLP -dependent α-decarboxylases, the homologues of HDC (***Figure 6.1***). In addition, Cys180 is unique of human HDC and is not present in other HDCs from different origin (***Figure 6.2***). Thus, HDCwt was produced and purified in recombinant form (***Figure 6.3***), revealing that this enzyme is present in solution in two species, that are in equilibrium depending on the concentration of reducing agent (***Figure 6.4***), suggesting the presence of a reversible intermolecular disulphide bridge between monomers. These two forms in solution, indeed, are both dimers (***Figure 6.5***), but they show slight structural differences, with an increased hydrodynamic radius (***Table 6.1***) and melting temperature (***Table 6.2***) for the completely oxidised form respect to the reduced one. The conformational rearrangement OxHDCwt→RedHDCwt is also accompanied by a slight perturbation of the active site microenvironment, as detected through spectroscopic (***Figure 6.6***), circular dichroism (***Figure 6.7***) and fluorescence (***Figure 6.8***) analyses, and a consequent alteration of kinetic parameters of the enzyme (***Table***

6.3): the oxidized form, indeed, is not only more stable than the reduced form, but also more active, with a 3-fold increase in catalytic efficiency, driven by the combination of both increase in k_{cat} and decrease in K_M.

As the equilibrium between the two HDCwt forms involves the presence of reversible disulphide bridge(s) between monomers, and the analysis of the solved HDC structure [18] highlights the face-to-face positioning of Cys180 in the two subunits (***Figure 6.9***), it would be supposed that this residue could be responsible for a disulphide bridge. Thus, the two single mutants HDCC180S and HDCC418S were produced and characterised. Interestingly, while HDCC418S features closely resemble those of HDCwt, HDCC180S mutant in insensible to reducing agent presence (***Figure 6.10***) both structurally (***Table 6.4***) and catalytically (***Table 6.5***), as it shows features close to those of RedHDCwt in all conditions. Taken together, these data individuate Cys180 as the residue involved in RedHDC→OxHDC switch, responsible for the increase in both protein stability and catalytic efficiency.

It follows that the solved HDC structure [18] is more likely corresponding to the reduced form of the enzyme. In collaboration with University of Roma "La Sapienza", the possible structure of OxHDCwt was modelled starting from the solved one, and molecular dynamics simulations were undertaken in order to evaluate structural rearrangements during the conformational transitions between the two HDC forms [362]. These analyses show that the covalent bond in Cys-Cys pair at position 180 leads to a conformational rearrangement of HDC resulting in subtle alterations at the active site, in agreement with slight differences evidenced by spectroscopic analyses as well as by kinetic features. Moreover, the increased stability of OxHDCwt could be due to the additional sulphur-sulphur covalent bond, that also causes a rearrangement of the overall protein structure determining an increase in hydrodynamic diameter, in line with DLS measurements.

Since Cys180 was individuated as a redox-sensitive switch in human HDC, a possible S-glutathionylation modification of this residue was investigated. This post-translational modification, indeed, occurs in response to oxidative or nitrosative stress and results in protein-specific functional changes (i.e. activation or deactivation) [370]. However, no S-glutathionylation was detected after HDC treatment with H_2O_2, resembling a mild oxidative condition, and GSH, suggesting

that HDC could not be target of this post-translational modification (***Figure 6.11***). Moreover, forcing thiols oxidation with diamide treatment followed by GSH incubation clearly shows S-glutathionylation of HDCwt, but also of HDCC180 mutant, indicating that cysteine(s) modification does not regard Cys180, maybe because strongly linked in the intermolecular disulphide bridge.

Taken together, these data highlight a redox-related regulation of HDC, which joins the short list of PLP enzymes that present redox-sensitive cysteine residues [363-369]. Interestingly, among PLP enzymes, the cysteine switch appears to be a peculiar and unique feature of human HDC, even if, at present, it is not easy to envisage a physiological role of this redox sensor in HDC. Taking into account that cell environment is highly reducing, it is reasonable to suggest that HDC is mainly reduced under physiological conditions. However, in cancer cells, where redox potential is altered, increased oxidizing conditions could favour the more stable and active OxHDC, leading to an increased histamine production. In this view, RedHDC→OxHDC switch could explain why in some cellular oxidative stress-linked pathologies, such as cholangiocarcinoma, histamine content results higher than in physiological conditions. Moreover, this HDC feature could be interesting also in other tumour types, in which the enzyme could participate in the positive feedback loop that fix tumour microenvironment in a "constant inflammation" state, necessary for its own development.

The different catalytic behaviour of the two HDC forms was investigated through stopped-flow analyses. RedHDC in presence of histidine shows a slow increase at 422 concomitantly with a slow decrease at 332 nm (***Figure 6.12***), followed by a decay back to the 332 nm peak when substrate is consumed (***Figure 6.13***). On the contrary, only a fast reaction of the 415 nm peak to form an external aldimine with a maximum at about 420 nm was detected for OxHDC, followed by a decay to a peak at around 400 nm (***Figure 6.14***), but an independent slower reaction of the 332 nm peak to form a 388 nm peak is present, and predominates during the steady state (***Figure 6.15***). The formation and decay of this 388 nm peak is too slow to be catalytically competent, so it may be a branch intermediate of the main pathway. Alternatively, it would be another form of enzyme, which reacts more slowly and which does not interconvert with the 415 nm-form. Further

analyses will be performed in order to deeply characterize the different catalytical behaviour between the two HDC forms, but it is suggested that different/alternative catalytic steps or reaction intermediates might characterise each HDC form. Study of these differences could be useful in the unravelling how a reaction intermediate stabilisation can influence catalysis or substrate release.

Considering the higher catalytic efficiency of OxHDC respect to RedHDC, the development of specific inhibitors directed toward the first form are highly desirable. Thus, several compounds, individuated as possible HDC inhibitors through a bioinformatic screening in collaboration with University of Roma "La Sapienza" (***Figure 6.16***), were tested on OxHDC under saturating concentrations of substrate, and residual enzyme activity was calculated (***Figure 6.17***). Even if other analyses have to be performed, such as the evaluation of a possible competitive inhibition mechanism at L-histidine concentrations around enzyme K_M, two of them showed to decrease OxHDC activity, with a 25 to 50% maximum extent, respectively. Moreover, compounds identified as effective share common structural features (***Figure 6.18***) that can be the basis of a second bioinformatic screening following a rational-based drug discovering approach, as already applied for AADC with good results [52].

Chapter 7

AADC and HDC can be regulated by phosphorylation

7.1. Bioinformatic analyses of AADC and HDC predict phosphorylation sites

Bioinformatic analyses of AADC and HDC predicted phosphorylation sites identified, for both sequences, multiple possible phosphorylation sites for many different kinases, among which PKA, PKC, cell cycle control protein kinase 2 (cdc2), casein kinase 2 (CK2) and p38 mitogen-activated protein kinases (p38MAPK). Starting from literature data [69-72,78-81], attention was focused on PKA predicted phosphorylation sites. Therefore, the position of corresponding residues in enzyme structures was analysed, in order to eliminate those located in protein core or solvent inaccessible surfaces.

Three possible PKA phosphorylation sites in AADC, but no one in HDC, were identified (***Table 7.1***).

Enzyme	Kinase	NetPhos score	Amino acid
AADC	PKA	0.757	Ser220
		0.722	Ser416
		0.663	Thr320
	PKC	0.764	Thr323
		0.711	Ser193
		0.694	Ser104
		0.583	Ser429
HDC	PKC	0.766	Ser194
		0.715	Thr472
		0.679	Thr105
		0.619	Thr327
		0.505	Ser329

Table 7.1. Bioinformatic analyses results of AADC and HDC predicted phosphorylation sites after position analyses of residues.
Bioinformatic analyses of AADC and HDC possible phosphorylation sites were performed using NetPhos 3.1 free online server (http://www.cbs.dtu.dk/services/NetPhos) using the corresponding amino acid sequences of the cloned genes.
Underlined residues: predicted sites in AADC and HDC corresponding residues.

On the contrary, PKC possible phosphorylation sites are not only more represented, but also involve the same residues in both enzymes, underlined in ***Table 7.1***.

Interestingly, identified putative phosphorylation residues, matching in the two enzymes, are located close to active site (***Figure 7.1***).

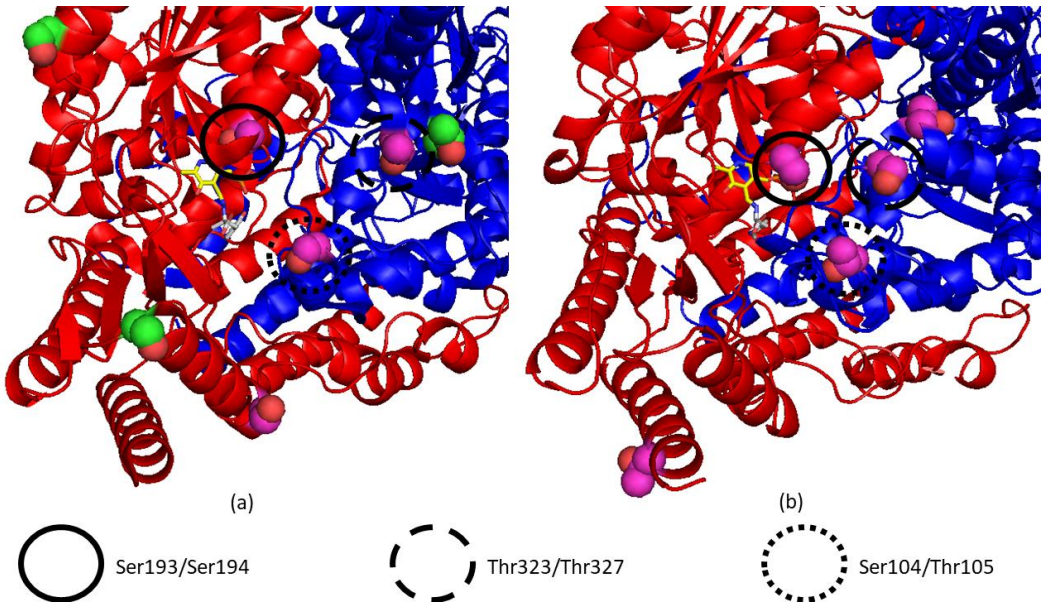

Figure 7.1. Cartoon representation of (a) AADC and (b) HDC predicted phosphorylation sites matching in the two enzymes.
(a): pig kidney AADC (PDB code 1JS6); (b): human HDC (PDB code 4E1O).
The represented structures of are taken from PDB and rendered with PyMol.
For both enzymes the two monomers are colored in red and blue, respectively, while PLP is shown as sticks. The predicted phosphorylation sites are represented as spheres and colored as kinase target (green for PKA, purple for PKC).

7.2. Ser193 is phosphorylated after AADC phosphorylation assay

The *in vitro* phosphorylation assay mixture, prepared as reported in *Chapter 5*, was send to "Proteomics and Mass Spectrometry Core Facility" of Athens University (Georgia, USA). Mass spectrometry data revealed that Ser193 residue, one of those identified by bioinformatic analyses, was found to be phosphorylated in about 15% of AADC protein.

7.3. Activity analyses after AADC phosphorylation reveal ions concentration-dependent AADC activity and increased affinity for L-DOPA

Considering the identified phosphorylation site proximity to enzyme active site, activity assay of AADC in presence of L-DOPA after phosphorylation of enzyme was performed, in order to evaluate if kinetic parameters are affected by this post-translational modification. Phosphorylated AADC was produced setting the most widely used *in vitro* phosphorylation conditions, using a 10:1 ratio between target protein and PKA, respectively, and performing the assay in 50 mM This-HCl buffer pH 7.5 in presence of 10 mM $MgCl_2$ and 1 mM ATP. After incubation of this mixture at 37 °C for 30 minutes, aliquots of phosphorylation mix were used to perform AADC activity assay in standard conditions, as described in *Chapter 5*.

As shown in ***Table 7.2***, even if calculated k_{cat} after AADC phosphorylation (AADC-P) is almost equal to that of the non-treated enzyme, K_M of AADC-P is about 1.5-fold lower respect to AADC, whit a total increase in enzyme catalytic efficiency of about 2 times after phosphorylation.

Enzyme	**k_{cat}** s^{-1}	**K_M** mM	**k_{cat}/K_M** $s^{-1}mM^{-1}$
AADC[152]	7.6 ± 0.1	0.11 ± 0.01	69.09 ± 6.34
AADC-P	7.90 ± 0.16	0.068 ± 0.010	116.18 ± 17.25

Table 7.2. Calculated kinetic parameters of AADC-P for L-DOPA.

These data seem to suggest a possible effect of phosphorylation on the affinity of AADC for L-DOPA.

Even if 10 mM $MgCl_2$ is the commonly used Mg^{2+} concentration in *in vitro* PKA phosphorylation assays, previously unpublished data suggest that high concentration of $MgCl_2$ could slightly inhibit AADC activity, thus possibly counteracting the phosphorylation effect. To test this hypothesis, the same phosphorylation mixture was set without ATP but with 10 mM $MgCl_2$ to assess if there is and how much consistent is the effect of Mg^{2+} on AADC activity subsequent measurement. As shown in ***Table 7.3***, incubation of AADC with 10 mM $MgCl_2$

slightly decrease k_{cat} and increase K_M of the enzyme for L-DOPA respect to the non-treated enzyme, resulting in a reduction of enzyme catalytic efficiency.

Enzyme	k_{cat} s^{-1}	K_M mM	k_{cat}/K_M $s^{-1}mM^{-1}$
AADC[152]	7.6 ± 0.1	0.11 ± 0.01	69.09 ± 6.34
AADC	6.75 ± 0.44	0.14 ± 0.03	48.21 ± 10.80
AADC-P	7.90 ± 0.16	0.068 ± 0.010	116.18 ± 17.25

Table 7.3. Calculated kinetic parameters of AADC-P for L-DOPA.

Therefore, AADC phosphorylation was performed decreasing the concentration of $MgCl_2$ from 10 to 1 mM in incubation mix. Surprisingly, subsequent measurement of kinetic parameters reveals that AADC-P k_{cat} slightly increases respect to the non-phosphorylated enzyme, while the K_M decreases by a factor of about 3.5 (***Table 7.4***), and catalytic efficiency increase of about 4 times.

Enzyme	k_{cat} s^{-1}	K_M mM	k_{cat}/K_M $s^{-1}mM^{-1}$
AADC[152]	7.6 ± 0.1	0.11 ± 0.01	69.09 ± 6.34
AADC	6.75 ± 0.44	0.14 ± 0.03	48.21 ± 10.80
AADC-P	7.90 ± 0.16	0.068 ± 0.010	116.18 ± 17.25
	8.63 ± 0.33	0.032 ± 0.009	269.69 ± 76.55

Table 7.4. Calculated kinetic parameters of AADC-P for L-DOPA.

These analyses suggest that incubation of AADC with high concentrations of Mg^{2+} can slightly inhibit enzymatic activity, so only 1 mM $MgCl_2$ was used during phosphorylating incubation of enzyme in following analyses. In addition, AADC-P kinetic parameters detection following low $MgCl_2$ concentration condition for phosphorylation assay shows not only a maximum increase in k_{cat}, which nevertheless seems to be not so affected, but it especially shows a drastic reduction of K_M respect to the non-phosphorylated enzyme, with a global 4-fold increase in catalytic efficiency (k_{cat}/K_M), strongly suggesting that phosphorylation might increase the affinity of AADC for this substrate.

7.4. Activity analyses after AADC phosphorylation with L-5HTP and L-phenylalanine reveal a common increased substrate affinity

In order to investigate if phosphorylation can affect the affinity for only L-DOPA or if it can lead to a more general structural protein modification that increases the affinity of all AADC substrates, kinetic parameters of AADC after phosphorylation were measured in presence of 5-HTP. As shown in ***Table 7.5***, even if AADC-P k_{cat} for this substrate is almost the same respect to the non-phosphorylated enzyme, a concomitantly decrease of K_M value was measured, which is around the assay detection limit.

Enzyme	**k_{cat}** s^{-1}	**K_M** mM	**k_{cat}/K_M** $s^{-1}mM^{-1}$
AADC	1.01 ± 0.02	0.038 ± 0.007	26.58 ± 4.93
AADC-P	1.10 ± 0.07	0.013 ± 0.004	84.61 ± 26.58

Table 7.5. Calculated kinetic parameters of AADC-P for L-5HTP.

Therefore, in presence of 5-HTP, like for L-DOPA, AADC after phosphorylation treatment shows a slight increase in k_{cat} and a more pronounced decrease in K_M, with a total 3-fold increase in catalytic efficiency. This increase seems to be lower than that for L-DOPA, even if it has to be taken into consideration that the really low K_M measured value is close to the assay detection limit.

AADC can decarboxylate also other amino acids, such as L-phenylalanine, L-tyrosine and L-tryptophan to their corresponding amines. Accordingly, AADC activity after phosphorylation treatment was tested in presence of L-phenylalanine using the same procedure. For this substrate, as previously detected for L-DOPA and L-5HTP, a slight increase in k_{cat} (***Table 7.6***) and an about 1.5-fold decrease in K_M respect to the non-phosphorylated enzyme can be observed, with a 2-fold total increase in efficiency.

Enzyme	k_{cat} s^{-1}	K_M mM	k_{cat}/K_M $s^{-1}mM^{-1}$
AADC	0.128 ± 0.013	14.35 ± 3.73	0.009 ± 0.002
AADC-P	0.173 ± 0.020	9.23 ± 1.90	0.019 ± 0.004

Table 7.6. Calculated kinetic parameters of AADC-P for L-phenylalanine.

7.5. Preliminary data:

Regulation of HDC by phosphorylation seems to be form-dependent

Incubation of HDC in phosphorylating mix followed by mass spectrometry analysis revealed that, after phosphorylation treatment, Ser194 residue, corresponding to Ser193 in AADC, is phosphorylated in about 5% of total protein, even less than AADC phosphorylation extent (around 15%).

Previous analyses (see *Chapter 6*) demonstrate that HDC efficiency responds to reducing/non-reducing environment due to the presence of a disulphide bridge between the two protein monomers involving Cys180 residues. This disulphide bridge is reversible and its formation forces a structural rearrangement that increases both the stability of the enzyme and the catalytic efficiency. Therefore, kinetic parameters of HDC after phosphorylation treatment (HDC-P), performed in the same conditions of AADC, were measured not only to compare them with those of AADC-P and possibly detect a different effect of this post-translational modification between the two enzymes, but also to detect, if present, a different effect between the two forms of HDC (OxHDC and RedHDC). For this reason, incubation of HDC in phosphorylating mix and subsequent measurement of its kinetic parameters using the standard activity assay were performed for both enzymatic forms. ***Table 7.7*** summarize the corresponding data.

Enzyme	k_{cat} s^{-1}	K_M mM	k_{cat}/K_M $s^{-1}mM^{-1}$
OxHDC	1.10 ± 0.05	0.033 ± 0.006	33.3 ± 6.2
OxHDC-P	1.03 ±0.10	0.094 ± 0.033	10.96 ± 3.99
RedHDC	0.70 ± 0.02	0.064 ± 0.008	10.9 ± 1.4
RedHDC-P	1.03 ± 0.02	0.032 ± 0.004	32.19 ± 4.07

Table 7.7. ***Calculated kinetic parameters of HDC-P for L-histidine.***

While OxHDC after phosphorylation (OxHDC-P) shows a slight decrease in k_{cat} and an increase in K_M of about 3-fold respect to OxHDC, RedHDC-P presents an increased k_{cat} and a half K_M respect to the corresponding non-phosphorylated form of the enzyme. While OxHDC shows a 3-fold increase in catalytic efficiency respect to the reduced form, after phosphorylation treatment the ratio is reverse, with an efficiency 3 times lower for OxHDC-P respect to RedHDC-P.

7.6. Partial conclusions and future prospects

Despite their great number and wide distribution in nature, only few PLP dependent enzymes have been reported to undergo phosphorylation [371] and, among these, phosphorylation can activate, inhibit or seems to have no structural or functional effect, sometimes with conflicting results. Few papers have been published reporting that both AADC and HDC purified from tissues can be phosphorylated, in particular by PKA [69-72,78-81]. Since phosphorylation is a common and widespread strategy of enzyme regulation, it could be interesting to understand the role, if present, of this post-translational modification in human AADC and HDC: these two homologous enzymes, indeed, produce important neurotransmitters that behave also as signalling mediators outside CNS, and their post-translational modification might be a fast response to environmental stimuli.

Bioinformatic analyses predicted many possible phosphorylation sites for both proteins: among those solvent-accessible, identified residues are not only conserved between the two enzymes (***Table 7.1***), but also closed to active site (***Figure 7.1***). An *in vitro* PKA phosphorylation assay was set for AADC and mass spectrometry analysis was performed, allowing not only the quantification of phosphorylation extent, but also the individuation of involved residue(s). Interestingly, results indicate that PKA phosphorylation occurs on Ser193, the closest residue to the active site among those previously individuated through bioinformatic analysis (***Figure 7.1***).

Considering that phosphorylation at this aminoacidic position could influence active site microenvironment and/or catalytic activity of the enzyme, incubation of AADC in phosphorylating conditions (AADC-P) was followed by measurements of its kinetic parameters using the traditional activity assay (***Table 7.2***). Interestingly, meanwhile it was also found that AADC seems to be slightly inhibited in presence of high $MgCl_2$ concentrations (***Table 7.3***): it might be interesting to investigate, through some focused experiment, the concentration-dependency of AADC inhibition, together with the evaluation of a similar effect of, for example, $CaCl_2$. No data have been so far published, indeed, about a possible ions-dependent inhibition of AADC.

AADC kinetic parameters measurement after phosphorylation revealed that enzyme shows not only an increase of catalytic efficiency toward all tested substrates, i.e. L-DOPA, 5-HTP and L-phenylalanine (***Tables 7.4, 7.5 and 7.6***, respectively), but also the same mechanism of activation for all of them: the increase in catalytic efficiency, indeed, is mainly due to a decrease in K_M for all substrates, strongly suggesting that phosphorylation could increase the affinity of AADC for its substrates.

Even if many other experiments should be performed in order to confirm these data, for example artificial mutants changing serine in aspartate and/or glutamate as positive controls for the negative charge presence at that particular location, and molecular dynamics simulations in order to evaluate differences in possible location/orientation of substrates in phosphorylated enzyme active site respect to the non-phosphorylated one, these results strongly support an effect of Ser193 phosphorylation on AADC. In addition, this measured activity alteration is due to a low portion of AADC-P in tested mix, since mass spectrometry detected only a 15% of phosphorylated protein in these assay conditions, i.e. the common ones used for *in vitro* PKA phosphorylation assay. One would expect that the measured phosphorylation effect might be greater in presence of a higher amount of AADC-P in solution: therefore, it could be interesting to evaluate phosphorylation efficiency using PKC, since this was the kinase predicted to preferentially phosphorylate Ser193 (***Table 7.1***), without ruling out the possibility that PKC could phosphorylate other residue(s).

Preliminary results on HDC, phosphorylated using the same conditions as AADC, and further tested for kinetic parameters, show an interesting behaviour. HDC after phosphorylation, indeed, seems to switch its efficiency between the two forms of the enzyme: while the non-phosphorylated HDC is more efficient in L-histidine decarboxylation when present in solution in oxidized form, the phosphorylated one is more efficient in reduced form (***Table 7.7***). Phosphorylation of HDC results in the same behaviour of phosphorylated AADC when HDC is in the reduced form (i.e. increase of catalytic efficiency), or in an opposite behaviour (i.e. decrease of catalytic efficiency) when HDC is in the oxidized form, peculiar of this enzyme. Since mass spectrometry analysis revealed that the phosphorylated

residue is Ser194, corresponding to Ser193 individuated for AADC, and thus close to enzyme active site (***Figure 7.1***), the opposite effect of phosphorylation at this residue in the two HDC enzymatic forms could be at least partially linked to conformational differences at the active site between them, as predicted through molecular modelling [362]. Interestingly, the amount of HDC-P was even lower than AADC-P, with only a 5% phosphorylated protein in these assay conditions, suggesting again the option of testing PKC possible phosphorylation, as the latter one was the kinase predicted to phosphorylate HDC by bioinformatic screening.

Chapter 8

iPSCs differentiation into midbrain dopaminergic neurons allows the evaluation of dopamine synthetizing and degradative enzymes expression and equilibria

8.1. Establishing a stable and reproducible model is essential for pathological mechanisms investigation

All iPSCs lines used in this study were previously reprogrammed in hosting laboratory using a non-integrating Sendai RNA virus from skin fibroblasts [372] of two patients carrying mutations in AADC gene and one age-matched control subject. In addition, each iPSCs line was tested to be phenotypically homogeneous and karyotypically normal. Pluripotency was assessed by immunofluorescence for OCT3/4 and TRA-1-60, TRA-1-80, and NANOG and quantitative reverse transcriptase-polymerase chain reaction (qRT-PCR) for *OCT4*, c*MYC*, *SOX2*, and *KLF4*, all genes involved in maintenance of pluripotent state. Moreover, pluripotency was confirmed by in vitro spontaneous differentiation into three germ layer derivatives, i.e. mesoderm, endoderm, ectoderm, through SMA, TUJ1, SOX17 immunocytochemical expression. In addition, the ability of properly developing into DA neurons was already confirmed for each cell line, together with the strength and reproducibility of cellular model, through a set of analyses already performed in the research group. In particular, cell lines were analysed at day 11 for midbrain neural progenitor population quality assessment: immunocytochemistry quantification of positive cells for developing midbrain unique co-expression of FOXA2 and LMX1A, and qRT-PCR analysis of increased expression level of different transcription factors involved in midbrain DA neurons differentiation (*FOXA2*, *LMX1A*, *LMX1B*, EN1 and EN2) together with decreased expression of pluripotency-related transcription factors (*OCT4*, *NANOG*) compared

to respective iPSCs lines. Cell lines were also previously analysed at day 65, i.e. at complete DA neurons maturation, for the immunocytochemical detection of mature neurons markers (MAP2 and TH) as well as for their qRT-PCR expression (MAP2, TH, NURR1, PITX3, SNCA). Finally, further analyses were performed in order to evaluate the disease-specific clinical-like phenotype of Patients lines, such as quantification of AADC activity and evaluation of its substrates accumulation and/or their metabolites decrease, using the same experiment setup used for disease diagnosis.

8.2. iPSCs require standardised conditions for culture reproducibility

Use of feeder-free conditions, i.e. Corning® Matrigel® as matrix, eliminates the inherent biological variability of feeder cells, in line with recent efforts focused on improving the reproducibility of iPSCs culture by simplifying and removing undefined components from all aspects of culture system (media, matrices and passaging reagents). Human iPSCs grow as compact, multicellular colonies characterized by distinct borders (***Figure 1(a)***). Healthy colonies merge together seamlessly, and can be multi-layered in the centre, resulting in dense clusters of cells. Individual cells are tightly packed, exhibit a high nuclear-to-cytoplasm ratio and have prominent nucleoli (***Figure 1(b)***).

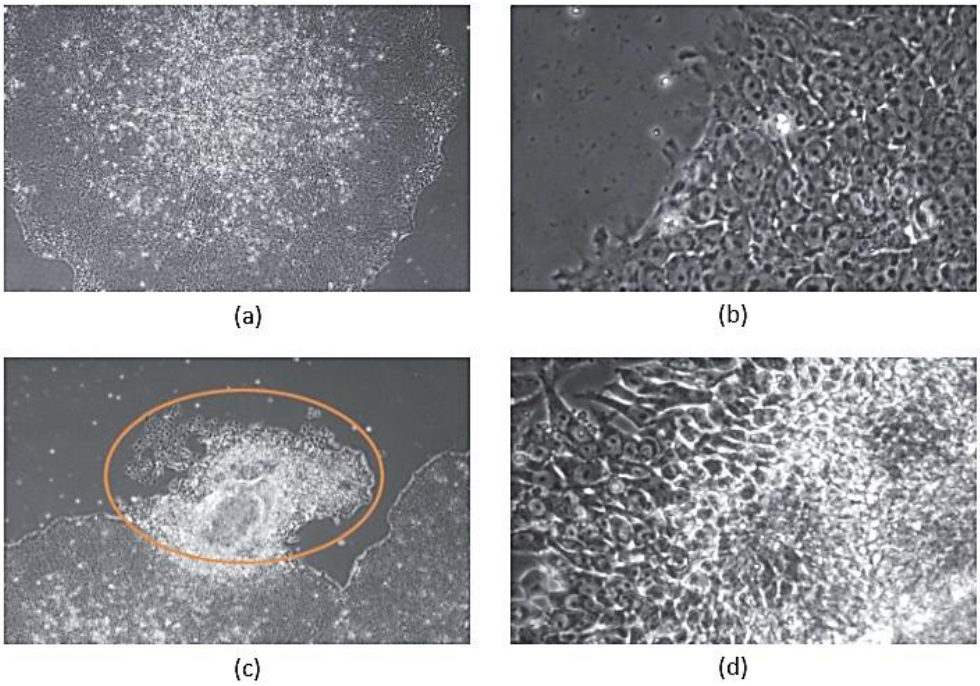

Figure 8.1. Bright field images of human iPSCs morphology.
(a,b) Undifferentiated human iPSC cells.
(c,d) Areas of spontaneous differentiation (orange circle) at the border of an undifferentiated iPSCs colony.
Images are taken using 20x (a,c) and 40x (b,d) magnifications.

However, iPSCs can undergo undesired spontaneous differentiation, characterized by loss of colony border integrity (***Figure 8.1(c)***), regions of irregular cell morphology within a colony (***Figure 8.1(d)***), and/or the emergence of other cell types, usually linked to too low or too high colony density. Proper colony density is, indeed, a critical aspect of iPSCs culturing, so it is fundamental to adjust plating density in order to maintain the culture at the desired confluence (i.e. increase/decrease split ratio). iPSCs are ready to passage when the majority of colonies are large, compact, and have centres that are dense compared to their edges.

8.3. Dopaminergic neurons maturation can be followed by a gradual cell morphology change

Both Control and Patients iPSCs were differentiated using the protocol descripted in *Chapter 5*. During differentiation procedure, based on two main phases in which iPSCs are pushed toward midbrain DA neurons progenitors

development and subsequently driven over DA neurons maturation, cells show morphological features consistent with developing steps on bright field images (***Figure 8.2***): spherical embryoid bodies plating lead to the formation of adherent cultures, to further create neural progenitor cells and begin the DA neuron patterning, with the progressive development of neural projections branching out from round and dense somas.

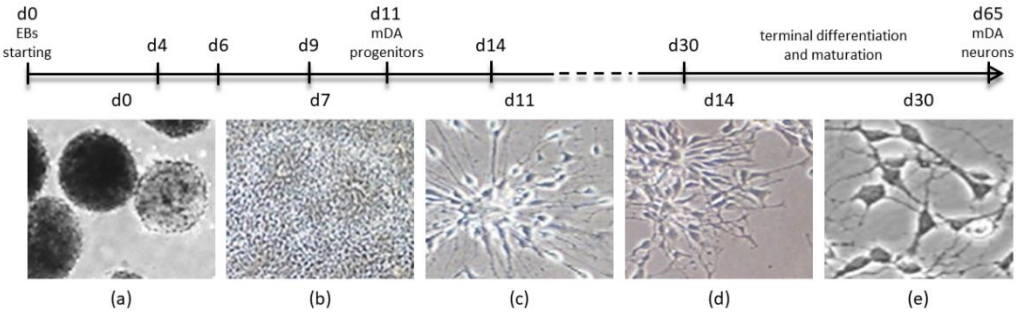

Figure 8.2. Bright field images of differentiation procedure.
BF images were taken at different times during differentiation procedure, i.e. (a) d0, (b) d7, (c) d11, (d) d14, (e) d30 of protocol descripted in Materials and Methods section. Images are taken using 20x (a,b) and 40x (c,d,e) magnifications.

8.4. Dopaminergic neurons properly differentiate from both Control and Patients iPSCs

Immunofluorescence analysis after 65 days of differentiation was performed in order to establish efficiency in deriving DA neurons. Cell's nucleus was stained using DAPI, while the number of neurons present in cell population was detected through immunostaining for MAP2, a major component of neuronal cytoskeleton [373]. In addition, cells were also stained for TH in order to quantify specific dopaminergic population among the total neuronal content. Representative immunofluorescence images of each analysed line are presented in ***Figure 8.3***.

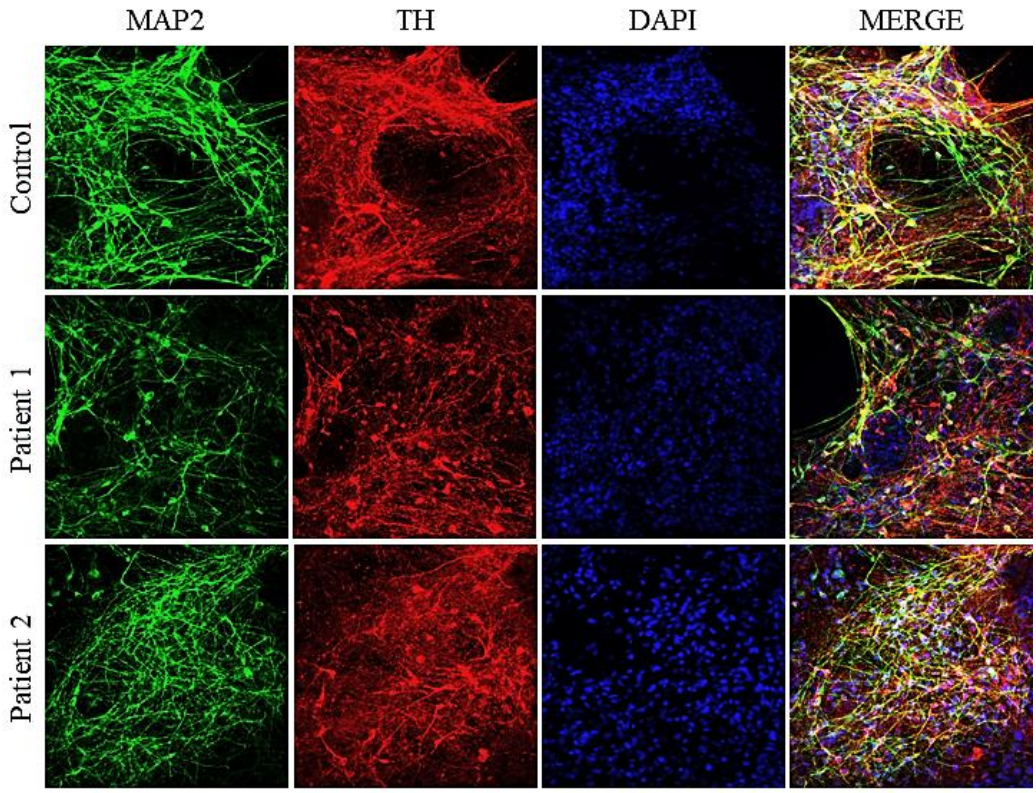

Figure 8.3. Immunofluorescence analysis of d65 iPSCs-derived neurons.
iPSCs-derived differentiations are co-stained for DAPI, MAP2 and TH markers. Images were taken using 20x magnification.

Quantification of general neuronal and specific DA neurons content was performed as reported in *Chapter 5* using Image J software, to assess the percentage of MAP2 and TH/MAP2 double-positive cell. Percentage of MAP2-positive cells is 48.54 ± 2.78 for Control, 47.60 ± 3.28 for Patient 1 and 50.60 ± 1.69 for Patient 2, indicative of a comparable neuronal content between Control and Patients lines (***Figure 8.4(a)***). All cells lines also show a relatively comparable range of TH positive cells among the MAP2 positive ones, with percentages of 40.83 ± 5.57 for Control and 36.43 ± 4.37 and 34.61 ± 4.80 for Patient 1 and Patient 2, respectively (***Figure 4(b)***).

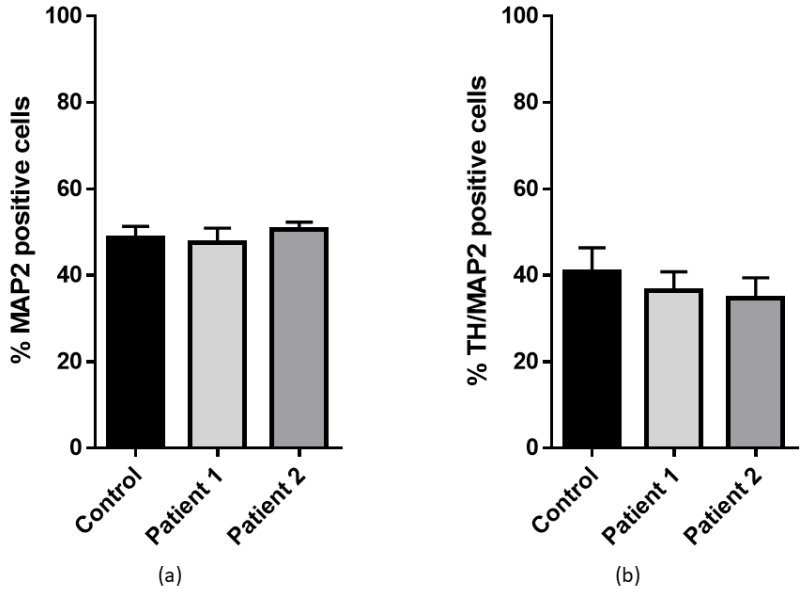

Figure 8.4. Quantification of d65 iPSCs-derived neurons.
(a) Quantification of MAP2-positive cells as percentage of total cells.
(b) Quantification od TH/MAP2 double-positive cells as a percentage of total cells.
Counting is performed in triplicate for each cell line differentiation and a total n = 3 measurements is used for data elaboration. Error bars represent s.e.m.

Collected data are in line with previously data from hosting research group and original followed protocol [347], confirming an efficient differentiation process for both Control and Patients iPSCs. In addition, total and DA neurons percentages in Patients lines are consistent with Control, indicating that Patients iPSCs fully differentiate into midbrain DA neurons with the same efficiency of Control ones, thus suggesting that deficiency in AADC activity does not alter the neuronal development and does not trigger neurogenerative response.

8.5. Controls neurons do not show AADC phosphorylation in standard culturing conditions

Immunoprecipitation (IP) of AADC was performed in order to enrich the sample in protein content with the purpose of detecting a possible enzyme phosphorylated portion. Western blot following AADC IP was subsequently analysed using an anti-phosphorylated serine antibody. AADC detection after IP procedure clearly shows an enrichment without protein loss during washing steps (***Figure 8.5(a)***), while GAPDH, generally used as internal loading control and still

present after pre-cleaning procedure, is lost during washing steps, supporting the specificity direction of analysis (***Figure 8.5(b)***).

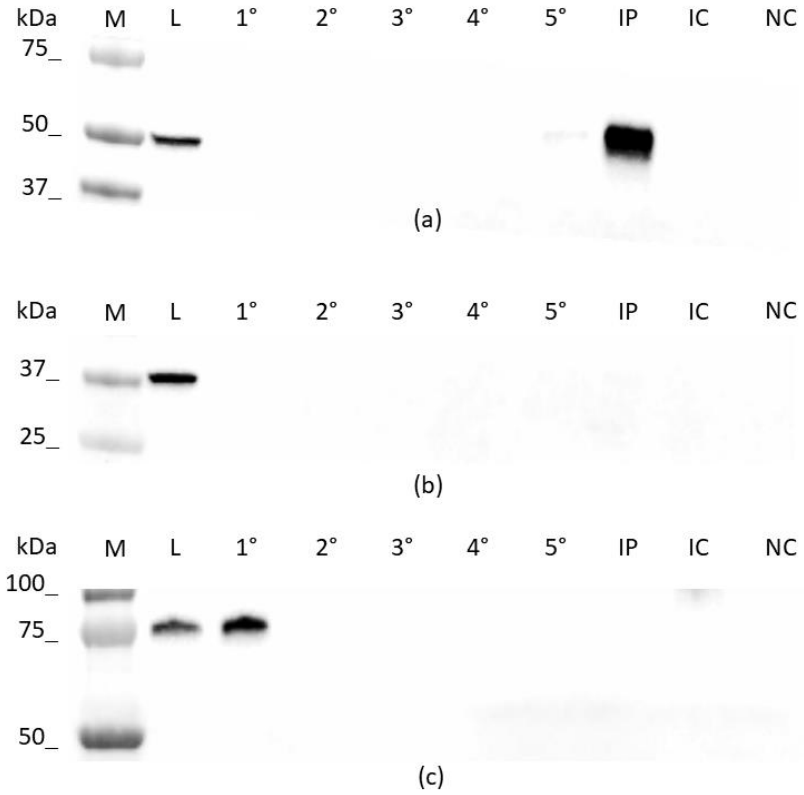

Figure 8.5. Western blotting analysis of AADC immunoprecipitation and phosphorylation in Control iPSCs-derived neurons.
(a) *Detection of AADC. (b) Detection of GAPDH. (c) Detection of phosphorylated serine. M: molecular weight marker; L: pre-cleaned cell lysate; 1°, 2°, 3°, 4° and 5°: sequential washing steps; IP: immunoprecipitated sample; IC: isotype control; NC: negative control.*

However, the same membrane blotted with an anti-phosphorylated serine antibody does not show any positivity at AADC corresponding molecular weight (***Figure 8.5(c)***). Thus, even if immunoprecipitation enrichment in AADC content worked, this analysis does not detect any amount of phosphorylated protein, suggesting that, at least in standard cell culture conditions, AADC is not subject to regulation by this particular post-translational modification.

8.6. AADC expression is altered in Patients-derived neurons compared to Control

AADC expression in Control and Patients neurons was investigated through immunocytochemistry analysis at day 65, in a double staining with TH.

Representative acquired image is presented in ***Figure 8.6***, showing that AADC expression is widely distributed in whole neurons, in both soma and projections.

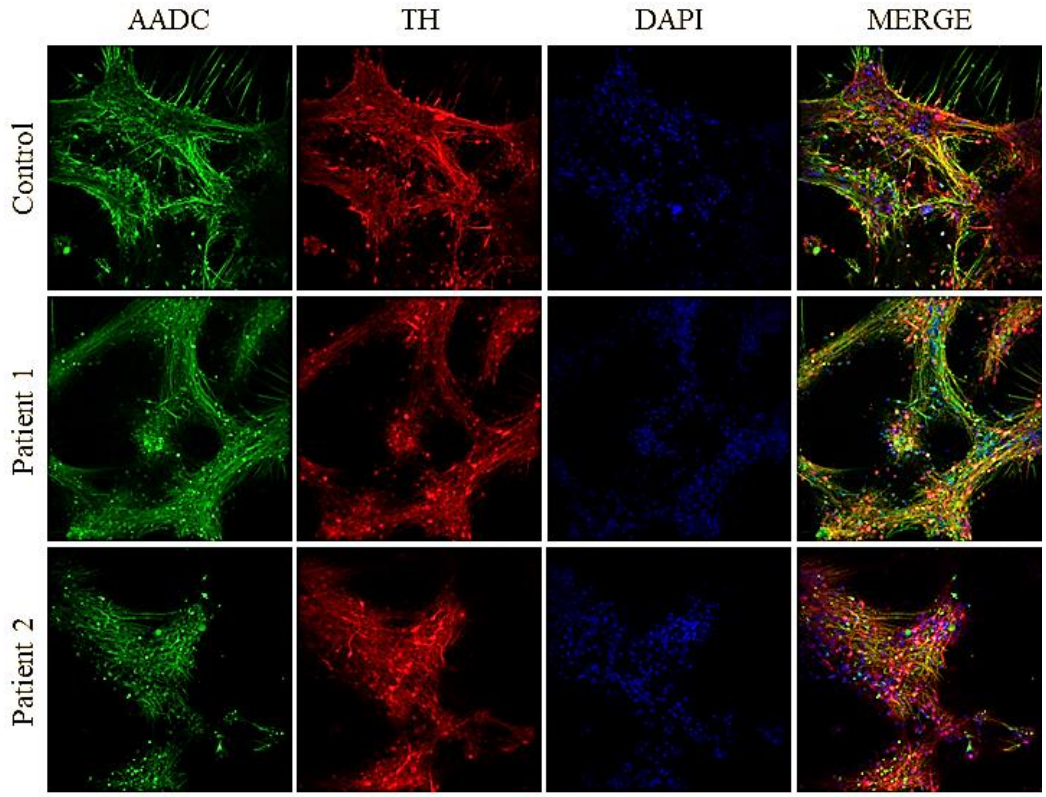

Figure 8.6. Immunofluorescence analysis of AADC expression in iPSCs-derived neurons.
iPSCs-derived differentiations are co-stained for DAPI, AADC and TH markers.
Images were taken using 20x magnification.

A visual inspection of stained samples suggests that AADC may be less expressed in Patient 2 than in Control and Patient 1 that in general show a more intense signal. This observation could be in line with Patient 2 genotype, since a premature stop codon in one of AADC codifying alleles might likely result in a lower total amount of protein.

Therefore, total AADC content in Control and Patients mature neurons was evaluated through western blot analysis, using GAPDH as sample loading control. Representative acquired image is presented in ***Figure 8.7(a)***: Patient 1 shows an AADC band stronger than Control, while in Patient 2 AADC seems to be highly under-expressed.

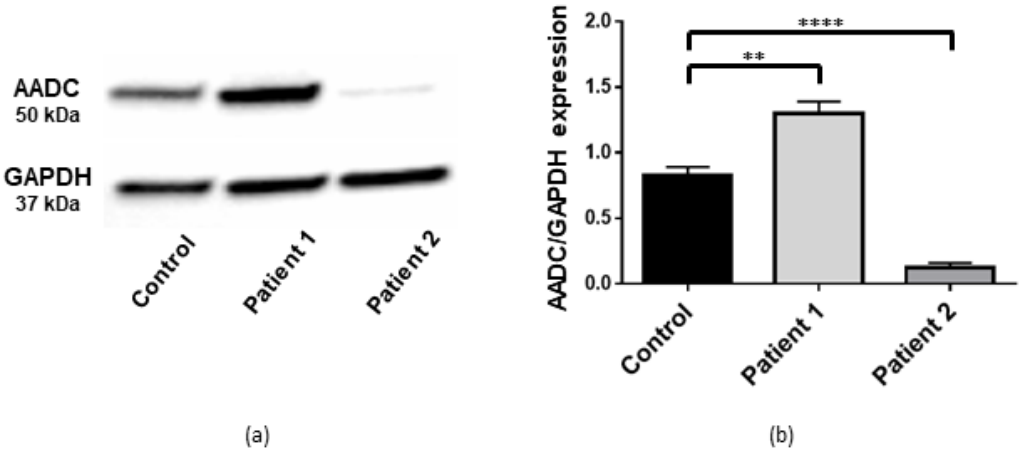

Figure 8.7. AADC expression in Control and Patients iPSCs-derived neurons.
(a) Representative western blot analysis.
*(b) Quantification of AADC expression normalised to GAPDH respective expression in each cell line. **: p = 0.0018; ****: p < 0.0001. A total of n = 5 measurements is used for data elaboration. Error bars represent s.e.m.*

Quantification analysis of 5 western blots, performed with distinct differentiation samples for each cell line (***Figure 8.7(b)***), confirms an increased AADC content in Patient 1 iPSCs-derived neurons respect to Control ones ($p = 0.0018$), and a very significant lower expression of protein in Patient 2 neurons ($p < 0.0001$), confirming immunocytochemistry analysis detection.

While AADC low expression level in Patient 2 might be predictable according to genotype, i.e. a premature stop codon in one of the two encoding alleles, Patient 1, characterised by a homologous missense mutation, shows an AADC content higher than in Control line.

8.7. MAO-A and MAO-B expression alteration seems to be AADC-variant dependent

Considering AADC differential expression in Patients and Control iPSCs-derived neurons, it was interesting to investigate if the expression of other enzymes belonging to DA homeostasis pathway is altered as well. In particular, attention was focused on MAO-A and MAO-B, two main enzymes responsible for DA degradation in CNS. Both Patients show a decreased MAO-A expression level respect to Control, even more consistent for Patient 2 ($p = 0.0443$ for Patient 1 and

p = 0.012 for Patient 2), as detected from western blot analyses (***Figure 8.8(a)***) and their quantifications (***Figure 8.9(b)***).

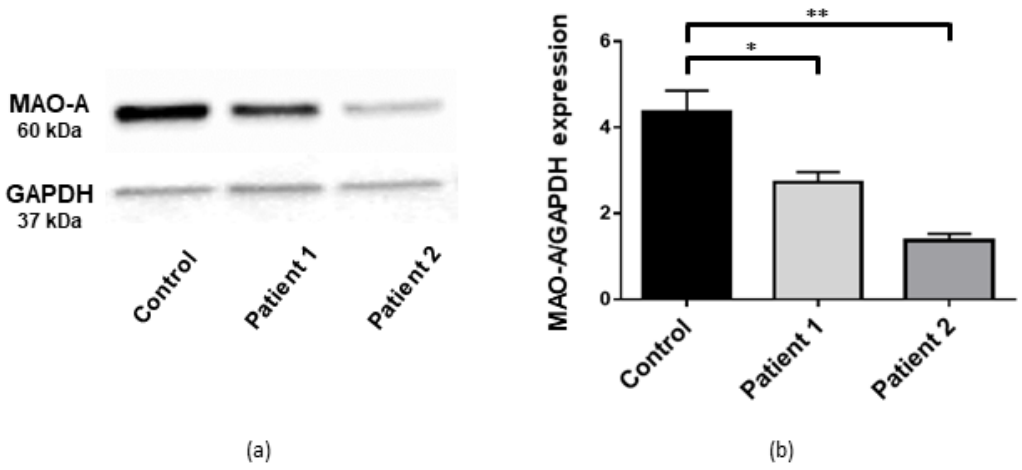

Figure 8.8. MAO-A expression in Control and Patients iPSCs-derived neurons.
(a) Representative western blot analysis.
*(b) Quantification of MAO-A expression normalised to GAPDH respective expression in each cell line. *: p = 0.0443; **: p = 0.0012. A total of n = 5 measurements is used for data elaboration. Error bars represent s.e.m.*

MAO-B expression, instead, seems to behaves differently, with a slight increase for Patient 1 (p = 0.0029) and a strong decrease for Patient 2 (p < 0.0001) respect to Control (***Figure 8.9***).

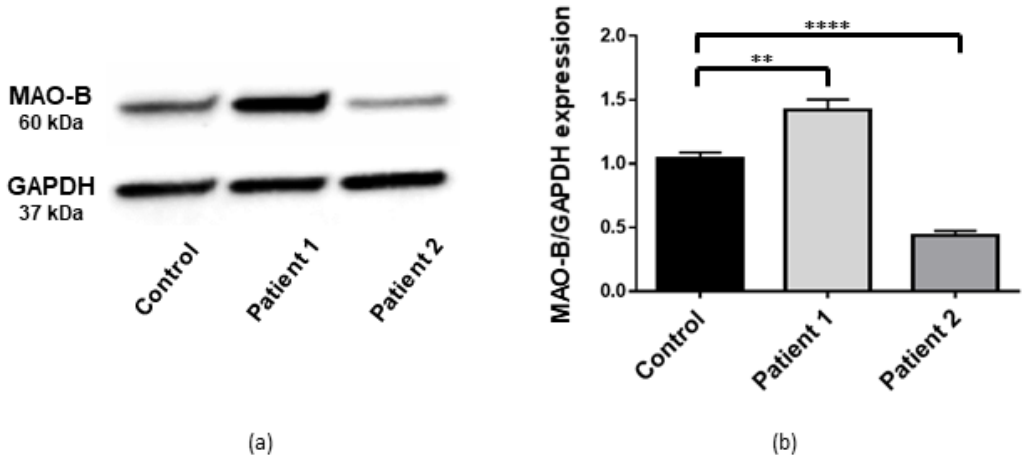

Figure 8.9. MAO-B expression in Control and Patients iPSCs-derived neurons.
(a) Representative western blot analysis.
*(b) Quantification of MAO-B expression normalised to GAPDH respective expression in each cell line. **: p = 0.0029; **: p < 0.0001. A total of n = 5 measurements is used for data elaboration. Error bars represent s.e.m.*

In summary, a very low expression of both MAO-A and MAO-B is detected for Patient 2 compared to Control, while Patient 1 show a lower expression of MAO-A but a higher expression of MAO-B. In addition, MAO-A total levels, normalised to GAPDH for each cell line, are significantly higher than MAO-B ones. Interestingly, MAO-B expression pattern resemble AADC expression one, with an increase in Patient 1 and a decrease in Patient 2, while MAO-A is lower for both Patients compare to Control. Taken together, these analyses may suggest that DA degradative enzymes content in Patients could be regulated in response to DA and/or AADC levels, in general in response to DA synthetizing pathway alterations.

In order to further investigate differential expression of MAO-A/B, immunocytochemistry analyses were performed to evaluate enzyme-specific cell-subtype expression, in particular for Control and Patient 2, which are expected to show a higher difference, as suggested from western blot analyses.

A visual inspection of whole stained samples, indeed, confirms that MAO-A is less expressed in Patient 2 than in Control, which in general shows a more intense signal.

As shown in ***Figure 8.10***, MAO-A expression co-localises with TH, both in Control and Patient 2 neuronal soma, but it is also expressed in TH negative cells, i.e. other cell types, usually present in samples since differentiation process toward midbrain DA neurons do not present a complete efficiency.

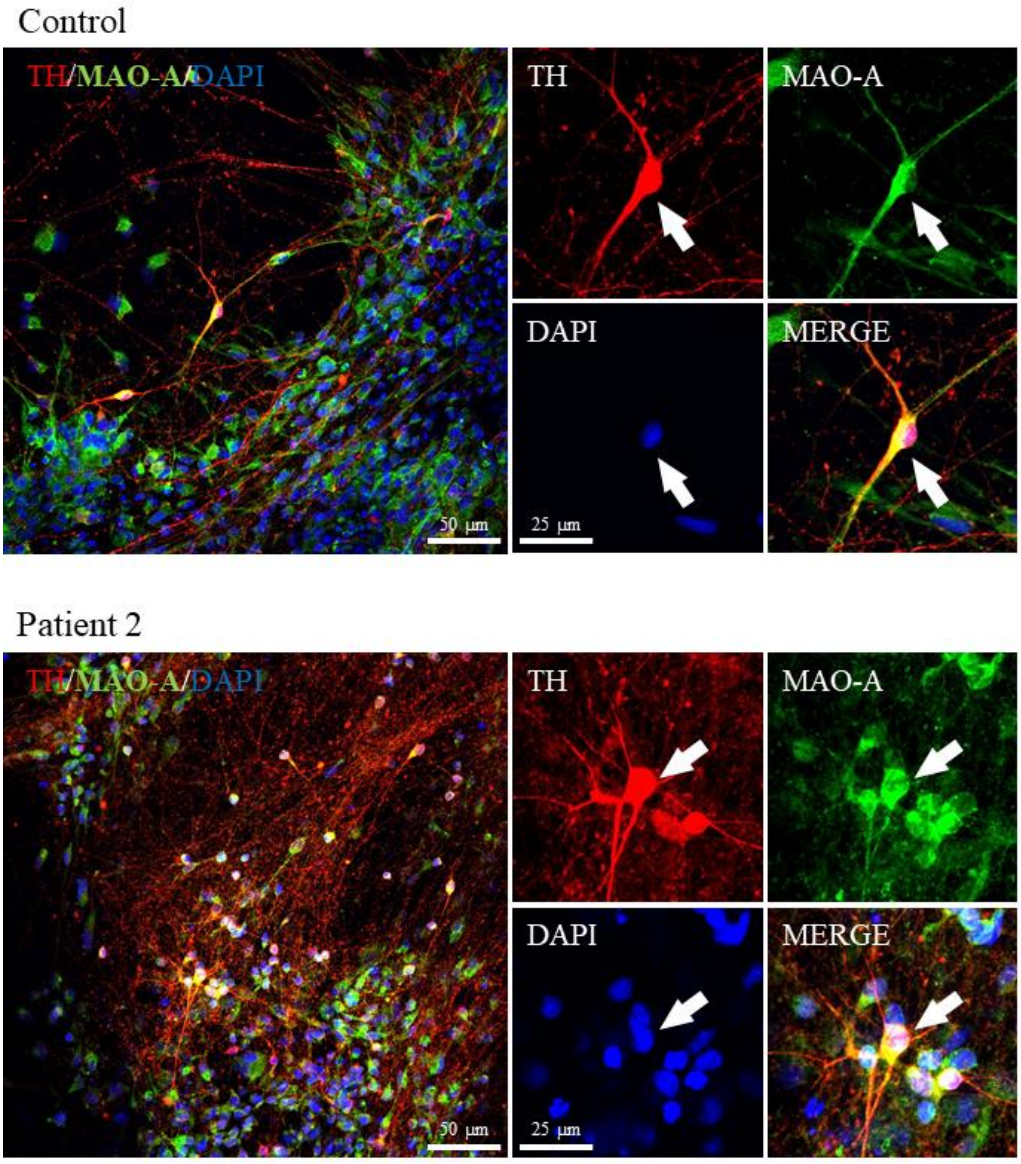

Figure 8.10. Immunofluorescence analysis of MAO-A expression in iPSCs-derived neurons.
iPSCs-derived differentiations are co-stained for DAPI, TH and MAO-A markers.
White arrows point to markers co-localisation.
Images were taken using 20x and 40x magnifications.

Samples were therefore double-stained for MAO-A and glial fibrillary acidic protein (GFAP), an intermediate filament protein expressed by glia cells, including astrocytes (***Figure 8.11***), to unravel if MAO-A positive and TH negative cells individuated in the previous analysis could possibly be glia cells.

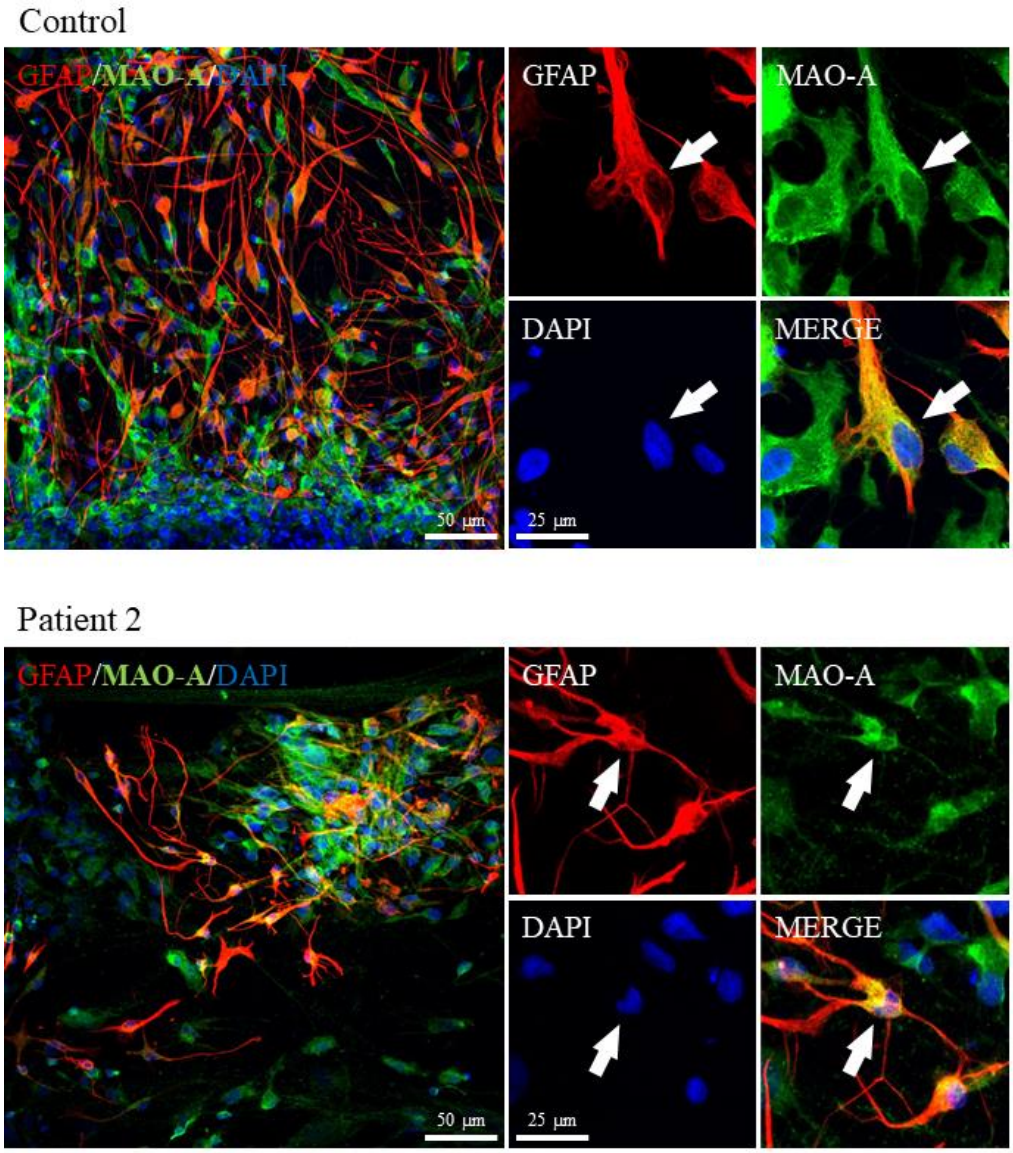

Figure 8.11. Immunofluorescence analysis of MAO-A expression in glia cells.
iPSCs-derived differentiations are co-stained for DAPI, GFAP and MAO-A markers. White arrows point to markers co-localisation. Images were taken using 20x and 40x magnifications.

As shown in ***Figure 8.11***, MAO-A co-localises also with GFAP, indicating that its widespread signal is linked to its expression not only in DA neurons, but also in glia cells.

The same set of experiments were performed to analyse MAO-B expression. Surprisingly, no TH and MAO-B double-positive cells are detected (***Figure 8.12***), since MAO-B signal does not co-localise with TH signal.

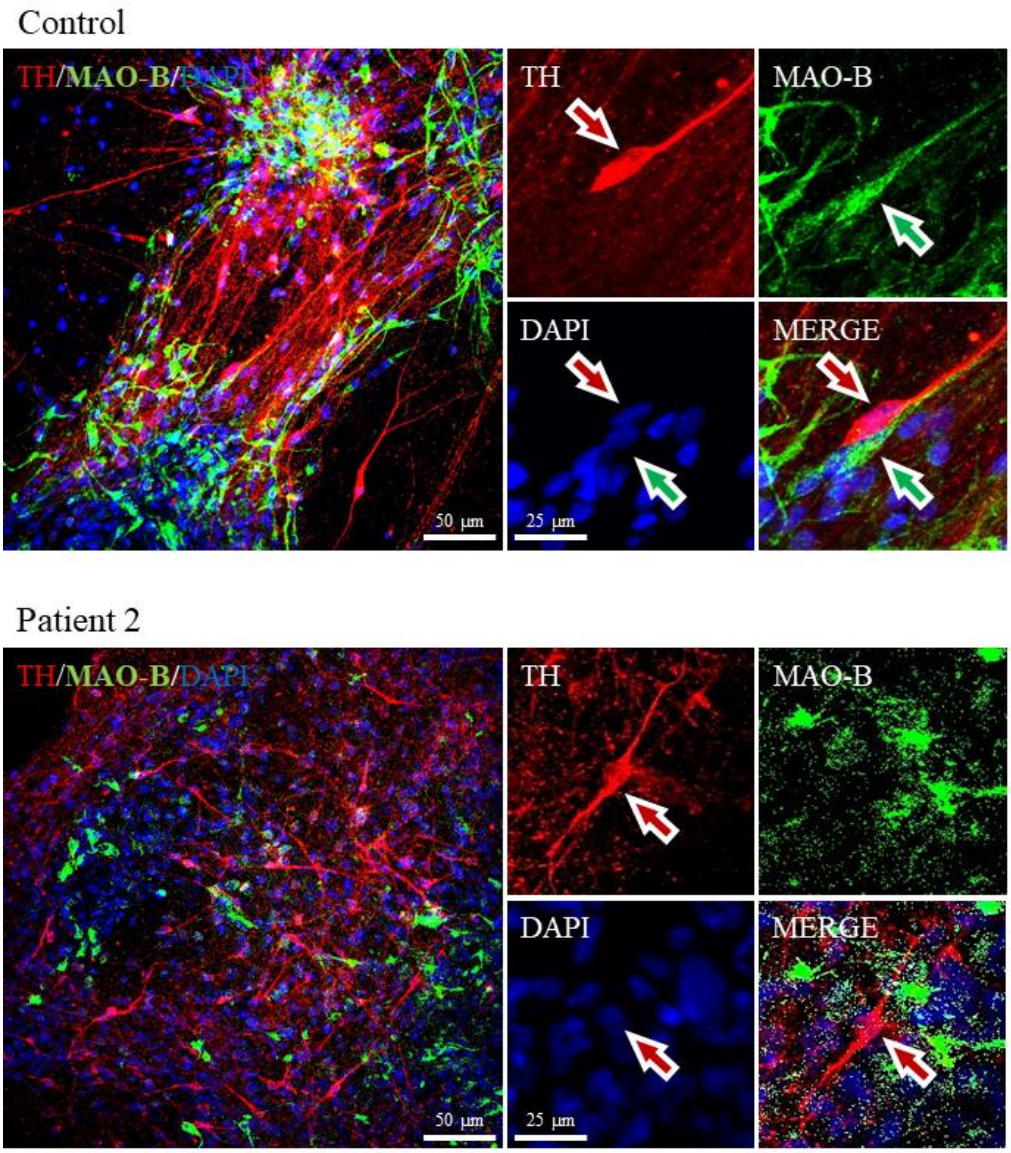

Figure 8.12. Immunofluorescence analysis of MAO-B expression in iPSCs-derived neurons.
iPSCs-derived differentiations are co-stained for DAPI, TH and MAO-B markers.
Coloured arrows indicate the corresponding marker.
Images were taken using 20x and 40x magnifications.

Interestingly, MAO-B and GFAP double staining (***Figure 8.13***) confirms that MAO-B expression is mainly localised in glia cells.

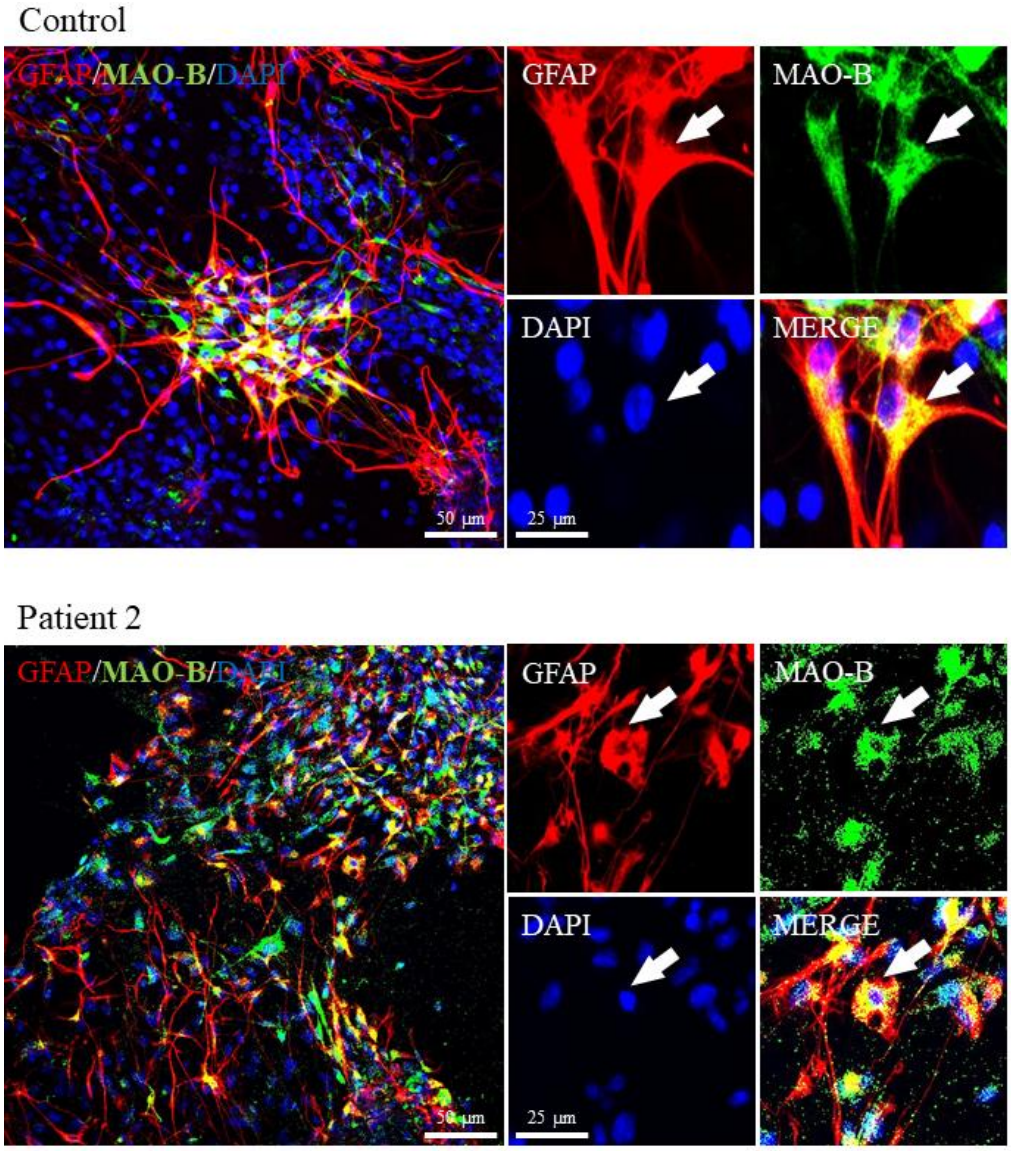

Figure 8.13. Immunofluorescence analysis of MAO-B expression in glia cells.
iPSCs-derived differentiations are co-stained for DAPI, GFAP and MAO-B markers.
White arrows point to markers co-localisation.
Images were taken using 20x and 40x magnifications.

In summary, immunocytochemistry analyses showed that MAO-A is widely express in both DA neurons and glia cells, while MAO-B is mainly expressed in glia cells, and not in DA neurons. Moreover, further considerations can be made about glia cells phenotype in cell lines. In Patient 2, indeed, glia cells seem to be less structured, with smaller nuclei and consistently under-developed branches respect to Control line (***Figures 8.11 and 8.13***). Considering that in Patient 1 glia cells do not show this strong alteration (data not shown), and glia cells are the mainly responsible for MAO-B expression, Patient 1 very low MAO-B content

might be linked to an altered glia cells phenotype. The same consideration cannot be made for MAO-A, that is expressed both in glia cells and neurons, because, at least from these analyses, it cannot certainly be determined which cell type among them and in which extent both and/or one of them could contribute to MAO-A expression alteration in Patients respect to Control.

8.8. Partial conclusions and future prospects

One of the main challenges in studying human neurological diseases is the lack of human-derived samples, mainly due to their inaccessibility, making it difficult to model diseases and improve pathophysiology understanding. Moreover, animal models often do not faithfully recapitulate human clinical phenotype [374], thus it is hoped that disease-modelling and therapy testing will become easier using human iPSCs. However, maintenance and propagation of human iPSCs in feeder-free conditions requires the use of complex media formulations, in combination with careful handling techniques, to maintain high quality cultures at each passage (***Figure 8.1(a)***). In addition, iPSCs cultures has to be routinely checked, and cleaned if necessary, in order to prevent, or remove, spontaneous differentiations spots (***Figure 8.1(b)***) that can substantially affect the differentiation outcome.

Human iPSCs differentiation into midbrain DA neurons shows a gradual cell morphology acquisition (***Figure 8.2***). However, subsequent investigations about pathophysiology mechanisms underlying the disease require good quality samples, and, since it is well known that human iPSCs lines are subject to variable differentiation efficiencies [375], each differentiation is checked at day 65 for its DA neurons content by immunocytochemistry (***Figure 8.3***), followed by markers quantification (***Figure 8.4***), to ensure that it is qualitatively in line with model standards.

A first set of analyses was performed in order to detect, if present, AADC in its phosphorylated form, as previously suggested by *in vitro* experiments (see *Chapter 6*). Even if enzyme immunoprecipitation was performed with the aim to load a higher amount of enzyme, no signal was found in western blotting analysis using an anti-phosphorylated serine antibody (***Figure 8.5***), at least in Control standard culturing conditions. However, the highly dynamic feature of this post-translational modification, together with the static state that characterises an *in vitro* cellular model, not subjected to any environmental and internal stimulus in standard conditions, might have affected the possible presence of phosphorylated AADC. Therefore, it could be interesting to perform the experiment after chemical as well as ion channels-mediated stimulation of neurons.

As AADC expression showed to be wide distributed in differentiated lines, but with a putative weaker immunofluorescent signal in Patient2 (***Figure 8.6***), western blotting analyses were performed in order to check Patients lines AADC content respect to Control one. As expected from genetic background, i.e. compound heterozygosis with a premature stop codon in one allele, Patient 2 shows a decreased protein level (***Figure 8.7***), but, surprisingly, in Patient 1, which is homozygous for a missense mutation, protein amount is significantly higher than in Control. This result definitely deserves further investigation. One possible hypothesis could be related to an intrinsic feature of this particular AADC variant, R347G: the arginine to glycine mutation, indeed, was already characterised *in vitro* for structural/functional alterations [22], revealing that this substitution results in the destruction of a hydrogen bonds network, including Arg347, involved in proper positioning of catalytic loop, and consequently catalytic Tyr332 [20], at the active site of AADC upon substrate binding. Considering the peculiar flexibility of the catalytic loop, that also makes the loop "open" conformation more likely to be proteolyzed [25], it could be assumed that an arginine to glycine mutation close to the catalytic loop might make it less flexible and consequently less susceptible to proteolytic cleavage. In this view, the higher AADC content in Patient 1 samples could be due not to a higher protein expression but rather to a higher stability of this particular AADC variant. This hypothesis is now under investigation through a range of experiments in order to evaluate R347G mutant intrinsic stability.

Another possibility might be the existence of a positive feedback mechanism that tends to increase AADC content with the aim to compensate the low DA release. Further experiments have to be performed in order to confirm/disprove this hypothesis. In particular, it might be interesting to analyse AADC cDNA levels through qRT-PCR to check for an increase in protein transcription in Patients respect to Control.

Looking at the complexity of dopaminergic pathway, it has been considered interesting to evaluate if its upstream alteration could have any effect on downstream equilibria. Thus, attention was focused on two of the main enzymes responsible for DA degradation, MAO-A and MAO-B, performing western blot and immunocytochemistry analyses. MAO-A, widely express in both DA neurons and

glia cells (***Figures 8.9 and 8.10***), was found to be downregulated in both Patients compare to Control line (***Figure 8.7***), even if with a higher extent in Patient 2. MAO-B, instead, was found to be higher expressed in Patient 1 respect to Control line, but an opposite behaviour was detected for Patient 2 (***Figure 8.8***), a pattern similar to that of AADC amount. Interestingly, MAO-B was found to be expressed mainly in glia cells, and not in DA neurons (***Figures 8.11 and 8.12***). Moreover, glia cells of Patient 2, which present the greater extent of MAO-B and MAO-A decrease, clearly show a morphological alteration compared to Control line (***Figures 10 and 12***).

Even if these preliminary results require further investigations, the suggestion that not only alteration of DA synthetic pathway in neurons, but also alteration of neurons-astrocytes interplay, could underlie the pathophysiologic mechanisms of AADC Deficiency is a new and interesting prospective. Recent findings strongly highlighted astrocytes role not only in provide neurons with metabolic and structural support, but also in information processing, through modulation of synaptic activity and plasticity, neurotransmitters homeostasis, neurogenesis and brain wiring, and structural and functional alterations of this cell type were already associated with many human brain pathological conditions [376]. Since dysregulations of astrocytes functions and interplay with neurons contribute to the development and progression of various neurological diseases, targeting astrocytes could be an alternative and/or supporting approach for the development of novel and effective therapies to treat brain disorders, and, maybe, also AADC Deficiency.

Chapter 9

Conclusions

AADC and HDC are two homologous enzymes responsible for the synthesis of DA/serotonin and histamine, respectively, as well as other modulators. All of these molecules are main protagonists or regulators of several physiological pathways, fundamental both in CNS and in peripheral tissues. Alterations of their homeostasis, indeed, cause and/or participate in the development and progression of several pathological conditions, often severe and disabling. Consequently, AADC and HDC activity modulation might be useful in pathophysiological understanding of several diseases as well as in improving/developing new therapeutic strategies. However, despite the fact that both enzymes are of fundamental importance, the knowledge of biochemical features of AADC and HDC is poor and fragmented.

Human wild-type HDC production and purification in recombinant form revealed that this enzyme is present in solution in two species (RedHDCwt and OxHDCwt), that are in equilibrium depending on the concentration of reducing agent, due to the presence of an intermolecular reversible disulphide bridge between monomers, involving residue Cys180. This feature has been extensively investigated using *in vitro* biochemical technics, revealing that the two enzymatic forms show slight structural differences in their whole arrangement, as well as slight perturbation of the active site microenvironment. As consequence, OxHDCwt results not only more stable, but also more active than RedHDCwt. Even if, at present, it is not easy to envisage a physiological role of this redox RedHDC→OxHDC switch, it seems to be a peculiar and unique feature of human HDC among PLP-dependent enzymes. Taking into account that the cell environment is highly reducing, it is reasonable to suggest that HDC is mainly reduced under physiological conditions. However, in cancer cells, where redox potential is altered, the increased oxidizing conditions could favour the more stable and active OxHDC, leading to an increased histamine production. This HDC feature

could be responsible for the high histamine content characterising some cellular oxidative stress-linked pathologies, such as cholangiocarcinoma, and could be interesting also in other tumour types, in which the enzyme might participate in the positive feedback loop that fix tumour microenvironment in a "constant inflammation" state, necessary for its development. Moreover, in this view, the development of specific inhibitors directed toward OxHDC is highly desirable.

On the other side, AADC limited literature studies about enzyme phosphorylation have driven an *in vitro* deep characterization of the impact of this possible post-translational modification on enzyme activity. The phosphorylated residue was individuated to be Ser193, close to active site. Moreover, AADC kinetic parameters measurements after phosphorylation assay revealed that the enzyme shows not only an increase of catalytic efficiency toward all tested substrates, i.e. L-DOPA, L-5HTP and L-phenylalanine, but also the same mechanism of activation for all of them: increase in catalytic efficiency, is mainly due to a decrease in K_M, strongly suggesting that phosphorylation might increase the affinity of AADC for all its substrates. However, AADC in its phosphorylated form was not found in iPSCs-derived dopaminergic neurons, at least in standard culturing conditions. It should be considered, nevertheless, that the highly dynamic feature of this post-translational modification, together with the static state that characterise an *in vitro* cellular model, not subjected to any environmental and internal stimulus in standard conditions, might have affected the possible presence of phosphorylated AADC.

iPSCs-derived dopaminergic neurons of AADC Deficiency patients were used as cell model to evaluate enzyme content in Patients' lines respect to Control one, revealing that higher AADC amount is found in a patient harbouring the homozygous missense mutation R347G, possibly due to the existence of a positive feedback mechanism that tends to increase AADC content with the aim to compensate the low DA release, or to a higher stability of the specific AADC variant. Interestingly, the analysis of other dopaminergic pathway enzymes, in particular MAO-A and MAO-B, both in expression levels and in cell-specific localisation, suggested that not only alteration of DA levels, but also alteration of neurons-astrocytes interplay, could participate in pathophysiological mechanisms

of AADC Deficiency. Thus, targeting astrocytes might be an alternative and/or supporting approach for the development of novel and effective therapies to treat brain disorders, and, maybe, also AADC Deficiency.

Altogether, data and information obtained from the performed experiments have increased AADC and HDC knowledge, as well as paved the way for new hypothesis regarding possible efforts in the development of new disease treatments.

Chapter 10

Bibliography

[1] Percudani R, Peracchi A, "A genomic overview of pyridoxal-phosphate-dependent enzymes." *EMBO Rep* (2003) 4(9):850-854.

[2] Metzler DE, Snell EE, "Deamination of serine. I. Catalytic deamination of serine and cysteine by pyridoxal and metal salts." *J Biol Chem* (1952) 198(1):353-361.

[3] Metzler DE, Snell EE, Deamination of serine. II. D-Serine dehydrase, a vitamin B6 enzyme from Escherichia coli." *J Biol Chem* (1952) 198(1):363-373.

[4] Metzler, DE, Snell EE, "Some transamination reactions involving vitamin B6." *J Am Chem Soc* (1952) 74, 5.

[5] Braunstein, AE, Shemyakin MM, *Biokhimiya* (1953) 18.

[6] Braunstein AE, "The Enzymes" *Academic Press: New York* (1960).

[7] Braunstein AE, "Chemical and biological aspects of pyridoxal catalysis" *Pergamon Press: New York* (1963).

[8] Grishin NV, Phillips MA, Goldsmith EJ, "Modeling of the spatial structure of eukaryotic ornithine decarboxylases." Protein Sci (1995) 4(7):1291-1304.

[9] Schneider G, Käck H, Lindqvist Y, "The manifold of vitamin B6 dependent enzymes." *Structure* (2000) 8(1):R1-R6.

[10] Sandmeier E, Hale TI, Christen P, "Multiple evolutionary origin of pyridoxal-5'-phosphate-dependent amino acid decarboxylases." *Eur J Biochem* (1994) 221(3):997-1002.

[11] Burkhard P, Dominici P, Borri-Voltattorni C, Jansonius JN, Malashkevich VN, "Structural insight into Parkinson's disease treatment from drug-inhibited DOPA decarboxylase." *Nat Struct Biol* (2001) 8(11):963-967.

[12] Montioli R, Cellini B, Borri Voltattorni C, "Molecular insights into the pathogenicity of variants associated with the aromatic amino acid decarboxylase deficiency." *J Inherit Metab Dis* (2011) 34(6):1213-1224.

[13] Paiardini A, Bossa F, Pascarella S, "Evolutionarily conserved regions and hydrophobic contacts at the superfamily level: The case of the fold-type I, pyridoxal-5'-phosphate-dependent enzymes." *Protein Sci* (2004) 13(11):2992-3005.

[14] Paiardini A, Giardina G, Rossignoli G, Voltattorni CB, Bertoldi M, "New Insights Emerging from Recent Investigations on Human Group II Pyridoxal 5'-Phosphate Decarboxylases." *Curr Med Chem* (2017) 24(3):226-244.

[15] Finn RD, Coggill P, Eberhardt RY, Eddy SR, Mistry J, Mitchell AL, Potter SC, Punta M, Qureshi M, Sangrador-Vegas A, Salazar GA, Tate J3, Bateman A, "The Pfam protein families database: towards a more sustainable future." *Nucleic Acids Res* (2016) 44(D1):D279-D285.

[16] Boutet E, Lieberherr D, Tognolli M, Schneider M, Bansal P, Bridge AJ, Poux S, Bougueleret L, Xenarios I, "UniProtKB/Swiss-Prot, the Manually Annotated Section of the UniProt KnowledgeBase: How to Use the Entry View." *Methods Mol Biol* (2016) 1374:23-54.

[17] Jansonius JN, "Structure, evolution and action of vitamin B6-dependent enzymes." *Curr Opin Struct Biol* (1998) 8(6):759-769.

[18] Komori H, Nitta Y, Ueno H, Higuchi Y, "Structural study reveals that Ser-354 determines substrate specificity on human histidine decarboxylase." *J Biol Chem* (2012) 287: 29175-29183.

[19] Fenalti G, Law RH, Buckle AM, Langendorf C, Tuck K, Rosado CJ, Faux NG, Mahmood K, Hampe CS, Banga JP, Wilce M, Schmidberger J, Rossjohn J, El-Kabbani O, Pike RN, Smith AI, Mackay IR, Rowley MJ, Whisstock JC, "GABA production by glutamic acid decarboxylase is regulated by a dynamic catalytic loop." *Nat Struct Mol Biol* (2007) 14: 280-286.

[20] Bertoldi M, Gonsalvi M, Contestabile R, Voltattorni CB, "Mutation of tyrosine 332 to phenylalanine converts dopa decarboxylase into a decarboxylation-dependent oxidative deaminase." *J Biol Chem* (2002) 277(39):36357-36362.

[21] Bertoldi M, Frigeri P, Paci M, Voltattorni CB, "Reaction specificity of native and nicked 3,4-dihydroxyphenylalanine decarboxylase." *J Biol Chem* (1999) 274(9):5514-5521.

[22] Montioli R, Paiardini A, Kurian MA, Dindo M, Rossignoli G, Heales SJ, Pope S, Voltattorni CB, Bertoldi M, "The novel R347g pathogenic mutation of aromatic amino acid decarboxylase provides additional molecular insights into enzyme catalysis and deficiency." *Biochim Biophys Acta* (2016) 1864(6):676-682.

[23] Langendorf CG, Tuck KL, Key TL, Fenalti G, Pike RN, Rosado CJ, Wong AS, Buckle AM, Law RH, Whisstock JC, "Structural characterization of the mechanism through which human glutamic acid decarboxylase auto-activates." *Biosci Rep* (2013) 33(1):137-144.

[24] Giardina G, Montioli R, Gianni S, Cellini B, Paiardini A, Voltattorni CB, Cutruzzolà F, "Open conformation of human DOPA decarboxylase reveals the mechanism of PLP addition to Group II decarboxylases." *Proc Natl Acad Sci USA* (2011) 108(51):20514-20519.

[25] Matsuda N, Hayashi H, Miyatake S, Kuroiwa T, Kagamiyama H, "Instability of the apo form of aromatic L-amino acid decarboxylase in vivo and in vitro: implications for the involvement of the flexible loop that covers the active site." *J Biochem* (2004) 135(1):33-42.

[26] Kass I, Hoke DE, Costa MG, Reboul CF, Porebski BT, Cowieson NP, Leh H, Pennacchietti E, McCoey J, Kleifeld O, Borri Voltattorni C, Langley D, Roome B, Mackay IR, Christ D, Perahia D, Buckle M, Paiardini A, De Biase D, Buckle AM, "Cofactor-dependent conformational heterogeneity of GAD65 and its role in autoimmunity and neurotransmitter homeostasis." *Proc Natl Acad Sci USA* (2014) 111(25):E2524-E2529.

[27] Dunathan HC, "Conformation and reaction specificity in pyridoxal phosphate enzymes." *Proc Natl Acad Sci USA* (1966) 55:712-716.

[28] Livanova NB, Chebotareva NA, Eronina TB, Kurganov BI, "Pyridoxal 5'-phosphate as a catalytic and conformational cofactor of muscle glycogen phosphorylase B." *Biochemistry* (2002) 67(10):1089-1098.

[29] Huang X, and Miller W, Adv Appl Math (1991) 12:373-381; https://fasta.bioch.virginia.edu/fasta_www2/fasta_www.cgi?rm=lalign&pgm=lal.

[30] Borri Voltattorni C, Minelli A, Borri P, “Interaction of L-alphamethyl-alpha-hydrazino-3,4 dihydroxyphenylpropionic acid with dopa-decarboxylase from pig kidney” *FEBS Lett* (1977) 75:277-280.

[31] Borri Voltattorni C, Minelli A, Borri P, “Interaction of N-(DLseryl)N'-(2,3,4-trihydroxybenzyl)-hydrazine with L-dopa decarboxylase from pig kidney.” *Experientia* (1977) 33:158-160.

[32] Borri Voltattorni C, Minelli A, Borri P, “The interaction of 2,3,4-trihydroxybenzylhydrazine with DOPA decarboxylase from pig kidney.” *Life Sci* (1981) 28:103-108.

[33] Montioli R, Voltattorni CB, Bertoldi M, “Parkinson's Disease: Recent Updates in the Identification of Human Dopa Decarboxylase Inhibitors.” Curr Drug Metab (2016) 17(5):513-518.

[34] McCormick DB, Snell EE, “Pyridoxal Kinase of Human Brain and Its Inhibition by Hydrazine Derivatives.” *Proc Natl Acad Sci USA* (1959) 45:1371-1379.

[35] Bender DA, Smith WR, “Inhibition of kynurenine hydrolase by benserazide, carbidopa and other aromatic hydrazine derivatives: evidence for sub-clinical iatrogenic niacin deficiency.” *Biochem Soc Trans* (1978) 6:120-122.

[36] Kelley JL, Miller CA, White HL, “Inhibition of histidine decarboxylase. Derivatives of histidine.” *J Med Chem* (1977) 20(4):506-509.

[37] Snape TJ, Astles AM, Davies J, “Understanding the chemical basis of drug stability and degradation”, *The Pharmaceutical Journal* (2010)

[38] Lee YH, Kim KH, Yoon IK, Lee KE, Chun IK, Rhie JY, Gwak HS, “Pharmacokinetic evaluation of formulated levodopa methyl ester nasal delivery systems.” *Eur J Drug Metab Pharmacokineti* (2014) 39:237–242.

[39] Scaturro AL, De Caro V, Campisi G, Giannola LI, “Potential transbuccal delivery of L-dopa methylester prodrug: Stability in the environment of the oral cavity and ability to cross the mucosal tissue.” *Drug Deliv* (2016) 23:2355–2362.

[40] Djaldetti R, Melamed E, “Levodopa ethylester: A novel rescue therapy for response fluctuations in Parkinson’s disease.” *Ann Neurol* (1996) 39:400–404.

[41] Maycock AL, Aster SD, Patchett AA, “Inactivation of 3-(3,4-dihydroxyphenyl)alanine decarboxylase by 2-(fluoromethyl)-3-(3,4-dihydroxyphenyl)alanine.” *Biochemistry* (1980) 19:709-718.

[42] Kubota H, Hayashi H, Watanabe T, Taguchi Y, Wada H, “Mechanism of inactivation of mammalian L-histidine decarboxylase by (S)-α- fluoromethylhistidine.” *Biochemical Pharmacology* (1984) 33(7):983-990.

[43] Strunecká A, Patočka J, Connett P, “Fluorine in medicine.” *Journal of Applied Biomedicine* (2004) 2:141-150.

[44] Arellano M., Malet-Martino M, Martino R, Gires P, “The anticancer drug 5-fluorouracil is metabolized by the isolated perfused rat liver and in rats into highly toxic fluoroacetate.” *Br J Cancer* (1998) 77:79-86.

[45] Struneck A, Patočka J, “Pharmacological and toxicological effects of aluminofluoride complexes.” *Fluoride* (1999) 32:230-242.

[46] Struneck A, Patočka J, “Aluminofluoride complexes: A useful tool in laboratory investigations, but a hidden danger for living organisms?” *Chemistry: From Fundamentals to Application* (2002) pp 271-282.

[47]Bertoldi M, Gonsalvi M, Voltattorni CB, “Green tea polyphenols: novel irreversible inhibitors of dopa decarboxylase.” *Biochem Biophys Res Commun* (2001) 284:90-93.

[48]Rodríguez-Caso C, Rodríguez-Agudo D, Sánchez-Jiménez F, Medina MA, “Green tea epigallocatechin-3-gallate is an inhibitor of mammalian histidine decarboxylase.” *CMLS Cell Mol Life Sci* (2003) 60:1760–1763.

[49]Ren J, Zhang Y, Jin H, Yu J, Zhou Y, Wu F, Zhang W, “Novel inhibitors of human DOPA decarboxylase extracted from Euonymus glabra Roxb.” *ACS Chem Biol* (2014) 9:897-903.

[50]Nitta Y, Kikuzaki H, Azuma T, Ye Y, Sakaue M, Higuch Y, Komori H, Ueno H, “Inhibitory activity of Filipendula ulmaria constituents on recombinant human histidine decarboxylase.” *Food Chemistry* (2013) 138:1551–1556.

[51]Inami Y, Matsui Y, Hoshino T, Murayama C, Norimoto H, “Inhibitory activity of the flower buds of Lonicera japonica Thunb against histamine production and L-histidine decarboxylase in human keratinocytes.” *Molecules* (2014) 19(6):8212-9.

[52]Daidone F, Montioli R, Paiardini A, Cellini B, Macchiarulo A, Giardina G, Bossa F, Borri Voltattorni C, “Identification by virtual screening and in vitro testing of human DOPA decarboxylase inhibitors.” *PLoS One* (2012) 7:e31610.

[53]Castro-Oropeza R, Pino-Angeles A, Khomutov MA, Urdiales JL, Moya-Garcìa AA, Vepsalainen J, Persson L, Sarabia F, Khomutov A, Sànchez-Jimènez F, “Aminooxy analog of histamine is an efficient inhibitor of mammalian L-histidine decarboxylase: combined in silico and experimental evidence.” *Amino Acids* (2014) 46:621–631.

[54]Yamamoto J, Fukui T, Suzuki K, Tanaka S, Yatsunami K, Ichikawa A, “Expression and characterization of recombinant mouse mastocytoma histidine decarboxylase.” *Biochim Biophys Acta* (1993) 1216:431–440.

[55]Yatsunami K, Tsuchikawa M, Kamada M, “Comparative studies of human recombinant 74- and 54-kDa L-histidine decarboxylase.” *J Biol Chem* (1995) 270:30813–30817.

[56]Tanaka S, Nemoto K, Yamamura E, Ohmura S, Ichikawa A, “Degradation of the 74 kDa form of L-histidine decarboxylase via the ubiquitin–proteasome pathway in a rat basophilic/mast cell line (RBL-2H3).” *FEBS Lett* (1997) 417:203–207.

[57]Tanaka S, Nemoto K, Yamamura E, Ichikawa A, “Intracellular localization of the 74- and 53-kDa forms of L-histidine decarboxylase in a rat basophilic/mast cell line, RBL-2H3.” *J Biol Chem* (1998) 273:8177–8182.

[58]Tanaka S, Deai K, Konomi A, Takahashi K, Yamane H, Sugimoto Y, “Expression of L-histidine decarboxylase in granules of elicited mouse polymorphonuclear leukocytes.” *Eur J Immunol* (2004) 34:1472–1482.

[59]Suzuki S, Tanaka S, Nemoto K, Ichikawa A, “Membrane targeting and binding of the 74-kDa form of mouse L-histidine decarboxylase via its carboxyl-terminal sequence.” *FEBS Lett* (1998) 437:44–48.

[60]Furuta K, Nakayama K, Sugimoto Y, Ichikawa A, Tanaka S, “Activation of histidine decarboxylase through post-translational cleavage by caspase-9 in a mouse mastocytoma P-815.” *J.Biol.Chem.*(2007) 282:13438–13446.

[61]Tanaka S, Fukui T, Yamamoto J, Shima Y, Kume T, Ohgo M, “Processing and activation of recombinant mouse mastocytoma histidine decarboxylase in the particulate fraction of Sf9 cells by porcine pancreatic elastase.” *Biochim Biophys Acta* (1995) 1253:9–12.

[62]Hadjiconstantinou M, Rossetti Z, Silvia C, Krajnc D, Neff NH, “Aromatic L-amino acid decarboxylase activity of the rat retina is modulated in vivo by environmental light.” *J Neurochem* (1988) 51(5):1560-1564.

[63]Rossetti ZL, Silvia CP, Krajnc D, Neff NH, Hadjiconstantinou M, “Aromatic L-amino acid decarboxylase is modulated by D1 dopamine receptors in rat retina.” *J Neurochem* (1990) 54(3):787-791.

[64]Rossetti Z, Krajnc D, Neff N H, Hadjiconstantinou M, “Modulation of retinal aromatic L-amino acid decarboxylase via alpha 2 adrenoceptors.” *J Neurochem* (1989) 52:647-652.

[65]Zhu MY, Juorio AV, Paterson IA, Boulton AA, “Regulation of aromatic L-amino acid decarboxylase by dopamine receptors in the rat brain.” *J Neuroehem* (1992) 58:63-641.

[66]Hadjiconstantinou M, Wemlinger TA, Silvia CP, Hubble JP, Neff NH, “Aromatic L-amino acid decarboxylase activity of mouse striatum is modulated via dopamine receptors.” *J Neurochem* (1993) 60:2175-2180.

[67]Zhu MY, Juorio AV, Paterson IA, Boulton AA, “Regulation of striatal aromatic L-amino acid decarboxylase: Effects of blockade or activation of dopamine receptors.” *Eur J Pharmacol* (1993) 238:157-164.

[68]Kemp BE, Pearson RB, “Protein kinase recognition sequence motifs.” *Trends Biochem Sci* (1990) 15:342-346.

[69]Young EA, Neff NH, Hadjiconstantinou M, “Evidence for cyclic AMP-mediated increase of aromatic L-amino acid decarboxylase activity in the striatum and midbrain.” *J Neurochem* (1993) 60:2331-2333.

[70]Young EA, Neff NH, Hadjiconstantinou M, “Phorbol ester administration transiently increases aromatic Lamino acid decarboxylase activity of the mouse striatum and midbrain.” *J Neurochem* (1994) 63:594-597.

[71]Duchemin AM, Berry MD, Neff NH, Hadjiconstantinou M, “Phosphorylation and activation of brain aromatic L-amino acid decarboxylase by cyclic AMP-dependent protein kinase.” *J Neurochem* (2000) 75:725-731.

[72]Tehranian R, Montoya SE, Van Laar AD, Hastings TG, Perez RG, “Alpha-synuclein inhibits aromatic amino acid decarboxylase activity in dopaminergic cells.” *J Neurochem* (2006) 99(4):1188-1196.

[73]Creese I, Sibley DR, Hamblin MW, Left SE, “The classification of dopamine receptors: relationship to radioligand binding.” *Ann Rev Neurosci* (1983) 6:43-71.

[74]Kebabian JW, Calne DB, “Multiple receptors for dopamine.” *Nature* (1979) 277:93-96.

[75]Zhu MY, Juorio AV, Paterson IA, Boulton AA, “Regulation of aromatic L-amino acid decarboxylase in rat striatal synaptosomes: Effects of dopamine receptor agonists and antagonists.” *Brit J Pharmacol* (1994) 112:23-30.

[76]Jafferji SS, Michell RH, “Stimulation of phosphatidylinositol turn-over by histamine, 5-hydroxytryptamine and adrenaline in the longitudinal smooth muscle of guinea pig ileum.” Biochem Pharmacol (1976) 25:1429-1430.

[77]Roth BL, Chuang DM, “Multiple mechanisms of serotonergic signal transduction.” Life Sci (1987) 41:1051-1064.

[78]Hammar L, “Mammalian histidine decarboxylase: effect by protein kinase on mouse mastocytoma histidine decarboxylase.” *Agents Actions* (1983) 13(2-3):246-249.

[79]Huszti Z, Magyar K, “Regulation of histidine decarboxylase activity in rat hypothalamus in vitro by ATP and cyclic AMP: enzyme inactivation under phosphorylating conditions.” *Agents Actions* (1984) 14(3-4):546-549.

[80]Huszti Z, Magyar K, “Stimulation of hypothalamic histidine decarboxylase by calcium-calmodulin and protein kinase (cAMP-dependent) inhibitor.” *Agents Actions* (1987) 20(3-4):233-235.

[81]Savany A, Cronenberger L, “Relationship between the multiple forms of rat gastric histidine decarboxylase: effects of conditions favouring phosphorylation and dephosphorylation.” *Biochem Int* (1990) 20(2):363-374.

[82]Borri Voltattorni C, Bertoldi M, “Dopa decarboxylase”, *Encyclopedia of Molecular Medicine* (2002) vol 2, pp 1089-1093.

[83]Hurley MJ, Jenner P, "What has been learnt from study of dopamine receptors in Parkinson's disease?" *Pharmacol Ther* (2006) 111(3):715–728.

[84]Hussain T, Lokhandwala MF, "Renal dopamine receptors and hypertension." *Exp Biol Med* (2003) 228(2):134–142.

[85]Ricci A, Mignini F, Tomassoni D, Amenta F, "Dopamine receptor subtypes in the human pulmonary arterial tree." *Auton Autacoid Pharmacol* (2006) 26(4):361–369.

[86]Cavallotti C, Massimo M, Paolo B, Maurizio S, Fiorenzo M, "Dopamine receptor subtypes in the native human heart." *Heart and Vessels* (2010) 25(5):432–437.

[87]Hoyer D, Clarke DE, Fozard JR, Hartig PR, Martin GR, Mylecharane EJ, Saxena PR, Humphrey PP, "International Union of Pharmacology classification of receptors for 5-hydroxytryptamine (Serotonin)." *Pharmacol Rev* (1994) 46(2):157–203.

[88]Eisenhofer G, Kopin IJ, Goldstein DS, "Catecholamine metabolism: a contemporary view with implications for physiology and medicine." *Pharmacological Reviews* (2004) 56(3):331–49.

[89]Amin F, Davidson M, Davis KL, "Homovanillic acid measurement in clinical research: a review of methodology." *Schizophrenia Bulletin* (1992) 18(1):123–148.

[90]Sulzer D, Zecca L, "Intraneuronal dopamine-quinone synthesis: a review." *Neurotoxicity Research* (2000) 1(3):181–195.

[91]Miyazaki I, Asanuma M, "Dopaminergic neuron-specific oxidative stress caused by dopamine itself." *Acta Medica Okayama* (2008) 62(3):141–150.

[92]Schultz W, "Multiple dopamine functions at different time courses." *Annual Review of Neuroscience* (2007) 30:259–188.

[93]Björklund A, Dunnett SB, "Dopamine neuron systems in the brain: an update." *Trends in Neurosciences* (2007) 30(5):194–202.

[94]Dahlstroem A, Fuxe K, "Evidence for the existence of monoamine-containing neurons in the central nervous system. I. Demonstration of monoamines in the cell bodies of brain stem neurons." *Acta Physiologica Scandinavica. Supplementum* (1964) SUPPL 232:1–55.

[95]Malenka RC, Nestler EJ, Hyman SE, "Chapter 6: Widely Projecting Systems: Monoamines, Acetylcholine, and Orexin." *Molecular Neuropharmacology: A Foundation for Clinical Neuroscience*, 2nd ed (2009) pp 147–148, 154–157.

[96]Paulus W, Schomburg ED, "Dopamine and the spinal cord in restless legs syndrome: does spinal cord physiology reveal a basis for augmentation?" *Sleep Medicine Reviews* (2006) 10(3):185–196.

[97]Ben-Jonathan N, Hnasko R, "Dopamine as a prolactin (PRL) inhibitor." Endocrine Reviews (2001) 22(6):724–763.

[98]Missale C, Nash SR, Robinson SW, Jaber M, Caron MG, "Dopamine receptors: from structure to function." *Physiological Reviews* (1998) 78(1):189–225.

[99]Rubí B, Maechler P, "Minireview: new roles for peripheral dopamine on metabolic control and tumor growth: let's seek the balance." *Endocrinology* (2010) 151(12):5570–5581.

[100] Buttarelli FR, Fanciulli A, Pellicano C, Pontieri FE, "The dopaminergic system in peripheral blood lymphocytes: from physiology to pharmacology and potential applications to neuropsychiatric disorders." *Current Neuropharmacology* (2011) 9(2):278–288.

[101] Sarkar C, Basu B, Chakroborty D, Dasgupta PS, Basu S, "The immunoregulatory role of dopamine: an update." *Brain, Behavior, and Immunity* (2010) 24(4):525–528.

[102] Frazer A, Hensler JG, "Understanding the neuroanatomical organization of serotonergic cells in the brain provides insight into the functions of this neurotransmitter." *Basic Neurochemistry* (1999) Sixth ed.

[103] Binder MD, Hirokawa N, *Encyclopedia of neuroscience* (2009) p. 705.

[104] Blier P, El Mansari M, "Serotonin and beyond: therapeutics for major depression." *Philosophical Transactions of the Royal Society of London. Series B, Biological Sciences* (2013) 368(1615):20120536.

[105] Chilmonczyk Z, Bojarski AJ, Pilc A, Sylte I, "Functional Selectivity and Antidepressant Activity of Serotonin 1A Receptor Ligands." *International Journal of Molecular Sciences* (2015) 16(8):18474–18506.

[106] King MW, "Serotonin." *The Medical Biochemistry Page, Indiana University School of Medicine* (2009).

[107] Berger M, Gray JA, Roth BL, "The expanded biology of serotonin". Annual Review of Medicine (2009) 60:355–366.

[108] Rang HP, *Pharmacology* (2003) p 187.

[109] Vanhoutte PM, "Serotonin and the vascular wall." International Journal of Cardiology (1987) 14(2):189–203.

[110] Marieb EN, *Essentials of Human Anatomy & Physiology*, 8th ed (2009) p 336.

[111] Lesurtel M, Graf R, Aleil B, Walther DJ, Tian Y, Jochum W, Gachet C, Bader M, Clavien PA, "Platelet-derived serotonin mediates liver regeneration." *Science* (2006) 312(5770):104–107.

[112] Collet C, Schiltz C, Geoffroy V, Maroteaux L, Launay JM, de Vernejoul MC, "The serotonin 5-HT2B receptor controls bone mass via osteoblast recruitment and proliferation." *FASEB Journal* (2008) 22(2):418–427.

[113] Yadav VK, Ryu JH, Suda N, Tanaka KF, Gingrich JA, Schütz G, Glorieux FH, Chiang CY, Zajac JD, Insogna KL, Mann JJ, Hen R, Ducy P, Karsenty G, "Lrp5 controls bone formation by inhibiting serotonin synthesis in the duodenum." *Cell* (2008) 135(5):825–837.

[114] Burchett SA, Hicks TP, "The mysterious trace amines: protean neuromodulators of synaptic transmission in mammalian brain." *Prog Neurobiol* (2006) 79(5–6):223–246.

[115] Broadley KJ, "The vascular effects of trace amines and amphetamines." *Pharmacol Ther* (2010) 125(3):363–375.

[116] Miller GM, "The emerging role of trace amine-associated receptor 1 in the functional regulation of monoamine transporters and dopaminergic activity." *J Neurochem* (2011) 116(2):164–176.

[117] Standaert DG, Walsh RR, "Pharmacology of dopaminergic neurotransmission." *Principles of Pharmacology: The Pathophysiologic Basis of Drug Therapy* (2011) pp 186–206.

[118] Kaasinen V, Vilkman H, Hietala J, Någren K, Helenius H, Olsson H, Farde L, Rinne J, "Age-related dopamine D2/D3 receptor loss in extrastriatal regions of the human brain." *Neurobiology of Aging* (2000) 21(5):683–688.

[119] Ota M, Yasuno F, Ito H, Seki C, Nozaki S, Asada T, Suhara T, "Age-related decline of dopamine synthesis in the living human brain measured by positron emission tomography with L-[beta-11C]DOPA." *Life Sciences* (2006) 79(8):730–736.

[120] Wang E, Snyder SD, *Handbook of the aging brain* (1988).

[121] Dickson DV, "Neuropathology of movement disorders." *Parkinson's disease and movement disorders* (2007) pp 271–283.

[122] Obeso JA, Rodriguez-Oroz MC, Goetz CG, Marin C, Kordower JH, Rodriguez M, Hirsch EC, Farrer M, Schapira AH, Halliday G, "Missing pieces in the Parkinson's disease puzzle." *Nature Medicine* (2010) 16(6):653–661.

[123] Schulz-Schaeffer WJ, "The synaptic pathology of alpha-synuclein aggregation in dementia with Lewy bodies, Parkinson's disease and Parkinson's disease dementia." Acta Neuropathologica (2010) 120(2):131–143.

[124] Jankovic J, "Parkinson's disease: clinical features and diagnosis." *Journal of Neurology, Neurosurgery, and Psychiatry* (2008) 79(4):368–376.

[125] Parker KL, Lamichhane D, Caetano MS, Narayanan NS, "Executive dysfunction in Parkinson's disease and timing deficits." *Frontiers in Integrative Neuroscience* (2013) 7:75.

[126] Caballol N, Martí MJ, Tolosa E, "Cognitive dysfunction and dementia in Parkinson disease." *Movement Disorders* (2007) 22:S358–66.

[127] Kalia LV, Lang AE, "Parkinson's disease." *Lancet* (2015) 386(9996):896–912.

[128] Lesage S, Brice A, "Parkinson's disease: from monogenic forms to genetic susceptibility factors." *Human Molecular Genetics* (2009) 18:R48–59.

[129] Samii A, Nutt JG, Ransom BR, "Parkinson's disease". *Lancet* (2004) 363(9423):1783–93.

[130] The National Collaborating Centre for Chronic Conditions, "Symptomatic pharmacological therapy in Parkinson's disease." *Parkinson's Disease* (2006) pp 59–100.

[131] Nord M, "Levodopa pharmacokinetics: from stomach to brain. A study on patients with Parkinson's disease." *Linköping University Electronic Press* (2017) p 10.

[132] Goldenberg MM, "Medical management of Parkinson's disease." *P & T* (2008) 33(10):590–606.

[133] Pedrosa DJ, Timmermann L, "Review: management of Parkinson's disease." Neuropsychiatric Disease and Treatment (2013) 9:321–340.

[134] The National Collaborating Centre for Chronic Conditions, "Palliative care in Parkinson's disease." *Parkinson's Disease* (2006) pp 147–151.

[135] de Lau LM, Breteler MM, "Epidemiology of Parkinson's disease." *The Lancet. Neurology* (2006) 5(6):525–535.

[136] AFF008E: Observational Phase 1b Follow-up Extension Study for Patients With Parkinson's Disease After Immunization With AFFITOPE® PD01A, ClinicalTrials.gov Identifier: NCT01885494.

[137] Kriks S, Shim JW, Piao J, Ganat YM, Wakeman DR, Xie Z, Carrillo-Reid L, Auyeung G, Antonacci C, Buch A, "Dopamine neurons derived from human ES cells efficiently engraft in animal models of Parkinson's disease." *Nature* (2011) 480:547-551.

[138] Grealish S, Diguet E, Kirkeby A, Mattsson B, Heuer A, Bramoulle Y, Van Camp N, Perrier AL, Hantraye P, Björklund A, “Human ESC derived dopamine neurons show similar preclinical efficacy and potency to fetal neurons when grafted in a rat model of Parkinson’s disease.” *Cell Stem Cell* (2014) 15:653-665.

[139] Muramatsu S, Okuno T, Suzuki Y, Nakayama T, Kakiuchi T, Takino N, Iida A, Ono F, Terao K, Inoue N, Nakano I, Kondo Y, Tsukada H, “Multitracer assessment of dopamine function after transplantation of embryonic stem cell derived neural stem cells in a primate model of Parkinson’s disease.” *Synapse* (2009) 63:541-548.

[140] Cho MS, Hwang DY, Kim DW, “Efficient derivation of functional dopaminergic neurons from human embryonic stem cells on a large scale.” *Nat Protoc* (2008) 3:1888–1894.

[141] Wu J, Xiao H, Sun H, Zou L, Zhu LQ, "Role of dopamine receptors in ADHD: a systematic meta-analysis." *Molecular Neurobiology* (2012) 45(3):605–620.

[142] Ilieva IP, Hook CJ, Farah MJ, "Prescription Stimulants' Effects on Healthy Inhibitory Control, Working Memory, and Episodic Memory: A Meta-analysis." *Journal of Cognitive Neuroscience* (2015) 27(6):1069–1089.

[143] Spencer RC, Devilbiss DM, Berridge CW, "The cognition-enhancing effects of psychostimulants involve direct action in the prefrontal cortex." *Biological Psychiatry* (2015) 77(11):940–950.

[144] Wood PB, "Role of central dopamine in pain and analgesia." *Expert Review of Neurotherapeutics* (2008) 8(5):781–797.

[145] Connolly BS, Lang AE, "Pharmacological treatment of Parkinson disease: a review." *JAMA* (2014) 311(16):1670–1683.

[146] Flake ZA, Scalley RD, Bailey AG, "Practical selection of antiemetics." *American Family Physician* (2004) 69(5):1169–1174.

[147] Goodman LS, Brunton LL, Chabner B, Knollmann BC, *Goodman and Gilman's pharmacological basis of therapeutics*. (2001) pp 459–461.

[148] de Wit R, Aapro M, Blower PR, "Is there a pharmacological basis for differences in 5-HT3-receptor antagonist efficacy in refractory patients?" *Cancer Chemotherapy and Pharmacology* (2005) 56(3):231–238.

[149] Brun L, Ngu LH, Keng WT, Ch’ng GS, Choy YS, Hwu WL, Lee WT, Willemsen MA, Verbeek MM, Wassenberg T, Regal L, Orcesi S, Tonduti D, Accorsi P, Testard H, Abdenur JE, Tay S, Allen GF, Heales S, Kern I, Kato M, Burlina A, Menegold C, Hoffmann GF, Blau N, “Clinical and biochemical features of aromatic L-amino acid decarboxylase deficiency.” *Neurology* (2010) 75:64-71.

[150] Pons R, Ford B, Chiriboga CA, Clayton PT, Hinton V, Hyland K, Sharma R, De Vivo DC, “Aromatic L-amino acid decarboxylase deficiency: clinical features, treatment, and prognosis.” *Neurology* (2004) 62(7):1058-1065.

[151] Hyland K, Clayton PT, “Aromatic amino acid decarboxylase deficiency in twins.” *J Inherit Metab Dis* (1990) 13(3):301-304.

[152] Montioli R, Dindo M, Giorgetti A, Piccoli S, Cellini B, Voltattorni CB, “A comprehensive picture of the mutations associated with aromatic amino acid decarboxylase deficiency: from molecular mechanisms to therapy implications.” Hum Mol Genet (2014) 23:5429-5440.

[153] Montioli R, Janson G, Paiardini A, Bertoldi M, Borri Voltattorni C, “Heterozygosis in aromatic amino acid decarboxylase deficiency: Evidence for a positive interallelic

complementation between R347Q and R358H mutations." *IUBMB Life* (2018) 70(3):215-223.

[154] Lee NC, Shieh YD, Chien YH, Tzen KY, Yu IS, Chen PW, Hu MH, Hu MK, Muramatsu S, Ichinose H, Hwu WL, "Regulation of the dopaminergic system in a murine model of aromatic L-amino acid decarboxylase deficiency." *Neurobiol Dis* (2013) 52:177-190.

[155] Lee NC, Chien YH, Hu MH, Liu WS, Chen PW, Wang WH, Tzen KY, Byrne BJ, Hwu WL, "Treatment of congenital neurotransmitter deficiencies by intracerebral ventricular injection of an adeno-associated virus serotype 9 vector." *Hum Gene Ther* (2014) 25(3):189-198.

[156] Christine CW, Starr PA, Larson PS, Eberling JL, Jagust WJ, Hawkins RA, VanBrocklin HF, Wright JF, Bankiewicz KS, Aminoff MJ, "Safety and tolerability of putaminal AADC gene therapy for Parkinson disease." *Neurology* (2009) 73(20):1662-1669.

[157] Lee NC, Muramatsu S, Chien YH, Liu WS, Wang WH, Cheng CH, Hu MK, Chen PW, Tzen KY, Byrne BJ, Hwu WL, "Benefits of Neuronal Preferential Systemic Gene Therapy for Neurotransmitter Deficiency." *Mol Ther* (2015) 23(10):1572-1581.

[158] Hwu WL, Muramatsu S, Tseng SH, Tzen KY, Lee NC, Chien YH, Snyder RO, Byrne BJ, Tai CH, Wu RM, "Gene therapy for aromatic L-amino acid decarboxylase deficiency." *Sci Transl Med* (2012) 4(134):134ra61.

[159] "A Clinical Trial for Treatment of Aromatic L-amino Acid Decarboxylase (AADC) Deficiency Using AAV2-hAADC - An Expansion" *ClinicalTrials.gov* Identifier: NCT02926066.

[160] "A Single-Stage, Adaptive, Open-label, Dose Escalation Safety and Efficacy Study of AADC Deficiency in Pediatric Patients (AADC)" *ClinicalTrials.gov* Identifier: NCT02852213.

[161] Hill SJ, Ganellin CR, Timmerman H, Schwartz JC, Shankley NP, Young JM, Schunack W, Levi R, Haas HL, "International Union of Pharmacology. XIII. Classification of histamine receptors." *Pharmacol Rev* (1997) 49(3):253–278.

[162] Ohtsu H, Watanabe T, "New function of histamine found in histidine decarboxylase gene knockout mice." *Biochem Biophys Res Commun* (2003) 305:443-447.

[163] Brown RE, Stevens DR, Haas HL, "The Physiology of Brain Histamine." *Progress in Neurobiology* 63(6):637–672.

[164] Panula P, Nuutinen S, "The histaminergic network in the brain: basic organization and role in disease." *Nat Rev Neurosci* (2013) 14:472-487.

[165] Håkanson R, Sundler F, "Histamine-producing cells in the stomach and their role in the regulation of acid secretion." *Scand J Gastroenterol Suppl* (1991) 180:88-94.

[166] Ashina K, Tsubosaka Y, Nakamura T, Omori K, Kobayashi K, Hori M, Ozaki H, Murata T, "Histamine Induces Vascular Hyperpermeability by Increasing Blood Flow and Endothelial Barrier Disruption In Vivo." *PLoS One* (2015) 10(7):e0132367.

[167] Metcalfe D, Baram D, Mekori J, "Mast cells." *Physiol Rev* (1997) 77:1033–1079.

[168] Leurs R, Smit MJ, Timmerman H, "Molecular pharmacological aspects of histamine receptors." *Pharmacol Ther* (1995) 66:413–463.

[169] Garbuzenko E, Nagler A, Pickholtz D, "Human mast cells stimulate fibroblast proliferation, collagen synthesis and lattice contraction: a direct role for mast cells in skin fibrosis." *Clin Exp Allergy* (2002) 32:237-246.

[170] Fitzsimons C, Engel N, Policastro L, “Regulation of phospholipase C activation by the number of H2 recepotrs during Ca2-induced differentiation of mouse keratinocytes.” *Biochem Pharmacol* (2002) 63:1785-96.

[171] Rodríguez-Martínez G, Velasco I, García-López G, Solís KH, Flores-Herrera H, Díaz NF, Molina-Hernández A, “Histamine is required during neural stem cell proliferation to increase neuron differentiation.” *Neuroscience* (2012) 216:10-17.

[172] Brandes LJ, Bogdanovic RP, Tong J, Davie JR, LaBella FS, “Intracellular histamine and liver regeneration: high affinity binding of histamine to chromatin, low affinity binding to matrix, and depletion of a nuclear storage pool following partial hepatectomy.” *Biochem Biophys Res Commun* (1992) 184(2):840-847.

[173] Bartus RT, Emerich DF, “Cholinergic markers in Alzheimer disease.” *JAMA* (1999) 282(23):2208e2209.

[174] Thirupathi AT, Akshitha CS, Sony K, Baqi MA, Rambabu K, Kumar VV, Mahender B, Venkateshwar Rao KN, “UPDATES ON ALZHEIMERS DISESASE”, *J Hosp Pharmacy* (2017) 12(2) Supplement Issue-A.

[175] Burns A, Iliffe S, "Alzheimer's disease." *BMJ* (2009) 338:b158.

[176] Povova J, Ambroz P, Bar M, Pavukova V, Sery O, Tomaskova H, “Epidemiological of and risk factors for Alzheimer's disease: a review.” *Biomed Pap Med Fac Univ Palacky Olomouc Czech Repub* (2012)156(2):108e114.

[177] Ballard C, Gauthier S, Corbett A, Brayne C, Aarsland D, Jones E, "Alzheimer's disease." *Lancet* (2011) 377(9770):1019–1031.

[178] Allgaier M, Allgaier C, “An update on drug treatment options of Alzheimer's disease.” *Front Biosci* (2014) 19:1345-1354.

[179] Bennett DA, Holtzman DM, “Immunization therapy for Alzheimer disease?” *Neurology* (2005) 64(1):10-12.

[180] Blandina P, Efoudebe M, Cenni G, Mannaioni P, Passani MB, “Acetylcholine, histamine, and cognition: two sides of the same coin.” *Learn Mem* (2004) 11(1):1-8.

[181] Dere E, Zlomuzica A, De Souza Silva MA, Ruocco LA, Sadile AG, Huston JP, “Neuronal histamine and the interplay of memory, reinforcement and emotions.” *Behav Brain Res* (2010) 215(2):209-220.

[182] Passani MB, Blandina P, “Histamine receptors in the CNS as targets for therapeutic intervention.” *Trends Pharmacol Sci* (2011) 32(4):242-249.

[183] Airaksinen MS, Paetau A, Paljarvi L, Reinikainen K, Riekkinen P, Suomalainen R, “Histamine neurons in human hypothalamus: anatomy in normal and Alzheimer diseased brains.” *Neuroscience* (1991) 44(2):465-481.

[184] Airaksinen MS, Reinikainen K, Riekkinen P, Panula P, “Neurofibrillary tangles and histamine-containing neurons in Alzheimer hypothalamus.” *Agents Actions* (1991) 33(1-2):104-107.

[185] Ishunina TA, van Heerikhuize JJ, Ravid R, Swaab DF, “Estrogen receptors and metabolic activity in the human tuberomamillary nucleus: changes in relation to sex, aging and Alzheimer's disease.” *Brain Res* (2003) 988(1-2):84-96.

[186] Higuchi M, Yanai K, Okamura N, Meguro K, Arai H, Itoh M, “Histamine H(1) receptors in patients with Alzheimer's disease assessed by positron emission tomography.” *Neuroscience* (2000) 99(4):721-729.

[187] Zlomuzica A, Dere D, Dere E, “The histamine H1 receptor and recollection-based discrimination in a temporal order memory task in the mouse.” *Pharmacol Biochem Behav* (2013) 111:58-63.

[188] Zlomuzica A, Ruocco LA, Sadile AG, Huston JP, Dere E, “Histamine H1 receptor knockout mice exhibit impaired spatial memory in the eight-arm radial maze.” *Br J Pharmacol* (2009) 157(1):86-91.

[189] Ambree O, Buschert J, Zhang W, Arolt V, Dere E, Zlomuzica A, “Impaired spatial learning and reduced adult hippocampal neurogenesis in histamine H1-receptor knockout mice.” *Eur Neuropsychopharmacol* (2014) 24(8):1394-1404.

[190] Bernardino L, Eiriz MF, Xapelli S, Grade S, Rosa A, Cortes L, “Histamine is a proneurogenic factor on subventricular zone stem/progenitor cells a new approach for brain repair therapies.” *Int J Dev Neurosci* (2010) 28(8):666-667.

[191] Bernardino L, Eiriz MF, Santos T, Xapelli S, Grade S, Rosa AI, “Histamine stimulates neurogenesis in the rodent subventricular zone.” *Stem Cells* (2012) 30(4):773-784.

[192] Molina-Hernandez A, Rodriguez-Martinez G, Escobedo-Avila I, Velasco I, “Histamine up-regulates fibroblast growth factor receptor 1 and increases FOXP2 neurons in cultured neural precursors by histamine type 1 receptor activation: conceivable role of histamine in neurogenesis during cortical development in vivo.” *Neural Dev* (2013) 8:4.

[193] Maruszak A, Pilarski A, Murphy T, Branch N, Thuret S, “Hippocampal neurogenesis in Alzheimer's disease: is there a role for dietary modulation?” *J Alzheimers Dis* (2014) 38(1):11-38.

[194] Mirshafiey A, Matsuo H, Nakane S, Rehm BH, Koh CS, Miyoshi S, “Novel immunosuppressive therapy by M2000 in experimental multiple sclerosis.” *Immunopharmacology and Immunotoxicology* (2005) 27(2):255265.

[195] Mattson MP, Taub DD, “Ancient viral protein enrages astrocytes in multiple sclerosis.” *Nat Neurosci* (2004) (10):1021-1023.

[196] Ichigi J, “Histamine release from mast cells of EAE rats by G(i) protein dependent and IgE-dependent pathways.” *Journal of Molecular Neuroscience* (1999) 13(1-2):93-99.

[197] Musio S, Gallo B, Scabeni S, “A key regulatory role for histamine in experimental autoimmune encephalomyelitis: disease exacerbation in histidine decarboxylase-deficient mice.” *Journal of Immunology* (2006) 176(1):17-26.

[198] Lindsey LK, Meng F, Alpini G, Francis H, “Histamine and histamine receptor regulation of gastrointestinal cancers.” *Transl Gastrointest Cancer* (2012) 1:215–227.

[199] Ghosh AK, Hirasawa N, Ohtsu H, “Defective angiogenesis in the inflammatory granulation tissue in histidine decarboxylase-deficient mice but not in mast cell-deficient mice.” *J Exp Med* (2002) 195:973-982.

[200] Kanda N, Watanabe S, “Histamine Inhibits the Production of Interferon-induced Protein of 10 kDa in Human Squamous Cell Carcinoma and Melanoma.” *J Invest Dermatol* (2002) 119:1411-1419.

[201] Landis SH, Murray T, Bolden S, Wingo PA, "Cancer statistics, 1998." *Ca* (1998) 48(1):6–29.

[202] Patel T, "Worldwide trends in mortality from biliary tract malignancies." *BMC Cancer* (2002) 2:10.

[203] Tietz PS, Larusso NF, "Cholangiocyte biology." *Current Opinion in Gastroenterology* (2006) 22(3):279–287.

[204] Holzinger F, Z'graggen K, Büchler MW, "Mechanisms of biliary carcinogenesis: a pathogenetic multi-stage cascade towards cholangiocarcinoma." *Annals of Oncology* (1999) 10(Suppl 4):122–126.

[205] Chapman RW, "Risk factors for biliary tract carcinogenesis." *Annals of Oncology* (1999) 10(Suppl 4):308–311.

[206] Tsaitas C, Semertzidou A, Sinakos E, "Update on inflammatory bowel disease in patients with primary sclerosing cholangitis." *World Journal of Hepatology* (2014) 6(4):178–187.

[207] Yamamoto M, Takasaki K, Yoshikawa T, "Lymph node metastasis in intrahepatic cholangiocarcinoma." *Japanese Journal of Clinical Oncology* (1999) 29(3):147–150.

[208] Farley DR, Weaver AL, Nagorney DM, ""Natural history of unresected cholangiocarcinoma: patient outcome after noncurative intervention." *Mayo Clinic Proceedings* (1995) 70(5):425–429.

[209] Rosen CB, Nagorney DM, Wiesner RH, Coffey RJ, La Russo NF, "Cholangiocarcinoma complicating primary sclerosing cholangitis." *Annals of Surgery* (1991) 213(1):21–25.

[210] Alpini G, Prall RT, LaRusso NF, "The pathobiology of biliary epithelia." *The Liver: Biology & Pathobiology*, 4th ed (2001) pp 421– 435.

[211] Munshi MK, Priester S, Gaudio E, Yang F, Alpini G, Mancinelli R, Wise C, Meng F, Franchitto A, Onori P, Glaser SS, "Regulation of biliary proliferation by neuroendocrine factors: implications for the pathogenesis of cholestatic liver diseases." *Am J Patho*l (2011) 178(2):472-484.

[212] Alvaro D, Mancino MG, Glaser S, Gaudio E, Marzioni M, Francis H, Alpini G, "Proliferating cholangiocytes: a neuroendocrine compartment in the diseased liver." *Gastroenterology* (2007) 132:415– 431.

[213] Kanno N, LeSage G, Glaser S, Alpini G, "Regulation of cholangiocytes bicarbonate secretion." *Am J Physiol Gastrointest Liver Physiol* (2001) 281:G612–G625.

[214] Alpini G, Glaser S, Ueno Y, Pham L, Podila PV, Caligiuri A, LeSage G, LaRusso NF, "Heterogeneity of the proliferative capacity of rat cholangiocytes after bile duct ligation." *Am J Physiol Gastrointest Liver Physiol* (1998) 274:G767–G775.

[215] Kanno N, LeSage G, Glaser S, Alvaro D, Alpini G, "Functional heterogeneity of the intrahepatic biliary epithelium." *Hepatology* (2000) 31:555–561.

[216] Glaser S, Benedetti A, Marucci L, Alvaro D, Baiocchi L, Kanno N, Caligiuri A, Phinizy JL, Chowdhury U, Papa E, LeSage G, Alpini G, "Gastrin inhibits cholangiocyte growth in bile duct-ligated rats by interaction with cholecystokinin-B/Gastrin receptors via D-myo-inositol 1,4,5-triphosphate-, Ca(2+)-, and protein kinase C alpha-dependent mechanisms." *Hepatology* (2000) 32:17–25.

[217] Francis H, Glaser S, Demorrow S, Gaudio E, Ueno Y, Venter J, Dostal D, Onori P, Franchitto A, Marzioni M, Vaculin S, Vaculin B, Katki K, Stutes M, Savage J, Alpini G, "Small mouse cholangiocytes proliferate in response to H1 histamine receptor stimulation by activation of the IP3/CaMK I/CREB pathway." *Am J Physiol Cell Physiol* (2008) 295:C499 –C513.

[218] Mancinelli R, Franchitto A, Gaudio E, Onori P, Glaser S, Francis H, Venter J, Demorrow S, Carpino G, Kopriva S, White M, Fava G, Alvaro D, Alpini G, "After damage of large bile ducts by gamma-aminobutyric acid, small ducts replenish the biliary

tree by amplification of calcium-dependent signaling and de novo acquisition of large cholangiocyte phenotypes." *Am J Pathol* (2010) 176:1790 –1800.

[219] Francis H, DeMorrow S, Venter J, Onori P, White M, Gaudio E, Francis T, Greene JF, Tran S, Meininger CJ, Alpini G, "Inhibition of histidine decarboxylase ablates the autocrine tumorigenic effects of histamine in human cholangiocarcinoma." *Gut* (2012) 61:753-764.

[220] Ercan-Sencicek AG, Stillman AA, Ghosh AK, Bilguvar K, O'Roak BJ, Mason CE, Abbott T, Gupta A, King RA, Pauls DL, Tischfield JA, Heiman GA, Singer HS, Gilbert DL, Hoekstra PJ, Morgan TM, Loring E, Yasuno K, Fernandez T, Sanders S, Louvi A, Cho JH, Mane S, Colangelo CM, Biederer T, Lifton RP, Gunel M, State MW, "L-histidine decarboxylase and Tourette's syndrome." *N Engl J Med* (2010) 362(20):1901-1908.

[221] Fernandez TV, Sanders SJ, Yurkiewicz IR, Ercan-Sencicek AG, Kim YS, Fishman DO, Raubeson MJ, Song Y, Yasuno K, Ho WS, "Rare copy number variants in tourette syndrome disrupt genes in histaminergic pathways and overlap with autism." *Biol Psychiatry* (2012) 71:392–402.

[222] Karagiannidis I, Dehning S, Sandor P, Tarnok Z, Rizzo R, Wolanczyk T, Madruga-Garrido M, Hebebrand J, Nothen MM, Lehmkuhl G, "Support of the histaminergic hypothesis in Tourette syndrome: association of the histamine decarboxylase gene in a large sample of families." *Journal of medical genetics* (2013) 50:760–764.

[223] Leckman JF, "Tourette's syndrome." *Lancet* (2002) 360(9345):1577-1586.

[224] Robertson MM1, Eapen V, Cavanna AE, "The international prevalence, epidemiology, and clinical phenomenology of Tourette syndrome: a cross-cultural perspective." *J Psychosom Res* (2009) 67(6):475-483.

[225] Scahill L1, Tanner C, Dure L, "The epidemiology of tics and Tourette syndrome in children and adolescents." *Adv Neurol* (2001) 85:261-271.

[226] Canitano R, Vivanti G, "Tics and Tourette syndrome in autism spectrum disorders." *Autism: the international journal of research and practice* (2007) 11:19–28.

[227] Hirschtritt ME, Lee PC, Pauls DL, Dion Y, Grados MA, Illmann C, King RA, Sandor P, McMahon WM, Lyon GJ, "Lifetime prevalence, age of risk, and genetic relationships of comorbid psychiatric disorders in Tourette syndrome." *JAMA Psychiatry* (2015) 72:325–333.

[228] Singer HS, Wong DF, Brown JE, Brandt J, Krafft L, Shaya E, Dannals RF, Wagner HN Jr, "Positron emission tomography evaluation of dopamine D-2 receptors in adults with Tourette syndrome." *Adv Neurol* (1992) 58:233-239.

[229] Denys D, de Vries F, Cath D, Figee M, Vulink N, Veltman DJ, van der Doef TF, Boellaard R, Westenberg H, van Balkom A, Lammertsma AA, van Berckel BN, "Dopaminergic activity in Tourette syndrome and obsessive-compulsive disorder." *Eur Neuropsychopharmacol* (2013) 23(11):1423-1431.

[230] Bloch MH, "Emerging treatments for Tourette's disorder." *Curr Psychiatry Rep* (2008) 10(4):323-330.

[231] Canales JJ, Graybiel AM, "Patterns of gene expression and behavior induced by chronic dopamine treatments." *Ann Neurol* (2000) 47(4 Suppl 1):S53-59.

[232] Rapanelli M, Frick LR, Pogorelov V, Ota KT, Abbasi E, Ohtsu H, Pittenger C, "Dysregulated intracellular signaling in the striatum in a pathophysiologically grounded model of Tourette syndrome." *Eur Neuropsychopharmacol* (2014) 24(12):1896-1906.

[233] Baldan LC, Williams KA, Gallezot JD, Pogorelov V, Rapanelli M, Crowley M, Anderson GM, Loring E, Gorczyca R, Billingslea E, Wasylink S, Panza KE, Ercan-Sencicek AG, Krusong K, Leventhal BL, Ohtsu H, Bloch MH, Hughes ZA, Krystal JH, Mayes L, de Araujo I, Ding YS, State MW, Pittenger C, "Histidine decarboxylase deficiency causes tourette syndrome: parallel findings in humans and mice." *Neuron* (2014) 81(1):77-90.

[234] Rapanelli M, "The magnificent two: histamine and the H3 receptor as key modulators of striatal circuitry." *Prog Neuropsychopharmacol Biol Psychiatry* (2017) 73:36-40.

[235] Thomson JA, Itskovitz-Eldor J, Shapiro SS, Waknitz MA, Swiergiel JJ, Marshall VS, Jones JM, "Embryonic stem cell lines derived from human blastocysts." *Science* (1998) 282(5391):1145-1147.

[236] Takahashi K, Yamanaka S, "Induction of pluripotent stem cells from mouse embryonic and adult fibroblast cultures by defined factors." *Cell* (2006) 126(4):663-676.

[237] Okita K, Ichisaka T, Yamanaka S, "Generation of germline-competent induced pluripotent stem cells". *Nature* (2007) 448(7151): 313–317.

[238] Maherali N, Sridharan R, Xie W, Utikal J, Eminli S, Arnold K, Stadtfeld M, Yachechko R, Tchieu J, Jaenisch R, Plath K, Hochedlinger K, "Directly reprogrammed fibroblasts show global epigenetic remodeling and widespread tissue contribution." *Cell Stem Cell* (2007) 1(1):55-70.

[239] Wernig M, Meissner A, Foreman R, Brambrink T, Ku M, Hochedlinger K, Bernstein BE, Jaenisch R, "In vitro reprogramming of fibroblasts into a pluripotent ES-cell-like state." *Nature* (2007) 448(7151):318-324.

[240] Takahashi K, Tanabe K, Ohnuki M, Narita M, Ichisaka T, Tomoda K, Yamanaka S, "Induction of pluripotent stem cells from adult human fibroblasts by defined factors." *Cell* (2007) 131(5):861-872.

[241] Yu J, Vodyanik MA, Smuga-Otto K, Antosiewicz-Bourget J, Frane JL, Tian S, Nie J, Jonsdottir GA, Ruotti V, Stewart R, Slukvin II, Thomson JA, "Induced pluripotent stem cell lines derived from human somatic cells." *Science* (2007) 318(5858):1917-1920.

[242] Maherali N, Ahfeldt T, Rigamonti A, Utikal J, Cowan C, Hochedlinger K, "A high-efficiency system for the generation and study of human induced pluripotent stem cells." *Cell Stem Cell* (2008) 3(3):340-345.

[243] Aasen T, Raya A, Barrero MJ, Garreta E, Consiglio A, Gonzalez F, Vassena R, Bilić J, Pekarik V, Tiscornia G, Edel M, Boué S, Izpisúa Belmonte JC, "Efficient and rapid generation of induced pluripotent stem cells from human keratinocytes." *Nat Biotechnol* (2008) 26(11):1276-1284.

[244] Staerk J, Dawlaty MM, Gao Q, Maetzel D, Hanna J, Sommer CA, Mostoslavsky G, Jaenisch R, "Reprogramming of human peripheral blood cells to induced pluripotent stem cells." *Cell Stem Cell* (2010) 7(1):20-24.

[245] Loh YH, Hartung O, Li H, Guo C, Sahalie JM, Manos PD, Urbach A, Heffner GC, Grskovic M, Vigneault F, Lensch MW, Park IH, Agarwal S, Church GM, Collins JJ, Irion S, Daley GQ, "Reprogramming of T cells from human peripheral blood." *Cell Stem Cell* (2010) 7(1):15-19.

[246] Zhou T, Benda C, Dunzinger S, Huang Y, Ho JC, Yang J, Wang Y, Zhang Y, Zhuang Q, Li Y, Bao X, Tse HF, Grillari J, Grillari-Voglauer R, Pei D, Esteban MA, "Generation of human induced pluripotent stem cells from urine samples." *Nat Protoc* (2012) 7(12):2080-9.

[247] Takeda J, Seino S, Bell GI, "Human Oct3 gene family: cDNA sequences, alternative splicing, gene organization, chromosomal location, and expression at low levels in adult tissues." *Nucleic Acids Res* (1992) 20(17):4613-4620.

[248] Boyer LA, Lee TI, Cole MF, Johnstone SE, Levine SS, Zucker JP, Guenther MG, Kumar RM, Murray HL, Jenner RG, Gifford DK, Melton DA, Jaenisch R, Young RA, "Core transcriptional regulatory circuitry in human embryonic stem cells." *Cell* (2005) 122(6):947-956.

[249] Niwa H, Miyazaki J, Smith AG, "Quantitative expression of Oct-3/4 defines differentiation, dedifferentiation or self-renewal of ES cells." *Nat Genet* (2000) 24(4):372-376.

[250] Masui S, Nakatake Y, Toyooka Y, Shimosato D, Yagi R, Takahashi K, Okochi H, Okuda A, Matoba R, Sharov AA, Ko MS, Niwa H, "Pluripotency governed by Sox2 via regulation of Oct3/4 expression in mouse embryonic stem cells." *Nat Cell Biol* (2007) 9(6):625-635.

[251] Shields JM, Christy RJ, Yang VW, "Identification and characterization of a gene encoding a gut-enriched Krüppel-like factor expressed during growth arrest." *J Biol Chem* (1996) 271(33):20009-20017.

[252] Chen X, Johns DC, Geiman DE, Marban E, Dang DT, Hamlin G, Sun R, Yang VW, "Krüppel-like factor 4 (gut-enriched Krüppel-like factor) inhibits cell proliferation by blocking G1/S progression of the cell cycle." *J Biol Chem* (2001) 276(32):30423-30428.

[253] Dang DT, Chen X, Feng J, Torbenson M, Dang LH, Yang VW, "Overexpression of Krüppel-like factor 4 in the human colon cancer cell line RKO leads to reduced tumorigenicity." *Oncogene* (2003) 22(22):3424-3430.

[254] Yoon HS, Yang VW, "Requirement of Krüppel-like factor 4 in preventing entry into mitosis following DNA damage." *J Biol Chem* (2004) 279(6):5035-5041.

[255] Yoon HS, Chen X, Yang VW, "Kruppel-like factor 4 mediates p53-dependent G1/S cell cycle arrest in response to DNA damage." *J Biol Chem* (2003) 278(4):2101-2105.

[256] Yoon HS, Ghaleb AM, Nandan MO, Hisamuddin IM, Dalton WB, Yang VW, "Krüppel-like factor 4 prevents centrosome amplification following gamma-irradiation-induced DNA damage." *Oncogene* (2005) 24(25):4017-4025.

[257] Rowland BD, Bernards R, Peeper DS, "The KLF4 tumour suppressor is a transcriptional repressor of p53 that acts as a context-dependent oncogene." *Nat Cell Biol* (2005) 7(11):1074-1082.

[258] McConnell BB, Ghaleb AM, Nandan MO, Yang VW, "The diverse functions of Krüppel-like factors 4 and 5 in epithelial biology and pathobiology." *Bioessays* (2007) 29(6):549-557.

[259] Wang B, Zhao MZ, Cui NP, Lin DD, Zhang AY, Qin Y, Liu CY, Yan WT, Shi JH, Chen BP, "Krüppel-like factor 4 induces apoptosis and inhibits tumorigenic progression in SK-BR-3 breast cancer cells." *FEBS Open Bio* (2015) 5:147-154.

[260] Whitlock NC, Bahn JH, Lee SH, Eling TE, Baek SJ, "Resveratrol-induced apoptosis is mediated by early growth response-1, Krüppel-like factor 4, and activating transcription factor 3." *Cancer Prev Res* (2011) 4(1):116-127.

[261] Chen Y, McGee J, Chen X, Doman TN, Gong X, Zhang Y, Hamm N, Ma X, Higgs RE, Bhagwat SV, Buchanan S, Peng SB, Staschke KA, Yadav V, Yue Y, Kouros-Mehr H, "Identification of druggable cancer driver genes amplified across TCGA datasets." *PLoS One* (2014) 9(5):e98293.

[262] Mitsui K, Tokuzawa Y, Itoh H, Segawa K, Murakami M, Takahashi K, Maruyama M, Maeda M, Yamanaka S, “The homeoprotein Nanog is required for maintenance of pluripotency in mouse epiblast and ES cells.” *Cell* (2003) 113(5):631-642.

[263] Rodda DJ, Chew JL, Lim LH, Loh YH, Wang B, Ng HH, Robson P, “Transcriptional regulation of nanog by OCT4 and SOX2.” *J Biol Chem* (2005) 280(26):24731-24737.

[264] Thomson M, Liu SJ, Zou LN, Smith Z, Meissner A, Ramanathan S, “Pluripotency factors in embryonic stem cells regulate differentiation into germ layers.” *Cell* (2011) 145(6):875-889.

[265] Polesskaya A, Cuvellier S, Naguibneva I, Duquet A, Moss EG, Harel-Bellan A, "Lin-28 binds IGF-2 mRNA and participates in skeletal myogenesis by increasing translation efficiency." *Genes & Development* (2007) 211(9):1125–1138.

[266] Yang DH, Moss EG, "Temporally regulated expression of Lin-28 in diverse tissues of the developing mouse." Gene Expression Patterns (2003) 3(6): 719–726.

[267] Stadtfeld M, Nagaya M, Utikal J, Weir G, Hochedlinger K, “Induced pluripotent stem cells generated without viral integration.” *Science* (2008) 322(5903):945-949.

[268] Zhou W, Freed CR, “Adenoviral gene delivery can reprogram human fibroblasts to induced pluripotent stem cells.” *Stem Cells* (2009) 27(11):2667-2674.

[269] Okita K, Nakagawa M, Hyenjong H, Ichisaka T, Yamanaka S, “Generation of mouse induced pluripotent stem cells without viral vectors.” *Science* (2008) 322(5903):949-953.

[270] Huangfu D, Maehr R, Guo W, Eijkelenboom A, Snitow M, Chen AE, Melton DA, “Induction of pluripotent stem cells by defined factors is greatly improved by small-molecule compounds.” *Nat Biotechnol* (2008) 26(7):795-797.

[271] Shi Y, Desponts C, Do JT, Hahm HS, Schöler HR, Ding S, “Induction of pluripotent stem cells from mouse embryonic fibroblasts by Oct4 and Klf4 with small-molecule compounds.” *Cell Stem Cell* (2008) 3(5):568-574.

[272] Hou P, Li Y, Zhang X, Liu C, Guan J, Li H, Zhao T, Ye J, Yang W, Liu K, Ge J, Xu J, Zhang Q, Zhao Y, Deng H, “Pluripotent stem cells induced from mouse somatic cells by small-molecule compounds.” *Science* (2013) 341(6146):651-654.

[273] Judson RL, Babiarz JE, Venere M, Blelloch R, “Embryonic stem cell-specific microRNAs promote induced pluripotency.” *Nat Biotechnol* (2009) 27(5):459-461.

[274] Bao X, Zhu X, Liao B, Benda C, Zhuang Q, Pei D, Qin B, Esteban MA, “MicroRNAs in somatic cell reprogramming.” *Curr Opin Cell Biol* (2013) 25(2):208-214.

[275] Shi Y, Kirwan P, Smith J, Robinson HP, Livesey FJ, “Human cerebral cortex development from pluripotent stem cells to functional excitatory synapses.” *Nat Neurosci* (2012) 15(3):477-486.

[276] Maury Y, Côme J, Piskorowski RA, Salah-Mohellibi N, Chevaleyre V, Peschanski M, Martinat C, Nedelec S, “Combinatorial analysis of developmental cues efficiently converts human pluripotent stem cells into multiple neuronal subtypes.” *Nat Biotechnol* (2015) 33(1):89-96.

[277] Cajánek L, Ribeiro D, Liste I, Parish CL, Bryja V, Arenas E, “Wnt/beta-catenin signaling blockade promotes neuronal induction and dopaminergic differentiation in embryonic stem cells.” *Stem Cells* (2009) 27(12):2917-2927.

[278] Douvaras P, Fossati V, “Generation and isolation of oligodendrocyte progenitor cells from human pluripotent stem cells.” *Nat Protoc* (2015) 10(8):1143-1154.

[279] Shaltouki A, Peng J, Liu Q, Rao MS, Zeng X, “Efficient generation of astrocytes from human pluripotent stem cells in defined conditions.” *Stem Cells* (2013) 31(5):941-952.

[280] Laflamme MA, Chen KY, Naumova AV, Muskheli V, Fugate JA, Dupras SK, Reinecke H, Xu C, Hassanipour M, Police S, O'Sullivan C, Collins L, Chen Y, Minami E, Gill EA, Ueno S, Yuan C, Gold J, Murry CE, “Cardiomyocytes derived from human embryonic stem cells in pro-survival factors enhance function of infarcted rat hearts.” *Nat Biotechnol* (2007) 25(9):1015-1024.

[281] Mummery C, Ward-van Oostwaard D, Doevendans P, Spijker R, van den Brink S, Hassink R, van der Heyden M, Opthof T, Pera M, de la Riviere AB, Passier R, Tertoolen L, “Differentiation of human embryonic stem cells to cardiomyocytes: role of coculture with visceral endoderm-like cells.” *Circulation* (2003) 107(21):2733-2740.

[282] Kehat I, Kenyagin-Karsenti D, Snir M, Segev H, Amit M, Gepstein A, Livne E, Binah O, Itskovitz-Eldor J, Gepstein L, “Human embryonic stem cells can differentiate into myocytes with structural and functional properties of cardiomyocytes.” *J Clin Invest* (2001) 108(3):407-414.

[283] Burridge PW, Matsa E, Shukla P, Lin ZC, Churko JM, Ebert AD, Lan F, Diecke S, Huber B, Mordwinkin NM, Plews JR, Abilez OJ, Cui B, Gold JD, Wu JC, “Chemically defined generation of human cardiomyocytes.” *Nat Methods* (2014) 11(8):855-860.

[284] Roelandt P, Vanhove J, Verfaillie C, “Directed differentiation of pluripotent stem cells to functional hepatocytes.” *Methods Mol Biol* (2013) 997:141-147.

[285] Schwartz RE, Linehan JL, Painschab MS, Hu WS, Verfaillie CM, Kaufman DS, “Defined conditions for development of functional hepatic cells from human embryonic stem cells.” *Stem Cells Dev* (2005) 14(6):643-655.

[286] Basma H, Soto-Gutiérrez A, Yannam GR, Liu L, Ito R, Yamamoto T, Ellis E, Carson SD, Sato S, Chen Y, Muirhead D, Navarro-Alvarez N, Wong RJ, Roy-Chowdhury J, Platt JL, Mercer DF, Miller JD, Strom SC, Kobayashi N, Fox IJ, “Differentiation and transplantation of human embryonic stem cell-derived hepatocytes.” *Gastroenterology* (2009) 136(3):990-999.

[287] Zirra A, Wiethoff S, Patani R, “Neural Conversion and Patterning of Human Pluripotent Stem Cells: A Developmental Perspective.” *Stem Cells Int* (2016) 2016:8291260.

[288] Arenas E, Denham M, Villaescusa JC, “How to make a midbrain dopaminergic neuron.” *Development* (2015) 142(11):1918-1936.

[289] Chi CL, Martinez S, Wurst W, Martin GR, “The isthmic organizer signal FGF8 is required for cell survival in the prospective midbrain and cerebellum.” *Development* (2003) 130(12):2633-2644.

[290] Martinez S, Crossley PH, Cobos I, Rubenstein JL, Martin GR, “FGF8 induces formation of an ectopic isthmic organizer and isthmocerebellar development via a repressive effect on Otx2 expression.” *Development* (1999) 126(6):1189-1200.

[291] Basson MA, Echevarria D, Ahn CP, Sudarov A, Joyner AL, Mason IJ, Martinez S, Martin GR, “Specific regions within the embryonic midbrain and cerebellum require different levels of FGF signalling during development.” *Development* (2008) 135(5):889-898.

[292] Sato T, Nakamura H, “The Fgf8 signal causes cerebellar differentiation by activating the Ras-ERK signalling pathway.” *Development* (2004) 131(17):4275-4285.

[293] Suzuki-Hirano A, Sato T, Nakamura H, "Regulation of isthmic Fgf8 signal by sprouty2." *Development* (2005) 132(2):257-265.

[294] Lin W, Metzakopian E, Mavromatakis YE, Gao N, Balaskas N, Sasaki H, Briscoe J, Whitsett JA, Goulding M, Kaestner KH, Ang SL, "Foxa1 and Foxa2 function both upstream of and cooperatively with Lmx1a and Lmx1b in a feedforward loop promoting mesodiencephalic dopaminergic neuron development." *Dev Biol* (2009) 333(2):386-396.

[295] Ono Y, Nakatani T, Sakamoto Y, Mizuhara E, Minaki Y, Kumai M, Hamaguchi A, Nishimura M, Inoue Y, Hayashi H, Takahashi J, Imai T, "Differences in neurogenic potential in floor plate cells along an anteroposterior location: midbrain dopaminergic neurons originate from mesencephalic floor plate cells." *Development* (2007) 134(17):3213-3225.

[296] Andersson E, Tryggvason U, Deng Q, Friling S, Alekseenko Z, Robert B, Perlmann T, Ericson J, "Identification of intrinsic determinants of midbrain dopamine neurons." *Cell* (2006) 124(2):393-405.

[297] Deng Q, Andersson E, Hedlund E, Alekseenko Z, Coppola E, Panman L, Millonig JH, Brunet JF, Ericson J, Perlmann T, "Specific and integrated roles of Lmx1a, Lmx1b and Phox2a in ventral midbrain development." *Development* (2011) 138(16):3399-3408.

[298] Andersson E, Jensen JB, Parmar M, Guillemot F, Björklund A, "Development of the mesencephalic dopaminergic neuron system is compromised in the absence of neurogenin 2." *Development* (2006) 133(3):507-516.

[299] Smidt MP, Asbreuk CH, Cox JJ, Chen H, Johnson RL, Burbach JP, "A second independent pathway for development of mesencephalic dopaminergic neurons requires Lmx1b." *Nat Neurosci* (2000) 3(4):337-341.

[300] Ferri AL, Lin W, Mavromatakis YE, Wang JC, Sasaki H, Whitsett JA, Ang SL, "Foxa1 and Foxa2 regulate multiple phases of midbrain dopaminergic neuron development in a dosage-dependent manner." *Development* (2007) 134(15):2761-2769.

[301] Stott SR, Metzakopian E, Lin W, Kaestner KH, Hen R, Ang SL, "Foxa1 and Foxa2 are required for the maintenance of dopaminergic properties in ventral midbrain neurons at late embryonic stages." *J Neurosci* (2013) 33(18):8022-8034.

[302] Chung S, Leung A, Han BS, Chang MY, Moon JI, Kim CH, Hong S, Pruszak J, Isacson O, Kim KS, "Wnt1-Lmx1a forms a novel autoregulatory loop and controls midbrain dopaminergic differentiation synergistically with the SHH-FoxA2 pathway." *Cell Stem Cell* (2009) 5(6):646-658.

[303] Prakash N, Brodski C, Naserke T, Puelles E, Gogoi R, Hall A, Panhuysen M, Echevarria D, Sussel L, Weisenhorn DM, Martinez S, Arenas E, Simeone A, Wurst W, "A Wnt1-regulated genetic network controls the identity and fate of midbrain-dopaminergic progenitors in vivo." *Development* (2006) 133(1):89-98.

[304] Gil M, McKinney C, Lee MK, Eells JB, Phyillaier MA, Nikodem VM, "Regulation of GTP cyclohydrolase I expression by orphan receptor Nurr1 in cell culture and in vivo." *J Neurochem* (2007) 101(1):142-150.

[305] Jankovic J, Chen S, Le WD, "The role of Nurr1 in the development of dopaminergic neurons and Parkinson's disease." *Prog Neurobiol* (2005) 77(1-2):128-138.

[306] Joseph B, Wallén-Mackenzie A, Benoit G, Murata T, Joodmardi E, Okret S, Perlmann T, "p57(Kip2) cooperates with Nurr1 in developing dopamine cells." *Proc Natl Acad Sci USA* (2003) 100(26):15619-15624.

[307] Saucedo-Cardenas O, Quintana-Hau JD, Le WD, Smidt MP, Cox JJ, De Mayo F, Burbach JP, Conneely OM, "Nurr1 is essential for the induction of the dopaminergic

phenotype and the survival of ventral mesencephalic late dopaminergic precursor neurons." *Proc Natl Acad Sci USA* (1998) 95(7):4013-4018.

[308] Smits SM, Ponnio T, Conneely OM, Burbach JP, Smidt MP, "Involvement of Nurr1 in specifying the neurotransmitter identity of ventral midbrain dopaminergic neurons." *Eur J Neurosci* (2003) 18(7):1731-1738.

[309] Castro DS, Hermanson E, Joseph B, Wallén A, Aarnisalo P, Heller A, Perlmann T, "Induction of cell cycle arrest and morphological differentiation by Nurr1 and retinoids in dopamine MN9D cells." *J Biol Chem* (2001) 276(46):43277-43284.

[310] Volpicelli F, Caiazzo M, Greco D, Consales C, Leone L, Perrone-Capano C, Colucci D'Amato L, di Porzio U, "Bdnf gene is a downstream target of Nurr1 transcription factor in rat midbrain neurons in vitro." *J Neurochem* (2007) 102(2):441-453.

[311] Zetterström RH, Solomin L, Jansson L, Hoffer BJ, Olson L, Perlmann T, "Dopamine neuron agenesis in Nurr1-deficient mice." *Science* (1997) 276(5310):248-250.

[312] Jacobs FM, Veenvliet JV, Almirza WH, Hoekstra EJ, von Oerthel L, van der Linden AJ, Neijts R, Koerkamp MG, van Leenen D, Holstege FC, Burbach JP, Smidt MP, "Retinoic acid-dependent and -independent gene-regulatory pathways of Pitx3 in meso-diencephalic dopaminergic neurons." *Development* (2011) 138(23):5213-5222.

[313] Veenvliet JV, Dos Santos MT, Kouwenhoven WM, von Oerthel L, Lim JL, van der Linden AJ, Koerkamp MJ, Holstege FC, Smidt MP, "Specification of dopaminergic subsets involves interplay of En1 and Pitx3." *Development* (2013) 140(16):3373-3384.

[314] Jacobs FM, van Erp S, van der Linden AJ, von Oerthel L, Burbach JP, Smidt MP, "Pitx3 potentiates Nurr1 in dopamine neuron terminal differentiation through release of SMRT-mediated repression." *Development* (2009) 136(4):531-540.

[315] Volpicelli F, De Gregorio R, Pulcrano S, Perrone-Capano C, di Porzio U, Bellenchi GC, "Direct regulation of Pitx3 expression by Nurr1 in culture and in developing mouse midbrain." *PLoS One* (2012) 7(2):e30661.

[316] Kadkhodaei B, Ito T, Joodmardi E, Mattsson B, Rouillard C, Carta M, Muramatsu S, Sumi-Ichinose C, Nomura T, Metzger D, Chambon P, Lindqvist E, Larsson NG, Olson L, Björklund A, Ichinose H, Perlmann T, "Nurr1 is required for maintenance of maturing and adult midbrain dopamine neurons." *J Neurosci* (2009) 29(50):15923-15932.

[317] van den Munckhof P, Luk KC, Ste-Marie L, Montgomery J, Blanchet PJ, Sadikot AF, Drouin J, "Pitx3 is required for motor activity and for survival of a subset of midbrain dopaminergic neurons." *Development* (2003) 130(11):2535-2542.

[318] Alvarez-Fischer D, Fuchs J, Castagner F, Stettler O, Massiani-Beaudoin O, Moya KL, Bouillot C, Oertel WH, Lombès A, Faigle W, Joshi RL, Hartmann A, Prochiantz A, "Engrailed protects mouse midbrain dopaminergic neurons against mitochondrial complex I insults." *Nat Neurosci* (2011) 14(10):1260-1266.

[319] Frim DM, Uhler TA, Galpern WR, Beal MF, Breakefield XO, Isacson O, "Implanted fibroblasts genetically engineered to produce brain-derived neurotrophic factor prevent 1-methyl-4-phenylpyridinium toxicity to dopaminergic neurons in the rat." *Proc Natl Acad Sci USA* (1994) 91(11):5104-5108.

[320] Hyman C, Hofer M, Barde YA, Juhasz M, Yancopoulos GD, Squinto SP, Lindsay RM, "BDNF is a neurotrophic factor for dopaminergic neurons of the substantia nigra." *Nature* (1991) 350(6315):230-232.

[321] Akerud P, Canals JM, Snyder EY, Arenas E, "Neuroprotection through delivery of glial cell line-derived neurotrophic factor by neural stem cells in a mouse model of Parkinson's disease." *J Neurosci* (2001) 21(20):8108-8118.

[322] Arenas E, Trupp M, Akerud P, Ibáñez CF, “GDNF prevents degeneration and promotes the phenotype of brain noradrenergic neurons in vivo.” *Neuron* (1995) 15(6):1465-1473.

[323] Beck KD, Valverde J, Alexi T, Poulsen K, Moffat B, Vandlen RA, Rosenthal A, Hefti F, “Mesencephalic dopaminergic neurons protected by GDNF from axotomy-induced degeneration in the adult brain.” *Nature* (1995) 373(6512):339-341.

[324] Choi-Lundberg DL, Lin Q, Chang YN, Chiang YL, Hay CM, Mohajeri H, Davidson BL, Bohn MC, “Dopaminergic neurons protected from degeneration by GDNF gene therapy.” *Science* (1997) 275(5301):838-841.

[325] Gash DM, Zhang Z, Ovadia A, Cass WA, Yi A, Simmerman L, Russell D, Martin D, Lapchak PA, Collins F, Hoffer BJ, Gerhardt GA, “Functional recovery in parkinsonian monkeys treated with GDNF.” *Nature* (1996) 380(6571):252-255.

[326] Kordower JH, Emborg ME, Bloch J, Ma SY, Chu Y, Leventhal L, McBride J, Chen EY, Palfi S, Roitberg BZ, Brown WD, Holden JE, Pyzalski R, Taylor MD, Carvey P, Ling Z, Trono D, Hantraye P, Déglon N, Aebischer P, “Neurodegeneration prevented by lentiviral vector delivery of GDNF in primate models of Parkinson's disease.” *Science* (2000) 290(5492):767-773.

[327] Lin LF, Doherty DH, Lile JD, Bektesh S, Collins F, “GDNF: a glial cell line-derived neurotrophic factor for midbrain dopaminergic neurons.” *Science* (1993) 260(5111):1130-1132.

[328] Rosenblad C, Martinez-Serrano A, Björklund A, “Intrastriatal glial cell line-derived neurotrophic factor promotes sprouting of spared nigrostriatal dopaminergic afferents and induces recovery of function in a rat model of Parkinson's disease.” *Neuroscience* (1998) 82(1):129-137.

[329] Tomac A, Lindqvist E, Lin LF, Ogren SO, Young D, Hoffer BJ, Olson L, “Protection and repair of the nigrostriatal dopaminergic system by GDNF in vivo.” *Nature* (1995) 373(6512):335-339.

[330] Wagner J, Akerud P, Castro D.S, Holm PC, Canals JM, Snyder EY, Perlmann T, Arenas E, “Induction of a midbrain dopaminergic phenotype in Nurr1-overexpressing neural stem cells by type 1 astrocytes.” *Nat Biotechnol* (1999) 17:653-659.

[331] Kawasaki H, Mizuseki K, Nishikawa S, Kaneko S, Kuwana Y, Nakanishi S, Nishikawa SI, Sasai Y, “Induction of midbrain dopaminergicneurons from ES cells by stromal cell-derived inducing activity.” *Neuron* (2000) 28:31-40.

[332] Lee SH, Lumelsky N, Studer L, Auerbach JM, McKay RD, “Efficient generation of midbrain and hindbrain neurons from mouse embryonic stem cells.” *Nat Biotechnol* (2000) 18:675-679.

[333] Kim JH, Auerbach JM, Rodríguez-Gómez JA, Velasco I, Gavin D, Lumelsky N, Lee SH, Nguyen J, Sánchez-Pernaute R, Bankiewicz K, “Dopamine neurons derived from embryonic stem cells function in an animal model of Parkinson’s disease.” *Nature* (2002) 418:50-56.

[334] Perrier AL, Tabar V, Barberi T, Rubio ME, Bruses J, Topf N, Harrison NL, Studer L, “Derivation of midbrain dopamine neurons from human embryonic stem cells.” *Proc Natl Acad Sci USA* (2004) 101:12543-12548.

[335] Park CH, Minn YK, Lee JY, Choi DH, Chang MY, Shim JW, Ko JY, Koh HC, Kang MJ, Kang JS, “In vitro and in vivo analyses of human embryonic stem cell-derived dopamine neurons.” *J Neurochem* (2005) 92:1265-1276.

[336] Zeng X, Cai J, Chen J, Luo Y, You ZB, Fotter E, Wang Y, Harvey B, Miura T, Backman C, "Dopaminergic differentiation of human embryonic stem cells." *Stem Cells* (2004) 22:925-940.

[337] Roy NS, Cleren C, Singh SK, Yang L, Beal MF, Goldman SA, "Functional engraftment of human ES cell-derived dopaminergic neurons enriched by coculture with telomerase-immortalized midbrain astrocytes." *Nat Med* (2006) 12:1259-1268.

[338] Friling S. Andersson E, Thompson LH, Jonsson ME, Hebsgaard JB, Nanou E, Alekseenko Z, Marklund U, Kjellander S, Volakakis N, "Efficient production of mesencephalic dopamine neurons by Lmx1a expression in embryonic stem cells." *Proc Natl Acad Sci USA* (2009) 106:7613-7618.

[339] Chambers SM, Fasano CA, Papapetrou EP, Tomishima M, Sadelain M, Studer L, "Highly efficient neural conversion of human ES and iPS cells by dual inhibition of SMAD signaling." *Nat Biotechnol* (2009) 27:275-280.

[340] Fasano CA, Chambers SM, Lee G, Tomishima MJ, Studer L, "Efficient derivation of functional floor plate tissue from human embryonic stem cells." *Cell Stem Cell* (2010) 6:336-347.

[341] Castelo-Branco G, Wagner J, Rodriguez FJ, Kele J, Sousa K, Rawal N, Pasolli HA, Fuchs E, Kitajewski J, Arenas E, "Differential regulation of midbrain dopaminergic neuron development by Wnt-1, Wnt-3a, and Wnt-5a." *Proc Natl Acad Sci USA* (2003) 100:12747-12752.

[342] Castelo-Branco G, Rawal N, Arenas E, "GSK-3beta inhibition/betacatenin stabilization in ventral midbrain precursors increases differentiation into dopamine neurons." *J Cell Sci* (2004) 117:5731-5737.

[343] Joksimovic M, Yun BA, Kittappa R, Anderegg AM, Chang WW, Taketo MM, McKay RDG, Awatramani RB, "Wnt antagonism of Shh facilitates midbrain floor plate neurogenesis." *Nat Neurosci* (2009) 12:125-131.

[344] Tang M, Villaescusa JC, Luo SX, Guitarte C, Lei S, Miyamoto Y, Taketo MM, Arenas E, Huang EJ, "Interactions of Wnt/betacatenin signaling and sonic hedgehog regulate the neurogenesis of ventral midbrain dopamine neurons." *J Neurosci* (2010) 30:9280-9291.

[345] Andersson ER, Salto C, Villaescusa JC, Cajanek L, Yang S, Bryjova L, Nagy II, Vainio SJ, Ramirez C, Bryja V, "Wnt5a cooperates with canonical Wnts to generate midbrain dopaminergic neurons in vivo and in stem cells." *Proc Natl Acad Sci USA* (2013) 110:E602-E610.

[346] Yang J, Brown A, Ellisor D, Paul E, Hagan N, Zervas M, "Dynamic temporal requirement of Wnt1 in midbrain dopamine neuron development." *Development* (2013) 140:1342-1352.

[347] Kirkeby A, Grealish S, Wolf DA, Nelander J, Wood J, Lundblad M, Lindvall O, Parmar M, "Generation of regionally specified neural progenitors and functional neurons from human embryonic stem cells under defined conditions." *Cell Rep* (2012) 1:703-714.

[348] Doi D, Samata B, Katsukawa M, Kikuchi T, Morizane A, Ono Y, Sekiguchi K, Nakagawa M, Parmar M, Takahashi J, "Isolation of human induced pluripotent stem cell-derived dopaminergic progenitors by cell sorting for successful transplantation." *Stem Cell Rep* (2014) 2:337-350.

[349] Chen Y, Stevens B, Chang J, Milbrandt J, Barres BA, Hell JW, "NS21: re-defined and modified supplement B27 for neuronal cultures." *J Neurosci Methods* (2008) 171(2):239-247.

[350] Ross CA, Akimov SS, “Human-induced pluripotent stem cells: potential for neurodegenerative diseases.” *Hum Mol Genet* (2014) 23(R1):R17-26.

[351] Pankratz MT, Li XJ, Lavaute TM, Lyons EA, Chen X, Zhang SC, “Directed neural differentiation of human embryonic stem cells via an obligated primitive anterior stage.” *Stem Cells* (2007) 25(6):1511-1520.

[352] Schwartz PH, Brick DJ, Stover AE, Loring JF, Müller FJ, “Differentiation of neural lineage cells from human pluripotent stem cells.” *Methods* (2008) 45(2):142-158.

[353] Suter DM, Krause KH, “Neural commitment of embryonic stem cells: molecules, pathways and potential for cell therapy.” *J Pathol* (2008) 215(4):355-368.

[354] Daadi MM, Steinberg GK, “Manufacturing neurons from human embryonic stem cells: biological and regulatory aspects to develop a safe cellular product for stroke cell therapy.” *Regen Med* (2009) 4(2):251-263.

[355] Hankowski KE, Hamazaki T, Umezawa A, Terada N, “Induced pluripotent stem cells as a next-generation biomedical interface.” Lab Invest (2011) 91(7):972-977.

[356] Robinton DA, Daley GQ, “The promise of induced pluripotent stem cells in research and therapy.” *Nature* (2012) 481(7381):295-305.

[357] Sherald AF, Sparrow JC, Wright TR, “A spectrophotometric assay for Drosophila dopa decarboxylase.” *Anal Biochem* (1973) 56:300-305.

[358] Komori H, Nitta Y, Ueno H, Higuchi Y, “Purification, crystallization and preliminary X-ray analysis of human histidine decarboxylase.” *Acta Crystallogr* (2012) 68:675−677.

[359] Fleming PJ, Fleming KG, “HullRad: Fast Calculations of Folded and Disordered Protein and Nucleic Acid Hydrodynamic Properties.” *Biophys J* (2018) 114:856−869.

[360] Johnson C, Huynh V, Hargrove L, Kennedy L, Graf-Eaton A, Owens J, Trzeciakowski JP, Hodges K, DeMorrow S, Han Y, Wong L, Alpini G, Francis H, “Inhibition of Mast Cell-Derived Histamine Decreases Human Cholangiocarcinoma Growth and Differentiation via c-Kit/Stem Cell Factor-Dependent Signaling.” *Am J Pathol* (2006) 186:123−133.

[361] Medina MA, Correa-Fiz F, Rodriguez-Caso C, Sanchez-Jimenez F, “A comprehensive view of polyamine and histamine metabolism to the light of new technologies.” *J Cell Mol Med* (2005) 9:854−864.

[362] Rossignoli G, Grottesi A, Bisello G, Montioli R, Borri Voltattorni C, Paiardini A, Bertoldi M, “Cysteine 180 Is a Redox Sensor Modulating the Activity of Human Pyridoxal 5'-Phosphate Histidine Decarboxylase.” *Biochemistry* (2018) 57(44):6336-6348.

[363] Conway ME, Yennawar N, Wallin R, Poole LB, Hutson SM, “Human mitochondrial branched chain aminotransferase: structural basis for substrate specificity and role of redox active cysteines.” *Biochim Biophys Acta Proteins Proteomics* (2003) 1647:61−65.

[364] Sagong HY, Kim KJ, “Lysine Decarboxylase with an Enhanced Affinity for Pyridoxal 5-Phosphate by Disulfide Bond-Mediated Spatial Reconstitution.” *PLoS One* (2017) 12:e0170163.

[365] Matsui D, Oikawa T, “Detection and function of the intramolecular disulfide bond in arginine racemase: an enzyme with broad substrate specificity.” *Chem Biodiversity* (2010) 7:1591-1602.

[366] Gavilanes F, Peterson D, Bullis B, Schirch L, “Structure and reactivity of cysteine residues in mitochondrial serine hydroxymethyltransferase.” *J Biol Chem* (1983) 258:13155-13159.

[367] Chitnumsub P, Ittarat W, Jaruwat A, Noytanom K, Amornwatcharapong W, Pornthanakasem W, Chaiyen P, Yuthavong Y, Leartsakulpanich U, “The structure of Plasmodium falciparum serine hydroxymethyltransferase reveals a novel redox switch that regulates its activities.” *Acta Crystallogr* (2014) 70:1517-1527.

[368] Coleman CS, Stanley BA, Pegg AE, “Effect of mutations at active site residues on the activity of ornithine decarboxylase and its inhibition by active site-directed irreversible inhibitors.” *J Biol Chem* (1993) 268:24572-24579.

[369] Hasse D, Andersson E, Carlsson G, Masloboy A, Hagemann M, Bauwe H, Andersson I, “Structure of the homodimeric glycine decarboxylase P-protein from Synechocystis sp. PCC 6803 suggests a mechanism for redox regulation.” *J Biol Chem* (2013) 288:35333-35345.

[370] Dalle-Donne I, Rossi R, Colombo G, Giustarini D, Milzani A, “Protein S-glutathionylation: a regulatory device from bacteria to humans.” *Trends Biochem Sci* (2009) 34(2):85-96.

[371] Rossignoli G, Phillips RS, Astegno A, Menegazzi M, Voltattorni CB, Bertoldi M, “Phosphorylation of pyridoxal 5'-phosphate enzymes: an intriguing and neglected topic.” *Amino Acid*. (2018) 50(2):205-215.

[372] Fusaki N, Ban H, Nishiyama A, Saeki K, Hasegawa M, “Efficient induction of transgene-free human pluripotent stem cells using a vector based on Sendai virus, an RNA virus that does not integrate into the host genome.” *Proc Jpn Acad Ser B Phys Biol Sci* (2009) 85(8):348-62.

[373] Przyborski SA, Cambray-Deakin MA, “Developmental regulation of MAP2 variants during neuronal differentiation in vitro.” Brain Res Dev Brain Res (1995) 89(2):187-201.

[374] Heilker R, Traub S, Reinhardt P, Schöler HR, Sterneckert J, “iPS cell derived neuronal cells for drug discovery.” *Trends Pharmacol Sci* (2014) 35(10):510-519.

[375] Ji P, Manupipatpong S, Xie N, Li Y, “Induced Pluripotent Stem Cells: Generation Strategy and Epigenetic Mystery behind Reprogramming.” *Stem Cells Int* (2016) 2016:8415010.

[376] Dossi E, Vasile F, Rouach N, “Human astrocytes in the diseased brain.” *Brain Res Bull* (2018) 136:139-156.

Chapter 11

Publications

1. Montioli R, Paiardini A, Kurian MA, Dindo M, **Rossignoli G**, Heales SJR, Pope S, Voltattorni CB, Bertoldi M, "The novel R347g pathogenic mutation of aromatic amino acid decarboxylase provides additional molecular insights into enzyme catalysis and deficiency." *Biochim Biophys Acta* (2016) 1864(6):676-682.
2. Paiardini A, Giardina G, **Rossignoli G**, Voltattorni CB, Bertoldi M, "New Insights Emerging from Recent Investigations on Human Group II Pyridoxal 5'-Phosphate Decarboxylases." *Curr Med Chem* (2017) 24(3):226-244.
3. **Rossignoli G**, Phillips RS, Astegno A, Menegazzi M, Voltattorni CB, Bertoldi M, "Phosphorylation of pyridoxal 5'-phosphate enzymes: an intriguing and neglected topic." *Amino Acids* (2018) 50(2):205-215.
4. **Rossignoli G**, Grottesi A, Bisello G, Montioli R, Borri Voltattorni C, Paiardini A, Bertoldi M, "Cysteine 180 Is a Redox Sensor Modulating the Activity of Human Pyridoxal 5'-Phosphate Histidine Decarboxylase." *Biochemistry* (2018) 57(44):6336-6348.

Biochimica et Biophysica Acta 1864 (2016) 676–682

Contents lists available at ScienceDirect

Biochimica et Biophysica Acta

journal homepage: www.elsevier.com/locate/bbapap

The novel R347g pathogenic mutation of aromatic amino acid decarboxylase provides additional molecular insights into enzyme catalysis and deficiency

Riccardo Montioli [a,1], Alessandro Paiardini [b,1], Manju A. Kurian [c,d], Mirco Dindo [a], Giada Rossignoli [a], Simon J.R. Heales [e,f], Simon Pope [f], Carla Borri Voltattorni [a], Mariarita Bertoldi [a,*]

[a] Department of Neurosciences, Biomedicine and Movement, University of Verona, Verona, Italy
[b] Department of Biology and Biotechnology "Charles Darwin", La Sapienza University of Roma, Roma, Italy
[c] Developmental Neurosciences, UCL-Institute of Child Health, London, UK
[d] Department of Neurology, Great Ormond Street Hospital, London, UK
[e] Clinical Chemistry, Great Ormond Street Hospital, London, UK
[f] Neurometabolic Unit, National Hospital of Neurology and Neurosurgery, UK

ARTICLE INFO

Article history:
Received 9 November 2015
Received in revised form 15 March 2016
Accepted 15 March 2016
Available online 17 March 2016

Keywords:
AADC deficiency
Aromatic amino acid decarboxylase
Pathogenic variant
Pyridoxal 5′-phosphate

ABSTRACT

We report here a clinical case of a patient with a novel mutation (Arg347 → Gly) in the gene encoding aromatic amino acid decarboxylase (AADC) that is associated with AADC deficiency. The variant R347G in the purified recombinant form exhibits, similarly to the pathogenic mutation R347Q previously studied, a 475-fold drop of k_{cat} compared to the wild-type enzyme. In attempting to unravel the reason(s) for this catalytic defect, we have carried out bioinformatics analyses of the crystal structure of AADC-carbidopa complex with the modelled catalytic loop (residues 328–339). Arg347 appears to interact with Phe103, as well as with both Leu333 and Asp345. We have then prepared and characterized the artificial F103L, R347K and D345A mutants. F103L, D345A and R347K exhibit about 13-, 97-, and 345-fold k_{cat} decrease compared to the wild-type AADC, respectively. However, unlike F103L, the R347G, R347K and R347Q mutants as well as the D345A variant appear to be more defective in catalysis than in protein folding. Moreover, the latter mutants, unlike the wild-type protein and the F103L variant, share a peculiar binding mode of dopa methyl ester consisting of formation of a quinonoid intermediate. This finding strongly suggests that their catalytic defects are mainly due to a misplacement of the substrate at the active site. Taken together, our results highlight the importance of the Arg347-Leu333-Asp345 hydrogen-bonds network in the catalysis of AADC and reveal the molecular basis for the pathogenicity of the variants R347. Following the above results, a therapeutic treatment for patients bearing the mutation R347G is proposed.

© 2016 Elsevier B.V. All rights reserved.

1. Introduction

Aromatic amino acid decarboxylase (AADC) deficiency is a rare autosomal recessive disorder (OMIM #608643) caused by the deficit of Dopa or aromatic amino acid decarboxylase (AADC), a pyridoxal 5′-phosphate (PLP) enzyme, which catalyses the conversion of L-Dopa and L-5-hydroxytryptophan to dopamine and serotonin, respectively. The main structural and functional properties of AADC have been recently reviewed [1]. In AADC deficiency, impaired enzyme activity is mainly due to point mutations in the *AADC* gene that lead to the synthesis of pathogenic variants. The most commonly reported symptoms of AADC deficiency include hypotonia, neurodevelopmental delay, oculogyric crises and complex movement disorder with autonomic features [2,3]. Studies of cerebrospinal fluid are key to diagnosis, showing reduced levels of 5-hydroxyindoleacetic acid and homovanillic acid together with elevated concentrations of L-Dopa, L-5-hydroxytryptophan and 3-O-methylDopa [4–6]. Diagnosis is confirmed by quantification of plasma AADC enzyme activity and *AADC* gene sequencing. To date, around 100 patients with homozygous or compound heterozygous mutations have been genotyped. Among them, 26 missense mutations have been identified, 18 of which are homozygous in the affected patients (http://www.biopku.org/home/jake.asp). Biochemical characterizations of the latter variants in the purified recombinant form of the enzyme, together with bioinformatics analyses, revealed that most of the examined variants displayed k_{cat} values linearly related to the magnitude of the near-UV CD signals and the ANS

Abbreviations: PLP, pyridoxal 5′-phosphate; AADC, aromatic amino acid decarboxylase; HDC, histidine decarboxylase; DME, dopa methyl ester; ANS, 1,8-anilinonaphtalene sulfonic acid; PMP, pyridoxamine 5′-phosphate; $K_{D(PLP)}$, equilibrium dissociation constant for PLP; TNB, 2,4,6-trinitrobenzene-1-sulfonic acid.

* Corresponding author at: Department of Neurosciences, Biomedicine and Movement, Section of Biological Chemistry, University of Verona, Strada Le Grazie, 8, 37134 Verona, Italy.
E-mail address: mita.bertoldi@univr.it (M. Bertoldi).

[1] RM and AP contribute equally to this work.

http://dx.doi.org/10.1016/j.bbapap.2016.03.011
1570-9639/© 2016 Elsevier B.V. All rights reserved.

emission fluorescence intensities [7]. These variants concern mutations of residues mapping to or interacting with loops 1 (aa 66–84), 2 (aa 100–110) and 3 (aa 323–357). Since the comparison of the crystal structure of the apo and holo forms of AADC highlights the relevance of these structural elements for the transition from the apo open form to the holo closed form [8], it was proposed that the pathogenicity of these mutations is due to incorrect apo-to-holo conversion [7]. The only exception is represented by the mutation R347Q which, although presenting no conformational alteration and maintaining a PLP binding affinity similar to that of the wild-type, exhibits severely decreased k_{cat} value [7]. To date, the reasons(s) for the loss of decarboxylase activity of this variant are unknown. Here we report a clinical case of a patient with a novel homozygous mutation, R347G, associated with AADC deficiency. This finding, together with the fact that the point mutation of Arg347 (to Gln or Gly) represents one of the most frequent pathogenic mutation and is present both in homozygous and in compound heterozygous states, urged us to undertake a detailed investigation on the molecular effects caused by the mutations of Arg347. The biochemical characterization of the variant R347G in the purified recombinant form reveals that it shares many structural and functional features with the variant R347Q. Thereafter we have explored by bioinformatics analyses the possible interactions of Arg347 in the crystal structure of the carbidopa-AADC complex in which the conformation of the mobile loop (residues 328–339), invisible in this structure, is modelled using the homologous region of histidine decarboxylase (HDC) as a template [9]. These studies, together with the biochemical characterization of the artificial mutants F103L, D345A, and R347K, allow us not only to identify the Arg347-Leu333-Asp345 triad as an important hydrogen bonds network for efficient catalysis of human AADC but also to unravel the molecular basis of the pathogenicity of the R347 mutations. Thus, our data provide potentially clinically translatable information for the therapy of patients harbouring pathogenic mutations at Arg347.

2. Materials and methods

2.1. Ascertainment of clinical case

Patient A was referred to a Tertiary Paediatric Neurology Centre with expertise in neurotransmitter disorders. Investigations and treatment strategies were investigated as part of routine clinical care.

2.2. Materials

PLP, L-Dopa, L-Dopa methyl ester (DME), 2,4,6-trinitrobenzene-1-sulfonic acid (TNB) and isopropyl-β-D-thiogalactopyranoside were purchased from Sigma-Aldrich. Protease inhibitor cocktail were purchased from Roche. The 1,8-anilinonaphtalene sulfonic acid (ANS) was purchased from Molecular Probes. The other chemicals were of the highest purity available.

2.3. Construction, expression and purification of the variants R347G, R347K, F103L and D345A

The R347G, R347K, F103L and D345A variants of AADC were constructed starting from the pDDChis construct that contains the complete open reading frame of the human AADC including a C-terminal 6xhis-tag and cloned into a pTrcHis2A expression vector [10]. Mutations were introduced by the QuikChange site-directed mutagenesis kit (Agilent Technologies) using the oligonucleotides 5′-CTGCATCG GCTTATCCTGGGCGGCAAG-3′ and its complement, 5′-GCTTATCACTGA CTACGGGCATTGGCAG-3′ and its complement, 5′-GGGCTTATCACTGA CTACAAGCATTGGCAG-3′ and its complement, 5′-GGCTTATC ACTGCCTACCGGCATTGG-3′ and its complement for F103L, R347G, R347K and D345A, respectively (the mutated codons are underlined). All the mutations were confirmed by the entire DNA sequence analysis. Expression plasmids of wild-type AADC [10], R347Q [7], F103L, R347G, R347K and D345A variants were used to transform *Escherichia coli* JM109 cells. Recombinant enzymes were expressed and purified by following the procedure previously described [10], and stored at −20 °C. The mutants yield after the standard purification was about 70% that of the wild-type enzyme. Protein concentrations were determined using the $\varepsilon_M = 142{,}000\ M^{-1}\ cm^{-1}$ at 280 nm and the PLP content of the enzymes was determined by releasing the coenzyme in the presence of 0.1 M NaOH and by using ε_M 6600 $M^{-1}\ cm^{-1}$ at 388 nm [11]. The purified variants were homogeneous as indicated by a single band upon migration in SDS-PAGE with mobility identical to that of the wild-type protein.

2.4. Spectroscopic measurements

Absorption measurements of F103L, R347G, R347Q, R347K, and D345A were performed using a Jasco V-550 spectrophotometer at a protein concentration of 10 μM in the absence or in the presence of 300 μM DME. CD measurements were made with a Jasco J-710 spectropolarimeter at a protein concentration of 6 μM. ANS binding spectra were recorded using a FP Jasco spectrofluorimeter setting at 5 nm excitation and emission bandwidths, following excitation at 365 nm of 1 μM enzyme sample that was previously incubated in the presence of 15 μM ANS for 1 h at 25 °C (in the dark) and in the presence of 20 μM PLP. All the spectroscopic measurements were carried out in 100 mM potassium phosphate buffer, pH 7.4, at 25 °C.

2.5. Apoenzyme preparation and coenzyme binding affinity

Apoenzyme was prepared as described previously [10]. The equilibrium dissociation constant for PLP, $K_{D(PLP)}$, of the variants R347G, R347K, F103L, and D345A was determined by measuring the quenching of the intrinsic fluorescence of 0.15 μM apoenzyme in the presence of PLP at concentrations ranging from 0.01 to 20 μM in 100 mM potassium phosphate buffer, pH 7.4 and by fitting the data to the following equation

$$Y = Y_{max}\frac{[E]_t + [PLP]_t + K_{D(PLP)} - \sqrt{\left([E]_t + [PLP]_t + K_{D(PLP)}\right)^2 - 4[E]_t[PLP]_t}}{2[E]_t}$$

where $[E]_t$ and $[PLP]_t$ represent the total concentrations of the enzyme and PLP, respectively, Y refers to the intrinsic quenching changes at a PLP concentration, [PLP], and Y_{max} refers to the fluorescence changes when all enzyme molecules are complexed with coenzyme. Curves fitting was performed using Origin® 7.03 (OriginLab).

2.6. Enzyme activity assay

The decarboxylase activity of the AADC variants was measured by a spectrophotometric assay as previously described [12] and modified [13]. Briefly, after an appropriate incubation time (a time within which a linear product formation is observed) of the enzyme in the presence of 2 mM L-Dopa and 10 μM PLP in a final volume of 250 μl, the reaction is stopped by heating at 100 °C for 1 min. Toluene (1.5 ml) and TNB (1 ml of a 4.3 mM solution) are then added, and the extraction of trinitrophenyldopamine is carried out at 42 °C for 1 h with continuous shaking. The concentration of trinitrophenyldopamine in the toluene layer is measured by using 12,400 $M^{-1}\ cm^{-1}$ as the molar extinction coefficient for trinitrophenyldopamine at 340 nm [14]. The kinetic parameters were determined by incubating the mutant recombinant proteins in the presence of different L-Dopa concentrations under saturating PLP concentration in 100 mM potassium phosphate buffer, pH 7.4. The concentrations of F103L, D345A, R347G, and R347K were 0.3 μM, 2 μM, 3 μM, and 5 μM, respectively, while the reaction times were 10 min for F103L and D345A, or 20 min for R347G and R347K. Data were fitted to the Michaelis–Menten equation.

2.7. HPLC analyses

Following incubation for 3 h in the presence of 300 μM DME in 100 mM potassium phosphate buffer, pH 7.4, at 25 °C, wild-type or variants AADC 10 μM were denatured by the addition of trichloroacetic acid to a final concentration of 5% (*v*/v). The quenched solutions were centrifuged to remove protein, and the supernatants were analysed by HPLC, using a Nucleodur 100–5 C18 (250 × 4.6 mm) (Macherey-Nagel) column connected to a Jasco PU-2080 Plus HPLC control system. The eluent was 50 mM potassium phosphate buffer, pH 2.35, at a flow rate of 1 ml/min. A Jasco UV-2075 Plus detector set at 295 nm was employed. Peaks corresponding to PLP and pyridoxamine 5′-phosphate (PMP) were integrated using the Jasco Borwin software. Standard curves of peak area as a function of PLP or PMP concentration were prepared.

2.8. Atomic coordinates and modelling

Atomic coordinates were taken from the Protein Data Bank (PDB): the ID code 1JS3 was used for AADC complexed with carbidopa and ID code 4E1O for HDC [9,15]. The visualization of structures and contacts analyses were performed using the Molecular Operating Environment (MOE) software. Energy minimization refinement, applying the AMBER99 force field, and the protonation state correction were performed using MOE software. Missing or substituted atoms and loop residues in AADC, either native or mutant, were modelled using MODELLER 9.10 [16] and the solved HDC loop (residues 328–346) [9]. Structural superimpositions were conducted using PyMol [17].

3. Results and discussion

3.1. Identification of a new homozygous mutation of AADC causing AADC deficiency

Patient A, a male infant, was referred for further investigation of neurodevelopmental delay. Routine diagnostic testing revealed a raised prolactin level and a vanilly lactate peak on urinary organic acids. A low homovanillic acid, low 5-hydroxyindoleacetic acid, raised 3-orthomethyl-dopa and 5-hydroxytryptophan were evident on cerebrospinal fluid neurotransmitter analysis. Plasma AADC enzyme activity was undetectable. Molecular genetic testing of *AADC* revealed a homozygous mutation, c.1039C > G (R347G) in the proband, with appropriate familial segregation. Pyridoxine and calcium folinate treatment were commenced initially, with some discernible clinical improvement in baseline tone and involuntary movements. Following this, the MAO inhibitor, Selegeline, was added and lead to further clinical improvement. A latter addition of the dopamine agonist, Pramipexole, has led to ongoing benefits. Overall there has been reduction of the frequency and severity of the oculogyric crises as well as further neurodevelopmental gains with improvement in axial and peripheral tone.

3.2. Impact of the R347G mutation on the structure and function of AADC

The spectroscopic features of the R347G variant in the purified recombinant form were compared with the corresponding ones of the wild-type AADC. No differences were observed between the far-UV CD spectra of the mutated and the wild-type forms of the enzyme (data not shown), suggesting that the mutation does not affect the overall secondary structure of AADC. As shown in Fig. 1 and inset, the R347G variant exhibited in the visible region absorbance and positive dichroic bands at 420 and 335 nm whose intensities were similar to the corresponding ones of the wild-type AADC. The R347G variant had a $K_{D(PLP)}$ value ~4-fold higher than that of the wild-type enzyme (Table 1). In order to evaluate the structural features of the mutated protein, near-UV CD spectra and ANS fluorescence spectra of this variant were monitored. When ANS binds to hydrophobic surfaces of proteins, it emits a fluorescence signal whose maximum wavelength (at around 450 nm)

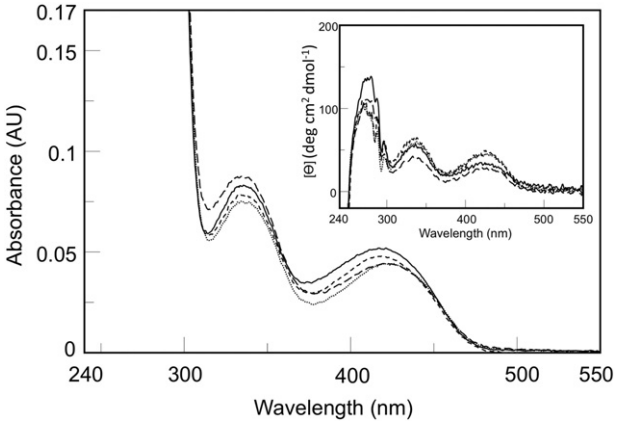

Fig. 1. Absorbance and CD spectra of wild-type AADC and variants. Absorption and CD (inset) spectra of (—) wild-type, (— — —) R347G, (-··) R347K, (–·–) F103L, and (·····) D345A at 10 μM enzyme concentration in 100 mM potassium phosphate buffer, pH 7.4.

is red-shifted and the intensity increases. The near-UV CD spectra of the holo and the apo forms of the R347G variant as well as the ANS emission spectra of the holo form revealed a modest decrease in the difference of the dichroic signals between the holo- and the apo- forms as well a slight increase of the ANS emission intensity of the holo form (data not shown), in comparison to the wild-type enzyme. Thus, these data fit the linear relation depicted in Fig. 2A, suggesting that the R347G mutation has a modest impact on the apo-holo transition. To determine the functional effects of replacing Arg347 by Gly, the steady-state kinetic parameters of the R347G variant were measured and compared to those of the wild-type enzyme (Table 1). The variant exhibits a very large drop in its catalytic efficiency, ~2760-fold, mainly driven by the ~475-fold decrease of its k_{cat} value. Interestingly, the location of the R347G variant on the curve in Fig. 2B is similar to that of the R347Q variant, suggesting that both variants R347Q and R347G behave similarly in sharing a sharp decrease in the k_{cat} value (corresponding to a residual catalytic activity of 1.1% and 0.2%, respectively), despite no or only modest conformational alterations. Based on these results, we have decided to gain further insights into the catalytic relevance of the large and positively charged side chain of Arg347 by using bioinformatics analyses aiming to identify the possible interaction(s) between Arg347 and other AADC residues.

3.3. Bioinformatics analyses

The position and possible interactions of Arg347 were analysed, starting from the coordinate file of the pig kidney AADC in complex with carbidopa (PDB file 1JS3). Arg347 belongs to loop 3 and maps near the active site cavity in proximity of the 328–339 loop. This is a mobile segment, invisible in the electron density maps, that seems to be important for the catalytic mechanism [15,18]. Before inspecting the structure, the protonation state of the molecule was corrected to mimic the physiological condition, and the structure was refined by

Table 1
Kinetic parameters and coenzyme binding affinity.

Enzyme	k_{cat} (s^{-1})	K_m (mM)	k_{cat}/K_m (s^{-1} mM^{-1})	$K_{D(PLP)}$ (nM)
Wild-type[a]	7.6 ± 0.1	0.11 ± 0.01	69 ± 6	43 ± 12
R347Q[b]	0.087 ± 0.005	0.49 ± 0.08	0.18 ± 0.03	54 ± 10
R347G	0.016 ± 0.001	0.64 ± 0.13	0.025 ± 0.05	178 ± 14
R347K	0.022 ± 0.003	0.31 ± 0.01	0.071 ± 0.011	214 ± 12
F103L	0.55 ± 0.09	0.15 ± 0.01	3.67 ± 0.007	98 ± 18
D345A	0.078 ± 0.001	0.60 ± 0.03	0.13 ± 0.65	150 ± 20

[a] Ref. [8].
[b] Ref. [6].

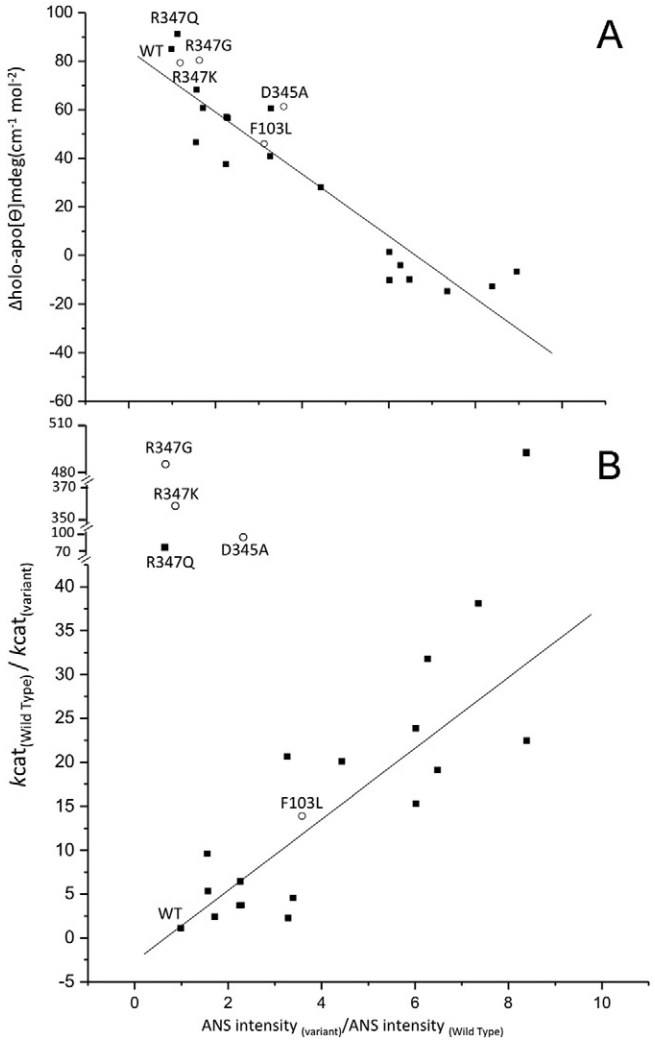

Fig. 2. Relationship between conformational and catalytic features of wild-type and variants. The position of wild-type AADC and variants R347G, R347Q, R347K, D345A and F103L are indicated. The solid symbol (■) represents positions of variants previously studied [7]. (A) Plot of difference of the magnitude of the near-UV dichroic signal of holo and the corresponding apo enzyme as a function of the ratio of ANS intensity of each variant and the wild-type, and (B) plot of the decrease of k_{cat} as a function of the increase of ANS intensity. The diagonal lines correspond to a linear fit, with R^2 values of −0.926 and 0.842 for (A) and (B), respectively.

energy minimization. As shown in Fig. 1 of SM, the side chain of Arg347 is predicted to form a hydrogen bond with the main chain oxygen of Phe103, an active site residue composing the hydrophobic cavity that hosts the substrate. The π system of Phe103 appears to be involved in the binding and orientation of the substrate as well as in stabilizing the position of the Tyr79 side chain [15]. Moreover, the proximity of Arg347 in the primary structure to the C-terminus of the loop (aa 328–339) missing in the structure, urged us to also explore the possible interaction(s) of this residue with those of the loop. Thus, we modelled the latter starting from the structure of AADC complexed with carbidopa, using the homologous region of HDC (PDB: 4E1O; residues 328–346) as template [9]. The modelling results obtained are shown in Figs. 3 and Fig. 2 of SM. Two main interactions are engaged by Arg347: 1) the guanidine moiety is placed at hydrogen-bond distance from the main-chain oxygen atom of Leu333 (~3.1 Å), the latter residue being adjacent to Tyr332, which is involved in the decarboxylase activity [18]; 2) the second one takes place between Arg347 and Asp345 (~2.4 Å), which also interacts also with the imidazole ring of His335 (~3.1 Å; Fig. 3). Therefore, it is predicted that there is a network of interactions involving residues Asp345, Arg347, His335 and Leu333, the role

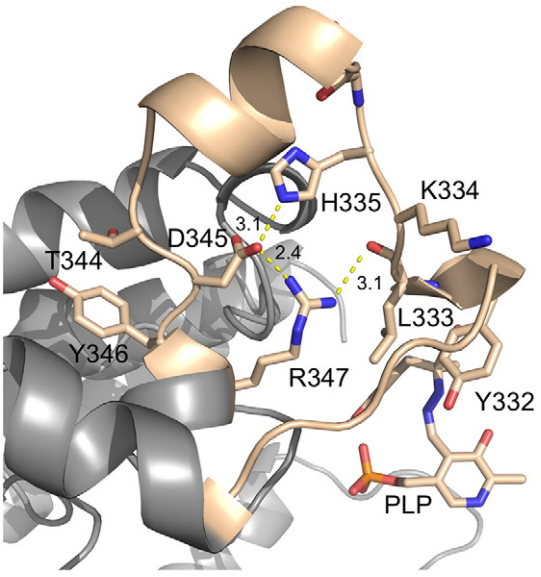

Fig. 3. Modelled mobile loop of human AADC (residues 326–346). The position of the loop (pink ribbons and sticks) is shown in the context of the AADC structure (grey ribbons). The predicted hydrogen bonds network involving Arg347, Asp345 and residues of the mobile loop (Leu333 and His335) is shown in yellow, together the relative distances (Å).

of which is probably to stabilize the closed conformation of the AADC catalytic loop. Similar interactions were also observed in the crystal structure of the close homologous human HDC (e.g., Asp345-His337; Fig. 2 of SM). However, in HDC the stabilization of residue Leu333 reasonably involves a hydrophobic interaction between its side-chain and Met347, which corresponds to Arg347 in human AADC. Since both interactions of Arg347 with Leu333 and Asp345 are missing in the R347G mutant, we have modelled the previously characterized pathogenic variant R347Q in an attempt to analyse the interactions of Gln347 with neighbouring residues. As shown in Fig. 4, the modelling study reveals that (i) the interaction (i.e., a hydrogen-bond) with Asp345 is still conserved, even if the minimum distance between the residues Gln347 and Asp345 (≥3.5 Å) is greater compared to the distance observed for the residues Arg347 and Asp345, and (ii) the interaction with Leu333 is completely lost, presumably leading to destabilization

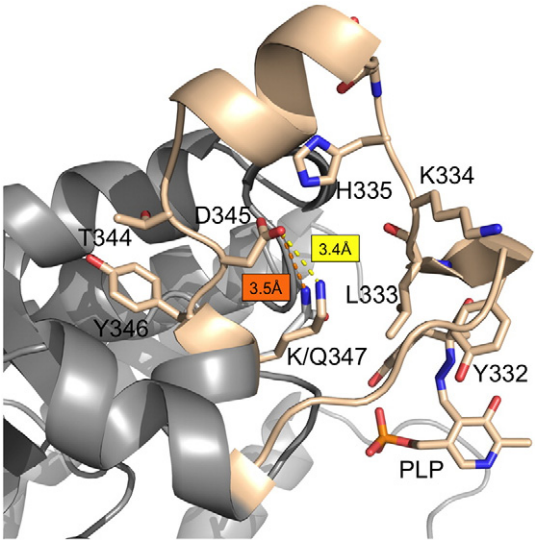

Fig. 4. Modelled R347Q and R347K mutants of human AADC. The position of the loop 326–346 (pink ribbons and sticks) is shown in the context of the dimeric AADC structure. Chain A is represented as grey ribbons. The distance (Å) between residues Gln/Lys347 and Asp345 is shown in yellow and orange, respectively.

of the catalytic loop. Therefore, we could reason that the Arg347-Leu333 interaction is pivotal for the proper positioning of the active site residue Tyr332 and that the lack of such interaction would result in impaired decarboxylase activity. We have also modelled an artificial R347K mutant that, according to our assumptions, was predicted to be engaged in a similar pattern of interactions as observed for the wild-type AADC. Interestingly, as shown in Fig. 4, the ε-amino group of Lys347 preserves the electrostatic interaction with Asp345 (≳3.4 Å), but, as in the case of the R347Q mutant, it loses the hydrogen-bond with the main-chain O atom of Leu333, leading us to suppose that such a mutant would also have exhibited a sharp decrease in catalytic activity similar to that observed for the mutants R347G and R347Q. Therefore, on the basis of all the above observations, we have prepared and characterized the F103L, D345A and R347K mutants.

3.4. Impact of the mutations F103L, D345A and R347K on the structural and functional properties of the wild-type AADC

The variants F103L, D345A, and R347K were expressed in *E. coli* and purified to homogeneity, as described in Methods section. A comparison of their far-UV CD spectra with that of the wild-type protein revealed superimposable features, indicating that substitution of Phe103, Asp345 or Arg347 for leucine, alanine or lysine, respectively, does not alter the secondary structure of the wild-type AADC, significantly (results not shown). The visible absorption and CD spectra of the variants F103L, D345A and R347K were similar to the corresponding spectra of wild-type AADC (Fig. 1 and inset). The $K_{D(PLP)}$ values of the variants F103L, D345A and R347K were ~2-, ~3.5-, and 5-fold, respectively, higher than the corresponding value of the wild-type enzyme (Table 1). Dichroic spectra in the near-UV region of both holo and apo form of the three variants together with the ANS fluorescence emission spectra of their holo forms were acquired and compared with the corresponding spectra of the wild-type protein. As shown in Fig. 2A, the plot of these data indicates that the examined mutations fit the linear correlation of the differences between the dichroic signals of holo and apo form against the ANS emission intensity of each holo mutant. The position of the F103L and D345A mutants on the curve is indicative of the meaningful impact of the mutations F103L and D345A on the apo-holo transition, even if less pronounced than that of mutations of residues mapping to loop 1 (H70T, H72Y, Y79C, P81L) [8]. On the other hand, the finding that the position of the R347K in this curve is similar to that of the wild-type AADC, R347Q and R347G variants strongly suggests that the mutation R347K does not alter the tertiary structure of holo-AADC. In order to find out if the mutations under study have an impact on decarboxylase activity, the steady-state kinetic parameters of the variants were measured (Table 1). The k_{cat}/K_m of the variants F103L, D345A, and R347K was decreased by ~19-, 530-, and 970-fold, respectively, in comparison with the wild-type AADC value. The decrease in catalytic efficiency is mainly driven by the decrease in k_{cat} (~14-fold in F103L, ~97-fold in D345A, and ≳345-fold in the case of R347K). When Phe103, belonging to the substrate binding pocket, and in van der Waals contact with the catecholic ring of carbidopa (a substrate analogue) [15], is substituted with a residue bearing an aliphatic side chain, there was a little change in the Km value.

As shown in Fig. 2B, F103L fits the linear relation between the structural and catalytic changes already identified for other AADC variants [7]. This result, in line with the fact that Phe103 maps to loop 2, suggests that mispositioning of the aromatic ring of Phe103 due to the loss of the interaction with R347 could not explain the remarkable loss of catalytic activity of the R347 variants (Table 1). On the other hand, it is evident that D345A and R347K do not fit the linear relation, taking in the plot a location similar to that of the wild-type protein and the other R347 variants (Fig. 2B). In other words, the drop in catalytic activity of the variants R347Q, R347G, R347K and D345A is definitely more consistent than the change in their conformation. These findings are in line with the bioinformatics analyses prediction and strongly suggest that the hydrogen bonds between Arg347 and both Asp345 and Leu333 are relevant for the catalytic mechanism of AADC. In this regard, it is of interest to note that both Arg347 and Asp345 residues are close to the dynamic catalytic loop (residues 328–339) of AADC, while Leu333 is in the middle of this loop. Previous spectroscopic and kinetic studies indicated that this catalytic loop undergoes a conformational change upon substrate binding, leading to a closure of the active site thereby achieving a conformational state that is productive for decarboxylation [19]. Indeed, site-directed mutagenesis has strongly suggested that Tyr332 performs the protonation of the Cα atom of the quinonoid intermediate which is crucial for the decarboxylation pathway [18].

3.5. Binding mode of variants with DME

Based on the above-mentioned results and considerations, we have decided to analyse the effects of the mutations under study on the formation of the external aldimine. This is the first intermediate that forms upon covalent binding of the substrate to the formyl group of the cofactor in PLP-enzymes while exchanging internal with external Schiff base through a gem-diamine intermediate [20]. PLP reactivity has been widely studied for this family of enzymes and the generally accepted hypothesis is based on Dunathan's proposal, published in 1966, suggesting that PLP-enzymes employ stereoelectronic effects to control their reaction specificity [21]. Dunathan's hypothesis assumes that enzymes place the bond to be broken of the external aldimine parallel to the p-system. In this way the developing p orbital is aligned for maximal overlap with the extended p system, lowering the energy of the transition state and increasing the reaction rate. In decarboxylases, the Cα-COO^- should be found in the orthogonal position to the p-system and its rupture allows the generation of a carboanionic quinonoid intermediate which is further protonated at the Cα leading to amine generation [22].

We have selected DME, a substrate analogue that contains an esterified carboxyl group and, therefore, is not susceptible to decarboxylation. For this reason, the AADC-DME complex appears to be a good model for studying the external aldimine intermediate. The absorption spectra upon addition of DME to the wild-type AADC and the variants under study have been registered up to 3 h, a time after which DME undergoes oxidation. As shown in Fig. 5, a prominent absorbance band centred at 398 nm, already attributed to the formation of the external aldimine, as well as a band at 325 nm characterize the complex of the wild-type enzyme or F103L with DME. This is similar to what was already seen for liver and kidney AADC [23,24]. On the contrary, we have noticed that DME added to R347G, R347Q, R347K, and D345A caused, in addition to the absorbance bands at 398 nm and 325 nm (the latter being more pronounced than for wild-type AADC and F103L), an absorbance band at 500 nm, typical of a quinonoid

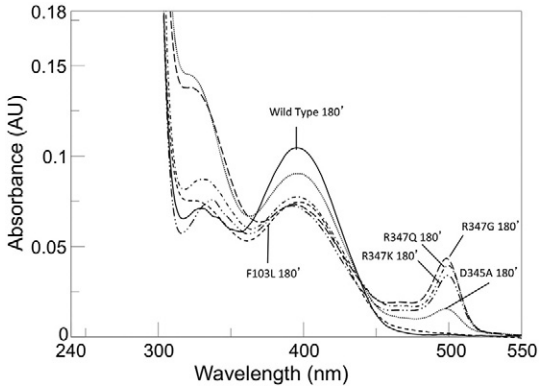

Fig. 5. Absorption spectra of the complex of wild-type and variants with DME. Absorption spectra of wild-type and variants (10 μM) after 3 h of incubation with 300 μM DME at 25 °C in 100 mM potassium phosphate buffer, pH 7.4.

intermediate. It was also observed that both 325 and 500 nm bands increased with time, concomitantly with the decrease of the 398 nm band. To determine if this reaction converts PLP into PMP or other coenzyme forms, aliquots were withdrawn after 3 h of incubation of the wild-type enzyme and the variants F103L, R347Q, or R347G or R347K or D345A with 300 μM DME. These samples were then subjected to HPLC analysis after total denaturation. Interestingly, it was found that, while the original PLP content of the wild-type AADC and the mutant F103L remained unchanged, about 10–15% of the PLP of mutants R347Q, R347G, R347K and D345A was converted into PMP.

These results may indicate that the reaction in mutants R347Q, R347G, R347K and D345A does not stop at the step of external aldimine formation. Instead, the appearance of the quinonoid species at 500 nm and the production of PMP are consistent with the suggestion of DME binding at the active site of the variants in a conformation orienting the Cα–H bond perpendicular to the plane of the cofactor system. In other words, such an event is indicative of a mispositioning of the external aldimine at the active site of these variants.

3.6. The structural and functional relevance of the Arg347-Leu333-Asp345 triad

Taken together, these results rule out the possibility that the lack of the interaction of Arg347 with the main chain oxygen of Phe103 could be responsible for decreased catalytic activity of the different R347 mutants. Rather, they point to a set of hydrogen bonds engaged by Arg347 with both Asp345 and Leu333 and its effect on the decarboxylase activity of the human AADC. As predicted by bioinformatics analyses, the disruption of both hydrogen bonds occurs upon mutation of Arg347 to Gly, while the disruption of one hydrogen bond takes place upon mutation of Arg347 to Gln or Lys or in mutant D345A. Since remarkable decreases in the k_{cat} (even if to different degree) is shared by all the tested R347 mutants and the D345 mutant, it is reasonable to suggest that the Arg347-Leu333-Asp345 hydrogen bonds network plays an important role in the catalysis of AADC. Moreover, the significant decrease in the k_{cat} values of R347G, R347Q, R347K, and D345A appears to be a consequence of an incorrect location of the external aldimine at their active site. These findings allow us to (i) indicate that Leu333, belonging to dynamic catalytic loop, and the Arg347 and Asp345 residues adjacent to it, are structural elements that impose important constrains on the alignment of the catalytic groups at the active site of the human AADC upon substrate binding, and (ii) offer an explanation for the molecular basis of the pathogenicity of the R347Q and R347G variants.

3.7. Therapeutic suggestions

Up to date, specific treatments guidelines are lacking for patients with AADC deficiency. Thus, a combination of pyridoxine, L-Dopa, MAO inhibitors and dopamine agonists is often administered in order to potentiate dopaminergic transmission. Like other diseases related to protein malfunctioning, an inherited mutation can be a catalytic and/or a folding mutation, thus altering protein function in different ways. For this reason, a detailed analysis into how missense mutations induce AADC deficit may provide a useful guidance for a proper therapeutic choice, and thereby improve clinical outcome. Only in the last three years studies performed using pathogenic AADC variants in the purified recombinant form have allowed identifying, at the protein and/or cellular level, their defects and, on these bases, stratify patients into different therapeutic categories [7,10,25]. Following this view, characterization of the variants R347Q and R347G provides the basis for delineate the most appropriate pharmacological therapy for patients bearing the pathogenic mutations of Arg347. The low k_{cat} value of the purified recombinant R347G strongly suggests that a dopamine agonist together with folinate could be the best way of assessing a good clinical response of patients bearing the R347G mutation. In fact, while the therapy with dopamine agonists could mime the dopamine effects, the one with folinic acid could not allow its depletion due to the conversion of accumulated L-Dopa into 3-*O*-methylDopa. The same therapy strategy could be applied to patients harbouring the R347Q variant. However, in the case of mutation R347G, which, unlike R347Q, has a 4-fold $K_{D(PLP)}$ value higher than that of the wild-type, the supplementation of pyridoxine could also be useful. All these considerations seem to be consistent with the improvement observed following the treatment of patient A.

4. Conclusion

A clinical case of a patient bearing a novel mutation in AADC, R347G, associated with severe enzyme activity deficiency is reported. Similarly to the pathogenic R347Q variant previously studied [7], the R347G mutant appears to be defective in catalysis rather than protein folding. The reason(s) for the dramatic loss of decarboxylase activity caused by the substitution of Arg347 with either Gly (~475-fold) or Gln (~87-fold) were investigated. The in silico modelling of the missing loop 328–339 of AADC structure predicted interactions of Arg347 with Asp345 and Leu333. Structural and functional features of the new designed mutants, D345A and R347K in recombinant AADC, strongly suggested that residues Arg347, Asp345, and Leu333, as well as their mutual interaction, are structural elements relevant for a proper location/orientation of the substrate and/or of the catalytic groups at or near the active site. Altogether, our data highlight the molecular defects caused by the mutations of Arg347, and allow us to suggest a therapeutic management of patients bearing the mutation R347G.

Supplementary data to this article can be found online at http://dx.doi.org/10.1016/j.bbapap.2016.03.011.

Transparency document

The Transparency document associated with this article can be found, in online version.

Acknowledgments

We are grateful to Prof. Moshe Finel, University of Helsinki, for carefully proof-reading the manuscript and correcting English. We thank the AADC research Trust (UK) for the interest in our research. This work was supported by grants from AADC research Trust (to C.B.V.) and from the University of Verona, FUR2014 (to M.B.).

References

[1] M. Bertoldi, Mammalian Dopa decarboxylase: structure, catalytic activity and inhibition, Arch. Biochem. Biophys. 546 (2014) 1–7.
[2] L. Brun, L.H. Ngu, W.T. Keng, G.S. Ch'ng, Y.S. Choy, W.L. Hwu, W.T. Lee, M.A. Willemsen, M.M. Verbeek, T. Wassenberg, L. Regal, S. Orcesi, D. Tonduti, P. Accorsi, H. Testard, J.E. Abdenur, S. Tay, G.F. Allen, S. Heales, I. Kern, M. Kato, A. Burlina, C. Manegold, G.F. Hoffmann, N. Blau, Clinical and biochemical features of aromatic L-amino acid decarboxylase deficiency, Neurology 75 (2010) 64–71.
[3] C. Manegold, G.F. Hoffmann, I. Degen, H. Ikonomidou, A. Knust, M.W. Laass, M. Pritsch, E. Wilichowski, F. Horster, Aromatic L-amino acid decarboxylase deficiency: clinical features, drug therapy and follow-up, J. Inherit. Metab. Dis. 32 (2009) 371–380.
[4] K. Hyland, P.T. Clayton, Aromatic amino acid decarboxylase deficiency in twins, J. Inherit. Metab. Dis. 13 (1990) 301–304.
[5] K.J. Swoboda, K. Hyland, D.S. Goldstein, K.C. Kuban, L.A. Arnold, C.S. Holmes, H.L. Levy, Clinical and therapeutic observations in aromatic L-amino acid decarboxylase deficiency, Neurology 53 (1999) 1205–1211.
[6] G. Haliloglu, E. Vezir, L. Baydar, S. Onol, S. Sivri, T. Coskun, M. Topcu, When do we need to perform a diagnostic lumbar puncture for neurometabolic diseases? Positive yield and retrospective analysis from a tertiary center, Turk. J. Pediatr. 54 (2012) 52–58.
[7] R. Montioli, M. Dindo, A. Giorgetti, S. Piccoli, B. Cellini, C.B. Voltattorni, A comprehensive picture of the mutations associated with aromatic amino acid decarboxylase deficiency: from molecular mechanisms to therapy implications, Hum. Mol. Genet. 23 (2014) 5429–5440.
[8] G. Giardina, R. Montioli, S. Gianni, B. Cellini, A. Paiardini, C.B. Voltattorni, F. Cutruzzola, Open conformation of human DOPA decarboxylase reveals the

mechanism of PLP addition to Group II decarboxylases, Proc. Natl. Acad. Sci. U. S. A. 108 (2011) 20514–20519.
[9] H. Komori, Y. Nitta, H. Ueno, Y. Higuchi, Structural study reveals that Ser-354 determines substrate specificity on human histidine decarboxylase, J. Biol. Chem. 287 (2012) 29175–29183.
[10] R. Montioli, B. Cellini, C. Borri Voltattorni, Molecular insights into the pathogenicity of variants associated with the aromatic amino acid decarboxylase deficiency, J. Inherit. Metab. Dis. 34 (2011) 1213–1224.
[11] E.A. Peterson, H.A. Sober, Preparation of crystalline phosphorylated derivatives of vitamin B6, J. Am. Chem. Soc. 76 (1954) 169–175.
[12] A.F. Sherald, J.C. Sparrow, T.R. Wright, A spectrophotometric assay for Drosophila dopa decarboxylase, Anal. Biochem. 56 (1973) 300–305.
[13] A. Charteris, R. John, An investigation of the assay of dopamine using trinitrobenzensulphonic acid, Anal. Biochem. 66 (1975) 365–371.
[14] C. Streffer, A method for determining aromatic amino acid decarboxylase, Biochim. Biophys. Acta 139 (1967) 193–195.
[15] P. Burkhard, P. Dominici, C. Borri-Voltattorni, J.N. Jansonius, V.N. Malashkevich, Structural insight into Parkinson's disease treatment from drug-inhibited DOPA decarboxylase, Nat. Struct. Biol. 8 (2001) 963–967.
[16] B. Webb, A. Sali, Comparative protein structure modeling using MODELLER, Curr. Protoc. Bioinformatics 47 (2014) (5 6 1–5 6 32).
[17] E. Bramucci, A. Paiardini, F. Bossa, S. Pascarella, PyMod: sequence similarity searches, multiple sequence-structure alignments, and homology modeling within PyMOL, BMC Bioinf. 13 (Suppl. 4) (2012) S2.
[18] M. Bertoldi, M. Gonsalvi, R. Contestabile, C.B. Voltattorni, Mutation of tyrosine 332 to phenylalanine converts dopa decarboxylase into a decarboxylation-dependent oxidative deaminase, J. Biol. Chem. 277 (2002) 36357–36362.
[19] M. Bertoldi, P. Frigeri, M. Paci, C.B. Voltattorni, Reaction specificity of native and nicked 3,4-dihydroxyphenylalanine decarboxylase, J. Biol. Chem. 274 (1999) 5514–5521.
[20] R.A. John, Pyridoxal phosphate-dependent enzymes, Biochim. Biophys. Acta 1248 (1995) 81–96.
[21] H.C. Dunathan, Conformation and reaction specificity in pyridoxal phosphate enzymes, Proc. Natl. Acad. Sci. U. S. A. 55 (1966) 712–716.
[22] M.D. Toney, Controlling reaction specificity in pyridoxal phosphate enzymes, Biochim. Biophys. Acta 1814 (2011) 1407–1418.
[23] P.S. Moore, M. Bertoldi, P. Dominici, C. Borri Voltattorni, Aromatic amino acid methyl ester analogs form quinonoidal species with Dopa decarboxylase, FEBS Lett. 412 (1997) 245–248.
[24] H. Hayashi, H. Mizuguchi, H. Kagamiyama, Rat liver aromatic L-amino acid decarboxylase: spectroscopic and kinetic analysis of the coenzyme and reaction intermediates, Biochemistry 32 (1993) 812–818.
[25] R. Montioli, E. Oppici, B. Cellini, A. Roncador, M. Dindo, C.B. Voltattorni, S250F variant associated with aromatic amino acid decarboxylase deficiency: molecular defects and intracellular rescue by pyridoxine, Hum. Mol. Genet. 22 (2013) 1615–1624.

Send Orders for Reprints to reprints@benthamscience.ae

Current Medicinal Chemistry, **2017**, *24*, **1-19**

REVIEW ARTICLE

New Insights Emerging from Recent Investigations on Human Group II Pyridoxal 5'-Phosphate Decarboxylases

Alessandro Paiardini[1], Giorgio Giardina[2], Giada Rossignoli[3], Carla Borri Voltattorni[3] and Mariarita Bertoldi[3,*]

[1]*Department of Biology and Biotechnology "Charles Darwin", La Sapienza University of Rome, Rome 00185, Italy;* [2]*Department of Biochemical Sciences "A. Rossi Fanelli", La Sapienza, University of Rome, Rome 00185, Italy;* [3]*Department of Neuroscience, Biomedicine and Movement, University of Verona, Verona, Italy*

ARTICLE HISTORY

Received: July 20, 2016
Revised: October 23, 2016
Accepted: November 08, 2016

DOI: 10.2174/0929867324666161123093339

Abstract: Aromatic amino acid, cysteine sulfinic acid, glutamate and histidine decarboxylases, belonging to group II of pyridoxal 5'-phosphate-dependent enzymes, catalyze the synthesis of dopamine/serotonin, hypotaurine, γ-aminobutyric acid and histamine, respectively. Considering that these reaction products are all essential bioactive molecules, group II decarboxylases have been long studied from an evolutionary, biochemical and pharmacological standpoint. Despite the fact that they all belong to a common fold-type, during evolution each decarboxylase has evolved unique structural elements responsible for its substrate specificity. Combining a literature update with bioinformatic analyses, this review focuses on some structural determinants shared by these enzymes revealing their intrinsic substrate specificity and highlighting the importance of some residues/regions for catalytic competence. In particular, two key structural features emerge: 1) a mobile catalytic loop, and 2) an open-to-close conformation accompanying the apo-holo transition. Drawing attention on these elements is crucial in correlating subtle structural modifications to functional properties for the understanding, at a molecular level of a pathological condition. This is corroborated by the increasingly important role played by these decarboxylases in several different pathological states (autoimmune diseases, type I diabetes, Parkinson's disease, aromatic amino acid decarboxylase deficiency, Tourette's syndrome and cholangiocarcinoma).

Keywords: Pyridoxal 5'-phosphate, aromatic amino acid decarboxylase, cysteine sulfinic acid decarboxylase, glutamate decarboxylase, histidine decarboxylase, type I diabetes, Stiff-person syndrome, Parkinson's disease, aromatic amino acid decarboxylase deficiency, Tourette's syndrome, cholangiocarcinoma.

GROUP II DECARBOXYLASES: A SUBFAMILY OF PYRIDOXAL 5'-PHOSPHATE (PLP) ENZYMES

Enzymes containing PLP are ubiquitous in biology, performing essential reactions in metabolism of amino acids and amines [1]. These enzymes catalyze a wide variety of reactions, including transamination, racemization, α- and β-decarboxylation, retro-aldol cleavage, β- and γ-elimination and β- and γ-substitution. The basic role of PLP in all these reactions has been understood since the 1950s from the seminal work of Metzler and Snell in the United States of America [2-4] and of Braunstein and colleagues in the former Union of the Soviet Socialist Republics [5-7]. The strongly electron withdrawing capability of the pyridinium ring was proposed to stabilize α- or β-carbanions on the amine or amino acid portion of substrates, thereby facilitating the wide variety of the reactions. The chemistry of these enzymatic reactions is thus controlled by the PLP cofactor, and PLP alone has been shown to perform many of these reactions, albeit at very slow rates. Therefore, it is the protein environment that con-

*Address correspondence to this author at the Department of Neuroscience, Biomedicine and Movement, Section of Biological Chemistry, University of Verona, Strada Le Grazie, 8, 37134, Verona, Italy; Tel: +39 0458027671; Fax: +39 0458027170; E-mail: mita.bertoldi@univr.it

0929-8673/17 $58.00+.00 **© 2017 Bentham Science Publishers**

fers the reaction specificity and enormous rate accelerations (by a factor of 10^{10} or more) typical of these enzymes. In the past seventy years, PLP-enzymes have been the subject of extensive research focused on the understanding of their structure-function relationships [8-14]. In these enzymes, PLP is invariably bound as an imine to the ε-amino group of a lysine residue of the protein in a structure known as the internal aldimine. After the initial binding of the substrate amino acid as a Michaelis complex, an external aldimine is formed between the C4' of the cofactor and the α-amino group of the substrate, which substitutes in the Schiff base linkage the ε-amino group of the PLP-binding lysine. Transimination (or transaldimination) itself is not a single step process. Indeed, it proceeds through a geminal diamine in which both enzyme and substrate amino groups are bound to C4' (Fig. **1**). Dunathan's hypothesis [15] predicts that the course of the reaction at this stage would depend on which of the three bonds to the α-carbon is held perpendicular to the plane of the coenzyme-imine π system by interactions between apoenzyme and substrate. This fundamental concept explains how reaction specificity is controlled and points on the role of polypeptide chain in directing the coenzyme intrinsic catalytic properties. Thus, the reaction catalyzed depends on which of the three α-substituents is lost, *i.e.* (i) elimination of CO_2 from Cα (α-decarboxylation), (ii) deprotonation (transamination, racemization, β-elimination and β- replacement, γ-elimination and γ-replacement), and (iii) elimination of the side chain of amino acids (α-synthesis and aldol cleavage) (Fig. **1**). In any case, this event results in the formation of a quinonoid intermediate in which the substrate and the cofactor generate a coplanar structure. An exception to this common mechanism is represented by PLP-dependent phosphorylases, where PLP does not act as an electrophilic catalyst but it participates in proton transfer acid-base reactions through its phosphate group [16].

The wide catalytic versatility of PLP-enzymes is accompanied by a limited structural diversity. In 1995 Grishin *et al.* [17] distributed PLP-enzymes into five different fold-types (from I to V) based on amino acid sequence comparison, predicted secondary structure and three-dimensional structures published theretofore [17]. This classification has been later updated with new information provided by progresses due to the increasing number of PLP-enzymes structure determinations [18].

The fold-type I, which is the most common one, is mainly typical of aminotransferases and of the majority of the α-decarboxylases, including human aromatic amino acid decarboxylase (AADC), cysteine sulfinic acid decarboxylase (CSAD), glutamate decarboxylase (GAD) and histidine decarboxylase (HDC) and also of enzymes which catalyse α- or γ-eliminations. Enzymes that catalyse β-elimination reactions belong to fold-type II, alanine racemase and a subset of decarboxylases (as eukaryotic ornithine decarboxylase) to fold-type III and D-alanine aminotransferase as well as few other enzymes to fold-type IV. Finally, the fold-type V comprises glycogen and starch phosphorylases.

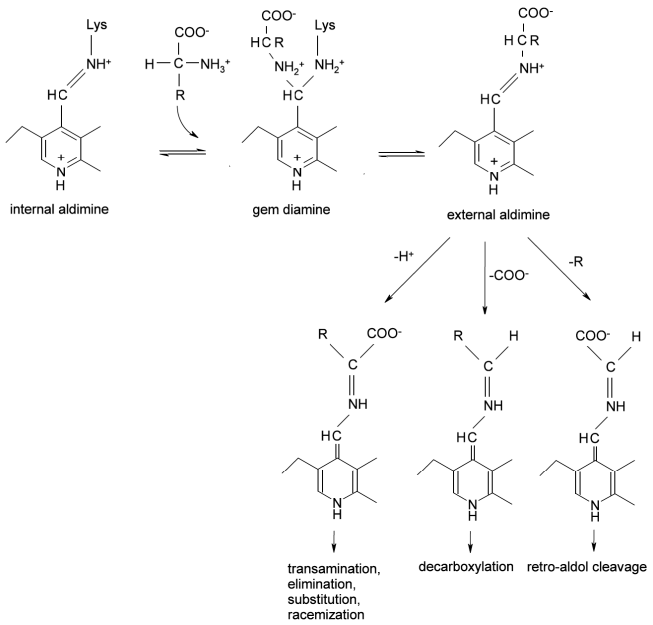

Fig. (1). Catalytic intermediates of PLP-catalyzed reactions in PLP-enzymes. The versatility of the cofactor allows multiple possible reaction pathways according to Dunathan's hypothesis [15].

In 1994, Sandmeier *et al.* [19] proposed a classification for PLP-decarboxylases considering their evolutionary relationships derived by amino acid sequence comparisons. According to this analysis, glycine decarboxylase, both from various prokaryotic and eukaryotic sources, is included in group

I. Group II comprises AADC, CSAD, HDC and GAD from prokaryotic and eukaryotic organisms. Prokaryotic ornithine, lysine and some arginine decarboxylases belong to group III. Finally, eukaryotic ornithine decarboxylases together with both prokaryotic and eukaryotic arginine decarboxylases and diaminopimelate decarboxylase are attributed to group IV. From that investigation [19] it is pointed out that decarboxylases have evolved along multiple lineages and even if some of them act on the same substrate, as or-

nithine decarboxylases, they might not belong to the same group [20-22].

Increasing knowledge, given by structural comparisons, reveals only two different PLP-binding folds for all decarboxylases. Group I, II and III decarboxylases share the PLP-binding motif of fold-type I. Instead, group IV decarboxylases belong to fold-type III.

The hallmarks of decarboxylases belonging to fold-type I are: a) a glycine-rich motif upstream from the PLP-lysine and b) an invariant aspartate residue interacting with the pyridine nitrogen [17, 19]. In fold-type III decarboxylases the PLP-lysine precedes the glycine-rich loop and the pyridine nitrogen positive charge interacts with the carboxy side chain of a glutamate residue which is part of a cluster of acidic residues [21, 22].

Table **1** presents some general characteristics and Fig. (**2**) shows substrates and products of the human group II decarboxylases that are the topics of this review.

HUMAN α-DECARBOXYLASES OF GROUP II: FUNCTIONAL PROPERTIES AND IMPLICATIONS IN DISEASES

AADC

AADC is a homodimeric α-decarboxylase that catalyzes the conversion of L-Dopa or 5- hydroxy-L-tryptophan to the important neurotransmitters dopamine or serotonin, respectively. The reported k_{cat} and K_m kinetic parameters for the pig enzyme are 4.3 ±0.2 s^{-1} and 0.070 ±0.005 mM for L-Dopa and 1.9 ±0.3 s^{-1} and 0.155 ±0.014 mM for 5-hydroxy-L-tryptophan in 50 mM Hepes pH 7.5 [23]. For the human enzyme, the values for L-Dopa are 7.6 ±0.1 s^{-1} and 0.11 ±0.01 mM in 100 mM potassium phosphate buffer pH 7.4 [24]. The enzyme is also able to catalyze the decarboxylation of other cathecol- or indole-related L-amino acids, and, for this reason, it is more appropriately defined aromatic amino acid decarboxylase rather than Dopa decarboxylase. In addition, AADC can catalyze multiple side reactions, such as oxidative deamination and half-transamination, depending on the presence or absence of molecular oxygen [23, 25].

AADC was found in mammalian tissues of neuronal origin, particularly in various areas of mammalian brain and in the sympathetic nervous system in cathecolamine- and serotonin- producing neurons as well as in adrenal and pineal glands and glial cells [26]. Moreover, the presence of the enzyme was also evidenced in nonneuronal tissues, mainly in liver and kidney, and, to a lower extent, in lung, spleen, and pancreas [26]. It is evident that, in neuronal tissues, AADC is devoted to the synthesis of neurotransmitters, while the function of AADC in nonneuronal tissues is far less clear. It has been reported that neuronal AADC could be phosphorylated and thus activated *in vitro* by either cAMP- or cGMP-dependent protein kinase [27, 28], even if the biological significance of this finding is still unknown [29]. Interestingly, Albert *et al.* [30] demon-

Table 1. Human PLP-dependent decarboxylases belonging to the group II.

Name	Acronym[1]	E.C.	Gene	Substrates	Products	Sequence[2]	Structures[3]
Aromatic-L-amino-acid decarboxylase	AADC	4.1.1.28	*DDC*	L-dopa 5-hydroxy-L-tryptophan	Dopamine 5-hydroxytryptamine	P20711 (DDC_HUMAN)	1JS34, 1JS64, 3RBF, 3RBL, 3RCH
Histidine decarboxylase	HDC	4.1.1.22	*HDC*	L-histidine	histamine	P19113 (DCHS_HUMAN)	4E1O
Glutamate decarboxylase 1	GAD67	4.1.1.15	*GAD1*	L-glutamate	4-aminobutanoate (GABA)	Q99259 (DCE1_HUMAN)	2OKJ, 3VP65
Glutamate decarboxylase 2	GAD65	4.1.1.15	*GAD2*	L-glutamate	4-aminobutanoate (GABA)	Q05329 (DCE2_HUMAN)	2OKK
Cysteine sulfinic acid decarboxylase	CSAD	4.1.1.29	*CSAD*	3-sulfino-Lalanine	hypotaurine	Q9Y600 (CSAD_HUMAN)	2JIS

[1]Abbreviation used in this review to indicate to the specific enzyme.
[2]Accession Code in UniProtKB [130].
[3]Accession Code in PDB.
[4]In the case of AADC, the enzyme from *S. scrofa* is also reported (90% sequence identity with the human enzyme).
[5]GAD65/67 chimaera.

strated that the single gene coding for AADC in both neuronal and nonneuronal tissues contains alternative promoters directing expression of neuronal and non-neuronal mRNA, differing only in their 5'- untranslated regions. Kinetic, mechanistic and inhibition studies carried out up to now on mammalian AADC enzymes were reported in a recent review [31].

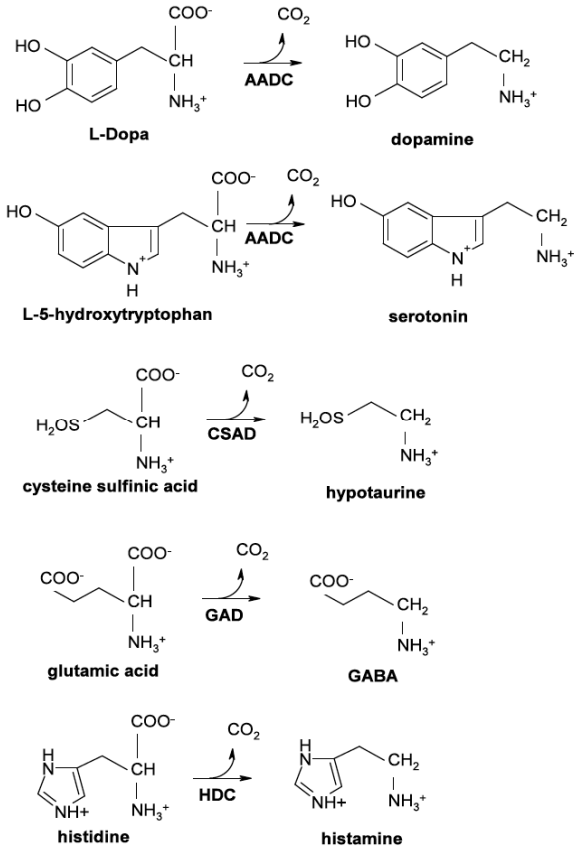

Fig. (2). Substrates and products of the human group II decarboxylases.

AADC is implicated in several clinic disorders. The enzyme is the target of drugs used in Parkinson's disease (PD), a neurodegenerative disease caused by the loss of dopaminergic neurons in *substantia nigra* region of the midbrain resulting in reduced level of dopamine at the neuronal terminals in the striatum [32, 33]. The current treatment for PD consists in the administration of L- Dopa along with a peripheral AADC inhibitor. The inhibitors commonly used are carbidopa (L-α-methyl-α-hydrazino-3,4-dihydroxyphenylpro-pionic acid) or benserazide ((RS)-2-amino-3-hydroxy- N'-(2,3,4-trihydroxybenzyl)propanehydrazide), both unable to cross the blood brain barrier. Benserazide is metabolically cleaved into serine and 2,3,4-trihydroxybenzylhydrazine which is the actual inhibitory molecule. The presence of a hydrazine moiety in both carbidopa and 2,3,4-trihydroxybenzylhydrazine is responsible for the irreversible binding of these inhibitors to the formyl group of PLP leading to the formation of a dead-end hydrazone.

The rationale of the therapy in Parkinsonism is based on the pharmacological principle that the L-Dopa-carbidopa/benserazide combination would reduce the degradation of L-Dopa to dopamine in the peripheral compartment and, consequently, increases the amount of dopamine available to the brain. Since both inhibitors presently available for clinical use lack AADC specificity and are responsible for various undesired side effects, the identification of highly selective and reversible AADC inhibitors has been the subject of recent investigations [34-36], reviewed in [37].

A genetic disorder involving AADC is AADC deficiency. It is an autosomal recessive neurometabolic disease (OMIM 608643) caused by inherited mutations in the *AADC* gene leading to malfunctioning of the enzyme. AADC deficiency is characterized by a cerebrospinal fluid profile of low homovanillic acid and 5-hydroxyindolacetic acid, high L-Dopa and 5-hydroxy-L-tryptophan [38-40]. The associated clinical features are hypotonia, neurodevelopmental delay, oculogyric crises and a complex movement disorder with autonomic features [41, 42]. Definitive diagnosis is further confirmed by the quantification of plasma AADC enzyme activity and finally through *AADC* gene sequencing. The genotyping of AADC deficiency patients (about 100 but they are rapidly increasing) identified more than 25 missense mutations on the *AADC* gene, present in both homozygous and in compound heterozygous patients. Biochemical, cell biology and bioinformatics analyses of the structural and functional consequences of missense mutations present in homozygous patients constitute a significant advancement on the understanding of the mechanism by which pathogenic mutations lead to AADC deficiency, thus allowing to suggest an appropriate therapeutic management [24, 43-45]. In particular, it was evidenced that the majority of mutations associated with AADC deficiency concerns residues involved in the proper transition of apo to holo enzyme [44]. This transition involves a large conformational change as reported in a following section regarding structural comparisons among decarboxylases (see below).

AADC is also regarded as a target of autoantibodies in autoimmune polyendocrine syndrome I (APS I) [46, 47], especially in patients with autoimmune hepatitis [48]. Some studies aimed to map human antibody epitopes on AADC revealed that autoantibodies to the C-

terminal region of the enzyme induce a significant inhibition of decarboxylase activity [48, 49]. These data constitute a first step for the understanding of the interrelation between autoantibody-mediated inhibition of enzymatic activity and epitope specificity.

CSAD

Among α-decarboxylases, CSAD is the less studied member so far. Its first partial characterization was performed on the enzyme extracted from calf brain [50]. The great deal of information on this enzyme is available from the mouse form. The protein is a homodimer of 55 kDa subunits [51] expressed in liver, kidney [52], adipose tissue [53], retina [54], mammary glands [55] and brain, although the level of its expression in the brain is still controversial [56, 57]. CSAD is responsible for the decarboxylation of cysteine sulfinic acid (or cysteic acid) into CO_2 and hypotaurine which is further oxidised to taurine, a molecule playing multiple roles in different biological processes: cell volume regulation, cell homeostasis, bile acids conjugation, mitochondrial tRNA modifications, central nervous and visual systems development [58-60]. This amino acid, the major product of cysteine metabolism, is considered conditionally essential in humans. The published results regarding kinetic parameters of the human CSAD concern the k_{cat}/K_m value reported to be 3550 ±880 $M^{-1}s^{-1}$ [61]. Instead, the reported values of k_{cat} and k_{cat}/K_m for the mouse enzyme are 6.6 s^{-1} and 33000 $M^{-1}s^{-1}$, respectively [57]. CSAD shares high sequence identity with GAD and with human GAD-like protein [57, 62], the latter performing also decarboxylation of cysteine sulfinic acid, involved in taurine synthesis and reported to be associated with bipolar syndrome [63]. Since the expression level of CSAD is low, taurine is often supplemented in diets, especially in infants, even if it is naturally present in foods such as seafood and meat. CSAD knockout mouse model evidenced the important physiological role played by the enzyme in modulating taurine concentration [64]. As AADC, also CSAD acts as autoantigen in APS-1, even if anti-CSAD reactivity has low frequency with respect to AADC or other α-decarboxylases [65].

GAD

GAD catalyzes the irreversible α-decarboxylation of L-glutamic acid to γ-aminobutyric acid (GABA) and CO_2, the former being the major inhibitory neurotransmitter of the mammalian brain [66, 67]. The enzyme was also found in nonneuronal tissues, including the pancreatic islet cell and kidney, where it performs signaling and trophic functions [68].

In addition to the primary decarboxylation reaction, the enzyme catalyzes a secondary slower half- transamination producing pyridoxamine 5'-phosphate (PMP) and succinic semialdehyde. This reaction converts holo form in the apo one, which, upon PLP binding, is reconverted into the active holo form. Of course, in the absence of PLP, a time-dependent GAD inactivation occurs. As a whole, these reactions represent the GAD activity cycle of apo and holoenzyme. In vertebrates, from fish to man, the enzyme exists as two isoforms, GAD67 and GAD65, with a molecular mass of 67kDa and 65kDa, respectively, each encoded by a different gene. A 75% sequence identity is shared by the two isoforms in the decarboxylase domain, being the difference only confined in the first 100-terminal amino acids [69]. The two isoforms have different intracellular distribution: GAD65 is found mainly in synaptic endings, whereas GAD67 is more uniformly distributed through the cell [70]. Notably, many features distinguish GAD67 and GAD65. First, GAD67 is cytosolic, while GAD65 is membrane-associated. Second, the apo forms of GAD67 and GAD65 exhibit different features with respect to interaction with PLP: (i) a lower PLP binding constant for GAD67 than for GAD65 [71], (ii) a much higher rate constant of the apo to holo conversion for GAD65 than for GAD67 [71], and (iii) a major propensity for GAD65 to be converted into the apo form in the presence of glutamate than for GAD67 [71, 72]. Thus, the regulatory role played in the apo/holo ratio could explain why GAD67 is mainly found in the holoform (therefore always active) and is thus responsible for the production of basal levels of GABA, while GAD65 is predominantly in the inactive apo form and is converted into the active holo form only in response to extra GABA requirement. Other compounds were found to play a different regulatory role of the two isoforms in the apo/holo cycle. ATP, which competes with PLP for apo GAD binding, slowed the activation of GAD65 but not that of GAD67 [71]. An opposite effect was observed in the presence of organic phosphate [71]. Again, although both GAD67 and GAD65 are regulated by phosphorylation, the regulation occurs in an opposite manner, *i.e.*, GAD67 is inhibited while GAD65 is activated by phosphorylation. This is consistent with the fact that the two isoforms have a different subcellular distribution and, thus, may be subjected to different regulation in responding to physiological conditions [73].

Another striking difference between GAD67 and GAD65 deserves note. Unlike GAD67, GAD65 is autoantigenic with autoantibodies identified in patients with autoantibodies type I diabetes and the Stiff-person

syndrome, a neurological disorder. It is of interest to notice that binding of autoantibodies causing inhibition of GAD65 *in vitro* occurs in regions such as the C-terminus of the enzyme that show difference in the structure and mobility with respect to GAD67 [72, 74-77] (see below).

The relevance of GAD in the clinical field is evidenced by the fact that abnormally low levels of GABA in the brain are associated with serious neurological disorders such as epilepsy [78], Huntington disease [79], Parkinson's disease [80], and Alzheimer's disease [81]. However, the pharmacological treatments are directed to regulate the levels of GABA by drug design strategy towards either the enzymes involved in GABA processing (such as GABA aminotransferase) or the GABA receptors.

HDC

HDC is the enzyme responsible for the synthesis of histamine from L-histidine. This multifunctional biogenic amine is involved in many physiological and pathological processes: neurotransmission, gastric secretion, anaphylactic reactions and cell proliferation [82].

The expression of HDC is regulated by several factors such as glucocorticoids, cAMP, calcium ions, protein kinase C activity as well as other kinase-related signalling pathways [83-86].

The characterization of human HDC is quite poor and the little available information is relatively recent since the mammalian enzymes are reported to be scarce and unstable proteins. Human HDC is expressed in mast cells, basophils, enterochromaffin-like cells in the stomach, brain neurons, or macrophages. Human and mouse HDC are translated as ~74kDa forms and then subjected to tissue- specific post-translational C-terminal proteolytic cleavage [87-91] to be converted into the catalytically active form [89, 92-94]. Processed isoforms range from ~53 to ~70 kDa, but the active ones are the 53-55 kDa isoforms [94-101]. The role of the C-terminal portion is to drive the HDC monomers to the endoplasmic reticulum before maturation, in order to regulate histamine production [101-103].

Many derivatives of histidine have been identified as inhibitors of HDC. Among them L-histidine methyl ester (HME) which binds to the active site of the enzyme forming an external aldimine that cannot undergo decarboxylation, and α-methylhistidine that behaves as a suicide inhibitor [104, 105]. Again, epigallocatechin 3-gallate [106] and phosphopyridoxyl histidine methylester [107] act as potent inhibitors of HDC. Recently, an aminooxy analog of histidine, 4(5)- aminooxymethylimidazole, was found to inhibit HDC with $IC_{50} \approx 2 \cdot 10^{-7}$ M [108].

HDC-deficient mice present a decreased number of mast cells that are altered in morphology and granular content [109]. The studies on these models confirm the functions of histamine related to contraction of smooth muscle, increase of vascular permeability and stimulation of gastric acid secretion. Moreover, they disclose other roles for this amine such as involvement in angiogenesis, inflammation, neurotransmission [110] and in several types of tumours. A recent paper concerning the available mouse models presents an overview of all the effects examined and evidences the complexity of histamine functions and the advantages/disadvantages in knockout studies versus pharmacological approach [111]. In summary, other systematic experimental data are necessary to unravel the multiple roles played by histamine.

Considering the involvement of the enzyme in pathological states, a truncated variant of HDC (W317X) is considered one of the genetic factors involved in Tourette's syndrome, a severe neuropsychiatric developmental disorder [112, 113]. The W317X mutation exerts a dominant- negative effect on HDC, resulting in lack of enzyme activity. However, recent studies have contradicted this hypothesis and stated that HDC mutations correlate poorly with this disorder [114]. It was also noted that the lack of HDC in mice results in increased locomotor and stereotypic behaviours, as well as increased anxiety [112, 113]. These findings point to a potential role for histaminergic neurotransmission in neurobehavioural actions, such as tics. Moreover, increased HDC activity was demonstrated to be related to multiple tumours growth and HDC was reported to be dysregulated in some cancers [115]. In particular, a critical role of HDC in cholangiocytes proliferation has been assessed [116, 117], although data supporting a role in cholangiocarcinoma are still preliminary.

Finally, as AADC and GAD, also HDC is an APS-1 autoantigen and in one patient, for the first time, a correlation between the presence of antibodies against APS-1 and the lack of gastric enterochromaffin-like cells [118] has been found.

STRUCTURAL COMPARISON OF HUMAN GROUP II α-DECARBOXYLASES: SIMILARITIES AND DIFFERENCES

Till the last century, no experimentally determined structure of any member of group II α- decarboxylases

was available yet. Starting from 2001, when the first crystal structure of a member of this family was solved, *i.e. Sus scrofa* AADC [119] (~90% sequence identity with the human homologous enzyme), we have witnessed a dramatic increase in the knowledge of the structural features of group II decarboxylases, which offers a detailed understanding of their similar enzymatic activities and highlights, at the same time, the key differences responsible for substrate specificity (Table **1**; [77, 120]). Most importantly, this wealth of structural information paves the way for a detailed understanding, at molecular level, of some pathological states associated to these enzymes.

The Overall Topology

From a structural and evolutionary standpoint, the decarboxylase domains of AADC, CSAD, GAD65/67 and HDC belong to the superfamily of fold-type I PLP-dependent enzymes, sharing a number of structural features that remained invariant upon the long evolutionary history of this superfamily [10] (Fig. **3A**). In particular, as in the case of every fold-type I enzyme, group II decarboxylases are structural and functional dimers. The dimer represents the obligate quaternary structure required to generate a functional enzyme [121]. Moreover, they maintain all of the seventeen structurally conserved regions and the appropriate positioning of key residues, which are crucial for keeping the fold-type I fold and binding the PLP cofactor [122]. A detailed comparison of the available sequences and structures of the decarboxylase domains of AADC, CSAD, GAD65, GAD67 and HDC suggests that this group of enzymes can be further clustered in two different evolutionary subgroups, comprising AADC and HDC in a first subgroup (root mean- square deviation, RMSD ≈ 0.8 Å), and GAD65/GAD67/CSAD in the other one (mean RMSD ≈ 0.5 Å) [19] (Fig. **3B**).

Each of the two monomers is composed of three distinct domains (Fig. **4**). A "large" domain, which consists of seven buried β-strands forming a β-sheet surrounded by eight α-helices, displays the α/β fold typical of fold-type I enzymes and hosts the PLP cofactor. A "C-terminal", or "small" domain, composed by a four-stranded antiparallel β-sheet and three α-helices, faces the opposite monomer.

Finally, a "N-terminal" domain, composed by two helices linked by an extended strand, represents a distinct structural tract of all the group II decarboxylases. The latter forms a clamp to the neighboring subunit, with the first helix of one subunit aligning antiparallel to the equivalent helix of the other subunit. It is suggested that this N-terminal domain is unlikely to represent an autonomous folding unit, but it is most likely stable only in the context of the dimer. The main function of this N-terminal domain would be to extend the interface between the two monomers [119]. A search of structurally similar domains, using the DALI server and the N-terminal domain of human AADC as query, highlights the presence of highly similar domains (RMSD < 3.0 Å over the entire N-terminal length) in other decarboxylases of bacterial origin (*i.e.*, PLP-dependent decarboxylase from *Sphaerobacter thermophiles*, PDB Code: 4RLG; tryptophan decarboxylase from *Ruminococcus gnavus*, PDB Code: 4OBV). Interestingly, an analysis of the Human Microbiome Project data demonstrates that at least 10% of the human population harbors at least one bacterium encoding a tryptophan decarboxylase in their gut community [123].

The N-terminal and the small C-terminal domains pack together *via* a short two-stranded sheet to close the monomer. The N- and C-terminal domains of each monomer form a structural and functional unit that is hypothesized to permit the large conformational changes accompanying the open-to-close switch of these enzymes (see below).

The Active Site Residues Interacting with the PLP Cofactor

The active site where the PLP cofactor lies is located at the monomer-monomer interface. The homologous residues of the five enzymes interacting with the PLP cofactor are very well conserved and are shown in Table **2** and Fig. (**5**). The PLP cofactor binds to an evolutionarily invariant Lys residue through a Schiff base linkage. As already mentioned above, the carboxylate group of a conserved Asp residue stabilizes, *via* an electrostatic interaction, the protonated pyridine nitrogen of PLP, providing the latter with a strong electrophilic nature necessary for the stabilization of carbanionic intermediates during the enzymatic catalysis. Another well conserved base-stacking His residue is positioned on the *re* face of the pyridine ring of PLP, while the *si* face makes a hydrophobic interaction with a conserved Ala residue. The oxygen atom in position 3 of PLP is stabilized *via* a hydrogen bond with a Thr residue. The phosphate group of PLP is further anchored to the protein through an extended hydrogen bond network. The α5-helix dipole from the large domain, which is well conserved in fold-type I enzymes, is also responsible for the proper stabilization of the negative phosphate moiety.

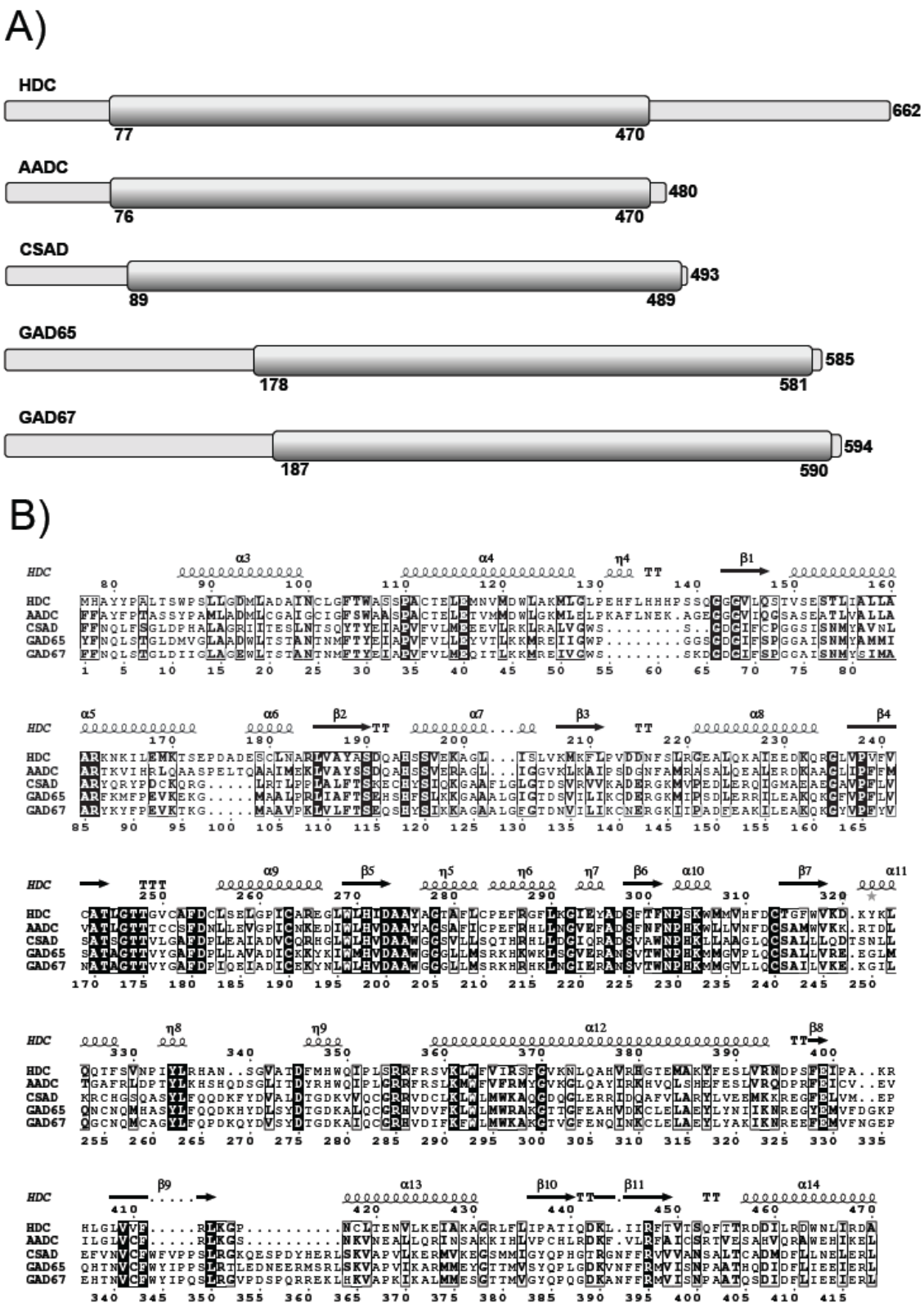

Fig. (3). A) Schematic representation of protein sequences of human group II decarboxylases. The length of each sequence is indicated on the right of each bar. The position of the decarboxylase domain (PFAM ID: PF00282; [69]) relative to each sequence is also shown. B) Multiple sequence alignment of human group II decarboxylases. Amino acid one-letter code is used. Dashes represent insertions and deletions. Invariant positions are boxed in black. The secondary structures of human HDC (PDB code 4E1O) are reported in the first line of each block: α-helices and β-strands are rendered as squiggles and arrows, respectively. ESPript ([134]; http://espript.ibcp.fr) was used to render this figure.

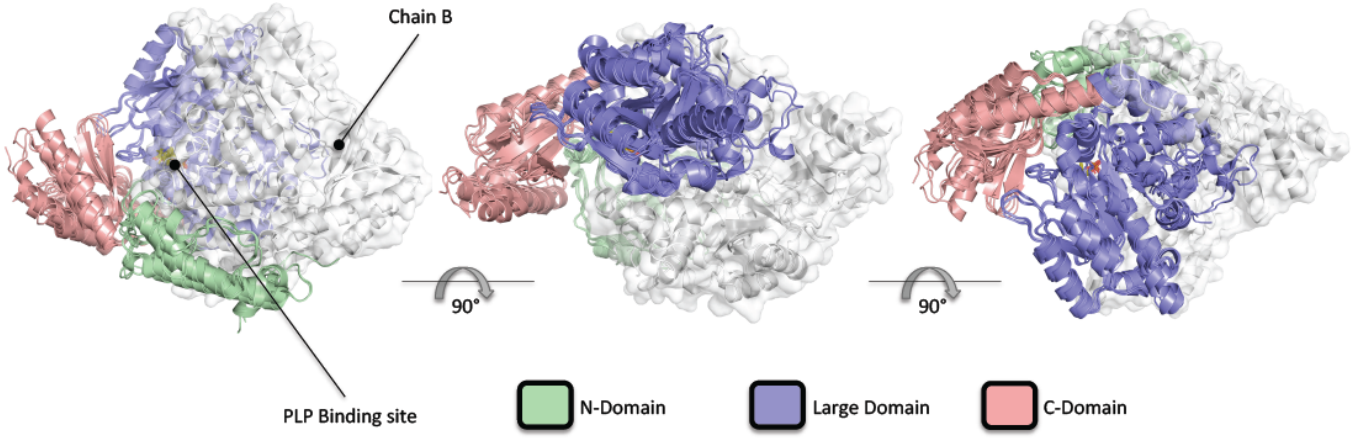

Fig. (4). Structural superposition of group II decarboxylases (HDC, AADC, GAD65, GAD67 and CSAD). In the case of AADC, the enzyme from *S. scrofa* was used. The N-terminal, large and C- terminal domains are represented in green, cyan and pink, respectively. Chain B is represented as grey cartoons and surface.

Table 2. Residues of group II decarboxylases interacting with PLP and substrates.

	PLP						Substrate	
	Schiff base	**N1**	**O3**	***Re* side**	***Si* side**	**Phosphate**	**α-carboxylate**	**Side-chain**
AADC	K303	D271	T246	H192	A273	S147, A148, S149, N300, H302	H192	T82, I101, H302
HDC	K305	D273	T248	H194	A275	V150, S151, N302, S354	H194	Y81, L102, S354
GAD67	K405	D373	T348	H291	A375	G252, A253, N402, H404, G456	R567	S192, N212, F214
GAD65	K396	D364	T339	H282	A366	G243, A244, N393, H395, G447	R558	S183, N203, F205
CSAD	K305	D273	T248	H191	A275	G152, S153, N302, H304, G357	R466	F94, S114, Y116

The Active Site Residues Interacting with the Ligands

AADC and HDC have been both crystallized in complex with their respective inhibitors carbidopa and HME, while the structures of GAD65 and GAD67 have been determined with their reaction product GABA. The structure of CSAD has been solved solely with the PLP cofactor bound as internal aldimine (data not published).

In AADC and HDC structures, the α-carboxylate moiety of the inhibitor is always placed approximately orthogonal to the plane of the PLP ring, in agreement with Dunathan's hypothesis [15] that foresees the perpendicular orientation of the scissile bond to the pyridine ring of PLP to allow the greatest overlap between the σand πorbitals during the transition state, as reported above. Crystallographic data on these complexes give therefore precious insights into the binding mode of substrates and inhibitors of human group II decarboxylases, and suggest at the same time how each enzyme is able to achieve reaction specificity and substrate selectivity.

The binding cleft where the ligands are bound is deeply buried into the active site cavity and extends underneath the *si* face of the pyridine ring of PLP. The

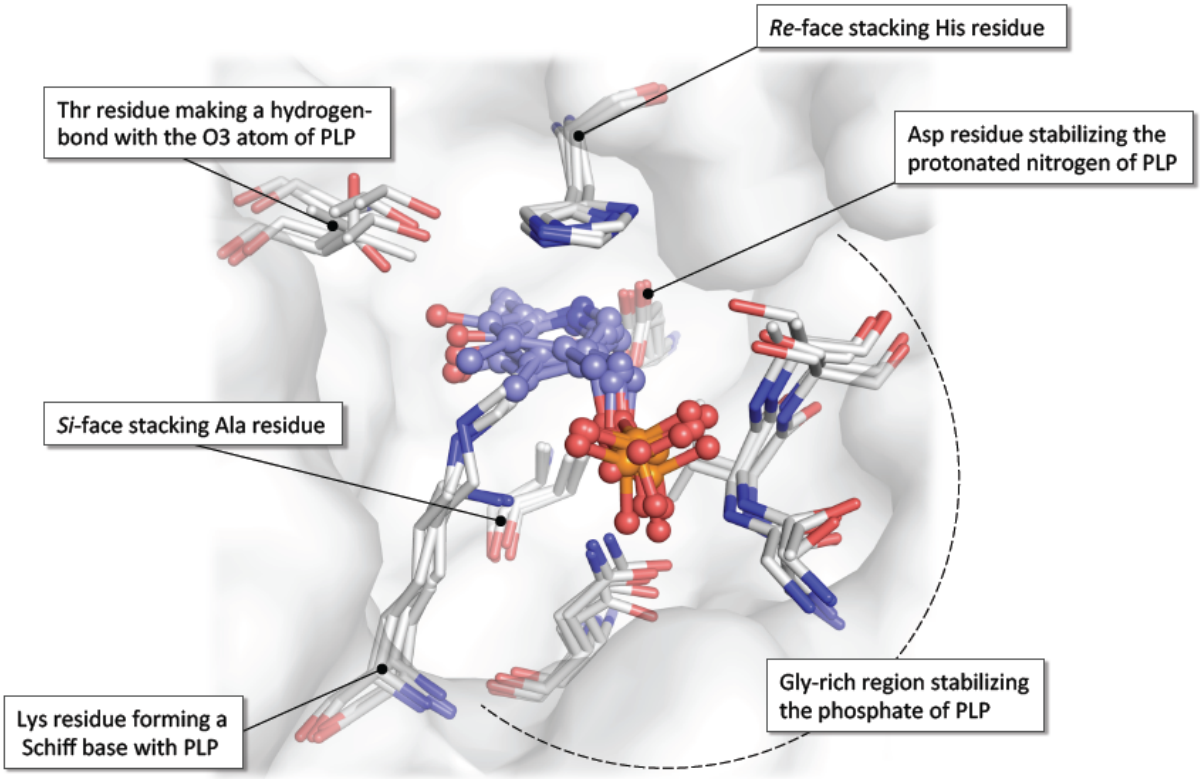

Fig. (5). Homologous residues (white sticks) of human group II decarboxylases interacting with the PLP cofactor (cyan ball-and-sticks).

homologous residues of the five enzymes interacting with the ligands are shown in Table **2**.

In the case of AADC, the inhibitor carbidopa forms a hydrazone linkage with PLP, mimicking the external aldimine enzyme-substrate intermediate. His192 and three structural water molecules interact with the α-carboxylate moiety of the inhibitor. Given the high structural similarity, it is expected that also the α-carboxylate groups of the substrates are involved in the same interactions. One of the catechol hydroxyl groups of the inhibitor makes a hydrogen bond with the side chain of Thr82**,** which is located at the bottom of the ligand binding cleft. The other hydroxyl group of the catechol is hydrogen bonded with the phosphate moiety of PLP, and is also placed at hydrogen bonding distance with the imidazole ring of His302. Modelling of another inhibitor of human AADC into the ligand binding cleft, benserazide, evidenced that the latter could be accommodated without any major adjustment of the side chains of the residues composing the cleft [35, 119].

A structural comparison of the substrate-binding pocket of HDC and AADC evidenced that the conformation of the inhibitors carbidopa and HME was quite similar [120], but highlighted at the same time key differences responsible for substrate specificity ferences responsible for substrate specificity (Fig. **6**). Like carbidopa, the imidazole ring of HME points toward the *si* face of the PLP-HME external aldimine, and makes two hydrogen-bonds with the main-chain of Tyr81 and a structural water molecule. Interestingly, the latter and a second water molecule in the substrate-binding pocket of HDC occupy the same position of the two hydroxyl groups of the cathecol ring of carbidopa. A crucial difference between the substrate-binding pocket of AADC and HDC is represented by the presence in the latter enzyme of a Ser residue, namely Ser354, which is replaced by a Gly in AADC. The imidazole ring of HME is at hydrogen bonding distance from Ser354, suggesting that the latter could be a key residue for substrate specificity. Indeed, the S354G mutation in HDC resulted in a decreased affinity for histidine, but at the same time an acquired ability to catalyze the decarboxylation of L-Dopa. It was therefore suggested that the mutation enlarged the size of the HDC substrate-binding pocket to permit the binding of a six-membered ring [120].

In the case of GAD65/GAD67/CSAD, the need to bind and select an aliphatic chain instead of an aromatic one imposes a narrower binding cleft compared to HDC and AADC, which is achieved by a structural

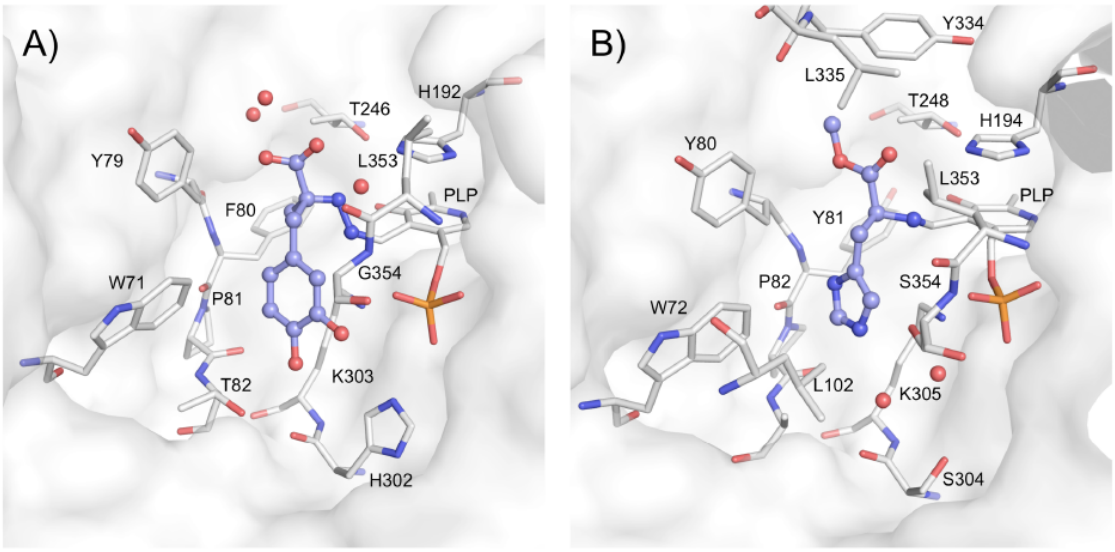

Fig. (6). Comparison of the active sites of A) AADC and B) HDC. Residues are labeled according to PDB numbering and shown as white sticks. Carbidopa and HME are shown as cyan ball-and-sticks.

modification of the loop region connecting the N-terminal with the large domain (Fig. **7**). An aromatic residue in AADC and HDC (Phe80 and Tyr81, respectively) twists the loop by making a stacking interaction with another Tyr residue of the large domain (Tyr274 and Tyr276, respectively) and creates the necessary space to bind aromatic ligands.

In the active site of GAD67, two discretely disordered conformations of GABA are observed. Though the resolution of the data precludes a full mechanistic interpretation on the GABA binding mode, nonetheless by comparing the structure of GAD67 with the other group II decarboxylases it appears quite clear that the side-chain of GAD65/GAD67 ligands occupy the same pocket and points toward the *si* face of the PLP cofactor. In particular, with the α-carboxylate moiety interacting with Arg567(GAD67)/Arg558(GAD65), the γ-carboxylate group would point to a cleft formed by Ser192(GAD67)/Ser183(GAD65), Asn212(GAD67)/Asn203(GAD65) and Phe214(GAD67)/Phe205 (GAD65). Interestingly, these three residues constitute a substrate recognition motif within the active site that is responsible for coordinating the respective preferred amino acid substrates of GAD and CSAD [61]. Introduction of the CSAD substrate recognition motif (Phe94, Ser114, and Tyr116) into GAD67 (GAD67: S192F/N212S/F214Y) resulted in an enzyme with a >700 fold switch in selectivity toward the decarboxylation of cysteine sulfinic acid over L-glutamic acid [61].

The Mobile Catalytic Loop

Human group II decarboxylases are all characterized by the presence of a highly flexible active site loop, which is important for the catalytic mechanism of decarboxylation (Fig. **8**) [77, 120, 124]. This 'catalytic loop' is located at the dimer interface and extends towards the active site of the other monomer in a closed conformation. It is well ordered and clearly assigned in the electron density map of HDC, CSAD and GAD67 [77, 120], whereas it was found mostly disordered and lacked electron density in the structures of AADC and GAD65 [77, 119]. Interestingly, several studies have shown that these loops are more prone to cleavage by proteases in the ligand-free form of the decarboxylases, whereas they are cleaved to a much lesser extent in the presence of substrates/inhibitors [125]. Therefore, structural and mechanistic data strongly suggest that before substrate binding, the loop adopts an 'open' conformation that is more solvent- exposed and prone to proteases cleavage, while after substrate binding and during catalysis, it could occlude the active site cleft and act as a lid for solvent shielding [77, 120, 124]. The latter assists the conversion of carboxylate to the more hydrophobic CO_2 product. Moreover, it has been also demonstrated that some loop residues take part in the catalytic mechanism. In GAD67 and HDC, a very well conserved residue (Tyr434/Tyr334 in GAD67/HDC, respectively) is placed into close proximity to the PLP-stacking His residue and GABA/HME [77, 120]. In the case of AADC, GAD and HDC, the loop Tyr→Phe substitution resulted in an enzyme unable to produce amines, clearly indicating that this residue is crucial for the decarboxylase activity [77, 120, 124]. Thus, it was suggested that the role of this conserved Tyr residue is to act as a proton donor to the negatively charged Cα atom of the carboanionic qui-

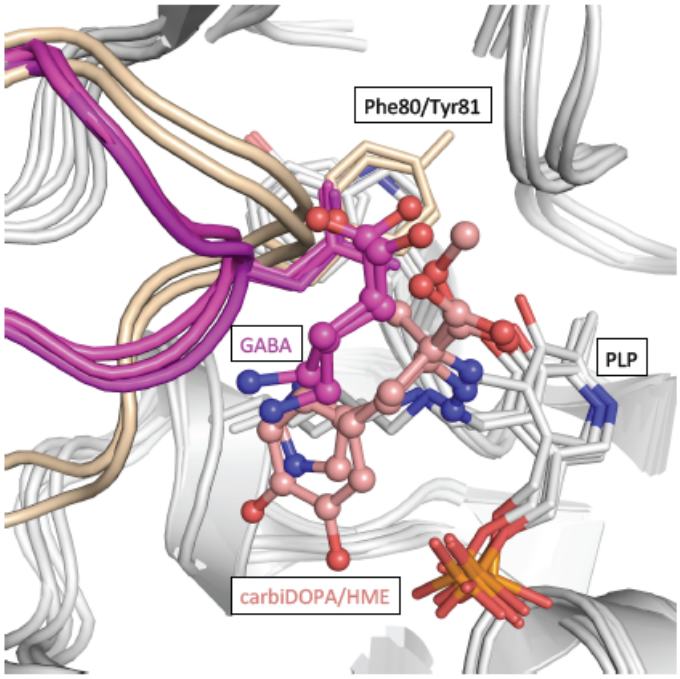

Fig. (7). Comparison of the substrate-specificty loop of decarboxylases. The loops of AADC and HDC with PLP bound to carbidopa or HME, respectively, are colored in beige, while the loops of GAD65, GAD67 with PLP-GABA and CSAD are depicted in magenta. Residues are labeled according to PDB numbering and shown as sticks. Carbidopa (pink), HME (pink) and GABA (magenta) are shown as ball-and-sticks.

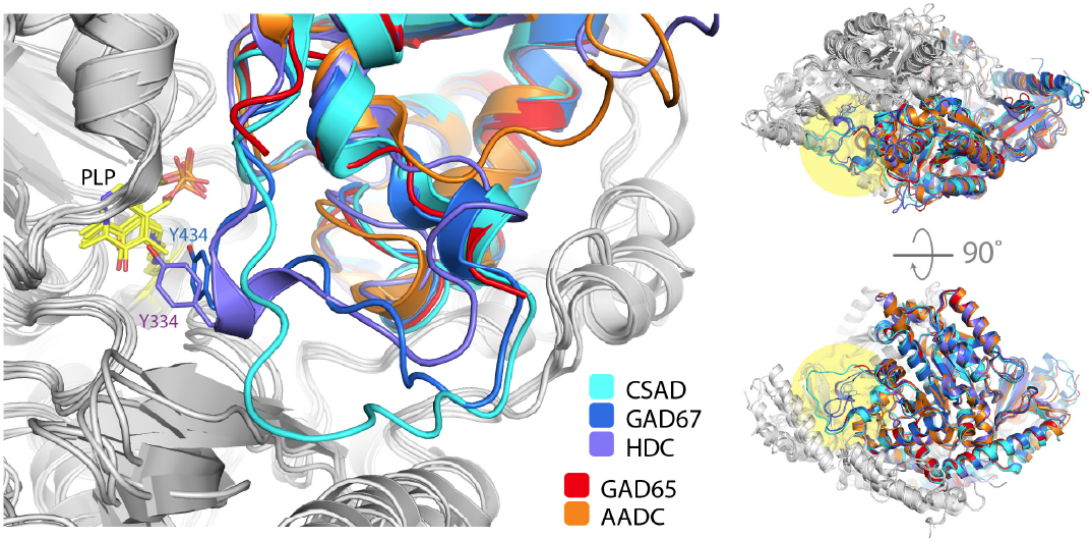

Fig. (8). Comparison of the mobile catalytic loop of group II decarboxylases. The loop is located at the dimer interface and extends towards the active site of the other monomer. The coordinates of the loops of GAD65 and AADC are missing due to the high flexibility of this region. Tyr334 and Tyr434 of HDC and GAD67, respectively, are shown as sticks.

nonoid intermediate [77, 120, 124]. The close proximity to the PLP-stacking His favors indeed this mechanism by lowering the pK$_a$ of Tyr. Although the conserved Tyr residue of the loop is crucial for catalysis, the other residues composing the loop are nonetheless important for the proper positioning and mechanism of the loop. Enzymatic studies on HDC and AADC have shown that also the surrounding loop region affects catalytic activity [45, 126], and have revealed the molecular basis for the pathogenicity of some variants (e.g. R347G and R347Q of AADC) in AADC deficiency [45].

As above mentioned, unlike the constitutively active GAD67, GAD65 undergoes auto-inactivation after catalyzing a side-reaction (*i.e.*, conversion of glutamate

to succinic semialdehyde acid), during which PLP is released as PMP [77, 127]. The very high mobility of the flexible loop of GAD65 was invoked as a possible reason promoting the side reaction and subsequent auto-inactivation. To test this hypothesis, Langendorf *et al.* created a panel of GAD65-67 chimaeras, including a GAD67$_{65loop}$ mutant [128]. Consequent structural and mechanistic analysis revealed that the conformational changes in the catalytic loop and auto-inactivation of the enzymes are also intimately linked to the conformation of the C-terminal domain [128] (see below) and, notably, that the very same structural features, which represent requirements for GAD enzymatic mechanism, distinguish GAD65 from GAD67 as a B cell autoantigen [72, 76].

The Open-to-Close Conformation

An interesting aspect of group II decarboxylases regulation that recently emerged, when the crystal structure of human *apo*-AADC was determined [129], forces us to reconsider the mechanism of PLP addition and preferential degradation of the *apo*- decarboxylases in a new perspective.

In 2011, Giardina *et al.* demonstrated that *apo*-AADC exists in an unexpected open conformation in which, compared with the AADC holoenzyme, the dimer subunits move up to 20Å apart and the two active sites become solvent-exposed (Fig. **9**) [129]. The open conformation is achieved through a rigid body quaternary rearrangement of the dimer around a fixed dimer interface, comprising only a helix-bundle of the N-terminal domain. Intriguingly, the *apo*-AADC structure was compared to an "open bivalve shell", with the interface between the N-domains functioning as the hinge [129]. The existence of such an open conformation of the *apo*-AADC implies that a large part of the *apo*-dimer interface is exposed, with the mobile catalytic loop of the active site (which connects the large domain to the C-terminal one) becoming more flexile and unstructured. Given that ubiquitin-ligases recognize unstructured regions of the target protein or newly exposed surfaces, these data could explain why *apo*-AADC is degraded at least 20-fold faster than the holoenzyme in rat brain cells [130].

In addition, as stated above, it should be also considered that many of the point mutations responsible for AADC deficiency map on residues present in regions of the apoenzyme involved in the transition to the holo form. A possible cause for the phenotype of the patients bearing these AADC mutations could be the inability to perform an efficient apo-to-holo active site closure.

The mechanism of selective degradation of *apo*-decarboxylases *in vivo* could represent a common strategy of this family to finely regulate the availability of the total enzyme and its activity, based on PLP abundance. Indeed, as in the case of AADC, it has been demonstrated that *holo*-GAD has a much higher stability than *apo*-GAD [131]. Recently, coupling molecular dynamics simulations and normal mode analyses with small-angle X-ray scattering and fluorescence spectroscopy data, Kass *et al.* described a similar conformational opening of *holo*-GAD65 and the dynamic communication between domains that drive this process [72], which involves a structural crosstalk between the mobile catalytic loop and the C-terminal domain, as previously mentioned. Intriguingly, an origami analogy was proposed illustrating the mechanism of dimer opening, which could be equally applicable to the *apo*→*holo* transitions of both AADC and GAD65 [72, 129]. Finally, it was concluded that this conformational plasticity of human GAD65, enabling regulation of GABA synthesis based on PLP availability, could have come at the cost of its involvement as a prevalent autoantigen in autoimmune Type-1-Diabetes [72].

Development of New Inhibitors and/or Pharmacological Chaperones Based on the Available Structural Data

As reported above, the wealth of structural information gained in recent years on group II decarboxylases provided us with a detailed description of the key similarities and differences that could be exploited for new therapeutic strategies. Indeed, the most effective drugs targeting members of this family are still lacking specificity, and are responsible for various side effects and adverse reactions.

CarbiDOPA and benserazide (more precisely, the metabolically derivative of benserazide, 2,3,4- trihydroxybenzylhydrazine), the AADC inhibitors employed clinically to treat Parkinson's disease, are both endowed with a hydrazine function, which irreversibly binds not only to AADC but also to free pyridoxal 5'-phosphate and pyridoxal 5'-phosphate-dependent enzymes [37]. In a recent effort to identify more specific inhibitors of AADC, a structure-based screening approach leaded to the identification of novel compounds with Ki values in the nanomolar range and, most importantly, unable to bind free PLP [35]. In this study, the peculiar interactions between the catechol moiety of CarbiDOPA and the AADC ligand binding cleft, as assessed by the visual inspection of the crystal structure, were exploited to derive a pharmacophore map

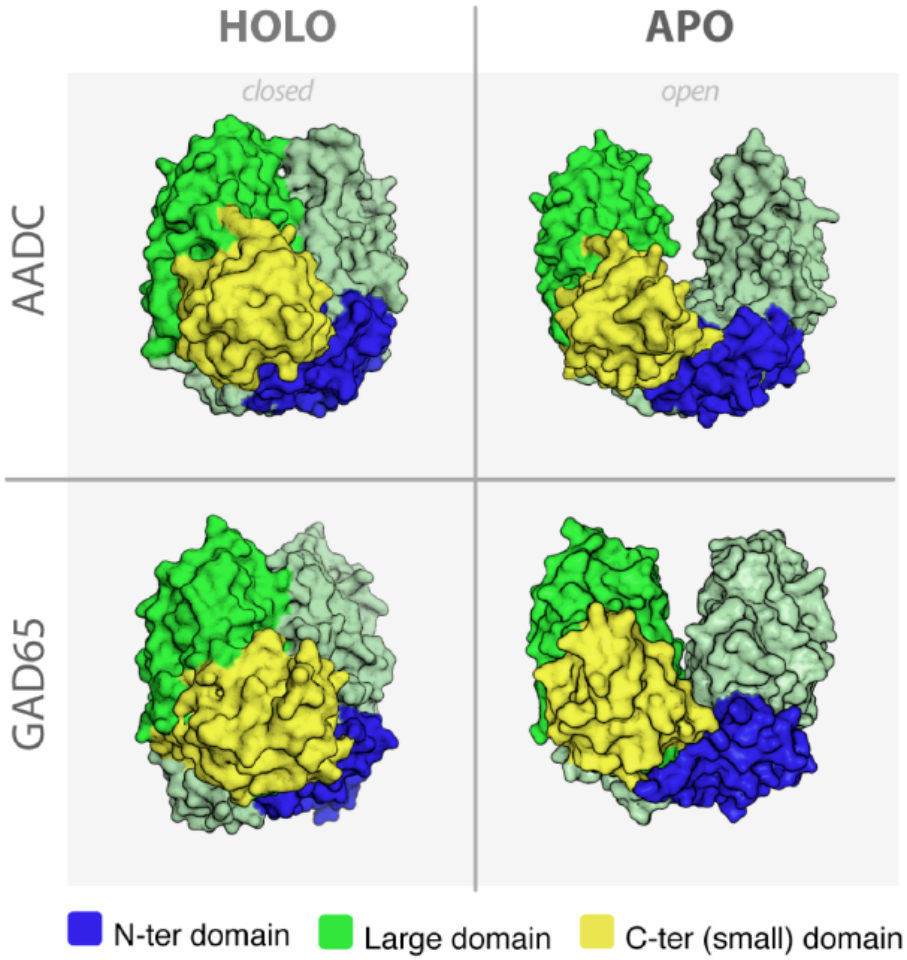

Fig. (9). Molecular surface representation of the open and closed dimers of AADC and GAD65 and the proposed mechanism of dimer opening in *holo* → *apo* conversion.

that, in turn, permitted the rational design of structure-based inhibitors. In addition, we recently examined the structural motifs involved in AADC inhibition shared by all the inhibitors identified so far [37]. Given the high structural similarity between AADC and HDC, it is conceivable that a similar approach, and/or subtle modifications of the scaffolds described in [35], could pave the way to the identification of HDC inhibitors. Indeed, as already mentioned, the Ser354 residue of HDC, which stabilizes the imidazole ring of the substrate, could act as a key determinant for inhibitor specificity.

Regulation of GABA levels in brain is mainly achieved by acting on GABA aminotransferase and/or GABA receptors [11] and transporters [132]. However, clinical disorders known to affect GABA metabolism and to lead to an excess of GABA could be treated also by targeting GAD enzymes. In this perspective, the structure-based design of inhibitors binding to the substrate recognition cleft of GAD65/GAD67/CSAD, which evolved to specifically bind aliphatic compounds, could represent a successful strategy. On the other hand, severe conditions as epilepsy and anxiety-related disorders (*e.g.,* panic disorder and post-traumatic stress disorder) are all associated with low levels of GABA [133]. As already discussed above, transiently stabilizing the catalytic loop region of GAD65 with inhibitors and/or pharmacological chaperones will possibly result in a dramatic increase in the GABA production levels.

Finally, acting on the selective degradation of apo-decarboxylases *in vivo,* for example with pharmacological chaperones able to rescue a productive enzyme conformation, could represent a common strategy in diverse diseases as AADC deficiency and Type-1-Diabetes.

CONCLUSION

Here we have i) reviewed the functional properties of the human PLP-α-decarboxylases AADC, CSAD, GAD and HDC, which belong to group II and synthe-

size important neurotransmitters, and (ii) provided the reader an up-date of their structural organization highlighting structural elements shared by these enzymes as well as those that differentiate them and are responsible for their substrate specificity. The current increase in the knowledge of the structure-function relationships of these decarboxylases makes this subject of topical interest in the purpose of fine tuning the therapy of several diseases (type I diabetes, PD, AADC deficiency, Tourette's syndrome, cholangiocarcinoma, APS-1) in which they are involved. The unraveling, from a molecular point of view, of their similar structural traits and of those underlying their individual substrate preference could help in facing the different diseases in which these decarboxylases are key players. In fact, residues of the mobile loop as well as those involved in the apo-to-holo transition could be envisaged as preferential targets for planning an oriented drug-design for finding more suitable drugs with therapeutic promise or for developing a pharmacological chaperone approach.

ABBREVIATIONS

AADC = aromatic amino acid decarboxylase

CSAD = cysteine sulfinic acid decarboxylase

HDC = histidine decarboxylase

GAD = glutamate decarboxylase

PLP = pyridoxal 5'-phosphate

PD = Parkinson's disease

APS I = polyendocrine syndrome I

GABA = γ-aminobutyric acid

PMP = pyridoxamine 5'-phosphate

HME = L-histidine methyl ester

RMSD = root mean-square deviation

CONFLICT OF INTEREST

The author(s) confirm that this article content has no conflict of interest.

ACKNOWLEDGEMENTS

Declared none.

REFERENCES

[1] Percudani, R.; Peracchi, A. A genomic overview of pyridoxal-phosphate-dependent enzymes. *EMBO Rep.,* **2003**, *4*(9), 850-854.

[2] Metzler, D.E.; Snell, E.E. Deamination of serine. I. Catalytic deamination of serine and cysteine by pyridoxal and metal salts. *J. Biol. Chem.,* **1952**, *198*(1), 353-361.

[3] Metzler, D.E.; Snell, E.E. Deamination of serine. II. D-Serine dehydrase, a vitamin B6 enzyme from Escherichia coli. *J. Biol. Chem.,* **1952**, *198*(1), 363-373.

[4] Metzler, D.E.; Snell, E.E. Some transamination reactions involving vitamin B6. *J. Am. Chem. Soc.,* **1952**, *74*, 5.

[5] Braunstein, A.E.; Shemyakin, M.M. *Biokhimiya,* **1953**, 18.

[6] Braunstein, A.E. *The Enzymes*; Academic Press: New York, **1960**.

[7] Braunstein, A.E. *Chemical and biological aspects of pyridoxal catalysis*; Pergamon Press: New York, **1963**.

[8] Hayashi, H. Pyridoxal enzymes: mechanistic diversity and uniformity. *J. Biochem.,* **1995**, *118*(3), 463-473.

[9] Eliot, A.C.; Kirsch, J.F. Pyridoxal phosphate enzymes: mechanistic, structural, and evolutionary considerations. *Annu. Rev. Biochem.,* **2004**, *73*, 383-415.

[11] Amadasi, A.; Bertoldi, M.; Contestabile, R.; Bettati, S.; Cellini, B.; di Salvo, M.L.; Borri-Voltattorni, C.; Bossa, F.; Mozzarelli, A. Pyridoxal 5-phosphate enzymes as targets for therapeutic agents. *Curr. Med. Chem.,* **2007**, *14*(12), 1291-1324.

[12] Toney, M.D. Pyridoxal phosphate enzymology. *Biochim. Biophys. Acta,* **2011**, *1814*(11), 1405-1406.

[13] Toney, M.D. Controlling reaction specificity in pyridoxal phosphate enzymes. *Biochim. Biophys. Acta,* **2011**, *1814*(11), 1407-1418.

[14] Phillips, R.S. Chemistry and diversity of pyridoxal-5-phosphate dependent enzymes. *Biochim. Biophys. Acta,* **2015**, *1854*(9), 1167-1174.

[15] Dunathan, H.C. Conformation and reaction specificity in pyridoxal phosphate enzymes. *Proc. Natl. Acad. Sci. USA,* **1966**, *55*(4), 712-716.

[16] Livanova, N.B.; Chebotareva, N.A.; Eronina, T.B.; Kurganov, B.I. Pyridoxal 5-phosphate as a catalytic and conformational cofactor of muscle glycogen phosphorylase B. *Biochemistry (Mosc.),* **2002**, *67*(10), 1089-1098.

[17] Grishin, N.V.; Phillips, M.A.; Goldsmith, E.J. Modeling of the spatial structure of eukaryotic ornithine decarboxylases. *Protein Sci.,* **1995**, *4*(7), 1291-1304.

[18] Schneider, G.; Käck, H.; Lindqvist, Y. The manifold of vitamin B6 dependent enzymes. *Structure,* **2000**, *8*(1), R1-R6.

[19] Sandmeier, E.; Hale, T.I.; Christen, P. Multiple evolutionary origin of pyridoxal-5-phosphate-dependent amino acid decarboxylases. *Eur. J. Biochem.,* **1994**, *221*(3), 997-1002.

[20] Momany, C.; Ernst, S.; Ghosh, R.; Chang, N.L.; Hackert, M.L. Crystallographic structure of a PLP-dependent ornithine decarboxylase from Lactobacillus 30a to 3.0 A resolution. *J. Mol. Biol.,* **1995**, *252*(5), 643-655.

[21] Kern, A.D.; Oliveira, M.A.; Coffino, P.; Hackert, M.L. Structure of mammalian ornithine decarboxylase at 1.6 A resolution: stereochemical implications of PLP-dependent amino acid decarboxylases. *Structure,* **1999**, *7*(5), 567-581.

[22] Almrud, J.J.; Oliveira, M.A.; Kern, A.D.; Grishin, N.V.; Phillips, M.A.; Hackert, M.L. Crystal structure of human ornithine decarboxylase at 2.1 A resolution: structural insights to antizyme binding. *J. Mol. Biol.,* **2000**, *295*(1), 7-16.

[23] Bertoldi, M.; Borri Voltattorni, C. Reaction of dopa decarboxylase with L-aromatic amino acids under aerobic and anaerobic conditions. *Biochem. J.,* **2000**, *352*(Pt 2), 533-538.

[24] Montioli, R.; Cellini, B.; Borri Voltattorni, C. Molecular insights into the pathogenicity of variants associated with the aromatic amino acid decarboxylase deficiency. *J. Inherit. Metab. Dis.,* **2011**, *34*(6), 1213-1224.

[25] Bertoldi, M.; Borri Voltattorni, C. Reaction and substrate specificity of recombinant pig kidney Dopa decarboxylase

under aerobic and anaerobic conditions. *Biochim. Biophys. Acta,* **2003**, *1647*(1-2), 42-47.

[26] Borri Voltattorni, C.; Bertoldi, M. Dopa decarboxylase. In: *Encyclopedia of Molecular Medicine*; Creighton, T., Ed.; John Wiley and Sons, Inc.: New York, **2002**; Vol. 2, pp. 1089-1093.

[27] Duchemin, A.M.; Berry, M.D.; Neff, N.H.; Hadjiconstantinou, M. Phosphorylation and activation of brain aromatic L-amino acid decarboxylase by cyclic AMP-dependent protein kinase. *J. Neurochem.,* **2000**, *75*(2), 725-731.

[28] Duchemin, A.M.; Neff, N.H.; Hadjiconstantinou, M.; Aromatic, L. Aromatic L-amino acid decarboxylase phosphorylation and activation by PKGIalpha *in vitro*. *J. Neurochem.,* **2010**, *114*(2), 542-552.

[29] Waymire, J.C.; Haycock, J.W. Lack of regulation of aromatic L-amino acid decarboxylase in intact bovine chromaffin cells. *J. Neurochem.,* **2002**, *81*(3), 589-593.

[30] Albert, V.R.; Lee, M.R.; Bolden, A.H.; Wurzburger, R.J.; Aguanno, A. Distinct promoters direct neuronal and non-neuronal expression of rat aromatic L-amino acid decarboxylase. *Proc. Natl. Acad. Sci. USA,* **1992**, *89*(24), 12053-12057.

[31] Bertoldi, M. Mammalian Dopa decarboxylase: structure, catalytic activity and inhibition. *Arch. Biochem. Biophys.,* **2014**, *546*, 1-7.

[32] Feany, M.B.; Bender, W.W. A Drosophila model of Parkinson's disease. *Nature,* **2000**, *404*, 394-398.

[33] Masliah, E.; Rockenstein, E.; Veinbergs, I.; Mallory, M.; Hashimoto, M.; Takeda, A.; Sagara, Y.; Sisk, A.; Mucke, L. Dopaminergic loss and inclusion body formation in alpha-synuclein mice: implications for neurodegenerative disorders. *Science,* **2000**, *287*(5456), 1265-1269.

[34] Cheng, P.; Zhou, J.; Qing, Z.; Kang, W.; Liu, S.; Liu, W.; Xie, H.; Zeng, J. Synthesis of 5-methyl phenanthridium derivatives: a new class of human DOPA decarboxylase inhibitors. *Bioorg. Med. Chem. Lett.,* **2014**, *24*(12), 2712-2716.

[35] Daidone, F.; Montioli, R.; Paiardini, A.; Cellini, B.; Macchiarulo, A.; Giardina, G.; Bossa, F.; Borri Voltattorni, C. Identification by virtual screening and *in vitro* testing of human DOPA decarboxylase inhibitors. *PLoS One,* **2012**, *7*(2), e31610.

[36] Ren, J.; Zhang, Y.; Jin, H.; Yu, J.; Zhou, Y.; Wu, F.; Zhang, W. Novel inhibitors of human DOPA decarboxylase extracted from Euonymus glabra Roxb. *ACS Chem. Biol.,* **2014**, *9*(4), 897-903.

[37] Montioli, R.; Voltattorni, C.B.; Bertoldi, M. Parkinsons Disease: Recent Updates in the Identification of Human Dopa Decarboxylase Inhibitors. *Curr. Drug Metab.,* **2016**, *17*(5), 513-518.

[38] Hyland, K.; Clayton, P.T. Aromatic amino acid decarboxylase deficiency in twins. *J. Inherit. Metab. Dis.,* **1990**, *13*(3), 301-304.

[39] Swoboda, K.J.; Hyland, K.; Goldstein, D.S.; Kuban, K.C.; Arnold, L.A.; Holmes, C.S.; Levy, H.L. Clinical and therapeutic observations in aromatic L-amino acid decarboxylase deficiency. *Neurology,* **1999**, *53*(6), 1205-1211.

[40] Haliloğlu, G.; Vezir, E.; Baydar, L.; Onol, S.; Sivri, S.; Coşkun, T.; Topçu, M. When do we need to perform a diagnostic lumbar puncture for neurometabolic diseases? Positive yield and retrospective analysis from a tertiary center. *Turk. J. Pediatr.,* **2012**, *54*(1), 52-58.

[41] Brun, L.; Ngu, L.H.; Keng, W.T.; Chng, G.S.; Choy, Y.S.; Hwu, W.L.; Lee, W.T.; Willemsen, M.A.; Verbeek, M.M.; Wassenberg, T.; Régal, L.; Orcesi, S.; Tonduti, D.; Accorsi, P.; Testard, H.; Abdenur, J.E.; Tay, S.; Allen, G.F.; Heales, S.; Kern, I.; Kato, M.; Burlina, A.; Manegold, C.; Hoffmann, G.F.; Blau, N. Clinical and biochemical features of aromatic L-amino acid decarboxylase deficiency. *Neurology,* **2010**, *75*(1), 64-71.

[42] Manegold, C.; Hoffmann, G.F.; Degen, I.; Ikonomidou, H.; Knust, A.; Laass, M.W.; Pritsch, M.; Wilichowski, E.; Hörster, F.; Aromatic, L. Aromatic L-amino acid decarboxylase deficiency: clinical features, drug therapy and follow-up. *J. Inherit. Metab. Dis.,* **2009**, *32*(3), 371-380.

[43] Montioli, R.; Oppici, E.; Cellini, B.; Roncador, A.; Dindo, M.; Voltattorni, C.B. S250F variant associated with aromatic amino acid decarboxylase deficiency: molecular defects and intracellular rescue by pyridoxine. *Hum. Mol. Genet.,* **2013**, *22*(8), 1615-1624.

[44] Montioli, R.; Dindo, M.; Giorgetti, A.; Piccoli, S.; Cellini, B.; Voltattorni, C.B. A comprehensive picture of the mutations associated with aromatic amino acid decarboxylase deficiency: from molecular mechanisms to therapy implications. *Hum. Mol. Genet.,* **2014**, *23*(20), 5429-5440.

[45] Montioli, R.; Paiardini, A.; Kurian, M.A.; Dindo, M.; Rossignoli, G.; Heales, S.J.; Pope, S.; Voltattorni, C.B.; Bertoldi, M. The novel R347g pathogenic mutation of aromatic amino acid decarboxylase provides additional molecular insights into enzyme catalysis and deficiency. *Biochim. Biophys. Acta,* **2016**, *1864*(6), 676-682.

[46] Rorsman, F.; Husebye, E.S.; Winqvist, O.; Björk, E.; Karlsson, F.A.; Kämpe, O. Aromatic-L-amino-acid decarboxylase, a pyridoxal phosphate-dependent enzyme, is a beta-cell autoantigen. *Proc. Natl. Acad. Sci. USA,* **1995**, *92*(19), 8626-8629.

[47] Husebye, E.S.; Gebre-Medhin, G.; Tuomi, T.; Perheentupa, J.; Landin-Olsson, M.; Gustafsson, J.; Rorsman, F.; Kämpe, O. Autoantibodies against aromatic L-amino acid decarboxylase in autoimmune polyendocrine syndrome type I. *J. Clin. Endocrinol. Metab.,* **1997**, *82*(1), 147-150.

[48] Candeloro, P.; Voltattorni, C.B.; Perniola, R.; Bertoldi, M.; Betterle, C.; Mannelli, M.; Giordano, R.; De Bellis, A.; Tiberti, C.; Laureti, S.; Santeusanio, F.; Falorni, A. Mapping of human autoantibody epitopes on aromatic L-amino acid decarboxylase. *J. Clin. Endocrinol. Metab.,* **2007**, *92*(3), 1096-1105.

[49] Bratland, E.; Wolff, A.S.; Haavik, J.; Kämpe, O.; Sköldberg, F.; Perheentupa, J.; Bredholt, G.; Knappskog, P.M.; Husebye, E.S. Epitope mapping of human aromatic L-amino acid decarboxylase. *Biochem. Biophys. Res. Commun.,* **2007**, *353*(3), 692-698.

[50] Heinämäki, A.A.; Perämaa, A.K.; Piha, R.S. Characterization of cerebral cysteine sulfinic acid decarboxylase. Molecular parameters and inhibition studies. *Acta Chem. Scand., B, Org. Chem. Biochem.,* **1982**, *36*(5), 287-290.

[51] Guion-Rain M-C, ; Portemer, C.; Chatagner, F. Rat liver cysteine sulfinate decarboxylase: purification, new appraisal of the molecular weight and determination of catalytic properties. *Biochim. Biophys. Acta,* **1975**, *384*(1), 265-276.

[52] Park, E.; Park, S.Y.; Wang, C.; Xu, J.; LaFauci, G.; Schuller-Levis, G. Cloning of murine cysteine sulfinic acid decarboxylase and its mRNA expression in murine tissues. *Biochim. Biophys. Acta,* **2002**, *1574*(3), 403-406.

[53] Ide, T.; Kushiro, M.; Takahashi, Y.; Shinohara, K.; Cha, S. mRNA expression of enzymes involved in taurine biosynthesis in rat adipose tissues. *Metabolism,* **2002**, *51*(9), 1191-1197.

[54] Lin, C.T.; Li, H.Z.; Wu, J.Y. Immunocytochemical localization of L-glutamate decarboxylase, gamma-aminobutyric acid transaminase, cysteine sulfinic acid decarboxylase, aspartate aminotransferase and somatostatin in rat retina. *Brain Res.,* **1983**, *270*(2), 273-283.

[55] Hu, J.M.; Ikemura, R.; Chang, K.T.; Suzuki, M.; Nishihara, M.; Takahashi, M. Expression of cysteine sulfinate decar-

boxylase mRNA in rat mammary gland. *J. Vet. Med. Sci.,* **2000**, *62*(8), 829-834.

[56] Tappaz, M.; Bitoun, M.; Reymond, I.; Sergeant, A. Characterization of the cDNA coding for rat brain cysteine sulfinate decarboxylase: brain and liver enzymes are identical proteins encoded by two distinct mRNAs. *J. Neurochem.,* **1999**, *73*(3), 903-912.

[57] Winge, I.; Teigen, K.; Fossbakk, A.; Mahootchi, E.; Kleppe, R.; Sköldberg, F.; Kämpe, O.; Haavik, J. Mammalian CSAD and GADL1 have distinct biochemical properties and patterns of brain expression. *Neurochem. Int.,* **2015**, *90*, 173-184.

[58] Huxtable, R.J. Physiological actions of taurine. *Physiol. Rev.,* **1992**, *72*(1), 101-163.

[59] Schuller-Levis, G.B.; Park, E. Taurine: new implications for an old amino acid. *FEMS Microbiol. Lett.,* **2003**, *226*(2), 195-202.

[60] Agnello, G.; Chang, L.L.; Lamb, C.M.; Georgiou, G.; Stone, E.M. Discovery of a substrate selectivity motif in amino acid decarboxylases unveils a taurine biosynthesis pathway in prokaryotes. *ACS Chem. Biol.,* **2013**, *8*(10), 2264-2271.

[62] Liu, P.; Torrens-Spence, M.P.; Ding, H.; Christensen, B.M.; Li, J. Mechanism of cysteine-dependent inactivation of aspartate/glutamate/cysteine sulfinic acid α-decarboxylases. *Amino Acids,* **2013**, *44*(2), 391-404.

[63] Chen, C.H.; Lee, C.S.; Lee, M.T.; Ouyang, W.C.; Chen, C.C.; Chong, M.Y.; Wu, J.Y.; Tan, H.K.; Lee, Y.C.; Chuo, L.J.; Chiu, N.Y.; Tsang, H.Y.; Chang, T.J.; Lung, F.W.; Chiu, C.H.; Chang, C.H.; Chen, Y.S.; Hou, Y.M.; Chen, C.C.; Lai, T.J.; Tung, C.L.; Chen, C.Y.; Lane, H.Y.; Su, T.P.; Feng, J.; Lin, J.J.; Chang, C.J.; Teng, P.R.; Liu, C.Y.; Chen, C.K.; Liu, I.C.; Chen, J.J.; Lu, T.; Fan, C.C.; Wu, C.K.; Li, C.F.; Wang, K.H.; Wu, L.S.; Peng, H.L.; Chang, C.P.; Lu, L.S.; Chen, Y.T.; Cheng, A.T. Variant GADL1 and response to lithium therapy in bipolar I disorder. *N. Engl. J. Med.,* **2014**, *370*(2), 119-128.

[64] Park, E.; Park, S.Y.; Dobkin, C.; Schuller-Levis, G. Development of a novel cysteine sulfinic Acid decarboxylase knockout mouse: dietary taurine reduces neonatal mortality. *J. Amino Acids,* **2014**, *2014*, 346809.

[65] Sköldberg, F.; Rorsman, F.; Perheentupa, J.; Landin-Olsson, M.; Husebye, E.S.; Gustafsson, J.; Kämpe, O. Analysis of antibody reactivity against cysteine sulfinic acid decarboxylase, a pyridoxal phosphate-dependent enzyme, in endocrine autoimmune disease. *J. Clin. Endocrinol. Metab.,* **2004**, *89*(4), 1636-1640.

[66] Mody, I.; De Koninck, Y.; Otis, T.S.; Soltesz, I. Bridging the cleft at GABA synapses in the brain. *Trends Neurosci.,* **1994**, *17*(12), 517-525.

[67] Bormann, J. The ABC of GABA receptors. *Trends Pharmacol. Sci.,* **2000**, *21*(1), 16-19.

[68] Reetz, A.; Solimena, M.; Matteoli, M.; Folli, F.; Takei, K.; De Camilli, P. GABA and pancreatic beta-cells: colocalization of glutamic acid decarboxylase (GAD) and GABA with synaptic-like microvesicles suggests their role in GABA storage and secretion. *EMBO J.,* **1991**, *10*(5), 1275-1284.

[69] Finn, R.D.; Coggill, P.; Eberhardt, R.Y.; Eddy, S.R.; Mistry, J.; Mitchell, A.L.; Potter, S.C.; Punta, M.; Qureshi, M.; Sangrador-Vegas, A.; Salazar, G.A.; Tate, J.; Bateman, A. The Pfam protein families database: towards a more sustainable future. *Nucleic Acids Res.,* **2016**, *44*(D1), D279-D285.

[70] Esclapez, M.; Tillakaratne, N.J.; Kaufman, D.L.; Tobin, A.J.; Houser, C.R. Comparative localization of two forms of glutamic acid decarboxylase and their mRNAs in rat brain supports the concept of functional differences between the forms. *J. Neurosci.,* **1994**, *14*(3 Pt 2), 1834-1855.

[71] Battaglioli, G.; Liu, H.; Martin, D.L. Kinetic differences between the isoforms of glutamate decarboxylase: implications for the regulation of GABA synthesis. *J. Neurochem.,* **2003**, *86*(4), 879-887.

[72] Kass, I.; Hoke, D.E.; Costa, M.G.; Reboul, C.F.; Porebski, B.T.; Cowieson, N.P.; Leh, H.; Pennacchietti, E.; McCoey, J.; Kleifeld, O.; Borri Voltattorni, C.; Langley, D.; Roome, B.; Mackay, I.R.; Christ, D.; Perahia, D.; Buckle, M.; Paiardini, A.; De Biase, D.; Buckle, A.M. Cofactor-dependent conformational heterogeneity of GAD65 and its role in autoimmunity and neurotransmitter homeostasis. *Proc. Natl. Acad. Sci. USA,* **2014**, *111*(25), E2524-E2529.

[73] Chou, C.C.; Modi, J.P.; Wang, C.Y.; Hsu, P.C.; Lee, Y.H.; Huang, K.F.; Wang, A.H.; Nan, C.; Huang, X.; Prentice, H.; Wei, J.; Wu, J.Y. Activation of Brain L-glutamate Decarboxylase 65 Isoform (GAD65) by Phosphorylation at Threonine 95 (T95). *Mol. Neurobiol.,* **2016**.

[74] Schwartz, H.L.; Chandonia, J.M.; Kash, S.F.; Kanaani, J.; Tunnell, E.; Domingo, A.; Cohen, F.E.; Banga, J.P.; Madec, A.M.; Richter, W.; Baekkeskov, S. High-resolution autoreactive epitope mapping and structural modeling of the 65 kDa form of human glutamic acid decarboxylase. *J. Mol. Biol.,* **1999**, *287*(5), 983-999.

[75] Söderbergh, A.; Myhre, A.G.; Ekwall, O.; Gebre-Medhin, G.; Hedstrand, H.; Landgren, E.; Miettinen, A.; Eskelin, P.; Halonen, M.; Tuomi, T.; Gustafsson, J.; Husebye, E.S.; Perheentupa, J.; Gylling, M.; Manns, M.P.; Rorsman, F.; Kämpe, O.; Nilsson, T. Prevalence and clinical associations of 10 defined autoantibodies in autoimmune polyendocrine syndrome type I. *J. Clin. Endocrinol. Metab.,* **2004**, *89*(2), 557-562.

[76] Arafat, Y.; Fenalti, G.; Whisstock, J.C.; Mackay, I.R.; Garcia de la Banda, M.; Rowley, M.J.; Buckle, A.M. Structural determinants of GAD antigenicity. *Mol. Immunol.,* **2009**, *47*(2-3), 493-505.

[77] Fenalti, G.; Law, R.H.; Buckle, A.M.; Langendorf, C.; Tuck, K.; Rosado, C.J.; Faux, N.G.; Mahmood, K.; Hampe, C.S.; Banga, J.P.; Wilce, M.; Schmidberger, J.; Rossjohn, J.; El-Kabbani, O.; Pike, R.N.; Smith, A.I.; Mackay, I.R.; Rowley, M.J.; Whisstock, J.C. GABA production by glutamic acid decarboxylase is regulated by a dynamic catalytic loop. *Nat. Struct. Mol. Biol.,* **2007**, *14*(4), 280-286.

[78] Gale, K. GABA in epilepsy: the pharmacologic basis. *Epilepsia,* **1989**, *30*(Suppl. 3), S1-S11.

[79] Wu, J.Y.; Bird, E.D.; Chen, M.S.; Huang, W.M. Abnormalities of neurotransmitter enzymes in Huntingtons chorea. *Neurochem. Res.,* **1979**, *4*(5), 575-586.

[80] Perry, T.L.; Hansen, S.; Lesk, D. [Plasma amino acid levels in children of patients with Huntingtons chorea]. *Neurology,* **1972**, *22*(1), 68-70. [Plasma amino acid levels in children of patients with Huntington's chorea].

[81] Sherif, F.M.; Ahmed, S.S. Basic aspects of GABA-transaminase in neuropsychiatric disorders. *Clin. Biochem.,* **1995**, *28*(2), 145-154.

[82] Medina, M.A.; Quesada, A.R.; Núñez de Castro, I.; Sánchez-Jiménez, F. Histamine, polyamines, and cancer. *Biochem. Pharmacol.,* **1999**, *57*(12), 1341-1344.

[83] Höcker, M.; Henihan, R.J.; Rosewicz, S.; Riecken, E.O.; Zhang, Z.; Koh, T.J.; Wang, T.C. Gastrin and phorbol 12-myristate 13-acetate regulate the human histidine decarboxylase promoter through Raf-dependent activation of extracellular signal-regulated kinase-related signaling pathways in gastric cancer cells. *J. Biol. Chem.,* **1997**, *272*(43), 27015-27024.

[84] Höcker, M.; Zhang, Z.; Koh, T.J.; Wang, T.C. The regulation of histidine decarboxylase gene expression. *Yale J. Biol. Med.,* **1996**, *69*(1), 21-33.

[85] Höcker, M.; Zhang, Z.; Merchant, J.L.; Wang, T.C. Gastrin regulates the human histidine decarboxylase promoter through an AP-1-dependent mechanism. *Am. J. Physiol.,* **1997**, *272*(4 Pt 1), G822-G830.

[86] Ichikawa, A.; Sugimoto, Y.; Tanaka, S. Molecular biology of histidine decarboxylase and prostaglandin receptors. *Proc. Jpn. Acad., Ser. B, Phys. Biol. Sci.,* **2010**, *86*(8), 848-866.

[87] Tran, V.T.; Snyder, S.H. Histidine decarboxylase. Purification from fetal rat liver, immunologic properties, and histochemical localization in brain and stomach. *J. Biol. Chem.,* **1981**, *256*(2), 680-686.

[88] Grzanna, R. Histidine decarboxylase: isolation and molecular characteristics. *Neurochem. Res.,* **1984**, *9*(7), 993-1009.

[89] Ohmori, E.; Fukui, T.; Imanishi, N.; Yatsunami, K.; Ichikawa, A. Purification and characterization of l-histidine decarboxylase from mouse mastocytoma P-815 cells. *J. Biochem.,* **1990**, *107*(6), 834-839.

[90] Savany, A.; Cronenberger, L. Properties of histidine decarboxylase from rat gastric mucosa. *Eur. J. Biochem.,* **1982**, *123*(3), 593-599.

[91] Savany, A.; Cronenberger, L. Isolation and properties of multiple forms of histidine decarboxylase from rat gastric mucosa. *Biochem. J.,* **1982**, *205*(2), 405-412.

[92] Taguchi, Y.; Watanabe, T.; Kubota, H.; Hayashi, H.; Wada, H. Purification of histidine decarboxylase from the liver of fetal rats and its immunochemical and immunohistochemical characterization. *J. Biol. Chem.,* **1984**, *259*(8), 5214-5221.

[93] Martin, S.A.; Bishop, J.O. Purification and characterization of histidine decarboxylase from mouse kidney. *Biochem. J.,* **1986**, *234*(2), 349-354.

[94] Yatsunami, K.; Tsuchikawa, M.; Kamada, M. Expression and characterization of human recombinant parental and mature L-histidine decarboxylases. *Methods Find. Exp. Clin. Pharmacol.,* **1995**, *17*(Suppl. C), 10-15.

[95] Joseph, D.R.; Sullivan, P.M.; Wang, Y.M.; Kozak, C.; Fenstermacher, D.A.; Behrendsen, M.E.; Zahnow, C.A. Characterization and expression of the complementary DNA encoding rat histidine decarboxylase. *Proc. Natl. Acad. Sci. USA,* **1990**, *87*(2), 733-737.

[96] Yamamoto, J.; Yatsunami, K.; Ohmori, E.; Sugimoto, Y.; Fukui, T.; Katayama, T.; Ichikawa, A. cDNA-derived amino acid sequence of L-histidine decarboxylase from mouse mastocytoma P-815 cells. *FEBS Lett.,* **1990**, *276*(1-2), 214-218.

[97] Dartsch, C.; Chen, D.; Persson, L. Multiple forms of rat stomach histidine decarboxylase may reflect posttranslational activation of the enzyme. *Regul. Pept.,* **1998**, *77*(1-3), 33-41.

[98] Fleming, J.V.; Wang, T.C. Amino- and carboxy-terminal PEST domains mediate gastrin stabilization of rat L-histidine decarboxylase isoforms. *Mol. Cell. Biol.,* **2000**, *20*(13), 4932-4947.

[99] Fajardo, I.; Urdiales, J.L.; Medina, M.A.; Sanchez-Jimenez, F. Effects of phorbol ester and dexamethasone treatment on histidine decarboxylase and ornithine decarboxylase in basophilic cells. *Biochem. Pharmacol.,* **2001**, *61*(9), 1101-1106.

[100] Fleming, J.V.; Wang, T.C. The production of 5355-kDa isoforms is not required for rat L-histidine decarboxylase activity. *J. Biol. Chem.,* **2003**, *278*(1), 686-694.

[101] Fleming, J.V.; Fajardo, I.; Langlois, M.R.; Sánchez-Jiménez, F.; Wang, T.C. The C-terminus of rat L-histidine decarboxylase specifically inhibits enzymic activity and disrupts pyridoxal phosphate-dependent interactions with L-histidine substrate analogues. *Biochem. J.,* **2004**, *381*(Pt 3), 769-778.

[102] Suzuki, S.; Tanaka, S.; Nemoto, K.; Ichikawa, A. Membrane targeting and binding of the 74-kDa form of mouse L-histidine decarboxylase *via* its carboxyl-terminal sequence. *FEBS Lett.,* **1998**, *437*(1-2), 44-48.

[103] Furuta, K.; Ichikawa, A.; Nakayama, K.; Tanaka, S. Membrane orientation of the precursor 74-kDa form of L-histidine decarboxylase. *Inflamm. Res.,* **2006**, *55*(5), 185-191.

[104] Kelley, J.L.; Miller, C.A.; White, H.L. Inhibition of histidine decarboxylase. Derivatives of histidine. *J. Med. Chem.,* **1977**, *20*(4), 506-509.

[105] Kollonitsch, J.; Perkins, L.M.; Patchett, A.A.; Doldouras, G.A.; Marburg, S.; Duggan, D.E.; Maycock, A.L.; Aster, S.D. Selective inhibitors of biosynthesis of aminergic neurotransmitters. *Nature,* **1978**, *274*(5674), 906-908.

[106] Rodríguez-Caso, C.; Rodríguez-Agudo, D.; Sánchez-Jiménez, F.; Medina, M.A. Green tea epigallocatechin-3-gallate is an inhibitor of mammalian histidine decarboxylase. *Cell. Mol. Life Sci.,* **2003**, *60*(8), 1760-1763.

[107] Wu, F.; Yu, J.; Gehring, H. Inhibitory and structural studies of novel coenzyme-substrate analogs of human histidine decarboxylase. *FASEB J.,* **2008**, *22*(3), 890-897.

[108] Castro-Oropeza, R.; Pino-Ángeles, A.; Khomutov, M.A.; Urdiales, J.L.; Moya-García, A.A.; Vepsäläinen, J.; Persson, L.; Sarabia, F.; Khomutov, A.; Sánchez-Jiménez, F. Aminooxy analog of histamine is an efficient inhibitor of mammalian L-histidine decarboxylase: combined in silico and experimental evidence. *Amino Acids,* **2014**, *46*(3), 621-631.

[109] Ohtsu, H.; Tanaka, S.; Terui, T.; Hori, Y.; Makabe-Kobayashi, Y.; Pejler, G.; Tchougounova, E.; Hellman, L.; Gertsenstein, M.; Hirasawa, N.; Sakurai, E.; Buzás, E.; Kovács, P.; Csaba, G.; Kittel A, ; Okada, M.; Hara, M.; Mar, L.; Numayama-Tsuruta, K.; Ishigaki-Suzuki, S.; Ohuchi, K.; Ichikawa, A.; Falus, A.; Watanabe, T.; Nagy, A. Mice lacking histidine decarboxylase exhibit abnormal mast cells. *FEBS Lett.,* **2001**, *502*(1-2), 53-56.

[110] Ohtsu, H.; Watanabe, T. New functions of histamine found in histidine decarboxylase gene knockout mice. *Biochem. Biophys. Res. Commun.,* **2003**, *305*(3), 443-447.

[111] Neumann, D.; Schneider, E.H.; Seifert, R. Analysis of histamine receptor knockout mice in models of inflammation. *J. Pharmacol. Exp. Ther.,* **2014**, *348*(1), 2-11.

[112] A.A. Stillman, A.K. Ghosh, K. Bilguvar, B.J. ORoak, C.E. Mason, T. Abbott, A. Gupta, R.A. King, D.L. Pauls, J.A. Tischfield, G.A. Heiman, H.S. Singer, D.L. Gilbert, P.J. Hoekstra, T.M. Morgan, E. Loring, K. Yasuno, T. Fernandez, S. Sanders, A. Louvi, J.H. Cho, S. Mane, C.M. Colangelo, T. Biederer, R.P. Lifton, M. Gunel, M.W. State, L-‐histidine decarboxylase and Tourettes syndrome. *N. Engl. J. Med.,* **2010**, *362*, 1901-1908.

[113] Bloch, M.; State, M.; Pittenger, C. Recent advances in Tourette syndrome. *Curr. Opin. Neurol.,* **2011**, *24*(2), 119-125.

[114] Dong, H.; Liu, W.; Liu, M.; Xu, L.; Li, Q.; Zhang, R.; Zhang, X.; Liu, S. Investigation of a Possible Role for the Histidine Decarboxylase Gene in Tourette Syndrome in the Chinese Han Population: A Family-Based Study. *PLoS One,* **2016**, *11*(8), e0160265.

[115] Cianchi, F.; Vinci, M.C.; Masini, E. Histamine in cancer: the dual faces of the coin. *Cancer Biol. Ther.,* **2008**, *7*(1), 36-37.

[116] Francis, H.; DeMorrow, S.; Venter, J.; Onori, P.; White, M.; Gaudio, E.; Francis, T.; Greene, J.F., Jr; Tran, S.; Meininger, C.J.; Alpini, G. Inhibition of histidine decarboxylase ablates the autocrine tumorigenic effects of histamine in human cholangiocarcinoma. *Gut,* **2012**, *61*(5), 753-764.

[117] Meng, F.; Onori, P.; Hargrove, L.; Han, Y.; Kennedy, L.; Graf, A.; Hodges, K.; Ueno, Y.; Francis, T.; Gaudio, E.; Francis, H.L. Regulation of the histamine/VEGF axis by miR-125b during cholestatic liver injury in mice. *Am. J. Pathol.,* **2014**, *184*(3), 662-673.

[118] Sköldberg, F.; Portela-Gomes, G.M.; Grimelius, L.; Nilsson, G.; Perheentupa, J.; Betterle, C.; Husebye, E.S.; Gustafsson, J.; Rönnblom, A.; Rorsman, F.; Kämpe, O. Histidine decarboxylase, a pyridoxal phosphate-dependent enzyme, is an autoantigen of gastric enterochromaffin-like cells. *J. Clin. Endocrinol. Metab.,* **2003**, *88*(4), 1445-1452.

[119] Burkhard, P.; Dominici, P. C. Borri--Voltattorni, J.N. Jansonius, V.N. Malashkevich, Structural insight into Parkinsons disease treatment from drug--inhibited DOPA decarboxylase. *Nat. Struct. Biol.,* **2001**, *8*, 963-967.

[120] Komori, H.; Nitta, Y.; Ueno, H.; Higuchi, Y. Structural study reveals that Ser-354 determines substrate specificity on human histidine decarboxylase. *J. Biol. Chem.,* **2012**, *287*(34), 29175-29183.

[121] Jansonius, J.N. Structure, evolution and action of vitamin B6-dependent enzymes. *Curr. Opin. Struct. Biol.,* **1998**, *8*(6), 759-769.

[122] Paiardini, A.; Bossa, F.; Pascarella, S. Evolutionarily conserved regions and hydrophobic contacts at the superfamily level: The case of the fold-type I, pyridoxal-5-phosphate-dependent enzymes. *Protein Sci.,* **2004**, *13*(11), 2992-3005.

[123] Williams, B.B.; Van Benschoten, A.H.; Cimermancic, P.; Donia, M.S.; Zimmermann, M.; Taketani, M.; Ishihara, A.; Kashyap, P.C.; Fraser, J.S.; Fischbach, M.A. Discovery and characterization of gut microbiota decarboxylases that can produce the neurotransmitter tryptamine. *Cell Host Microbe,* **2014**, *16*(4), 495-503.

[124] Bertoldi, M.; Gonsalvi, M.; Contestabile, R.; Voltattorni, C.B. Mutation of tyrosine 332 to phenylalanine converts dopa decarboxylase into a decarboxylation-dependent oxidative deaminase. *J. Biol. Chem.,* **2002**, *277*(39), 36357-36362.

[125] Bertoldi, M.; Frigeri, P.; Paci, M.; Voltattorni, C.B. Reaction specificity of native and nicked 3,4-dihydroxyphenylalanine decarboxylase. *J. Biol. Chem.,* **1999**, *274*(9), 5514-5521.

[126] Fleming, J.V.; Sánchez-Jiménez, F.; Moya-García, A.A.; Langlois, M.R.; Wang, T.C. Mapping of catalytically important residues in the rat L-histidine decarboxylase enzyme using bioinformatic and site-directed mutagenesis approaches. *Biochem. J.,* **2004**, *379*(Pt 2), 253-261.

[127] Martin, D.L.; Rimvall, K. Regulation of gamma-aminobutyric acid synthesis in the brain. *J. Neurochem.,* **1993**, *60*(2), 395-407.

[128] Langendorf, C.G.; Tuck, K.L.; Key, T.L.; Fenalti, G.; Pike, R.N.; Rosado, C.J.; Wong, A.S.; Buckle, A.M.; Law, R.H.; Whisstock, J.C. Structural characterization of the mechanism through which human glutamic acid decarboxylase auto-activates. *Biosci. Rep.,* **2013**, *33*(1), 137-144.

[129] Giardina, G.; Montioli, R.; Gianni, S.; Cellini, B.; Paiardini, A.; Voltattorni, C.B.; Cutruzzolà, F. Open conformation of human DOPA decarboxylase reveals the mechanism of PLP addition to Group II decarboxylases. *Proc. Natl. Acad. Sci. USA,* **2011**, *108*(51), 20514-20519.

[130] Matsuda, N.; Hayashi, H.; Miyatake, S.; Kuroiwa, T.; Kagamiyama, H. Instability of the apo form of aromatic L-amino acid decarboxylase *in vivo* and *in vitro*: implications for the involvement of the flexible loop that covers the active site. *J. Biochem.,* **2004**, *135*(1), 33-42.

[131] Chen, C.H.; Wu, S.J.; Martin, D.L. Structural characteristics of brain glutamate decarboxylase in relation to its interaction and activation. *Arch. Biochem. Biophys.,* **1998**, *349*(1), 175-182.

[132] Sałat, K.; Podkowa, A.; Mogilski, S.; Zaręba, P.; Kulig, K.; Sałat, R.; Malikowska, N.; Filipek, B. The effect of GABA transporter 1 (GAT1) inhibitor, tiagabine, on scopolamine-induced memory impairments in mice. *Pharmacol. Rep.,* **2015**, *67*(6), 1155-1162.

[133] Nuss, P. Anxiety disorders and GABA neurotransmission: a disturbance of modulation. *Neuropsychiatr. Dis. Treat.,* **2015**, *11*, 165-175.

[134] Boutet, E.; Lieberherr, D.; Tognolli, M.; Schneider, M.; Bansal, P.; Bridge, A.J.; Poux, S.; Bougueleret, L.; Xenarios, I. UniProtKB/Swiss-Prot, the Manually Annotated Section of the UniProt KnowledgeBase: How to Use the Entry View. *Methods Mol. Biol.,* **2016**, *1374*, 23-54.

DISCLAIMER: The above article has been published in Epub (ahead of print) on the basis of the materials provided by the author. The Editorial Department reserves the right to make minor modifications for further improvement of the manuscript.

PMID: 27881066

Amino Acids (2018) 50:205–215
https://doi.org/10.1007/s00726-017-2521-3

INVITED REVIEW

Phosphorylation of pyridoxal 5′-phosphate enzymes: an intriguing and neglected topic

Giada Rossignoli[1] · Robert S. Phillips[2,3] · Alessandra Astegno[4] · Marta Menegazzi[1] · Carla Borri Voltattorni[1] · Mariarita Bertoldi[1]

Received: 16 September 2017 / Accepted: 29 November 2017 / Published online: 4 December 2017
© Springer-Verlag GmbH Austria, part of Springer Nature 2017

Abstract

Pyridoxal 5′-phosphate (PLP)-dependent enzymes catalyze a wide range of reactions of amino acids and amines, with the exception of glycogen phosphorylase which exhibits peculiar both substrate preference and chemical mechanism. They represent about 4% of the gene products in eukaryotic cells. Although structure–function investigations regarding these enzymes are copious, their regulation by post-translational modifications is largely unknown. Protein phosphorylation is the most common post-translational modification fundamental in mediating diverse cellular functions. This review aims at summarizing the current knowledge on regulation of PLP enzymes by phosphorylation. Starting from the paradigmatic PLP-dependent glycogen phosphorylase, the first phosphoprotein discovered, we collect data in literature regarding functional phosphorylation events of eleven PLP enzymes belonging to different fold types and discuss the impact of the modification in affecting their activity and localization as well as the implications on the pathogenesis of diseases in which many of these enzymes are involved. The pivotal question is to correlate the structural consequences of phosphorylation among PLP enzymes of different folds with the functional modifications exerted in terms of activity or conformational changes or others. Although the literature shows that the phosphorylation of PLP enzymes plays important roles in mediating diverse cellular functions, our recapitulation of clue findings in the field makes clear that there is still much to be learnt. Besides mass spectrometry-based proteomic analyses, further biochemical and structural studies on purified native proteins are imperative to fully understand and predict how phosphorylation regulates PLP enzymes and to find the relationship between addition of a phosphate moiety and physiological response.

Keywords Pyridoxal 5′-phosphate enzymes · Phosphorylation · Regulation · Structure–function relationship

Abbreviations

PLP	Pyridoxal 5′-phosphate
PTM	Post-translational modification
TAT	Tyrosine aminotransferase
GABA	γ-Aminobutyric acid
GABA-T	γ-Aminobutyric acid transaminase
SPT	Serine palmitoyl transferase
GAD	Glutamate decarboxylase
DDC	DOPA decarboxylase
AADC	Aromatic amino acid decarboxylase
HDC	Histidine decarboxylase
CSAD	Cysteine sulfinic acid decarboxylase
SR	Serine racemase
CBS	Cystathionine β-synthase
ODC	Ornithine decarboxylase
PD	Parkinson's disease
PKA	Protein kinase A
PKC	Protein kinase C
PKG	Protein kinase G
CaMKII	Calcium–calmodulin dependent protein kinase II
LBC1	Long-chain base 1

Handling Editor: P. R. Jungblut.

✉ Mariarita Bertoldi
mita.bertoldi@univr.it

[1] Department of Neuroscience, Biomedicine and Movement, University of Verona, Strada Le Grazie, 8, 37134 Verona, Italy

[2] Department of Chemistry, University of Georgia, Athens, GA 30602, USA

[3] Department of Biochemistry and Molecular Biology, University of Georgia, Athens, GA 30602, USA

[4] Department of Biotechnology, University of Verona, Strada Le Grazie, 15, 37134 Verona, Italy

LBC2 Long-chain base 2
HSAN1 Autonomic neuropathy type 1
NMDA *N*-methyl-D-aspartate

Introduction

One of the main reasons for the extreme flexibility of proteins is the ability to respond to different cell environmental conditions, being modified and regulated by many factors. The regulation of enzyme activity in vivo by post-translational modification (PTM) provides a rapid way for cells to respond to changing physiological conditions, by modulating physico-chemical features, conformation, stability and activity, thus leading to a global altered protein function. PTMs are well-known mechanisms that trigger subtle changes in proteins and make them more suitable to face particular conditions.

Modern proteomic high-throughput mass spectrometry methods have permitted the identification of more than 200 different types of PTMs (Mann and Jensen 2003; Lu et al. 2013) spanning from phosphorylation, glycosylation, fatty acid linkage for membrane attachment, methylation, nitrosylation, glutathionylation, acetylation, ubiquitinylation, and many others (Seo and Lee 2004). Many platforms and databases have been developed to map all experimentally found modification consensus sequences to allow prediction of the sites more prone to specific PTM in every protein.

Phosphorylation was one of the first PTMs to be identified and is one of the most widespread, versatile and studied PTMs (Cohen 2000, 2002). It is a reversible covalent modification that could alter the function, the binding partners and the localization of proteins, thus determining the fine tuning of their biological activity. It is implied in many cellular processes such as signal transduction pathways, growth, differentiation and apoptosis. It has become more and more evident that alterations in phosphorylation pathways could cause or worsen pathological conditions such as cancer (Singh et al. 2017). This modification is carried out by a balanced interplay between kinases that phosphorylate a substrate protein using ATP as co-substrate, and phosphatases that are responsible for the removal of the phosphate (Hunter 1995). Phosphorylation commonly occurs on the hydroxy group of serine, threonine or tyrosine residues. There are 518 protein kinases known in the human genome, of which 428 are known or predicted to phosphorylate serine or threonine, while the other 90 react with tyrosine (Manning et al. 2002). The phosphorylation event could take place at only one or at multiple sites on a specific protein. Furthermore, a protein could be a substrate of a single or of multiple kinases, thus establishing complex cascade networks in response to a stimulus.

Because of their importance, kinases have been the subject of numerous studies on their classification and mechanism of action (Kornev et al. 2006; Taylor and Kornev 2011). It has been recently reported that many eukaryotic proteins (probably thousands) undergo phosphorylation during their lifespan (Venerando et al. 2017). Among them, pyridoxal 5′-phosphate (PLP)-dependent enzymes should not represent an exception. However, data concerning phosphorylation of PLP-enzymes are scarce: a search of the literature reveals that only 11 PLP-enzymes are known to be subject to phosphorylation.

From a structural point of view, PLP-enzymes are classified into five different fold types (from I to V) depending on their amino acid sequence, secondary structure and known spatial structures (Grishin et al. 1995; Schneider et al. 2000). Fold I, the largest, is the α-family, also known as the aminotransferase superfamily. Fold II is also known as the β-family, since many of its members catalyze reactions at the β-carbon. Fold III is the alanine racemase family, primarily containing racemases and some decarboxylases. Fold IV contains only D-amino acid and branched-chain amino acid aminotransferases. Glycogen phosphorylase is the only member of Fold V. The organization in fold types is useful to understand some structural constraints of the active site, the identity of the residues involved in catalysis and the conformational changes carried out by these enzymes upon cofactor and/or substrate binding. Despite their great numbers, wide distribution (Percudani and Peracchi 2003) and relevance for amino acid metabolism, only a few PLP-dependent enzymes have been shown to undergo phosphorylation. The aim of this review is to outline what is known at present about the involvement and the role (if already determined) of phosphorylation in the regulation of PLP enzymes that are subjected to it.

Glycogen phosphorylase

One of the best studied and classic examples of protein phosphorylation deals with a PLP-dependent enzyme, namely glycogen phosphorylase. The pioneering work carried out from the late 1930s to late 1950s by Carl and Gerty Cori, by Burnett and Kennedy, and finally by Fischer and Krebs, led to the demonstration that muscle glycogen phosphorylase exists in two forms (*a* and *b*), with the less active *b* form being converted into the active *a* form by phosphorylation, as well as by AMP binding (Johnson 1992). Glycogen phosphorylase is a unique PLP enzyme, since the substrate, glycogen, is a polysaccharide, and the phosphorolysis reaction is carried out by the 5′-phosphate group of the cofactor that has been proposed to behave in this case as an acid–base catalyst (Palm et al. 1990). However, a study with PLP phosphate analogs with altered pK_as suggested that the phosphate

remains a dianion throughout catalysis, and therefore, provides electrostatic rather than acid–base catalysis (Stirtan and Withers 1996). This is a property not shared by all the other PLP-dependent enzymes, which act on amino acids and amines, and utilize the aldimine and the conjugated pyridine ring as electron sinks, thus promoting catalysis. In these latter enzymes, the phosphate group functions mainly as a handle for the enzyme to bind the cofactor during the catalytic cycle, although in some cases it may also participate in catalysis (Phillips et al. 2014).

Glycogen phosphorylase exhibits three tissue-specific isozymes, found in muscle, liver and brain. Although the three isozymes have high sequence homology, they show significant differences in regulation. Liver glycogen phosphorylase is primarily regulated by phosphorylation on Ser-14 by phosphorylase kinase, in response to glucagon. Due to its key role in releasing glucose from the liver, this enzyme has emerged recently as a potential target for Type 2 antidiabetic drugs. Muscle glycogen phosphorylase is activated by both phosphorylation as well as ligands such as AMP, whereas brain glycogen phosphorylase is not activated by phosphorylation, but is activated by ligands such as AMP (Mathieu et al. 2017). The crystal structures of muscle and liver glycogen phosphorylase *a* and *b* have been determined (Sprang et al. 1988). The protein is a dimer and is allosterically activated by phosphorylation. In muscle glycogen phosphorylase, phosphorylation of Ser-14 results in conformational changes near the active site, despite a distance of about 40 Å between the serine phosphate and PLP (Fig. 1). In fact, in phosphorylase *b*, Ser-14 is in a disordered region and is not observed in the structure. The AMP-binding site is located near the phosphorylation site, and AMP binding results in similar structural changes as phosphorylation. These structural changes resulting from phosphorylation of Ser-14 of glycogen phosphorylase provide a paradigm for the structural effects of phosphorylation of other PLP-dependent enzymes.

PLP-dependent reactions of amino acids

The great majority of PLP enzymes act on amino acids rather than sugars with a general mechanism depicted in Fig. 2. The cofactor is covalently bound to the protein moiety through a Schiff base linkage of its aldehyde group with the ε-amino group of a lysine, forming the so-called internal aldimine. When an amino acid enters the active site, its α-amino group substitutes the ε-amino group of the lysine residue in a transaldimination reaction that leads to the *gem*-diamine that is subsequently converted into an external aldimine. From this step on, the reaction pathway to be undertaken depends on which of the bonds of the external aldimine is perpendicular to the imine-pyridine plane [Dunathan hypothesis (Dunathan 1966)]. This explains the enormous variety of reactions that could be catalyzed by PLP enzymes (Phillips 2015): transamination, α- and β-decarboxylation, β- and γ-elimination, racemization, β- and γ-substitution, retro-aldol cleavage and even oxidation.

In addition to the well-known glycogen phosphorylase, also tyrosine aminotransferase (TAT), γ-aminobutyric acid (GABA) aminotransferase (GABA-T), serine palmitoyltransferase (SPT), glutamate decarboxylase (GAD), DOPA decarboxylase (DDC), histidine decarboxylase (HDC), cysteine sulfinic acid decarboxylase (CSAD) belonging to fold-type I, serine racemase (SR) and cystathionine β-synthase (CBS) to fold-type II, and eukaryotic ornithine decarboxylase (ODC) to fold-type III (Grishin et al. 1995), have been found to be phosphorylated.

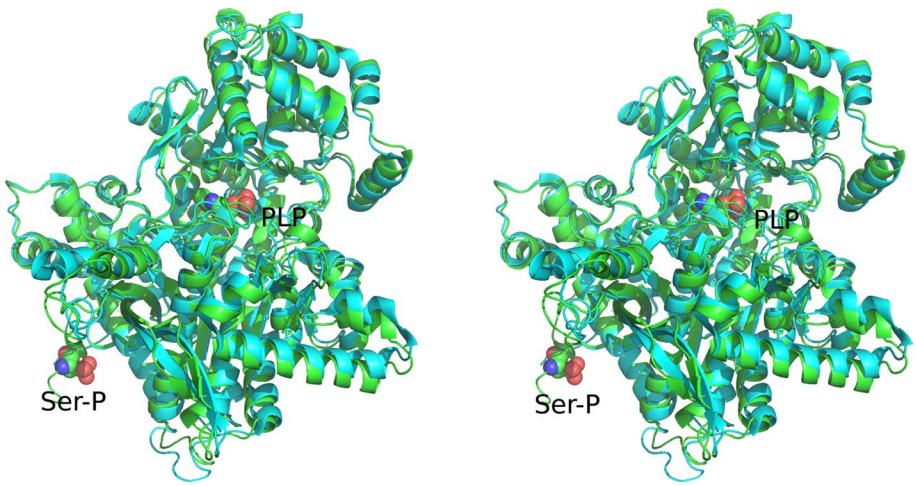

Fig. 1 Structure of Ser-14 phosphorylated glycogen phosphorylase. The structure of one subunit of rabbit muscle glycogen phosphorylase *a* overlaid on glycogen phosphorylase *b*, showing the position of the phosphoserine-14 and PLP as space-filling models. The green ribbon is phosphorylase *a* and the cyan ribbon is phosphorylase *b*. The figure was prepared with Pymol (the PyMOL Molecular Graphics System, version 1.7.2.1 Schrödinger, LLC) from protein structure files 1GPA and 1GPB (color figure online)

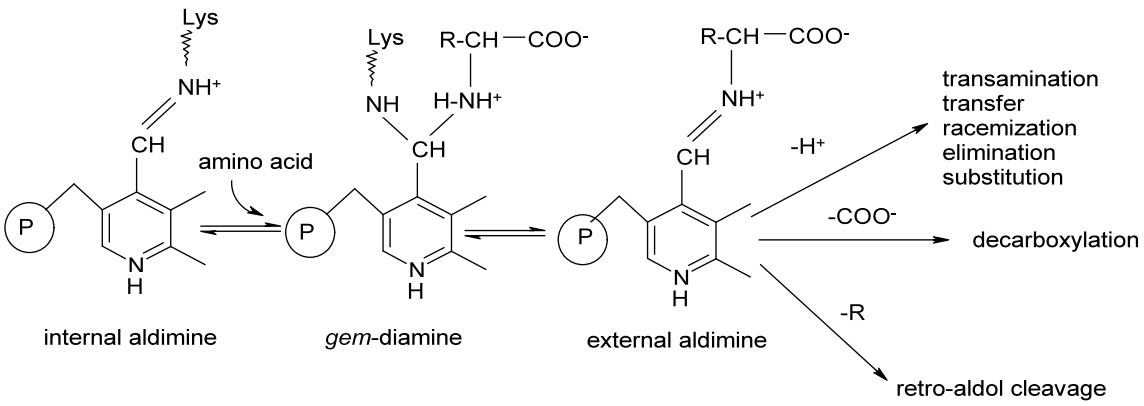

Fig. 2 Mechanism of reactions of PLP-enzymes. The cofactor PLP is covalently linked to the ε-aminic group of a lysine residue in the active site of a resting PLP enzyme in the so-called internal aldimine species. When an amino acidic substrate enters the active site, it makes a nucleophilic attack to the 4′-carbon of PLP generating a sp^3 species: the *gem*-diamine, which is subsequently converted into the external aldimine by substituting the ε-amino group of the lysine with the α-amino group of the substrate. Then, the reaction is directed into a precise direction depending on which of the bond of the α-carbon is perpendicular to the imine-pyridine plane and is thus chemically prone to be broken. This leads to the high versatility of reactions catalyzed by PLP enzymes. This mechanism is drawn according to the so-called Dunathan hypothesis (Dunathan 1966) and a huge amount of information on PLP enzymes recently revised by (John 1995; Phillips 2015)

Fold-type I decarboxylases: GAD, DDC, HDC, and CSAD

A recent review on this group of enzymes reveals many similarities as well as their major differences and specific features (Paiardini et al. 2017). Since these decarboxylases are responsible for the synthesis of essential molecules (neurotransmitters, bioactive amino acids and polyamines), it is conceivable that their activity should be finely tuned to respond to physiological conditions. Here, we review evidence that these enzymes can be phosphorylated, suggesting a possible interconnected regulation mechanism.

Among these decarboxylases, the most well-known is GAD, which catalyzes the a-decarboxylation of L-glutamate to GABA and is found in both prokaryotes and eukaryotes. In most vertebrates, the enzyme exists on two functional dimeric isoforms (GAD65 and GAD67) (Fenalti et al. 2007), while in plants (Gut et al. 2009; Astegno et al. 2015, 2016) and in *E. coli* and other enteric bacteria, it is characterized by a hexameric assembly (Capitani et al. 2003).

In mammals, GABA is a key inhibitory neurotransmitter in central nervous system and plays many fundamental roles in motor control, vision, as well as in brain plasticity-related processes such as memory, learning, locomotion, and during the development of the nervous system (Roberts 1975; Tower 1976; Hornykiewicz et al. 1976). It is also widely recognized that many clinical conditions including psychiatric disorders, spasticity, epilepsy, stiff-person syndrome, anxiety and cerebral ischemia involve imbalances in excitation and inhibition where GABA production is fundamental (Blum and Jankovic 1991; Sherman et al. 1991; Arias et al. 1992; Soghomonian and Laprade 1997; Kash et al. 1997).

The two human GAD isoforms, the membrane-anchored GAD65, and the cytosolic GAD67 (Erlander et al. 1991; Bu et al. 1992), are products of two independently regulated genes and expressed in different cerebral regions. Both of them utilize PLP as cofactor to perform catalysis. However, each of the two isoforms presents particular characteristics. GAD67 is present as holoenzyme, with the PLP cofactor bound as internal aldimine, while GAD65 is instead 50% in the apo form without bound PLP (Martin and Rimvall 1993). This was interpreted as suggesting GAD67 is responsible for basal GABA production, while GAD65 can be rapidly activated when higher neurotransmitter levels are required and cycles between an active holo form and an inactive apo form (Fenalti et al. 2007). Despite the high sequence identity and structural similarity of the two isoforms (Fenalti et al. 2007). GAD65 is an antigen in patients with type 1 diabetes and other autoimmune disorders, while GAD67 is rarely autoantigenic (Baekkeskov et al. 1987, 1990; Paiardini et al. 2017; Jayakrishnan et al. 2011). Recently, through a combined computational and experimental approach, it has been advanced that production of GAD65 autoantibodies could be related to cofactor-controlled conformational changes, due to the flexibility of some GAD65 structural elements, such as the C-terminal domain and the catalytic loop with respect to GAD67 (Kass et al. 2014; Langendorf et al. 2013). These determinants have been proposed to represent molecular bases for regulation of GABA production (Fenalti et al. 2007; Langendorf et al. 2013).

Both GAD65 and GAD67 have been reported to undergo phosphorylation (Bao et al. 1995; Hsu et al. 1999). Surprisingly, this modification exerts opposite functional effects for the two isoforms, since GAD65 is activated by phosphorylation while GAD67 is inhibited (Wei et al. 2004). The treatment in vitro of both GAD isoforms with three protein kinases (PKA, PKC and CaMKII) showed that PKCε is responsible for GAD65 phosphorylation, while PKA phosphorylates GAD67, and that in GAD67, Thr-91 is subjected to this modification (Wei et al. 2004). Similar to glycogen phosphorylase, the phosphorylation site in GAD67 is > 40 Å from the PLP (Fig. 3). Unfortunately, the structure is truncated on the N terminus, and Thr-91 is not visible in the structure. A model was proposed, taking into account the different regulation to which the two GAD proteins are subjected, due probably to their different responses to physiological conditions (Wei et al. 2004; Jin et al. 2003). In particular, it has been suggested that phosphorylation could alter the K_m for glutamate in a different manner for the two isoforms. In addition, the neuronal stimulation on the one hand activates both PKA and PKCε which phosphorylate GAD67 and GAD65, respectively, leading to an increase in GABA levels in vesicles which could then be released (Wei et al. 2004; Jin et al. 2003). However, it should be taken into account that the kinases and phosphatases that are involved in vivo are unknown and their identification represents an essential step for dissecting the signal pathways that regulate GABA neurotransmission (Wei and Wu 2008). A number of putative phosphorylation sites for both GAD65 and GAD67 have been proposed by means of bioinformatic prediction (Wei and Wu 2008). The effects of phosphorylation are not only limited to altered enzymatic activity but also to compartment localization. Phosphorylation of serine residues 3, 6, 10 and 13 in GAD65 regulates membrane anchoring without exerting any effect in catalysis (Namchuk et al. 1997). This has been proposed to be related to higher GAD65 membrane association under neuronal stimulation (Wei and Wu 2008). Other phosphorylation sites on GAD65 have been recently identified, unraveling the importance of Thr-95 in regulating activity and in the interplay with GAD67 following neuronal stimulation (Chou et al. 2017).

DDC (also known as aromatic amino acid decarboxylase, AADC) is a structurally similar α-decarboxylase whose role is the synthesis of the neurotransmitters, dopamine and serotonin, from the corresponding amino acids, L-Dopa and 5-hydroxytryptophan. DDC activity is reduced in regions of the brain in Parkinson's disease (PD), thus leading to low levels of dopamine. Pharmaceutical treatment of PD in the early stages is with L-Dopa and a peripheral DDC inhibitor such as carbidopa or benserazide. Information regarding phosphorylation of DDC is relatively scarce. A few papers have been published reporting that both recombinant and immunoprecipitated (from brain homogenates) DDC could be phosphorylated by the catalytic subunits of cyclic AMP-dependent protein kinase, and that the enzymatic activity increases in both cases (70% for the recombinant and 20% for the immunoprecipitated enzyme) (Duchemin et al. 2000). Moreover, interaction with α-synuclein, implicated in PD, has been reported to reduce phosphorylation levels of DDC (by 1.5-fold) probably by activation of a phosphatase such as protein phosphatase 2A (Tehranian et al. 2006). Concomitantly, a-synuclein leads to inhibition of DDC activity, a possible mechanism of dopamine homeostasis which is compromised in PD pathogenesis (Tehranian et al. 2006). Finally, cyclic guanosine monophosphate/protein kinase G (cGMP/PKG) has also been determined to phosphorylate DDC, increasing V_{max} by ~ 30% and K_m by ~ 60% (Duchemin et al. 2010). Activation of neuronal DDC by drugs that increase phosphorylation or allosteric activators could be a novel approach to treatment of PD. It is conceivable that an alteration or, more specifically, a decrease in phosphorylation level of DDC could be also involved in dysregulation of dopamine and serotonin observed in AADC deficiency, a rare genetic disease affecting *DDC/AADC* gene, causing neurological damages. In this sense, a treatment agent that acts increasing phosphorylation level could also be

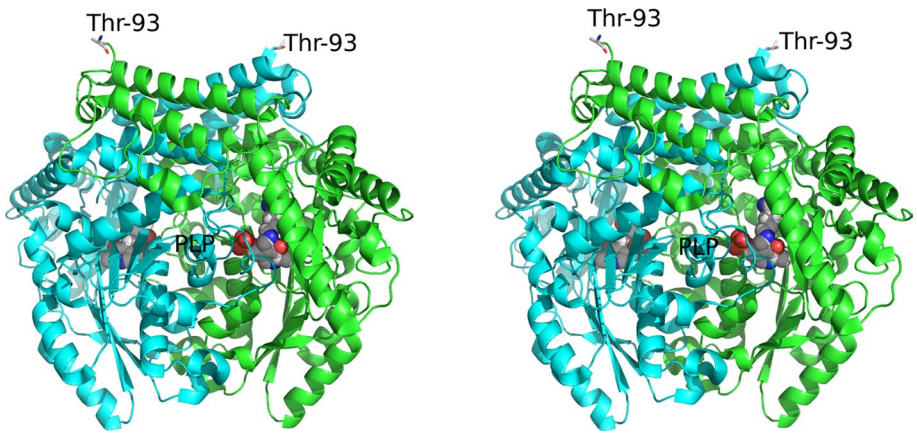

Fig. 3 Structure of Thr-91-phosphorylated glutamate decarboxylase. The structure of the dimer of GAD67, showing the relationship between the phosphorylation site and the active site. The N terminus of the protein was truncated at Thr-93, so the phosphorylation site at Thr-91 is not seen. The figure was prepared with Pymol (the PyMOL Molecular Graphics System, version 1.7.2.1 Schrödinger, LLC) from protein structure file 2OKJ

beneficial for patients carrying this genetic disease. However, no phosphorylation sites of DDC have been identified until now.

HDC is the only component of the biosynthetic pathway of histamine, an important biogenic amine with physiological regulatory roles in neurotransmission, gastric acid secretion and immune response. Thus, impairment of histamine metabolism is related to many pathological states such as inflammatory responses, peptic ulcer and several central nervous system disorders (Ohtsu 2010; Panula and Nuutinen 2013). More recently, new interesting relationships have been established between HDC expression and growth of different carcinoma types and neuroendocrine tumours, especially gastrointestinal cancers (Kennedy et al. 2012), especially cholangiocarcinoma (Francis et al. 2012). HDC is expressed as a 74 kDa inactive polypeptide (Fleming et al. 2004) and only after post-translational proteolysis of the C-terminal part, probably by caspase-9, the enzyme results in 53–55 kDa active isoforms (Dartsch et al. 1998). Since 30 years ago, papers have been published regarding possible HDC regulation by phosphorylation in rat hypothalamus or gastric mucosa extracts, with conflicting results. In vitro, hypothalamic HDC is inhibited by incubating the homogenate under phosphorylating conditions (ATP, cAMP, and Mg^{2+}) in the presence of a cAMP-dependent protein kinase (Huszti and Magyar 1984), and this effect is reversed by the addition of cAMP-dependent protein kinase inhibitor, enhancing HDC activity above control levels (Huszti and Magyar 1985). Although similar results are found also with the partially purified hypothalamic enzyme (Huszti and Magyar 1987), the incubation of gastric supernatant with various combinations of ATP, Mg^{2+}, cAMP and protein kinase under the blockade of endogenous phosphatases fails to alter significantly the enzyme activity. On the other hand, fractionated rat gastric mucosa enzyme distributes into multiple forms with different charges (Savany and Cronenberger 1982) and with the generation of less-negatively charged species in a time and temperature-dependent manner (Savany and Cronenberger 1988). In addition, in absence of PLP, gastric HDC is reversibly inactivated by phosphatase in a time and dose-dependent process (Savany and Cronenberger 1989) leading to the suggestion that dephosphorylation promotes and/or stabilizes apoenzyme formation. In fact, full reactivation is achieved by the addition of PLP, that at the same time reduces the number of forms with low negative charge (Savany and Cronenberger 1990), suggesting a relationship between the charge heterogeneity and the phosphorylation state.

CSAD is a recently identified decarboxylase involved in the production of taurine, which is involved in many biological processes. It has been reported that CSAD is activated when phosphorylated and inhibited when dephosphorylated. PKC is responsible for the phosphorylation reaction, while protein phosphatase 2C for phosphate removal (Tang et al. 1997). In particular, a neuronal stimulus resulting in taurine release, increases also taurine synthesis by activating PKC which in turns phosphorylates CSAD leading to an increase of taurine levels (Tang et al. 1997; Wu et al. 1998). This behaviour reminiscent of that of GAD65 and opposite to that of GAD67, highlighting the interplay of taurine and GABA in brain.

Fold-type I aminotransferases and acyltransferases: TAT, GABA-T and SPT

Phosphorylation of TAT and GABA-T was reported in papers published more than 40 years ago, in particular TAT is found phosphorylated in vivo and it is demonstrated that this modification does not alter enzyme activity (Lee and Nickol 1974). TAT is an enzyme active in the liver and whose role is to regulate the catabolism of tyrosine and phenylalanine. Its expression is modulated by cAMP and glucocorticoids in primary hepatocytes (Schmid et al. 1987) and cAMP-dependent protein kinase is considered to be responsible for phosphorylation (Spielholz et al. 1984; Pogson et al. 1986). The same kinase acts also on purified pig brain GABA-T and no effect of phosphorylation on enzyme kinetic properties is reported (Carr et al. 1986), even if no in-depth investigations on these phosphorylated aminotransferases have been carried out since then. Although no effects of phosphorylation on activity are seen with these enzymes in vitro, it is possible that phosphorylation can affect the interaction with other cell components in vivo, or their intracellular lifetime.

Some papers have recently been published on the phosphorylation of SPT, the first and rate-limiting enzyme of de novo sphingolipid biosynthetic pathway, that catalyses the condensation between L-serine and an acyl-CoA thioester substrate (typically palmitoyl-CoA). Despite the identification of some associated regulatory subunits, its core is a heterodimer composed by the subunits long-chain base 1 and 2 (LCB1 and LCB2) encoded by separate paralogous genes (Yard et al. 2007). Although only LCB2 contains the PLP-dependent catalytic site, LCB1 plays important roles in the regulation of the enzyme. Point mutations in both subunits are, indeed, associated with hereditary sensory and autonomic neuropathy type 1 (HSAN1), an autosomal-dominant genetic disorder characterized by peripheral neuropathy with signs of neuronal degeneration and minor limb injury development into extensive ulcerations with necessary amputation. HSAN1 is mainly due to a SPT substrate shift from L-serine to L-alanine, with consequent decrease in sphingolipids, and therefore, myelin production and simultaneously accumulation of atypical neurotoxic 1-deoxy-sphingolipids (1-deoxySL) (Penno et al. 2010). In

addition, wild-type SPT can metabolize L-alanine under certain conditions, associated with metabolic syndrome, type 2 diabetes and diabetic neuropathy (Othman et al. 2012, 2015). In particular, a fraction containing wild-type SPT extracted from CHO cells is found to be phosphorylated at Ser-384 of LCB2 subunit and phosphorylation is lost after alkaline phosphatase treatment. In addition, the mutation of this residue to phenylalanine, with the loss of the phosphorylation site, switches the substrate specificity of the enzyme from L-serine to L-alanine (Ernst et al. 2015). Despite the evidence of the alternative substrate preference of SPT, the physiological role of this dynamic regulation is still unknown. SPT phosphorylation was also found in BCR-ABL positive cells, a condition linked to the development of chronic myeloid leukemia (Taouji et al. 2013). LCB1, the other SPT subunit, is indeed phosphorylated at Tyr-164 in this cell types under basal condition and the inhibition of BCR-ABL with Imatinib decreases SPT phosphorylation, leading to a time and dose-dependent activation of the enzyme and its translocation from the endoplasmic reticulum to the Golgi apparatus. In addition, Tyr-164 mutation induces apoptosis in BCR-ABL-positive leukemia cells, identifying SPT as a potential therapeutic target to overcome Imatinib resistance.

Fold-type II: SR and CBS

L-Serine is racemized by SR to give D-serine, which binds to the glycine site as a co-agonist of the *N*-methyl D-aspartate (NMDA) receptors in various regions of the brain, exerting its effects in neurotoxicity and synaptic plasticity. Given the involvement of D-serine in neurodegenerative diseases and schizophrenia, the regulation by phosphorylation may be relevant in physiological and pathological mechanisms. SR is a tightly regulated enzyme by various factors: nucleotides, divalent cations, *S*-nitrosylation, other protein partners, and phosphorylation (Baumgart and Rodriguez-Crespo 2008). It was shown that phosphorylation at Thr-277 is typical of the 10% pool of membrane-associated mouse SR in non-neuronal cells (Balan et al. 2009). Mouse cytosolic SR has been found to be phosphorylated at Thr-71 and the enzymic activity, in terms of V_{max}, is increased following phosphorylation (Foltyn et al. 2010). This represents the main phosphorylation site on SR. Moreover, it has been demonstrated that PKC controls rat SR phosphorylation and thus D-serine production both in vitro and in vivo (Vargas-Lopes et al. 2011). Interestingly, this phosphorylation event inhibits SR in astrocytes and neurons (Vargas-Lopes et al. 2011). Since neither Thr-71 nor Thr-227 are conserved in human SR (the human corresponding residues are Ala-71 and Met-227), a search in phosphoproteomic analyses reveals that the human enzyme possesses multiple possible phosphorylation sites conserved also in mouse and rat: Ser-134, Tyr-207, Ser-212, Tyr-218, Ser-220, Ser-242 and Ser-339 (Klammer et al. 2012; Mertins et al. 2016). No in-depth investigation exists yet on the role of these residues regarding the structure–function relationship of SR.

Phosphorylation of human CBS has been reported in very recent papers (d'Emmanuele di Villa Bianca et al. 2015, 2016). Human CBS is a unique heme-containing enzyme that catalyzes the PLP-dependent condensation of homocysteine with serine to form cystathionine (Miles and Kraus 2004). Cystathionine is then cleaved by cystathionine γ-lyase (CGL) to give cysteine. CBS represents the first step in the transsulfuration pathway which connects the methionine cycle to cysteine production, therefore, its proper function is crucial for both cysteine and methionine metabolism. Accordingly, a compromised CBS activity or the absence of CBS leads to manifestation of CBS-deficient homocystinuria, a condition characterized by very high levels of plasma total homocysteine and methionine.

Recent studies have reported that the activity of human CBS within the urothelium, the epithelial lining the inner surface of human bladder, is regulated by phosphorylation (d'Emmanuele di Villa Bianca et al. 2015). The authors have demonstrated that CBS activity is specifically enhanced by phosphorylation at Ser227 in cGMP/PKG-dependent mechanism (d'Emmanuele di Villa Bianca et al. 2015, 2016). CBS is markedly expressed in the human urothelium (d'Emmanuele di Villa Bianca et al. 2015) representing the main enzymatic source of H_2S, which has been recently proposed as a new signal molecule in the control of bladder tone. In this context, the finding that CBS phosphorylation by PKG increases endogenous H_2S production (d'Emmanuele di Villa Bianca et al. 2015) suggests the possibility that the regulation of H_2S formation by CBS may involve CBS phosphorylation. Interestingly, CBS was found to be phosphorylated also on Ser-525 in a PKG-dependent manner, but without affecting H_2S production. This could be due to the localization of Ser-525 in the C-terminal regulatory domain which is the binding region of the allosteric activator *S*-adenosyl methionine. Therefore, phosphorylation of this serine residue may be implicated in the modulation of further features of CBS protein. Additional experiments are necessary to unravel the molecular mechanism underlying CBS activation by phosphorylation.

Fold-type III decarboxylases: eukaryotic ODC

ODC is the rate-limiting enzyme in polyamine biosynthesis, which is essential for cell division. The mammalian enzyme presents a consensus phosphorylation sequence for protein casein kinase II, and it has been reported that ODC, either recombinant mouse enzyme, or from intact mouse

overproducing ODC cells, can be phosphorylated at Ser-303 by casein kinase II (Rosenberg-Hasson et al. 1991). Studies with the wild-type and the S303A variant show that phosphorylation does not affect ODC activity as well as protein rate turnover (Rosenberg-Hasson et al. 1991). Reddy et al. (1996) reported that ODC could undergo multisite phosphorylation (in addition to that performed by casein kinase II) involving unidentified kinases that leads to ~ 50% increase in the V_{max} value and higher protein stability. Again, phosphorylation may affect the enzyme stability in vivo despite no direct effect on activity.

Concluding remarks and future perspectives

A search of the human phosphoproteomic data reveals that, although theoretically many PLP enzymes appear to be involved in phosphorylation regulatory pathways, only few of them are reported to be phosphorylated, at least until now. Apart from glycogen phosphorylase, for many of the others, the knowledge of how this modification affects enzyme function is unknown. Here, we show how difficult it is to interpret the possible modulation exerted by this modification, even for those enzymes whose structure is solved and the phosphorylation site(s) identified, as for example GAD or SR. The common feature appears to be the exposed position of the phosphorylation site in both enzymes. Moreover, the same modification could trigger different effects. This is also evident for these investigated PLP-enzymes where phosphorylation can activate, inhibit or have no effects. The relation among phosphorylation site, structural modification and functional effect is desirable to be obtained to shed light into complex metabolic regulation networks in which these enzymes are involved and often responsible for the first committed step in biosynthetic reactions of essential bioactive amines.

Since phosphorylation is a common and widespread strategy of regulation and interplay among transduction and metabolic pathways, it is of much interest to deepen the knowledge for PLP enzymes that represent the 4% of the enzyme activities present in a eukaryotic cells (Percudani and Peracchi 2003, 2009).

In perspective, the unraveling of the structure-to-function relationships of phosphorylation events for all known PLP enzymes and especially for those placed in key knots of physiological controlling routes is highly attractive. In addition, this information could be of great help also for PLP enzymes involved in hereditary pathogenic diseases, to concur in understanding complex phenotypes of patients bearing mutations that apparently lead to subtle modifications in protein structures. The study of regulation of PLP enzymes is at its beginning and needs to be further systematically undertaken.

Acknowledgements This work was supported by FUR2016, University of Verona, to MB.

Compliance with ethical standards

Conflict of interest The authors declare no conflict of interests.

Ethical statement The manuscript complies to the ethical rules applicable for the journal and the research does not involve data regarding humans or animals.

References

Arias C, Valero H, Tapia R (1992) Inhibition of brain glutamate decarboxylase activity is related to febrile seizures in rat pups. J Neurochem 58(1):369–373

Astegno A, Capitani G, Dominici P (2015) Functional roles of the hexamer organization of plant glutamate decarboxylase. Biochim Biophys Acta 1854(9):1229–1237. https://doi.org/10.1016/j.bbapap.2015.01.001

Astegno A, La Verde V, Marino V, Dell'Orco D, Dominici P (2016) Biochemical and biophysical characterization of a plant calmodulin: role of the N- and C-lobes in calcium binding, conformational change, and target interaction. Biochim Biophys Acta 1864(3):297–307. https://doi.org/10.1016/j.bbapap.2015.12.003

Baekkeskov S, Landin M, Kristensen JK, Srikanta S, Bruining GJ, Mandrup-Poulsen T, de Beaufort C, Soeldner JS, Eisenbarth G, Lindgren F et al (1987) Antibodies to a 64,000 Mr human islet cell antigen precede the clinical onset of insulin-dependent diabetes. J Clin Invest 79(3):926–934. https://doi.org/10.1172/JCI112903

Baekkeskov S, Aanstoot HJ, Christgau S, Reetz A, Solimena M, Cascalho M, Folli F, Richter-Olesen H, De Camilli P (1990) Identification of the 64 K autoantigen in insulin-dependent diabetes as the GABA-synthesizing enzyme glutamic acid decarboxylase. Nature 347(6289):151–156. https://doi.org/10.1038/347151a0

Balan L, Foltyn VN, Zehl M, Dumin E, Dikopoltsev E, Knoh D, Ohno Y, Kihara A, Jensen ON, Radzishevsky IS, Wolosker H (2009) Feedback inactivation of D-serine synthesis by NMDA receptor-elicited translocation of serine racemase to the membrane. Proc Natl Acad Sci USA 106(18):7589–7594. https://doi.org/10.1073/pnas.0809442106

Bao J, Cheung WY, Wu JY (1995) Brain L-glutamate decarboxylase. Inhibition by phosphorylation and activation by dephosphorylation. J Biol Chem 270(12):6464–6467

Baumgart F, Rodriguez-Crespo I (2008) D-Amino acids in the brain: the biochemistry of brain serine racemase. FEBS J 275(14):3538–3545. https://doi.org/10.1111/j.1742-4658.2008.06517.x

Blum P, Jankovic J (1991) Stiff-person syndrome: an autoimmune disease. Mov Disord 6(1):12–20. https://doi.org/10.1002/mds.870060104

Bu DF, Erlander MG, Hitz BC, Tillakaratne NJ, Kaufman DL, Wagner-McPherson CB, Evans GA, Tobin AJ (1992) Two human glutamate decarboxylases, 65-kDa GAD and 67-kDa GAD, are each encoded by a single gene. Proc Natl Acad Sci USA 89(6):2115–2119

Capitani G, De Biase D, Aurizi C, Gut H, Bossa F, Grutter MG (2003) Crystal structure and functional analysis of Escherichia coli glutamate decarboxylase. EMBO J 22(16):4027–4037. https://doi.org/10.1093/emboj/cdg403

Carr RK, Schlichter D, Spielholz C, Wicks WD (1986) In vitro phosphorylation of 4-aminobutyrate aminotransferase by cAMP

dependent protein kinase. J Cycl Nucleotide Protein Phosphor Res 11(1):11–23
Chou CC, Modi JP, Wang CY, Hsu PC, Lee YH, Huang KF, Wang AH, Nan C, Huang X, Prentice H, Wei J, Wu JY (2017) Activation of brain L-glutamate decarboxylase 65 isoform (GAD65) by phosphorylation at threonine 95 (T95). Mol Neurobiol 54(2):866–873. https://doi.org/10.1007/s12035-015-9633-0
Cohen P (2000) The regulation of protein function by multisite phosphorylation—a 25 year update. Trends Biochem Sci 25(12):596–601
Cohen P (2002) The origins of protein phosphorylation. Nat Cell Biol 4(5):E127–E130. https://doi.org/10.1038/ncb0502-e127
di Villa d'Emmanuele, Bianca R, Mitidieri E, Esposito D, Donnarumm E, Russo A, Fusco F, Ianaro A, Mirone V, Cirino G, Russo G, Sorrentino R (2015) Human cystathionine-β-synthase phosphorylation on serine227 modulates hydrogen sulfide production in human urothelium. PLoS ONE 10(9):e0136859. https://doi.org/10.1371/journal.pone.0136859
d'Emmanuele di Villa Bianca R, Mitidieri E, Fusco F, Russo A, Pagliara V, Tramontano T, Donnarumma E, Mirone V, Cirino G, Russo G, Sorrentino R (2016) Urothelium muscarinic activation phosphorylates CBSSer227 via cGMP/PKG pathway causing human bladder relaxation through H2S production. Sci Rep 6:31491. https://doi.org/10.1038/srep31491
Dartsch C, Chen D, Persson L (1998) Multiple forms of rat stomach histidine decarboxylase may reflect posttranslational activation of the enzyme. Regul Pept 77(1–3):33–41
Duchemin AM, Berry MD, Neff NH, Hadjiconstantinou M (2000) Phosphorylation and activation of brain aromatic L-amino acid decarboxylase by cyclic AMP-dependent protein kinase. J Neurochem 75(2):725–731
Duchemin AM, Neff NH, Hadjiconstantinou M (2010) Aromatic L-amino acid decarboxylase phosphorylation and activation by PKGIalpha in vitro. J Neurochem 114(2):542–552. https://doi.org/10.1111/j.1471-4159.2010.06784.x
Dunathan HC (1966) Conformation and reaction specificity in pyridoxal phosphate enzymes. Proc Natl Acad Sci USA 55(4):712–716
Erlander MG, Tillakaratne NJ, Feldblum S, Patel N, Tobin AJ (1991) Two genes encode distinct glutamate decarboxylases. Neuron 7(1):91–100
Ernst D, Murphy SM, Sathiyanadan K, Wei Y, Othman A, Laura M, Liu YT, Penno A, Blake J, Donaghy M, Houlden H, Reilly MM, Hornemann T (2015) Novel HSAN1 mutation in serine palmitoyltransferase resides at a putative phosphorylation site that is involved in regulating substrate specificity. Neuromol Med 17(1):47–57. https://doi.org/10.1007/s12017-014-8339-1
Fenalti G, Law RH, Buckle AM, Langendorf C, Tuck K, Rosado CJ, Faux NG, Mahmood K, Hampe CS, Banga JP, Wilce M, Schmidberger J, Rossjohn J, El-Kabbani O, Pike RN, Smith AI, Mackay IR, Rowley MJ, Whisstock JC (2007) GABA production by glutamic acid decarboxylase is regulated by a dynamic catalytic loop. Nat Struct Mol Biol 14(4):280–286. https://doi.org/10.1038/nsmb1228
Fleming JV, Fajardo I, Langlois MR, Sanchez-Jimenez F, Wang TC (2004) The C-terminus of rat L-histidine decarboxylase specifically inhibits enzymic activity and disrupts pyridoxal phosphate-dependent interactions with L-histidine substrate analogues. Biochem J 381(Pt 3):769–778. https://doi.org/10.1042/BJ20031553
Foltyn VN, Zehl M, Dikopoltsev E, Jensen ON, Wolosker H (2010) Phosphorylation of mouse serine racemase regulates D-serine synthesis. FEBS Lett 584(13):2937–2941. https://doi.org/10.1016/j.febslet.2010.05.022
Francis H, DeMorrow S, Venter J, Onori P, White M, Gaudio E, Francis T, Greene JF Jr, Tran S, Meininger CJ, Alpini G (2012) Inhibition of histidine decarboxylase ablates the autocrine tumorigenic effects of histamine in human cholangiocarcinoma. Gut 61(5):753–764. https://doi.org/10.1136/gutjnl-2011-300007
Grishin NV, Phillips MA, Goldsmith EJ (1995) Modeling of the spatial structure of eukaryotic ornithine decarboxylases. Protein Sci 4(7):1291–1304. https://doi.org/10.1002/pro.5560040705
Gut H, Dominici P, Pilati S, Astegno A, Petoukhov MV, Svergun DI, Grutter MG, Capitani G (2009) A common structural basis for pH- and calmodulin-mediated regulation in plant glutamate decarboxylase. J Mol Biol 392(2):334–351. https://doi.org/10.1016/j.jmb.2009.06.080
Hornykiewicz O, Lloyd KG, Davidson L (1976) The GABA system and function of the basal ganglia and Parkinson's disease. In: Chase TN, Tower DB, Roberts E (eds) GABA in nervous system function. Raven Press, New York, pp 479–485
Hsu CC, Thomas C, Chen W, Davis KM, Foos T, Chen JL, Wu E, Floor E, Schloss JV, Wu JY (1999) Role of synaptic vesicle proton gradient and protein phosphorylation on ATP-mediated activation of membrane-associated brain glutamate decarboxylase. J Biol Chem 274(34):24366–24371
Hunter T (1995) Protein kinases and phosphatases: the yin and yang of protein phosphorylation and signaling. Cell 80(2):225–236
Huszti Z, Magyar K (1984) Regulation of histidine decarboxylase activity in rat hypothalamus in vitro by ATP and cyclic AMP: enzyme inactivation under phosphorylating conditions. Agents Actions 14(3–4):546–549
Huszti Z, Magyar K (1985) Evidence for the role of cAMP-dependent protein kinase in the down-regulation of hypothalamic HD: reversal of cAMP-(ATP) induced inhibition of HD activity by the 'Walsh' inhibitor of cAMP-dependent protein kinase and by cyclic GMP. Agents Actions 16(3–4):240–243
Huszti Z, Magyar K (1987) Stimulation of hypothalamic histidine decarboxylase by calcium-calmodulin and protein kinase (cAMP-dependent) inhibitor. Agents Actions 20(3–4):233–235
Jayakrishnan B, Hoke DE, Langendorf CG, Buckle AM, Rowley MJ (2011) An analysis of the cross-reactivity of autoantibodies to GAD65 and GAD67 in diabetes. PLoS ONE 6(4):e18411. https://doi.org/10.1371/journal.pone.0018411
Jin H, Wu H, Osterhaus G, Wei J, Davis K, Sha D, Floor E, Hsu CC, Kopke RD, Wu JY (2003) Demonstration of functional coupling between gamma-aminobutyric acid (GABA) synthesis and vesicular GABA transport into synaptic vesicles. Proc Natl Acad Sci USA 100(7):4293–4298. https://doi.org/10.1073/pnas.0730698100
John RA (1995) Pyridoxal phosphate-dependent enzymes. Biochim Biophys Acta 1248(2):81–96
Johnson LN (1992) Glycogen phosphorylase: control by phosphorylation and allosteric effectors. FASEB J 6(6):2274–2282
Kash SF, Johnson RS, Tecott LH, Noebels JL, Mayfield RD, Hanahan D, Baekkeskov S (1997) Epilepsy in mice deficient in the 65-kDa isoform of glutamic acid decarboxylase. Proc Natl Acad Sci USA 94(25):14060–14065
Kass I, Hoke DE, Costa MG, Reboul CF, Porebski BT, Cowieson NP, Leh H, Pennacchietti E, McCoey J, Kleifeld O, Borri Voltattorni C, Langley D, Roome B, Mackay IR, Christ D, Perahia D, Buckle M, Paiardini A, De Biase D, Buckle AM (2014) Cofactor-dependent conformational heterogeneity of GAD65 and its role in autoimmunity and neurotransmitter homeostasis. Proc Natl Acad Sci USA 111(25):E2524–E2529. https://doi.org/10.1073/pnas.1403182111
Kennedy L, Hodges K, Meng F, Alpini G, Francis H (2012) Histamine and histamine receptor regulation of gastrointestinal cancers. Transl Gastrointest Cancer 1(3):215–227
Klammer M, Kaminski M, Zedler A, Oppermann F, Blencke S, Marx S, Muller S, Tebbe A, Godl K, Schaab C (2012) Phosphosignature predicts dasatinib response in non-small cell lung cancer.

Mol Cell Proteom 11(9):651–668. https://doi.org/10.1074/mcp.M111.016410
Kornev AP, Haste NM, Taylor SS, Eyck LF (2006) Surface comparison of active and inactive protein kinases identifies a conserved activation mechanism. Proc Natl Acad Sci USA 103(47):17783–17788. https://doi.org/10.1073/pnas.0607656103
Langendorf CG, Tuck KL, Key TL, Fenalti G, Pike RN, Rosado CJ, Wong AS, Buckle AM, Law RH, Whisstock JC (2013) Structural characterization of the mechanism through which human glutamic acid decarboxylase auto-activates. Biosci Rep 33(1):137–144. https://doi.org/10.1042/BSR20120111
Lee KL, Nickol JM (1974) Phosphorylation of tyrosine aminotransferase in vivo. J Biol Chem 249(18):6024–6026
Lu CT, Huang KY, Su MG, Lee TY, Bretana NA, Chang WC, Chen YJ, Huang HD (2013) DbPTM 3.0: an informative resource for investigating substrate site specificity and functional association of protein post-translational modifications. Nucleic Acids Res 41(database issue):D295–D305. https://doi.org/10.1093/nar/gks1229
Mann M, Jensen ON (2003) Proteomic analysis of post-translational modifications. Nat Biotechnol 21(3):255–261. https://doi.org/10.1038/nbt0303-255
Manning G, Whyte DB, Martinez R, Hunter T, Sudarsanam S (2002) The protein kinase complement of the human genome. Science 298(5600):1912–1934. https://doi.org/10.1126/science.1075762
Martin DL, Rimvall K (1993) Regulation of gamma-aminobutyric acid synthesis in the brain. J Neurochem 60(2):395–407
Mathieu C, Dupret JM, Rodrigues Lima F (2017) The structure of brain glycogen phosphorylase-from allosteric regulation mechanisms to clinical perspectives. FEBS J 284(4):546–554. https://doi.org/10.1111/febs.13937
Mertins P, Mani DR, Ruggles KV, Gillette MA, Clauser KR, Wang P, Wang X, Qiao JW, Cao S, Petralia F, Kawaler E, Mundt F, Krug K, Tu Z, Lei JT, Gatza ML, Wilkerson M, Perou CM, Yellapantula V, Huang KL, Lin C, McLellan MD, Yan P, Davies SR, Townsend RR, Skates SJ, Wang J, Zhang B, Kinsinger CR, Mesri M, Rodriguez H, Ding L, Paulovich AG, Fenyo D, Ellis MJ, Carr SA (2016) Proteogenomics connects somatic mutations to signalling in breast cancer. Nature 534(7605):55–62. https://doi.org/10.1038/nature18003
Miles EW, Kraus JP (2004) Cystathionine β-synthase: structure, function, regulation, and location of homocystinuria-causing mutations. J Biol Chem 279(29):29871–29874. https://doi.org/10.1074/jbc.R400005200
Namchuk M, Lindsay L, Turck CW, Kanaani J, Baekkeskov S (1997) Phosphorylation of serine residues 3, 6, 10, and 13 distinguishes membrane anchored from soluble glutamic acid decarboxylase 65 and is restricted to glutamic acid decarboxylase 65alpha. J Biol Chem 272(3):1548–1557
Ohtsu H (2010) Histamine synthesis and lessons learned from histidine decarboxylase deficient mice. Adv Exp Med Biol 709:21–31
Othman A, Rutti MF, Ernst D, Saely CH, Rein P, Drexel H, Porretta-Serapiglia C, Lauria G, Bianchi R, von Eckardstein A, Hornemann T (2012) Plasma deoxysphingolipids: a novel class of biomarkers for the metabolic syndrome? Diabetologia 55(2):421–431. https://doi.org/10.1007/s00125-011-2384-1
Othman A, Bianchi R, Alecu I, Wei Y, Porretta-Serapiglia C, Lombardi R, Chiorazzi A, Meregalli C, Oggioni N, Cavaletti G, Lauria G, von Eckardstein A, Hornemann T (2015) Lowering plasma 1-deoxysphingolipids improves neuropathy in diabetic rats. Diabetes 64(3):1035–1045. https://doi.org/10.2337/db14-1325
Paiardini A, Giardina G, Rossignoli G, Voltattorni CB, Bertoldi M (2017) New insights emerging from recent investigations on human group II pyridoxal 5′-phosphate decarboxylases. Curr Med Chem 24(3):226–244. https://doi.org/10.2174/0929867324666161123093339
Palm D, Klein HW, Schinzel R, Buehner M, Helmreich EJ (1990) The role of pyridoxal 5′-phosphate in glycogen phosphorylase catalysis. Biochemistry 29(5):1099–1107
Panula P, Nuutinen S (2013) The histaminergic network in the brain: basic organization and role in disease. Nat Rev Neurosci 14(7):472–487. https://doi.org/10.1038/nrn3526
Penno A, Reilly MM, Houlden H, Laura M, Rentsch K, Niederkofler V, Stoeckli ET, Nicholson G, Eichler F, Brown RH Jr, von Eckardstein A, Hornemann T (2010) Hereditary sensory neuropathy type 1 is caused by the accumulation of two neurotoxic sphingolipids. J Biol Chem 285(15):11178–11187. https://doi.org/10.1074/jbc.M109.092973
Percudani R, Peracchi A (2003) A genomic overview of pyridoxal-phosphate-dependent enzymes. EMBO Rep 4(9):850–854. https://doi.org/10.1038/sj.embor.embor914
Percudani R, Peracchi A (2009) The B6 database: a tool for the description and classification of vitamin B6-dependent enzymatic activities and of the corresponding protein families. BMC Bioinform 10:273. https://doi.org/10.1186/1471-2105-10-273
Phillips RS (2015) Chemistry and diversity of pyridoxal-5′-phosphate dependent enzymes. Biochim Biophys Acta 1854(9):1167–1174. https://doi.org/10.1016/j.bbapap.2014.12.028
Phillips RS, Scott I, Paulose R, Patel A, Barron TC (2014) The phosphate of pyridoxal-5′-phosphate is an acid/base catalyst in the mechanism of Pseudomonas fluorescens kynureninase. FEBS J 281(4):1100–1109. https://doi.org/10.1111/febs.12671
Pogson CI, Dickson AJ, Knowles RG, Salter M, Santana MA, Stanley JC, Fisher MJ (1986) Control of phenylalanine and tyrosine metabolism by phosphorylation mechanisms. Adv Enzyme Regul 25:309–327
Reddy SG, McLlheran SM, Cochran BJ, Worth LL, Bishop LA, Brown PJ, Knutson VP, Haddox MK (1996) Multisite phosphorylation of ornithine decarboxylase in transformed macrophages results in increased intracellular enzyme stability and catalytic efficiency. J Biol Chem 271(40):24945–24953
Roberts E (1975) The Nervous System. In: Tower DB (ed) The basic neurosciences, vol I. Raven Press, New York, pp 541–552
Rosenberg-Hasson Y, Strumpf D, Kahana C (1991) Mouse ornithine decarboxylase is phosphorylated by casein kinase-II at a predominant single location (serine 303). Eur J Biochem 197(2):419–424
Savany A, Cronenberger L (1982) Isolation and properties of multiple forms of histidine decarboxylase from rat gastric mucosa. Biochem J 205(2):405–412
Savany A, Cronenberger L (1988) Histidine decarboxylase from rat gastric mucosa: heterogeneity and enzyme forms modification. Biochem Int 16(3):559–570
Savany A, Cronenberger L (1989) Inactivation of rat gastric mucosal histidine decarboxylase by phosphatase. Biochem Int 19(2):429–438
Savany A, Cronenberger L (1990) Relationship between the multiple forms of rat gastric histidine decarboxylase: effects of conditions favouring phosphorylation and dephosphorylation. Biochem Int 20(2):363–374
Schmid E, Schmid W, Jantzen M, Mayer D, Jastorff B, Schutz G (1987) Transcription activation of the tyrosine aminotransferase gene by glucocorticoids and cAMP in primary hepatocytes. Eur J Biochem 165(3):499–506
Schneider G, Kack H, Lindqvist Y (2000) The manifold of vitamin B6 dependent enzymes. Structure 8(1):R1–R6
Seo J, Lee KJ (2004) Post-translational modifications and their biological functions: proteomic analysis and systematic approaches. J Biochem Mol Biol 37(1):35–44
Sherman AD, Davidson AT, Baruah S, Hegwood TS, Waziri R (1991) Evidence of glutamatergic deficiency in schizophrenia. Neurosci Lett 121(1–2):77–80

Singh V, Ram M, Kumar R, Prasad R, Roy BK, Singh KK (2017) Phosphorylation: implications in Cancer. Protein J 36(1):1–6. https://doi.org/10.1007/s10930-017-9696-z

Soghomonian JJ, Laprade N (1997) Glutamate decarboxylase (GAD67 and GAD65) gene expression is increased in a subpopulation of neurons in the putamen of Parkinsonian monkeys. Synapse 27(2):122–132. https://doi.org/10.1002/(SICI)1098-2396(199710)27:2<122:AID-SYN3>3.0.CO;2-G

Spielholz C, Carr K, Schlichter D, Wicks WD (1984) In vitro phosphorylation of tyrosine and 4-aminobutyrate aminotransferases by cAMP dependent protein kinase. Prog Clin Biol Res 144B:57–66

Sprang SR, Acharya KR, Goldsmith EJ, Stuart DI, Varvill K, Fletterick RJ, Madsen NB, Johnson LN (1988) Structural changes in glycogen phosphorylase induced by phosphorylation. Nature 336(6196):215–221. https://doi.org/10.1038/336215a0

Stirtan WG, Withers SG (1996) Phosphonate and alpha-fluorophosphonate analogue probes of the ionization state of pyridoxal 5′-phosphate (PLP) in glycogen phosphorylase. Biochemistry 35(47):15057–15064. https://doi.org/10.1021/bi9606004

Tang XW, Hsu CC, Schloss JV, Faiman MD, Wu E, Yang CY, Wu JY (1997) Protein phosphorylation and taurine biosynthesis in vivo and in vitro. J Neurosci 17(18):6947–6951

Taouji S, Higa A, Delom F, Palcy S, Mahon FX, Pasquet JM, Bosse R, Segui B, Chevet E (2013) Phosphorylation of serine palmitoyltransferase long chain-1 (SPTLC1) on tyrosine 164 inhibits its activity and promotes cell survival. J Biol Chem 288(24):17190–17201. https://doi.org/10.1074/jbc.M112.409185

Taylor SS, Kornev AP (2011) Protein kinases: evolution of dynamic regulatory proteins. Trends Biochem Sci 36(2):65–77. https://doi.org/10.1016/j.tibs.2010.09.006

Tehranian R, Montoya SE, Van Laar AD, Hastings TG, Perez RG (2006) Alpha-synuclein inhibits aromatic amino acid decarboxylase activity in dopaminergic cells. J Neurochem 99(4):1188–1196. https://doi.org/10.1111/j.1471-4159.2006.04146.x

Tower DB (1976) GABA in nervous system function. Raven Press, New York

Vargas-Lopes C, Madeira C, Kahn SA, Albino do Couto I, Bado P, Houzel JC, De Miranda J, de Freitas MS, Ferreira ST, Panizzutti R (2011) Protein kinase C activity regulates D-serine availability in the brain. J Neurochem 116(2):281–290. https://doi.org/10.1111/j.1471-4159.2010.07102.x

Venerando A, Cesaro L, Pinna LA (2017) From phosphoproteins to phosphoproteomes: a historical account. FEBS J. https://doi.org/10.1111/febs.14014

Wei J, Wu JY (2008) Post-translational regulation of L-glutamic acid decarboxylase in the brain. Neurochem Res 33(8):1459–1465. https://doi.org/10.1007/s11064-008-9600-5

Wei J, Davis KM, Wu H, Wu JY (2004) Protein phosphorylation of human brain glutamic acid decarboxylase (GAD)65 and GAD67 and its physiological implications. Biochemistry 43(20):6182–6189. https://doi.org/10.1021/bi0496992

Wu JY, Tang XW, Schloss JV, Faiman MD (1998) Regulation of taurine biosynthesis and its physiological significance in the brain. Adv Exp Med Biol 442:339–345

Yard BA, Carter LG, Johnson KA, Overton IM, Dorward M, Liu H, McMahon SA, Oke M, Puech D, Barton GJ, Naismith JH, Campopiano DJ (2007) The structure of serine palmitoyltransferase; gateway to sphingolipid biosynthesis. J Mol Biol 370(5):870–886. https://doi.org/10.1016/j.jmb.2007.04.086

Biochemistry

Article

Cite This: Biochemistry 2018, 57, 6336−6348

pubs.acs.org/biochemistry

Cysteine 180 Is a Redox Sensor Modulating the Activity of Human Pyridoxal 5′-Phosphate Histidine Decarboxylase

Giada Rossignoli,[†] Alessandro Grottesi,[‡] Giovanni Bisello,[†] Riccardo Montioli,[†] Carla Borri Voltattorni,[†] Alessandro Paiardini,[*,§] and Mariarita Bertoldi[*,†]

[†]Department of Neuroscience, Biomedicine and Movement, University of Verona, Strada Le Grazie, 8, 37134 Verona, Italy

[‡]Super Computing Applications and Innovation (CINECA), 00185 Rome, Italy

[§]Department of Biochemical Sciences "A. Rossi Fanelli", University "La Sapienza", Rome, P.zale A. Moro 5, 00185 Roma, Italy

Supporting Information

ABSTRACT: Histidine decarboxylase is a pyridoxal 5′-phosphate enzyme catalyzing the conversion of histidine to histamine, a bioactive molecule exerting its role in many modulatory processes. The human enzyme is involved in many physiological functions, such as neurotransmission, gastrointestinal track function, cell growth, and differentiation. Here, we studied the functional properties of the human enzyme and, in particular, the effects exerted at the protein level by two cysteine residues: Cys-180 and Cys-418. Surprisingly, the enzyme exists in an equilibrium between a reduced and an oxidized form whose extent depends on the redox state of Cys-180. Moreover, we determined that (i) the two enzymatic redox species exhibit modest structural changes in the coenzyme microenvironment and (ii) the oxidized form is slightly more active and stable than the reduced one. These data are consistent with the model proposed by bioinformatics analyses and molecular dynamics simulations in which the Cys-180 redox state could be responsible for a structural transition affecting the C-terminal domain reorientation leading to active site alterations. Furthermore, the biochemical properties of the purified C180S and C418S variants reveal that C180S behaves like the reduced form of the wild-type enzyme, while C418S is sensitive to reductants like the wild-type enzyme, thus allowing the identification of Cys-180 as the redox sensitive switch. On the other hand, Cys-418 appears to be a residue involved in aggregation propensity. A possible role for Cys-180 as a regulatory switch in response to different cellular redox conditions could be suggested.

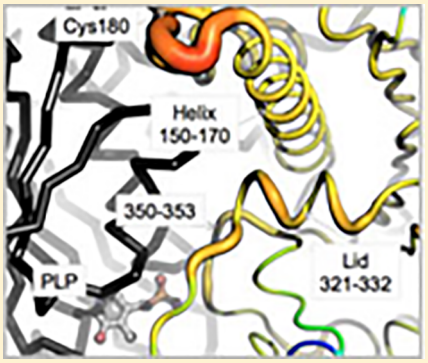

Histidine decarboxylase (HDC, EC 4.1.1.22) is a pyridoxal 5′-phosphate (PLP) enzyme that is responsible for the conversion of histidine to histamine. Histamine plays important roles in gastric acid secretion and immune responses and is also involved in cell growth, memory, appetite, and circadian rhythm regulation.[1] Impairment of histamine metabolism leads to multiple pathological states such as inflammatory responses, peptic ulcer, and several central nervous system disorders.[2,3]

From an evolutionary and structural point of view, HDC belongs to group II PLP-decarboxylases of fold type I. A recent review summarizes the spatial and functional correlations among the enzymes that belong to this group.[4] Although the prokaryotic HDC enzymes are mainly pyruvoyl-dependent (with the exception of a few Gram-negative bacteria such as *Morganella morganii* together with some *Enterobacter* and *Klebsiella* species), the eukaryotic, and thus the mammalian and human, enzymes are PLP-dependent. E. E. Snell and co-workers cloned, purified, and characterized the prokaryotic PLP HDCs.[5−11] Today, apart from a few mechanistic papers,[12] these prokaryotic decarboxylases are mainly studied for their role in contamination of food, especially fish, to find possible inhibitors that could prevent histamine accumulation.[13−15]

Mammalian HDC, which is different from the other homologous enzymes such as aromatic amino acid decarboxylase or glutamate decarboxylase,[4] has been poorly characterized until now, given its small quantities in the cell types where it is expressed: mast cells, a group of hypothalamic neurons, and enterochromaphin-like cells.[16,17] Indeed, its level is generally scarce also when it is cloned and expressed as a recombinant protein in bacterial systems. Moreover, the rat and mouse proteins, translated as 74 kDa inactive precursors, are very unstable and subjected to post-translational processing at the N- and C-termini.[18,19] The cleaved forms are active and range from 53 to 64 kDa, as seen in different cell types.[20−27] The minimum required for activity is 53 kDa,[28] which corresponds to the homologous domain of other PLP-decarboxylases. The mechanism of processing has been attributed to various systems such as calpains, proteasome, and caspase-9,[22,23,29−31] but it is far from being exhaustively elucidated.

Received: June 6, 2018
Revised: October 15, 2018
Published: October 22, 2018

Downloaded via UNIV DEGLI STUDI DI VERONA on November 11, 2018 at 22:06:10 (UTC).
See https://pubs.acs.org/sharingguidelines for options on how to legitimately share published articles.

© 2018 American Chemical Society

DOI: 10.1021/acs.biochem.8b00625
Biochemistry 2018, 57, 6336−6348

Besides its role in histamine production, HDC is now attracting attention because of its involvement in the cell proliferation of many tumors and in Tourette syndrome. Among tumors, cholangiocarcinoma is difficult to diagnose and has limited treatments being chemoresistant.[32,33] Surgical resection, the treatment of choice in such a case, is not always feasible given frequent late diagnosis.[34] Recently, it has been demonstrated that HDC expression is enhanced in cholangiocarcinoma, and the increased level of histamine secretion is related to tumor growth.[35] Treatment with an inhibitor of HDC, namely α-methyl-D,L-histidine, decreases HDC activity and slows cancer progression.[35,36] A few inhibitors of HDC have been further explored,[4] such as α-fluoromethylhistidine,[37] histidine methylester,[37] epigallocatechin gallate,[38] and 4(5)-aminooxymethylimidazole,[39] however with no direct clinical results.

Tourette syndrome, a developmental neuropsychiatric disorder, has been linked to a mutation, present in heterozygosis, in the *Hdc* gene. This gives rise to a deleted protein (W317X) with no decarboxylase activity.[40] However, despite contradictory reports, it has been recently confirmed both in humans and in *Hdc* knockout (KO) mouse models that HDC deficiency represents a rare cause of Tourette syndrome and that histamine−dopamine interconnections in the basal ganglia are an important knot of pathology.[41] This monoamine interplay has recently been reviewed by Pittenger.[42]

KO mice, generated in 2001,[43] gave insights into previously unknown pathophysiological functions of histamine, expanding its roles from taking part in allergic and neurological responses to being involved in different fields such as cardiology, immunology, and infectious diseases.[2]

The three-dimensional structure of active human HDC (residues 2−477) in complex with the inhibitory substrate analogue histidine methylester was determined in 2012 using an enzymatic form bearing a double-amino acid substitution (C180S and C418S) to increase protein stability and prevent nonspecific aggregation.[44,45] In the functionally active dimeric arrangement, Cys-180 belongs to the large domain of each monomer that is responsible for dimeric interface formation and faces near to the corresponding Cys-180 of the other monomer, while Cys-418 is located at the surface of the C-terminal small domain far from the other subunit. It has been demonstrated that the catalytic efficiency of the doubly substituted enzyme is not altered compared to that of the wild-type (WT) enzyme[45] with measured k_{cat} values 10-fold higher than the k_{cat} values reported for most mammalian HDCs (<0.1 s^{-1}).[46] A possible role for a regulation played by the redox state and/or by calcium levels was advanced.[46]

Here, we show, for the first time, that human WT HDC exists as an equilibrium between a cysteine-reduced (redHDC) and cysteine-oxidized (oxHDC) form. These two species exhibit slight structural and functional differences. In addition, we show that Cys-180 is responsible for the intermolecular disulfide-bound dimer (oxHDC) and provide insight into its properties, while Cys-418, in agreement with ref 44, could be involved in the propensity of HDC to aggregate.

MATERIALS AND METHODS

Materials. Pyridoxal 5′-phosphate (PLP), L-histidine (L-His), 2,4,6-trinitrobenzene-1-sulfonic acid (TNB), isopropyl β-D-thiogalactopyranoside (IPTG), protease inhibitor cocktail EDTA-free tablets, phenylmethanesulfonyl fluoride (PMSF), 2,4,6-trinitrobenzenesulfonic acid (TNB), 1,8-anilinonaphthalenesulfonic acid (ANS), dithiothreitol (DTT), β-mercaptoethanol (β-MeSH), glutathione (GSH), and all the other chemicals and reagents were purchased from Sigma-Aldrich and were of the highest purity available. The gene encoding human HDC was purchased from ORIGENE.

Multiple-Sequence Alignment of HDCs. Amino acid sequences from various sources were taken from the NCBI Web site (https://www.ncbi.nlm.nih.gov/) and aligned using the Clustal Omega tool (http://www.ebi.ac.uk/Tools/msa/clustalo/) keeping all parameters at their default values.

Plasmid Constructs. The gene encoding human HDC, carried by mammalian expression vector pCMV6, was amplified to obtain the gene sequence corresponding to the amino acid sequence Met-2−Cys-479, followed by the thrombin protease cleavage site. In addition, the restriction sites for the enzymes NdeI and XhoI were inserted upstream and downstream, respectively, for subcloning the modified *HDC* gene sequence upstream of the six-His tag into bacterial expression plasmid pET28a. The designed and synthesized (Eurofins Genomics) primers were 5′-AGGGACCATGGGC-ATGGAGCCTGAGGAGTACAGA-3′ for the forward primer and 5′-ATTTACTCGAG**GGATCCACGCGGAACCAG**AC-AGTGCTGACTCAGGAT-3′ for the reverse primer (the NdeI and XhoI restriction sites are underlined in the forward and reverse primers, respectively, while the thrombin cleavage site is shown in bold).

The C180S and C418S variants were constructed starting from the cloned gene in the pET28a expression vector. Mutations were introduced by the QuickChange site-directed mutagenesis kit (Agilent Technologies) using the oligonucleotides 5′-GCTGATGAGTCCAGCCTAAATGCCCGA-3′ and its complement and 5′-GGGTCCTAATAGTCTCACAGAA-AATGTG-3′ and its complement for C180S and C418S, respectively (the mutated codons are underlined) (Eurofins Genomics). The correct nucleotide sequences of the constructs were confirmed by DNA sequencing (BMR Genomics).

Expression and Purification. *Escherichia coli* BL21 (DE3) chemically competent cells were transformed by heat shock at 42 °C with the appropriate construct and grown in 6 L of Luria-Bertani (LB) broth supplemented with 35 mg/mL kanamycin. The cultures were grown at 37 °C to an OD_{600} of 0.4−0.6, and expression was induced with 0.5 mM IPTG for 15 h at 30 °C. Cells were harvested and resuspended in 20 mM sodium phosphate buffer (pH 7.4) containing 0.5 M NaCl, 20 mM imidazole, 50 μM PLP, 0.5 mM PMSF, and protease inhibitor cocktail, with the addition of 10 mM β-MeSH. Lysozyme was then added to a concentration of 0.2 mg/mL, and the culture was incubated for 20 min at room temperature. After a freeze−thaw cycle, leupeptin (1 μg/mL) and pepstatin (1 μg/mL) were added, and the suspension was centrifuged at 30000*g* for 30 min. The cleared lysate was diluted to ∼30 mg/mL and loaded onto a HisPrep FF 16/10 column (GE Healthcare) equilibrated with 20 mM sodium phosphate buffer (pH 7.4) containing 0.5 M NaCl and 20 mM imidazole in the presence of 10 mM β-MeSH. A linear gradient was then inserted (0 to 100% in 200 mL) with the same buffer containing 350 mM imidazole. Soluble HDC elutes as a symmetrical peak and was incubated with 100 μM PLP. Imidazole and unbound coenzyme were removed by extensive washing with 0.1 M potassium phosphate buffer (pH 7.4) and 10 mM β-MeSH, and the protein solution (redHDC) was concentrated in the same buffer using Amicon Ultra 10 concentrators (Millipore). The enzyme concentration was

DOI: 10.1021/acs.biochem.8b00625
Biochemistry 2018, 57, 6336−6348

determined by using an ε_M of 1.57 × 10^5 M^{-1} cm^{-1} at 280 nm,[47] and the PLP content was determined by releasing the coenzyme in 0.1 M NaOH using an ε_M of 6600 M^{-1} cm^{-1} at 388 nm.[48] The purity of the protein was detected by a single band corresponding to a molecular weight of ∼56 kDa in a 12% reducing sodium dodecyl sulfate−polyacrylamide gel electrophoresis (SDS−PAGE) gel.

Semidenaturing and Native PAGE. Semidenaturing 10% SDS−PAGE used to evaluate the presence of the intermolecular disulfide bond of 5 μg of HDC incubated with increasing concentrations of β-MeSH, DTT, or GSH (the concentrations are listed in the Results and Discussion) for 1 h and loaded with the addition of 4× nonreducing sample buffer.

Native PAGE analysis was performed under the same conditions as semidenaturing SDS−PAGE, but samples were loaded with the addition of 2× native sample buffer.

Size-Exclusion Liquid Chromatography Analyses. Size-exclusion liquid chromatography was used to prepare the fully oxidized HDC (oxHDC) starting from the reduced form. RedHDC was loaded onto a Sephacryl H-200 (16/60) (GE Healtcare) column equilibrated with 0.1 M potassium phosphate buffer (pH 7.4) and 0.15 M NaCl on an Akta FPLC system (GE Healthcare). The run, using the same buffer, was performed at a flow rate of 0.5 mL/min with detection at 280 nm. The protein eluted as a single symmetrical peak and was incubated with 100 μM PLP. Unbound coenzyme was removed by extensive washing with 0.1 M potassium phosphate buffer (pH 7.4), and the protein solution was concentrated in the same buffer using Amicon Ultra 10 concentrators (Millipore). The redox state of the eluted protein was determined by loading it onto a nonreducing denaturing (semidenaturing, see above) SDS−PAGE gel.

Size-exclusion liquid chromatography was used to determine the molecular dimensions of the holoenzyme (300 μg) in both oxidized and reduced forms. The samples were loaded on a Sephacryl H-200 (16/60) (GE Healtcare) column equilibrated with 0.1 mM potassium phosphate buffer (pH 7.4) and 0.15 M NaCl with the addition of 10 mM β-MeSH for redHDC, on an Akta FPLC system (GE Healthcare). The injection volume was 500 μL at a flow rate of 0.5 mL/min with detection at 280 nm. Three chromatographic experiments were run per sample, and Unicorn version 5.01 (GE Healthcare) was used to calculate the elution volume of each peak. The apparent molecular dimension of the eluting species was calculated by comparing their elution volume to that of a set of molecular weight standards under the same experimental conditions.

Spectroscopic Measurements. Absorption measurements were performed using a Jasco V-550 spectrophotometer at a protein concentration of 1 mg/mL under conditions specified in the Results and Discussion for each case.

Circular dichroism measurements were taken with a Jasco J-710 spectropolarimeter at a protein concentration of 1 mg/mL for near-ultraviolet (near-UV) and visible spectra or 0.1 mg/mL for far-UV spectra. The thermostability was determined by monitoring the circular dichroic signal at 222 nm at a concentration of 0.1 mg/mL and a temperature increase from 25 to 90 °C at a rate of 1.5 °C/min.

Fluorescence spectra were recorded using a FP-750 Jasco spectrofluorimeter setting at 5 nm excitation and emission bandwidths, following excitation at different wavelengths, specified in the Results and Discussion for each case.

All the spectroscopic measurements were taken in 0.1 M potassium phosphate buffer (pH 7.4) at 25 °C, with the addition of 10 mM β-MeSH or 10 mM GSH for redHDC.

Coenzyme Binding Affinity Measurements. The apoenzyme was prepared by incubating 10 μM redHDC or oxHDC with 50 mM phenylhydrazine at 25 °C for 2 h in 0.5 M potassium phosphate buffer (pH 6.8), with the addition of 10 mM β-MeSH for redHDC. The solution was then loaded on a desalting 26/10 column (GE Healthcare) preequilibrated with the same buffer without phenylhydrazine. The eluted enzyme was then concentrated using Amicon Ultra 10 concentrators (Millipore) and washed with 0.1 M potassium phosphate buffer (pH 7.4), with the addition of 10 mM β-MeSH for apo-redHDC.

The equilibrium apparent dissociation constant for PLP, $K_{D(PLP)}$, was determined by measuring the quenching of the intrinsic fluorescence of the 0.03 μM HDC apoenzyme in the presence of PLP at concentrations ranging from 0.005 to 20 μM in 0.1 mM potassium phosphate buffer (pH 7.4), with the addition of 10 mM β-MeSH for redHDC.

The data were fitted to the following equation:

$$Y = Y_{max}\frac{[E]_t + [PLP]_t + K_{D(PLP)} - \sqrt{[[E]_t + [PLP]_t + K_{D(PLP)}]^2 - 4[E]_t[PLP]_t}}{2[E]_t}$$

where $[E]_t$ and $[PLP]_t$ represent the total concentrations of the enzyme and PLP, respectively, Y refers to the intrinsic quenching changes at a PLP concentration, and Y_{max} refers to the fluorescence changes when all enzyme molecules are complexed with coenzyme.

Curve fitting was performed using Origin 8 Pro (OriginLab).

Dynamic Light Scattering Analysis. The dynamic light scattering (DLS) analyses were performed using the Zetasizer Nano S (ZEN1600) instrument (Malvern Instruments) with a constant 90° scattering angle and a 633 nm wavelength laser at 25 °C. The sample volume used for analysis was 0.8 mL at an enzyme concentration of 2 μM in 0.1 M potassium phosphate buffer (pH 7.4), with the addition of 10 mM β-MeSH for redHDC. A total of 100 scans were obtained for each sample, after an equilibration time of 10 min, and all samples were analyzed in triplicate.

Enzyme Activity Assay. The decarboxylase activity was measured by a stopped spectrophotometric assay already used for DOPA decarboxylase and useful for quantifying aromatic amines.[49] HDC (WT or variants, 0.3 μM) was incubated for an appropriate incubation time (a time within which linear product formation is observed) with 1 mM L-His and 10 μM PLP in a final volume of 250 μL in 0.1 M potassium phosphate buffer (pH 7.4), with the addition 1 mM GSH for redHDC. The reaction was then stopped by heating the mixture at 100 °C for 2 min. TNB (1 mL of a 4.3 mM solution) and toluene (1.5 mL) were added, and the extraction of trinitrophenylhistamine was performed at 42 °C for 45 min with continuous shaking. The concentration of the trinitrophenyl derivative in the toluene layer was measured by using a prepared calibration curve of absorbance at 340 nm as a function of trinitrophenyl derivative concentration. The measured ε_M is 11300 M^{-1} cm^{-1}

DOI: 10.1021/acs.biochem.8b00625
Biochemistry 2018, 57, 6336−6348

at 340 nm. The kinetic parameters were determined by incubating the enzyme in the presence of different L-His concentrations (0.025−2 mM) at a saturating PLP concentration, and the obtained data were fitted to the Michaelis−Menten equation using Origin 8 Pro (OriginLab).

Atomic Coordinates and Modeling. Atomic coordinates of human HDC (entry 4E1O[45]) were taken from the Protein Data Bank (PDB)[50] and used as a starting point to model the disulfide bond between the Cys-180 residues of the polypeptide chain. Modeling was done using MODELER, version 9.17,[51] and PyMod.[52] Subsequently, local steepest descent energy minimization in vacuum was performed to relieve local structural strain using GROMACS version 4.0.7[53] in conjunction with the GROMOS53a6 force field. The structural stability of the obtained model was assessed by a number of structure analysis tools. Ramachandran plot calculations, computed with PROCHECK,[54] exhibited optimal stereochemical quality, with 95.3% of the residues in the most favored region and only 0.5% of the residues in the disallowed regions. The energy profile calculated by the Dope score of the model suggests that the obtained disulfide bond is energetically consistent and reliable. Normal mode (NM) analysis of the structure of HDC with reduced Cys-180 residues was performed using the elastic network model (ENM), a fast and simple way to compute the low-frequency normal modes of a macromolecule,[55] as implemented in the *PyANM* tool.[56] The lowest-frequency normal mode was kept and used for visual analysis.

Molecular Dynamics (MD). All simulations have been performed using Gromacs version 2018.2. The structures were centered in cubic boxes with minimum distance of 0.9 nm between each atom of the protein and the box to reduce. The SPC water model[57] was used to solvate the system. The ionic strength was adjusted to make sure all simulations were electrically neutral. MD simulations were performed with periodic boundary conditions in the isothermal−isochoric ensemble (*NVT*), using an integration step of 2 fs at a constant temperature (300 K) using the velocity rescaling algorithm.[58] The particle mesh Ewald method[59] was used to calculate the long-range contribution (reciprocal space) of the electrostatic interactions using a cutoff radius of 1.0 nm. The Gromos53a6 force field[60] was used. Before production runs, all systems were subject to a minimization cycle and thermalization procedure to bring the temperature gradually to 300 K. All runs consisted of at least 100 ns MD simulations in an *NVT* ensemble. MD analysis was performed using Gromacs and was based on the equilibrated part of all simulations, that is, beyond 20 ns. Root-mean-square fluctuations were calculated using the Cα atom deviation with respect to their average position. Trajectories were projected onto selected eigenvectors to show main dominant protein motions. PLP was included in all simulations, and the topology parameter of the Gromos53a6 force field was obtained using the PRODRG server.[61] Figures were generated using the Pymol 2.0 software (The PyMOL Molecular Graphics System, version 2.0, Schrödinger, LLC).

RESULTS AND DISCUSSION

HDC Cys-180 Is the Only Cysteine Residue Not Conserved among HDCs. A multiple-sequence alignment of HDCs from mammals and other sources such as *Gallus*, *Drosophila*, *Danio*, and prokaryotic organisms shows that only one cysteine residue is not conserved among the 11 cysteine residues present in each subunit of the functionally active dimeric human HDC, namely Cys-180 (Figure 1). A further comparison of the sequences of HDCs with those of decarboxylases of group II, in particular with that of human aromatic amino acid decarboxylase, points out that six of the 11 cysteine residues of human HDC are shared, while the remaining four are typical of HDCs. Cys-418, the other cysteine residue replaced with serine in the crystallization papers by Komori and co-workers,[44,45] belongs to the latter group. Interestingly, HDCs from primates (*Gorilla gorilla*, *Pongo abelii*, *Pan paniscus*, *Pan troglodytes*, and many species of the genera *Macaco*) are predicted to have Cys-180, thus dating at least to primates the substitution responsible for the presence of this cysteine residue in the human protein. The fact that Cys-180 is not conserved and, at the same time together with Cys-418, contributes to protein stability[45] raises questions about the role it could play.

Human Wild-Type HDC Exists in an Equilibrium between a Reduced (redHDC) and an Oxidized (oxHDC) Form Controlled by Cys-180. Human HDC has been cloned in pET28a, transformed in BL21 *E. coli*, expressed, and purified with an affinity column as reported in Materials and Methods. The yield is 2−5 mg/L, and the enzyme is pure as evidenced by a single band in an SDS−PAGE gel (Figure S1) and contains 2 mol of PLP per dimer. It has been immediately noted that, depending on the reducing agent concentration, HDC presents one or two bands on a semidenaturing SDS−PAGE gel. The molecular weight of the slow mobility band suggests that it is a dimer, while the fastest band, at ∼56 kDa, corresponds to the monomer (Figure 2A and Figure S2A,B). β-MeSH, DTT, or GSH has been used as a reducing agent, showing in every case the same results. To obtain a fully reduced species, the reductant:protein dimer ratio should be an at least 2000-fold molar excess. A native PAGE performed at increasing GSH concentrations confirms that HDC is present as a dimer (Figure S2C). The dimeric arrangement is also exhibited by size-exclusion chromatography analysis showing that the two species elute at nearly the same volume (62.6 ± 0.1 and 61.8 ± 0.2 mL for redHDC and oxHDC, respectively) (Figure S2D).

The C180S and C418S variant HDCs have been cloned, expressed, and purified to homogeneity as revealed by a single band on an SDS−PAGE gel (data not shown), and both of them bind 2 mol of PLP/dimer. A semidenaturing SDS−PAGE performed under the same conditions as the wild-type method shows that C180S appears as a monomer at any GSH concentration, while C418S exists as oxidized/reduced species in equilibrium depending on the absence or presence of a reducing agent, a behavior strongly ressembling that of the WT (Figure 2B,C).

From these data, it can be inferred that HDC exists in a reduced and oxidized state depending on the presence of a reductant and that Cys-180 appears as a good candidate for an intersubunit disulfide bond of one subunit with the same residue of the neighboring subunit. No other cysteine residue is in fact present within 10 Å of Cys-180. In this regard, it is of interest that a possible role for regulation by the redox state was advanced.[46]

We have then undertaken a spectroscopic characterization to highlight possible differences in physicochemical signals between redHDC and oxHDC.

The Spectroscopic Analyses Reveal That redHDC and oxHDC Display Slight Structural Changes. The absorbance spectra of redHDC (in the presence of 10 mM GSH) and

DOI: 10.1021/acs.biochem.8b00625
Biochemistry 2018, 57, 6336−6348

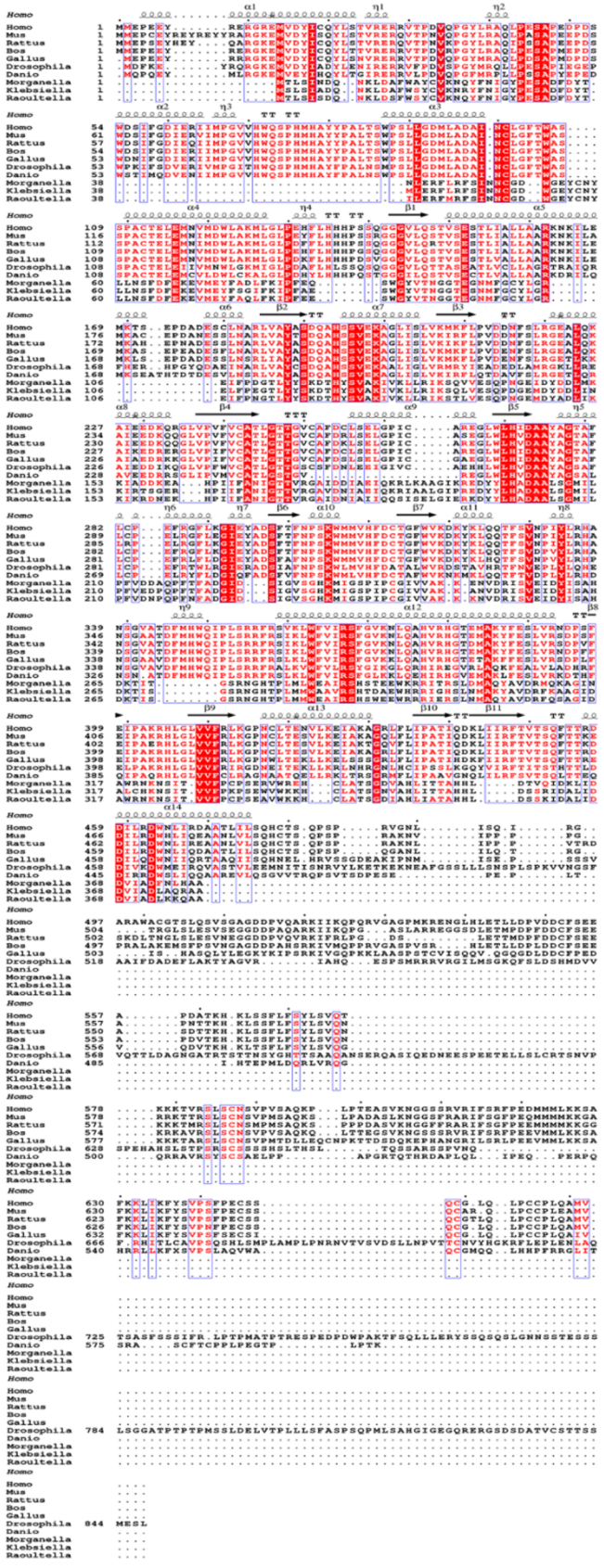

Figure 1. Multiple-sequence alignment of HDCs. Amino acid sequences from various sources were taken from the NCBI Web site (https://www.ncbi.nlm.nih.gov/) and are, in order, *Homo sapiens*, *Mus musculus*, *Rattus norvegicus*, *Bos taurus*, *Gallus gallus*, *Danio rerio*, *Drosophila melanogaster*, *Morganella morganii*, *Klebsiella aerogenes*, and *Raoultella planticola*. The one-letter amino acid code is used. Dashes represent insertions and deletions. Invariant positions are boxed in red. Similar residues are written in red characters. Homologous regions are boxed in light blue. The secondary structures of human HDC (PDB entry 4E1O) are reported in the first line of each block. α-Helices and β-strands are rendered as squiggles and arrows, respectively. ESPript (http://espript.ibcp.fr) was used to render this figure starting from a Clustal Omega alignment (http://www.ebi.ac.uk/Tools/msa/clustalo/).

Figure 1. continued

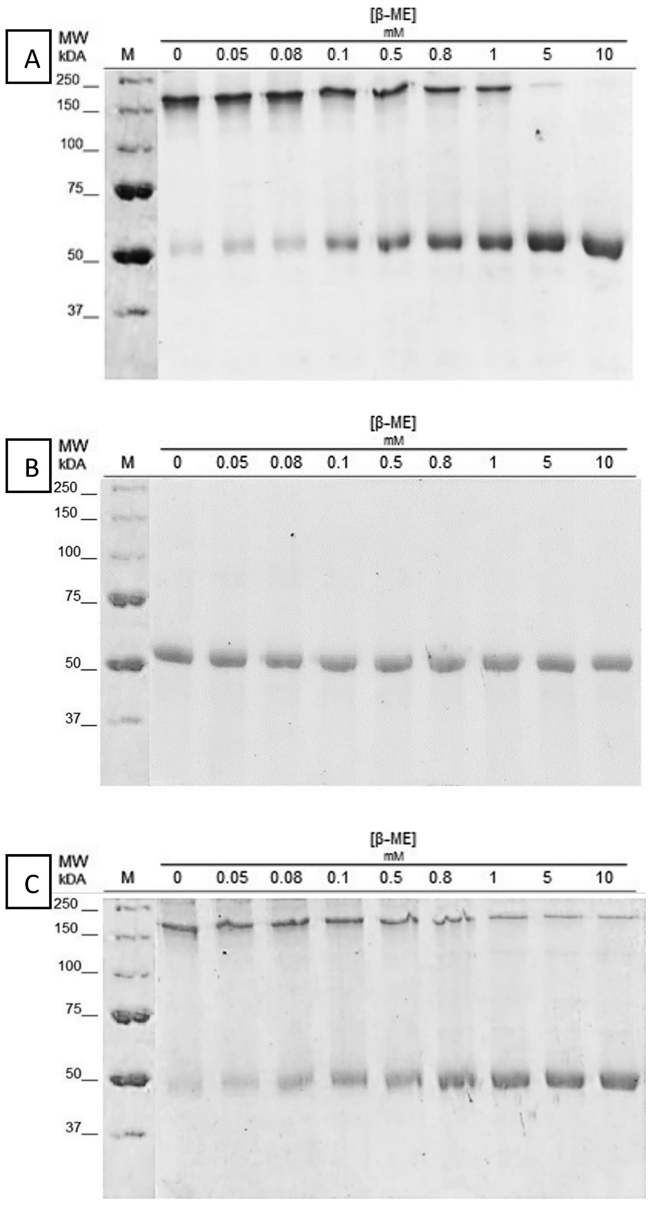

Figure 2. Semidenaturing 10% SDS−PAGE analysis of (A) WT, (B) C180S, and (C) C418S HDC with increasing β-MeSH concentrations. Five micrograms of (A) WT, (B) C180S, or (C) C418S HDC was incubated for 1 h at room temperature with the corresponding β-MeSH concentration in 0.1 M potassium phosphate buffer (pH 7.4). M, molecular weight marker.

DOI: 10.1021/acs.biochem.8b00625
Biochemistry 2018, 57, 6336−6348

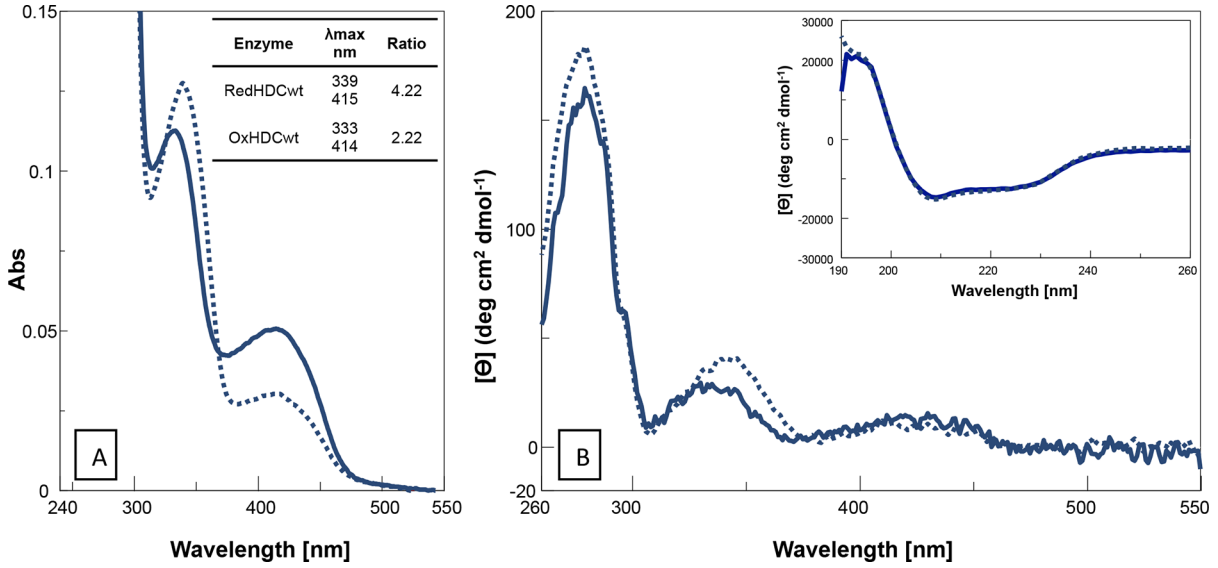

Figure 3. Spectroscopic characterization of WT HDC. (A) Absorbance and (B) near-UV and visible dichroic spectra of redHDC (dotted line) and oxHDC (straight line) were recorded at 1 mg/mL in 0.1 M potassium phosphate buffer (pH 7.4) without or with 20 mM GSH. The absorbance maximum wavelengths are reported in inset A. Inset B shows the far-UV spectra measured at 0.1 mg/mL in 0.1 M potassium phosphate buffer (pH 7.4) without or with 20 mM GSH.

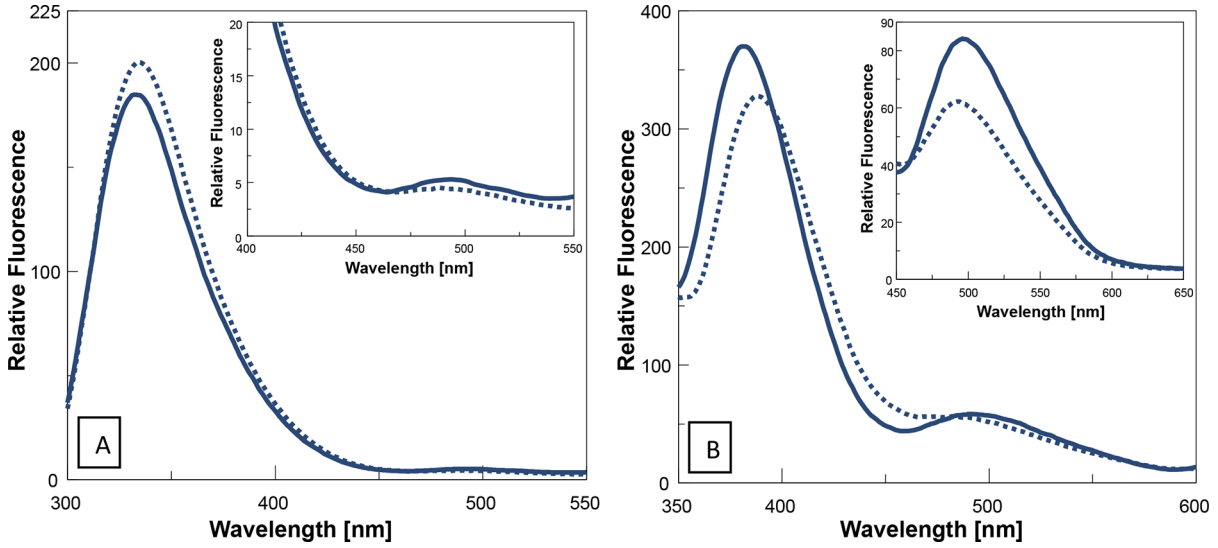

Figure 4. Emission fluorescence spectra of WT HDC. (A) Intrinsic fluorescence emission spectra of redHDC (dotted line) and oxHDC (straight line) after excitation at 280 nm. Spectra were recorded at 0.1 mg/mL in 0.1 M potassium phosphate buffer (pH 7.4) without or with 20 mM GSH. Inset A is a close-up of the fluorescence emission maximum in the 490 nm region. (B) Cofactor fluorescence emission spectra after excitation at 339 and 333 nm of redHDC (dotted line) and oxHDC (straight line), respectively, at 1 mg/mL in 0.1 M potassium phosphate buffer (pH 7.4) without or with 20 mM GSH. Inset B shows cofactor fluorescence emission spectra after excitation at 415 and 414 nm for redHDC and oxHDC, respectively.

oxHDC measured in 0.1 M potassium phosphate buffer (pH 7.4) show, in addition to the 280 nm band that can be attributed to the aromatic amino acids, the presence of two bands in the visible region with maxima at 339 and 415 nm for redHDC and at 333 and 414 nm for oxHDC. Besides the slight differences in wavelength maxima, the equilibrium between these two species is altered with 339 nm/415 nm and 333 nm/414 nm ratios of 4.22 and 2.22, respectively (Figure 3A). These species can be reasonably attributed to the enolimine and ketoenamine tautomers of the internal aldimine between PLP and Lys-304, and it can be thus suggested that the PLP microenvironment is altered in the two redox states of the enzyme.

The dichroic signals in the visible region reflect a similar coenzyme behavior displayed in absorbance, and in addition, the near-UV bands show a slight difference between redHDC and oxHDC (Figure 3B). The optical activities (millidegrees per absorbance unit at a fixed wavelength at the same protein concentration) for the enolimine and ketoenamine are 30.25 and 48.18 for redHDC and 24.53 and 20.12 for oxHDC, respectively, supporting the presence of an altered PLP microenvironment. Finally, the far-UV CD spectra are superimposable, indicative of a similar secondary structure content (inset Figure 3B).

Fluorescence data essentially provide the same information about the spectrophotometric and spectropolarimetric experi-

DOI: 10.1021/acs.biochem.8b00625
Biochemistry 2018, 57, 6336−6348

Table 1. Kinetic Parameters, Apparent Equilibrium Dissociation Constants for PLP, and Melting Temperatures of WT HDC and Its Variants[a]

enzyme	k_{cat} (s^{-1})	K_m (mM)	k_{cat}/K_m (s^{-1} mM^{-1})	$K_{D(PLP)}$ (nM)	T_m (°C)
redHDC WT	0.70 ± 0.02	0.064 ± 0.008	10.9 ± 1.4	32.8 ± 0.4	62.78 ± 0.06
oxHDC WT	1.10 ± 0.05	0.033 ± 0.006	33.3 ± 6.2	44.0 ± 0.3	65.97 ± 0.02
redHDC C180S	0.60 ± 0.02	0.057 ± 0.008	10.5 ± 1.5	–	–
oxHDC C180S	0.72 ± 0.02	0.062 ± 0.007	11.6 ± 1.3	30.5 ± 0.2	62.68 ± 0.04
redHDC C418S	0.74 ± 0.04	0.06 ± 0.01	12.3 ± 2.2	–	–
oxHDC C418S	1.05 ± 0.03	0.042 ± 0.007	25.0 ± 4.2	43.1 ± 0.2	65.49 ± 0.04

[a]From 0.05 to 2 mM L-His reacted with 0.075 nmol of each HDC species for 10 min in 250 μL of 0.1 M potassium phosphate buffer (pH 7.4) without or with 1 mM GSH. Dissociation constants for PLP were calculated from the measured enzyme intrinsic fluorescence quenching with an increasing concentration of the coenzyme as reported in Materials and Methods. Melting temperatures were calculated by dichroic changes at 222 nm as reported in Materials and Methods.

ments. Intrinsic fluorescence spectra recorded upon excitation at 280 nm show an emission band centered at 335 nm for redHDC and 333 nm for oxHDC with different relative intensities (207 vs 185). A red-shifted broad shoulder is present in oxHDC, emitting at 494 nm with a relative intensity of ∼5 for oxHDC suggesting an energy transfer and thus a different positioning of PLP with respect to aromatic amino acids. (Figure 4A). Cofactor emission fluorescence upon excitation of the enolimine tautomer at 339 and 333 nm for redHDC and oxHDC, respectively, shows emissions at 386 and 485 nm for redHDC and 381 and 491 nm for oxHDC. When the ketoenamine tautomer of the two species was excited at 415 nm (redHDC) and 414 nm (oxHDC), a band centered at 485 nm and at 496 nm was recorded (Figure 4B and inset). Altogether, these fluorescence results witnessed a modest change in the cofactor environment and in the interconnections among PLP and the surrounding residues in the two HDC forms.

These spectroscopic data suggest that redHDC and oxHDC present slight differences in all measured signals indicative of subtle structural changes. The optical activity values are also an expression of modest coenzyme-to-aromatic amino acid side chain microenvironment alterations. We thus investigated if these changes are related to the catalytic activity and to the stability of the enzyme.

OxHDC Is More Stable and More Active Than redHDC. The thermostability of the two enzymatic forms has been assessed by monitoring the dichroic signal at 222 nm with an increase in temperature from 25 to 90 °C at a rate of 1.5 °C/min. While the T_m of redHDC is 62.78 ± 0.06 °C, that of oxHDC is 65.97 ± 0.02 °C (Table 1), thus suggesting that the oxidized form of HDC is slightly more stable than the reduced form. DLS analyses show that the hydrodynamic diameter of redHDC is 9.90 ± 0.08 nm while that of oxHDC is 11.60 ± 0.04 nm. In addition, it should be pointed out that the theoretical diameter[62] is predicted to be 8 nm calculated on the basis of the determined structure of the double-mutant form (C180S/C418S)[45] that ressembles redHDC (see below).

Kinetic parameters of redHDC and oxHDC (Table 1) show that the catalytic efficiency of the oxidized form is 3-fold higher than that of the reduced form, and this is driven by the combination of both the 1.6-fold increase in k_{cat} and the 2-fold decrease in K_m. The apparent equilibrium dissociation constant for the coenzyme is quite similar, i.e., 33 nM for redHDC versus 44 nM for oxHDC.

Interestingly, the oxidized species is more active and more stable than the reduced form. Thus, we looked for a possible molecular cause as the basis for this different behavior.

The Cys-180 Redox State Is Responsible for a Structural Transition Affecting the C-Terminal Domain Reorientation and Could Be Responsible for Active Site Alterations. The availability of the recently determined crystal structure of human HDC (PDB entry 4E1O)[45] gave us the unprecedented opportunity to gain insights into the role of the intersubunit disulfide bridge of Cys-180 in controlling the structural rearrangement of human HDC and its catalysis. However, because Cys-180 was replaced with serine to prevent unwanted oligomerization,[45] we started our analysis by modeling the position of Cys-180 and the disulfide bridge in their reduced and oxidized forms, respectively (Figure 5). In

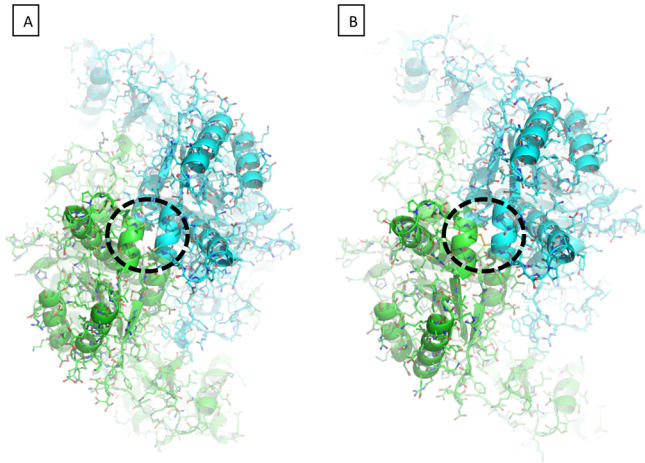

Figure 5. Modeling of WT HDC in its (A) reduced and (B) oxidized states. The two HDC subunits are represented as green and cyan cartoons and sticks, respectively. The dashed black circle indicates the position of the two Cys-180 residues.

their oxidized state, the two Cys-180 residues of each monomer are in a distance range (≈2.5 Å) that is compatible with the formation of an intersubunit disulfide bond. The latter, in turn, could be responsible for a "locking" of the two α-helices spanning residues 178−184 and comprising Cys-180, which face each other at the dimer interface. On the contrary, in the absence of the covalent bond between the two Cys residues, the two α-helices of redHDC are expected to freely move, because no other close contact is present. Indeed, an inspection of the physicochemical properties of the dimer interfaces of HDC and its close homologue aromatic amino acid decarboxylase (PDB entry 1JS3; root-mean-square deviation of ≈0.8 Å) in this region revealed that both enzymes (and other group II decarboxylases, e.g., glutamate decarbox-

DOI: 10.1021/acs.biochem.8b00625
Biochemistry 2018, 57, 6336−6348

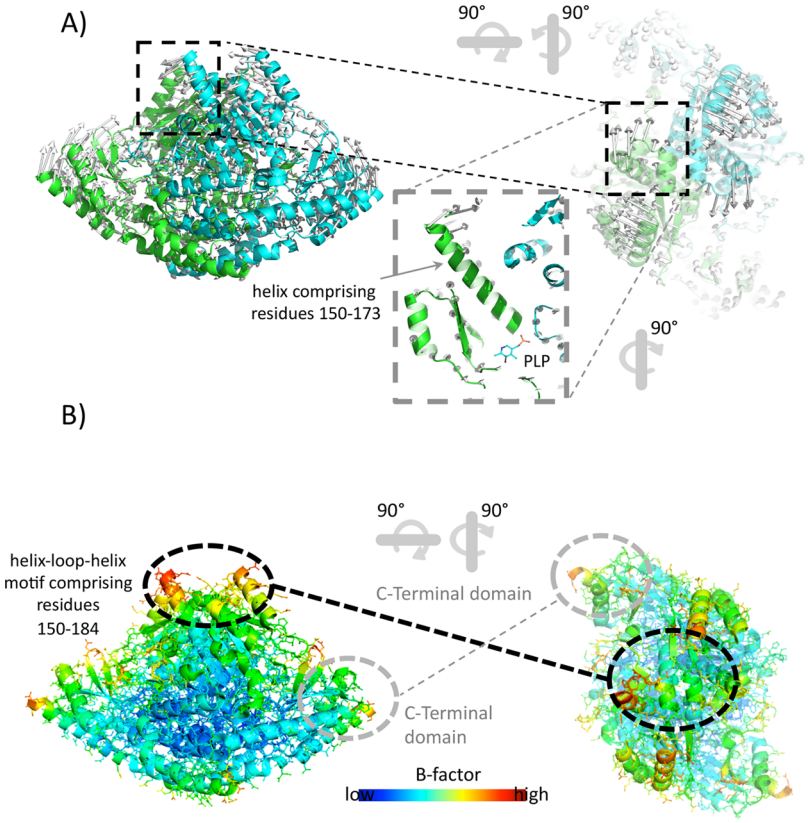

Figure 6. (A) NM analysis and (B) *B*-factors of WT HDC. (A) The two HDC subunits are represented as green and cyan cartoons. The gray arrows are trajectory vectors of the NM analysis. Each arrow's direction points in the direction where the residue will move, and each arrow's length indicates the moving scale for each residue. (B) Experimentally derived *B*-factor values, indicating local structural fluctuations, are in good agreement with NM analysis data.

ylase 65) share solvation properties that favor a partial opening.[4] Therefore, we reasoned that the presence or absence of a disulfide bridge between the Cys-180 residues of the HDC subunits[63] could lead to a subtle structural change, which in turn could be transmitted to the adjacent long α-helix of residues 150−173. The latter directly connects the α-helix of residues 178−184 to the active site of HDC. To test this hypothesis, we thus performed an all-Cα atom normal mode (NM) analysis of redHDC to investigate the conformational transitions of HDC. Indeed, it is well-known that NM analysis can probe large-amplitude motions that are often inaccessible to other atomistic simulations.[64] Moreover, NM analysis is insensitive to the presence of small molecules, such as PLP, in the context of large protein systems.

The NM symmetric rigid-body motions of the PLP binding and C-terminal domains of HDC, described by the lowest-frequency NM, are shown in Figure 6. According to NM analysis of human HDC, the magnitude of the structural fluctuations was highest at the C-terminal domains (CTDs) and at the flexible α-helix of residues 150−173 connecting the position of the α-helix residues of 178−184 and PLP (Figure 6A). Notably, HDC displayed a symmetric profile of fluctuations at the CTDs, as already observed in the close homologue glutamate decarboxylase.[65]

The obtained results of the NM simulations of HDC therefore suggested a tight coupling between the helix−loop−helix motif comprising residues 150−184 and the C-terminal domain of HDC, which in turn could drive a structural rearrangement of the two domains and of the catalytic loop lying at the interface between the N- and C-terminal domains of HDC. Interestingly, the conformation of the 150−184 helix−loop−helix motif comprises both Cys-180 and residues of the PLP binding cleft, directly linking therefore the redox state of Cys-180 to the position and stabilization of PLP. Most notably, the NM data corroborate the findings from the analysis of the structural flexibility of human HDC inferred from crystallographic *B*-factors[45] (Figure 6B), which can be used to assess the local dynamics of protein structures.[66]

To further corroborate the results obtained with coarse-grained NM analysis, MD simulations were performed to investigate the atomistic fluctuations of the PLP binding site as a function of the redox state of Cys-180. All simulations were 100 ns long, and all the analyses have been performed on the equilibrated part of all trajectories, i.e., after simulation for 20 ns. Insertion of a disulfide bridge between the Cys-180 residues of the two HDC subunits causes a general decrease in protein flexibility as measured by the root-mean-square fluctuation (RMSF) (see Materials and Methods). Figure 7 shows a comparison between the RMSF of the oxidized and reduced HDC for each monomer. As the plot shows, the introduction of a constraint in the S−S interchain disulfide bridge of Cys-180 confers upon oxHDC a generally higher rigidity compared to that of redHDC. From a structural viewpoint, the main RMSF differences between the oxidized and reduced HDC were localized on the helix encompassing residues 150−170.

We have checked the effect of conformational dynamics of helix 150−170 and all residues facing the active site on PLP mobility. In particular, we compared the flexibility (RMSF) of PLP atoms in the two HDC simulations and found that the RMSF in oxHDC was systematically lower than the

DOI: 10.1021/acs.biochem.8b00625
Biochemistry 2018, 57, 6336−6348

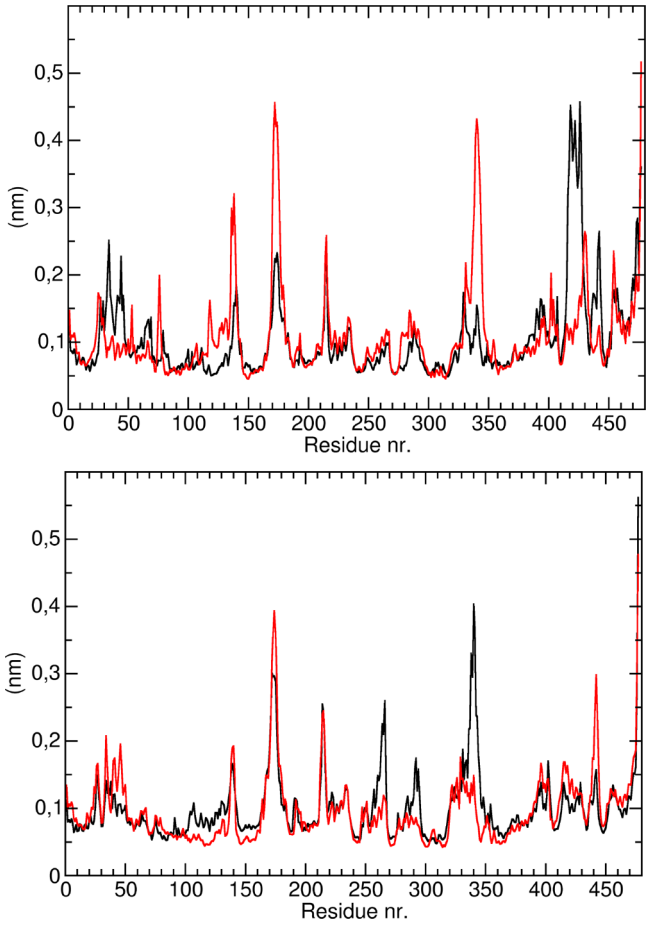

Figure 7. MD analysis of WT HDC in its reduced and oxidized states. Root-mean-square fluctuation of oxHDC (black) and redHDC (red) as a function of residue number for chain 1 (top) and chain 2 (bottom).

corresponding values for the PLP in the redHDC simulation (Figure 8), and this suggests that the disulfide bridge in Cys-180 affects the conformational mobility of the PLP moiety in its pocket by decreasing its conformational mobility

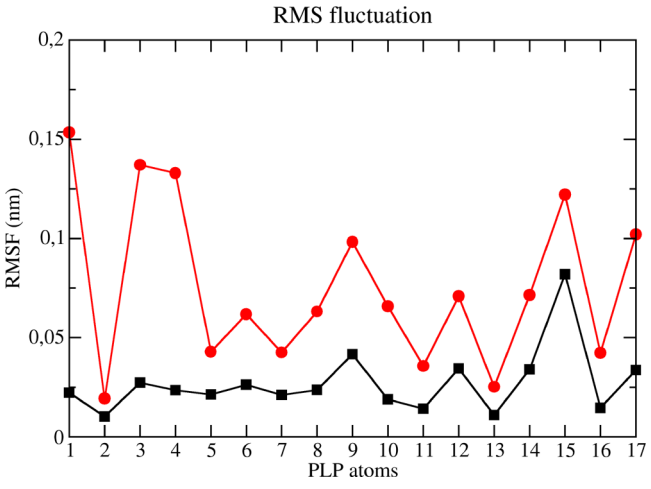

Figure 8. RMSF of PLP in oxNHD and redHDC. Root-mean-square fluctuation of PLP atoms with respect to their average position along the MD trajectories for the oxHDC simulation (black) and the redHDC simulation (red).

Further confirmation of this finding came from the essential dynamics analysis on the active site subset residues. This analysis showed that the overall fluctuation of the Cα atoms of active site residues (as calculated from the trace of the covariance matrix of positional atomic fluctuations of Cα atoms) was lower in oxHDC (0.32821 nm^2) than in redHDC (0.6821 nm^2). This confirms that the covalent bond in the Cys-Cys pair at position 180 confers a higher rigidity in the active site area.

In more detail, a ribbon representation of the HDC structure with a thickness and color scheme proportional to the difference between the RMSF of oxHDC and that of redHDC is reported in Figure 9 and a close-up inset. As shown, the N-

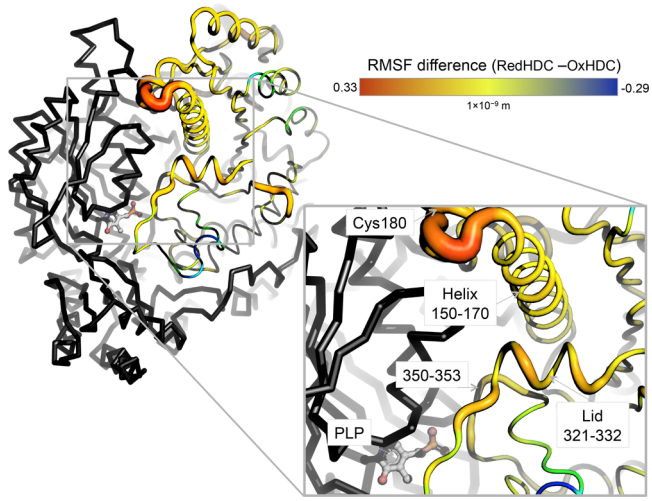

Figure 9. Difference between the RMSF of redHDC and that of oxHDC. Ribbon representation of the HDC structure with the difference between RMSF of redHDC and that of oxHDC mapped onto monomer A (rainbow scale going from 0.33 to −0.29 nm). Monomer B is colored gray. As shown in the inset, the N-terminal end of the redHDC is more flexible than its oxidized counterpart. This higher flexibility affects in turn the active site lid of HDC (residues 321−332) as well as the loop spanning residues 350−353.

terminal end of the redHDC is more flexible than its oxidized counterpart. This region is within the range of contact of either the active site lid of HDC (corresponding to residues 321−332) or the loop spanning residues 350−353 (comprising residues interacting with the phosphate moiety of PLP), which also show a higher flexibility in redHDC than in oxHDC. We suggest that this higher flexibility affects the pocket size hosting the PL, which in turn is more likely to have greater conformational freedom in redHDC than in oxHDC.

These bioinformatics data are in agreement with the slight differences evidenced by the spectroscopic analyses as well as by the kinetic features and by the protein thermal stability data between redHDC and oxHDC and suggest that oxidation could lead to a movement triggering subtle alterations at the active site. The stability could be due to the additional sulfur−sulfur covalent bond that causes a rearrangement of the overall protein structure determining an increase in the hydrodynamic diameter, as witnessed by DLS measurements. We then evaluated the functional properties of single variants C180S and C418S to gain insight into their specific contribution.

C180S Presents Features Similar to Those of redHDC, while C418S Is Sensitive to Reductants. The analyses of the absorbance, dichroic, and fluorescence properties of C180S

DOI: 10.1021/acs.biochem.8b00625
Biochemistry 2018, 57, 6336−6348

and C418S variants show that these species exhibit slight structural changes and no gross alterations in cofactor binding microenvironment (data not shown). We then focused our attention on the oxidized species of both variants because oxC180S should not form a disulfide-bound species and oxC418S should be less prone to aggregate. Interestingly, measurements of both the hydrodynamic diameter and of the thermostability show that oxC180S behaves like redHDC with a diameter of 10.56 ± 0.04 nm and a T_m value of 62.68 ± 0.04 °C, while oxC418S has a diameter of 11.6 ± 0.6 nm and a T_m of 65.49 ± 0.04 °C behaving like oxHDC. In addition, the functional features show that the catalytic efficiencies of both redC180S and oxC180S are almost identical to that of the redHDC while those of both redC418S and oxC418S are similar to those of redHDC and oxHDC, respectively (Table 1). No differences in PLP equilibrium binding constant are measured (Table 1).

Because it has been claimed that oxHDC tends to aggregate and for this reason the structure of the enzyme has been determined in the C180S/C418S double-mutant species,[45] we addressed this by concentrating 500 μL of 10 μM oxHDC, oxC180S, and oxC418S to 25 μL in an Amicon ultra device. The supernatants and the pellets (if present) were then run on an SDS gel under reducing and nonreducing conditions. We determined that a pellet was present in oxHDC and oxC180S solutions while no precipitation occurs with the oxC418S variant. Here, it follows that Cys-418 concurs in structural stability, although the molecular reason for the aggregation of oxHDC needs to be further investigated.

CONCLUSIONS

Even if human HDC belongs to the well-known group of the PLP-dependent α-decarboxylases, it is a poorly characterized protein, mainly because of its intrinsic instability. The only determined structure is that of the human protein engineered with two cysteine-for-serine substitutions (C180S and C418S) to increase its stability.[45] Here, for the first time, we provide evidence for the existence of an equilibrium between a reduced and an oxidized form of human HDC, the latter being slightly more active and stable than the former. We also identify Cys-180 as the residue that is responsible for this redox equilibrium. Bioinformatics analyses suggest a higher stability and active site alteration determined by the disulfide bridge in the oxHDC form. On this basis, human HDC may join the short list of PLP enzymes that present redox sensitive cysteine residues.[67−76] Interestingly, among PLP enzymes, the cysteine switch appears to be a peculiar and unique feature of human HDC. It has been documented that cysteine residues in proteins could play a role in the response to altered redox conditions in cancer.[77,78] At present, it is not easy to envisage a physiological role of this redox sensor in HDC. However, when the fact that the environment of a cell is highly reduced is taken into account, it is reasonable to suggest that HDC is mainly reduced under physiological conditions. However, in cancer cells, where redox conditions are altered, the highly oxidizing conditions could favor the more active and stable oxHDC. With this view in mind, it is worth mentioning that high histamine levels have been reported in cholangiocarcinoma, and the involvement of HDC in tumor progression was thus suggested.[35] Our results suggest that, under redox-altered conditions, the prevalence of oxHDC, which is more active and more stable because of the presence of an additional disulfide bridge involving Cys-180, could therefore lead to an increased level of production of histamine, which makes the pathological state worse. In this regard, the development of specific inhibitors directed toward oxHDC is highly desirable.

ASSOCIATED CONTENT

Supporting Information

The Supporting Information is available free of charge on the ACS Publications website at DOI: 10.1021/acs.biochem.8b00625.

SDS−PAGEs of the various steps of purification and the sensitivity to reducing agents (GSH, DTT, and β-MeSH) as well as size-exclusion chromatography analyses (PDF)

AUTHOR INFORMATION

Corresponding Authors

*Department of Neuroscience, Biomedicine and Movement, University of Verona, Strada Le Grazie, 8, 37134 Verona, Italy. Telephone: +39-0458027671. Fax: +39-0458027170. E-mail: mita.bertoldi@univr.it.

*Department of Biochemical Sciences "A. Rossi Fanelli", University "La Sapienza", Rome, P.zale A. Moro 5, Roma, Italy. Telephone: +39-0649917700. Fax: +39-0649917566. E-mail: alessandro.paiardini@uniroma1.it.

ORCID

Mariarita Bertoldi: 0000-0002-2337-9928

Funding

This work was supported by Grant FUR2017 (University of Verona) to M.B. and by AIRC Associazione Italiana Ricerca sul Cancro MFAG2017-Project Code 20447 and grants from Sapienza University of Rome, Italy (C26A149EC4), to A.P.

Notes

The authors declare no competing financial interest.

ACKNOWLEDGMENTS

The authors thank Dr. Alessandra Astegno (Department of Biotechnology, University of Verona) for the help with the native PAGE experiment.

ABBREVIATIONS

WT, wild-type; PLP, pyridoxal 5′-phosphate; HDC, histidine decarboxylase; oxHDC, oxidized HDC; redHDC, reduced HDC; DTT, dithiothreitol; β-MeSH, β-mercaptoethanol; GSH, glutathione; MD, molecular dynamics.

REFERENCES

(1) Medina, M. A., Quesada, A. R., Nunez de Castro, I., and Sanchez-Jimenez, F. (1999) Histamine, polyamines, and cancer. *Biochem. Pharmacol. 57*, 1341−1344.

(2) Ohtsu, H. (2010) Histamine synthesis and lessons learned from histidine decarboxylase deficient mice. *Adv. Exp. Med. Biol. 709*, 21−31.

(3) Panula, P., and Nuutinen, S. (2013) The histaminergic network in the brain: basic organization and role in disease. *Nat. Rev. Neurosci. 14*, 472−487.

(4) Paiardini, A., Giardina, G., Rossignoli, G., Voltattorni, C. B., and Bertoldi, M. (2017) New Insights Emerging from Recent Investigations on Human Group II Pyridoxal 5′-Phosphate Decarboxylases. *Curr. Med. Chem. 24*, 226−244.

(5) Guirard, B. M., Tanase, S., and Snell, E. E. (1984) Pyridoxal-P dependent bacterial histidine decarboxylase. *Prog. Clin. Biol. Res. 144A*, 235−244.

DOI: 10.1021/acs.biochem.8b00625
Biochemistry 2018, 57, 6336−6348

(6) Tanase, S., Guirard, B. M., and Snell, E. E. (1985) Purification and properties of a pyridoxal 5′-phosphate-dependent histidine decarboxylase from Morganella morganii AM-15. *J. Biol. Chem. 260*, 6738−6746.
(7) Hayashi, H., Tanase, S., and Snell, E. E. (1986) Pyridoxal 5′-phosphate-dependent histidine decarboxylase. Inactivation by alpha-fluoromethylhistidine and comparative sequences at the inhibitor- and coenzyme-binding sites. *J. Biol. Chem. 261*, 11003−11009.
(8) Snell, E. E., and Guirard, B. M. (1986) Pyridoxal phosphate-dependent histidine decarboxylase from Morganella AM-15. *Methods Enzymol. 122*, 139−143.
(9) Vaaler, G. L., Brasch, M. A., and Snell, E. E. (1986) Pyridoxal 5′-phosphate-dependent histidine decarboxylase. Nucleotide sequence of the hdc gene and the corresponding amino acid sequence. *J. Biol. Chem. 261*, 11010−11014.
(10) Vaaler, G. L., and Snell, E. E. (1989) Pyridoxal 5′-phosphate dependent histidine decarboxylase: overproduction, purification, biosynthesis of soluble site-directed mutant proteins, and replacement of conserved residues. *Biochemistry 28*, 7306−7313.
(11) Bhattacharjee, M. K., and Snell, E. E. (1990) Pyridoxal 5′-phosphate-dependent histidine decarboxylase. Mechanism of inactivation by alpha-fluoromethylhistidine. *J. Biol. Chem. 265*, 6664−6668.
(12) Tahanejad, F. S., and Naderi-Manesh, H. (2000) Quantum mechanical study of the intermediates formed following the reaction of the histidine decarboxylase's substrate and inhibitors with coenzyme. *Eur. J. Med. Chem. 35*, 283−289.
(13) Kim, D. H., Kim, K. B., Cho, J. Y., and Ahn, D. H. (2014) Inhibitory effects of brown algae extracts on histamine production in mackerel muscle via inhibition of growth and histidine decarboxylase activity of Morganella morganii. *J. Microbiol. Biotechnol. 24*, 465−474.
(14) Nitta, Y., Yasukata, F., Kitamoto, N., Ito, M., Sakaue, M., Kikuzaki, H., and Ueno, H. (2016) Inhibition of Morganella morganii Histidine Decarboxylase Activity and Histamine Accumulation in Mackerel Muscle Derived from Filipendula ulumaria Extracts. *J. Food Prot. 79*, 463−467.
(15) Wauters, G., Avesani, V., Charlier, J., Janssens, M., and Delmee, M. (2004) Histidine decarboxylase in Enterobacteriaceae revisited. *J. Clin Microbiol 42*, 5923−5924.
(16) Medina, M. A., Urdiales, J. L., Rodriguez-Caso, C., Ramirez, F. J., and Sanchez-Jimenez, F. (2003) Biogenic amines and polyamines: similar biochemistry for different physiological missions and biomedical applications. *Crit. Rev. Biochem. Mol. Biol. 38*, 23−59.
(17) Medina, M. A., Correa-Fiz, F., Rodriguez-Caso, C., and Sanchez-Jimenez, F. (2005) A comprehensive view of polyamine and histamine metabolism to the light of new technologies. *J. Cell. Mol. Med. 9*, 854−864.
(18) Joseph, D. R., Sullivan, P. M., Wang, Y. M., Kozak, C., Fenstermacher, D. A., Behrendsen, M. E., and Zahnow, C. A. (1990) Characterization and expression of the complementary DNA encoding rat histidine decarboxylase. *Proc. Natl. Acad. Sci. U. S. A. 87*, 733−737.
(19) Yamamoto, J., Yatsunami, K., Ohmori, E., Sugimoto, Y., Fukui, T., Katayama, T., and Ichikawa, A. (1990) cDNA-derived amino acid sequence of L-histidine decarboxylase from mouse mastocytoma P-815 cells. *FEBS Lett. 276*, 214−218.
(20) Taguchi, Y., Watanabe, T., Kubota, H., Hayashi, H., and Wada, H. (1984) Purification of histidine decarboxylase from the liver of fetal rats and its immunochemical and immunohistochemical characterization. *J. Biol. Chem. 259*, 5214−5221.
(21) Engel, N., Olmo, M. T., Coleman, C. S., Medina, M. A., Pegg, A. E., and Sanchez-Jimenez, F. (1996) Experimental evidence for structure-activity features in common between mammalian histidine decarboxylase and ornithine decarboxylase. *Biochem. J. 320* (2), 365−368.
(22) Viguera, E., Trelles, O., Urdiales, J. L., Mates, J. M., and Sanchez-Jimenez, F. (1994) Mammalian L-amino acid decarboxylases producing 1,4-diamines: analogies among differences. *Trends Biochem. Sci. 19*, 318−319.
(23) Olmo, M. T., Urdiales, J. L., Pegg, A. E., Medina, M. A., and Sanchez-Jimenez, F. (2000) In vitro study of proteolytic degradation of rat histidine decarboxylase. *Eur. J. Biochem. 267*, 1527−1531.
(24) Ohmori, E., Fukui, T., Imanishi, N., Yatsunami, K., and Ichikawa, A. (1990) Purification and characterization of l-histidine decarboxylase from mouse mastocytoma P-815 cells. *J. Biochem. 107*, 834−839.
(25) Dartsch, C., Chen, D., Hakanson, R., and Persson, L. (1999) Histidine decarboxylase in rat stomach ECL cells: relationship between enzyme activity and different molecular forms. *Regul. Pept. 81*, 41−48.
(26) Fleming, J. V., and Wang, T. C. (2000) Amino- and carboxy-terminal PEST domains mediate gastrin stabilization of rat L-histidine decarboxylase isoforms. *Mol. Cell. Biol. 20*, 4932−4947.
(27) Fajardo, I., Urdiales, J. L., Medina, M. A., and Sanchez-Jimenez, F. (2001) Effects of phorbol ester and dexamethasone treatment on histidine decarboxylase and ornithine decarboxylase in basophilic cells. *Biochem. Pharmacol. 61*, 1101−1106.
(28) Fleming, J. V., and Wang, T. C. (2003) The production of 53−55-kDa isoforms is not required for rat L-histidine decarboxylase activity. *J. Biol. Chem. 278*, 686−694.
(29) Olmo, M. T., Rodriguez-Agudo, D., Medina, M. A., and Sanchez-Jimenez, F. (1999) The pest regions containing C-termini of mammalian ornithine decarboxylase and histidine decarboxylase play different roles in protein degradation. *Biochem. Biophys. Res. Commun. 257*, 269−272.
(30) Rodriguez-Agudo, D., Olmo, M. T., Sanchez-Jimenez, F., and Medina, M. A. (2000) Rat histidine decarboxylase is a substrate for m-calpain in vitro. *Biochem. Biophys. Res. Commun. 271*, 777−781.
(31) Furuta, K., Nakayama, K., Sugimoto, Y., Ichikawa, A., and Tanaka, S. (2007) Activation of histidine decarboxylase through post-translational cleavage by caspase-9 in a mouse mastocytoma P-815. *J. Biol. Chem. 282*, 13438−13446.
(32) Gores, G. J. (2003) Cholangiocarcinoma: current concepts and insights. *Hepatology 37*, 961−969.
(33) Sirica, A. E. (2005) Cholangiocarcinoma: molecular targeting strategies for chemoprevention and therapy. *Hepatology 41*, 5−15.
(34) Aljiffry, M., Walsh, M. J., and Molinari, M. (2009) Advances in diagnosis, treatment and palliation of cholangiocarcinoma: 1990−2009. *World J. Gastroenterol 15*, 4240−4262.
(35) Francis, H., DeMorrow, S., Venter, J., Onori, P., White, M., Gaudio, E., Francis, T., Greene, J. F., Jr., Tran, S., Meininger, C. J., and Alpini, G. (2012) Inhibition of histidine decarboxylase ablates the autocrine tumorigenic effects of histamine in human cholangiocarcinoma. *Gut 61*, 753−764.
(36) Johnson, C., Huynh, V., Hargrove, L., Kennedy, L., Graf-Eaton, A., Owens, J., Trzeciakowski, J. P., Hodges, K., DeMorrow, S., Han, Y., Wong, L., Alpini, G., and Francis, H. (2016) Inhibition of Mast Cell-Derived Histamine Decreases Human Cholangiocarcinoma Growth and Differentiation via c-Kit/Stem Cell Factor-Dependent Signaling. *Am. J. Pathol. 186*, 123−133.
(37) Rodriguez-Caso, C., Rodriguez-Agudo, D., Moya-Garcia, A. A., Fajardo, I., Medina, M. A., Subramaniam, V., and Sanchez-Jimenez, F. (2003) Local changes in the catalytic site of mammalian histidine decarboxylase can affect its global conformation and stability. *Eur. J. Biochem. 270*, 4376−4387.
(38) Rodriguez-Caso, C., Rodriguez-Agudo, D., Sanchez-Jimenez, F., and Medina, M. A. (2003) Green tea epigallocatechin-3-gallate is an inhibitor of mammalian histidine decarboxylase. *Cell. Mol. Life Sci. 60*, 1760−1763.
(39) Castro-Oropeza, R., Pino-Angeles, A., Khomutov, M. A., Urdiales, J. L., Moya-Garcia, A. A., Vepsalainen, J., Persson, L., Sarabia, F., Khomutov, A., and Sanchez-Jimenez, F. (2014) Aminooxy analog of histamine is an efficient inhibitor of mammalian L-histidine decarboxylase: combined in silico and experimental evidence. *Amino Acids 46*, 621−631.
(40) Ercan-Sencicek, A. G., Stillman, A. A., Ghosh, A. K., Bilguvar, K., O'Roak, B. J., Mason, C. E., Abbott, T., Gupta, A., King, R. A., Pauls, D. L., Tischfield, J. A., Heiman, G. A., Singer, H. S., Gilbert, D.

DOI: 10.1021/acs.biochem.8b00625
Biochemistry 2018, 57, 6336−6348

L., Hoekstra, P. J., Morgan, T. M., Loring, E., Yasuno, K., Fernandez, T., Sanders, S., Louvi, A., Cho, J. H., Mane, S., Colangelo, C. M., Biederer, T., Lifton, R. P., Gunel, M., and State, M. W. (2010) L-histidine decarboxylase and Tourette's syndrome. *N. Engl. J. Med. 362*, 1901−1908.
(41) Castellan Baldan, L., Williams, K. A., Gallezot, J. D., Pogorelov, V., Rapanelli, M., Crowley, M., Anderson, G. M., Loring, E., Gorczyca, R., Billingslea, E., Wasylink, S., Panza, K. E., Ercan-Sencicek, A. G., Krusong, K., Leventhal, B. L., Ohtsu, H., Bloch, M. H., Hughes, Z. A., Krystal, J. H., Mayes, L., de Araujo, I., Ding, Y. S., State, M. W., and Pittenger, C. (2014) Histidine decarboxylase deficiency causes tourette syndrome: parallel findings in humans and mice. *Neuron 81*, 77−90.
(42) Pittenger, C. (2017) Histidine Decarboxylase Knockout Mice as a Model of the Pathophysiology of Tourette Syndrome and Related Conditions. *Handb. Exp. Pharmacol. 241*, 189−215.
(43) Ohtsu, H., Tanaka, S., Terui, T., Hori, Y., Makabe-Kobayashi, Y., Pejler, G., Tchougounova, E., Hellman, L., Gertsenstein, M., Hirasawa, N., Sakurai, E., Buzas, E., Kovacs, P., Csaba, G., Kittel, A., Okada, M., Hara, M., Mar, L., Numayama-Tsuruta, K., Ishigaki-Suzuki, S., Ohuchi, K., Ichikawa, A., Falus, A., Watanabe, T., and Nagy, A. (2001) Mice lacking histidine decarboxylase exhibit abnormal mast cells. *FEBS Lett. 502*, 53−56.
(44) Komori, H., Nitta, Y., Ueno, H., and Higuchi, Y. (2012) Purification, crystallization and preliminary X-ray analysis of human histidine decarboxylase. *Acta Crystallogr., Sect. F: Struct. Biol. Cryst. Commun. 68*, 675−677.
(45) Komori, H., Nitta, Y., Ueno, H., and Higuchi, Y. (2012) Structural study reveals that Ser-354 determines substrate specificity on human histidine decarboxylase. *J. Biol. Chem. 287*, 29175−29183.
(46) Sanchez-Jimenez, F., Pino-Angeles, A., Rodriguez-Lopez, R., Morales, M., and Urdiales, J. L. (2016) Structural and functional analogies and differences between histidine decarboxylase and aromatic l-amino acid decarboxylase molecular networks: Biomedical implications. *Pharmacol. Res. 114*, 90−102.
(47) Pace, C. N., Vajdos, F., Fee, L., Grimsley, G., and Gray, T. (1995) How to measure and predict the molar absorption coefficient of a protein. *Protein Sci. 4*, 2411−2423.
(48) Peterson, E. A., and Sober, H. A. (1954) Preparation of crystalline phosphorylated derivatives of vitamin B6. *J. Am. Chem. Soc. 76*, 169−175.
(49) Charteris, A., and John, R. (1975) An investigation of the assay of dopamine using trinitrobenzensulphonic acid. *Anal. Biochem. 66*, 365−371.
(50) Berman, H. M., Westbrook, J., Feng, Z., Gilliland, G., Bhat, T. N., Weissig, H., Shindyalov, I. N., and Bourne, P. E. (2000) The Protein Data Bank. *Nucleic Acids Res. 28*, 235−242.
(51) Webb, B., and Sali, A. (2014) Comparative Protein Structure Modeling Using MODELLER. *Curr. Protoc. Bioinf. 47*, 5.6.1−5.6.32.
(52) Bramucci, E., Paiardini, A., Bossa, F., and Pascarella, S. (2012) PyMod: sequence similarity searches, multiple sequence-structure alignments, and homology modeling within PyMOL. *BMC Bioinf. 13*, S2.
(53) Hess, B., Kutzner, C., van der Spoel, D., and Lindahl, E. (2008) GROMACS 4: Algorithms for Highly Efficient, Load-Balanced, and Scalable Molecular Simulation. *J. Chem. Theory Comput. 4*, 435−447.
(54) Laskowski, R. A., MacArthur, M. W., Moss, D. S., and Thornton, J. M. (1993) PROCHECK: a program to check the stereochemical quality of protein structures. *J. Appl. Crystallogr. 26*, 283.
(55) Tirion, M. M. (1996) Large Amplitude Elastic Motions in Proteins from a Single-Parameter, Atomic Analysis. *Phys. Rev. Lett. 77*, 1905−1908.
(56) Atilgan, A. R., Durell, S. R., Jernigan, R. L., Demirel, M. C., Keskin, O., and Bahar, I. (2001) Anisotropy of fluctuation dynamics of proteins with an elastic network model. *Biophys. J. 80*, 505−515.
(57) Berendsen, H. J. C., Postma, J. P. M., van Gunsteren, W. F., and Hermans, J. (1981) Interaction models for Water in Relation to Protein Hydration. In *Intermolecular forces. The Jerusalem symposia on quantum chemistry and biochemistry*, Vol. *14*, Springer, Dordrecht, The Netherlands.
(58) Bussi, G., Donadio, D., and Parrinello, M. (2007) Canonical sampling through velocity rescaling. *J. Chem. Phys. 126*, 014101.
(59) Darden, T., York, D., and Pedersen, L. (1993) Particle mesh Ewald: an N-log(N) method for Ewald sums in large systems. *J. Chem. Phys. 98*, 10089.
(60) Ponder, J. W., and Case, D. A. (2003) Force fields for protein simulations. *Adv. Protein Chem. 66*, 27−85.
(61) Schuttelkopf, A. W., and van Aalten, D. M. (2004) PRODRG: a tool for high-throughput crystallography of protein-ligand complexes. *Acta Crystallogr., Sect. D: Biol. Crystallogr. 60*, 1355−1363.
(62) Fleming, P. J., and Fleming, K. G. (2018) HullRad: Fast Calculations of Folded and Disordered Protein and Nucleic Acid Hydrodynamic Properties. *Biophys. J. 114*, 856−869.
(63) Giardina, G., Montioli, R., Gianni, S., Cellini, B., Paiardini, A., Voltattorni, C. B., and Cutruzzola, F. (2011) Open conformation of human DOPA decarboxylase reveals the mechanism of PLP addition to Group II decarboxylases. *Proc. Natl. Acad. Sci. U. S. A. 108*, 20514−20519.
(64) Batista, P. R., Robert, C. H., Marechal, J. D., Hamida-Rebai, M. B., Pascutti, P. G., Bisch, P. M., and Perahia, D. (2010) Consensus modes, a robust description of protein collective motions from multiple-minima normal mode analysis−application to the HIV-1 protease. *Phys. Chem. Chem. Phys. 12*, 2850−2859.
(65) Kass, I., Hoke, D. E., Costa, M. G., Reboul, C. F., Porebski, B. T., Cowieson, N. P., Leh, H., Pennacchietti, E., McCoey, J., Kleifeld, O., Borri Voltattorni, C., Langley, D., Roome, B., Mackay, I. R., Christ, D., Perahia, D., Buckle, M., Paiardini, A., De Biase, D., and Buckle, A. M. (2014) Cofactor-dependent conformational heterogeneity of GAD65 and its role in autoimmunity and neurotransmitter homeostasis. *Proc. Natl. Acad. Sci. U. S. A. 111*, E2524−2529.
(66) Schneider, B., Gelly, J. C., de Brevern, A. G., and Cerny, J. (2014) Local dynamics of proteins and DNA evaluated from crystallographic B factors. *Acta Crystallogr., Sect. D: Biol. Crystallogr. 70*, 2413−2419.
(67) Fleming, J. V., Sanchez-Jimenez, F., Moya-Garcia, A. A., Langlois, M. R., and Wang, T. C. (2004) Mapping of catalytically important residues in the rat L-histidine decarboxylase enzyme using bioinformatic and site-directed mutagenesis approaches. *Biochem. J. 379*, 253−261.
(68) Conway, M. E., Yennawar, N., Wallin, R., Poole, L. B., and Hutson, S. M. (2003) Human mitochondrial branched chain aminotransferase: structural basis for substrate specificity and role of redox active cysteines. *Biochim. Biophys. Acta, Proteins Proteomics 1647*, 61−65.
(69) Yennawar, N. H., Islam, M. M., Conway, M., Wallin, R., and Hutson, S. M. (2006) Human mitochondrial branched chain aminotransferase isozyme: structural role of the CXXC center in catalysis. *J. Biol. Chem. 281*, 39660−39671.
(70) Tremblay, L. W., and Blanchard, J. S. (2009) The 1.9 A structure of the branched-chain amino-acid transaminase (IlvE) from Mycobacterium tuberculosis. *Acta Crystallogr., Sect. F: Struct. Biol. Cryst. Commun. 65*, 1071−1077.
(71) Sagong, H. Y., and Kim, K. J. (2017) Lysine Decarboxylase with an Enhanced Affinity for Pyridoxal 5-Phosphate by Disulfide Bond-Mediated Spatial Reconstitution. *PLoS One 12*, e0170163.
(72) Matsui, D., and Oikawa, T. (2010) Detection and function of the intramolecular disulfide bond in arginine racemase: an enzyme with broad substrate specificity. *Chem. Biodiversity 7*, 1591−1602.
(73) Gavilanes, F., Peterson, D., Bullis, B., and Schirch, L. (1983) Structure and reactivity of cysteine residues in mitochondrial serine hydroxymethyltransferase. *J. Biol. Chem. 258*, 13155−13159.
(74) Chitnumsub, P., Ittarat, W., Jaruwat, A., Noytanom, K., Amornwatcharapong, W., Pornthanakasem, W., Chaiyen, P., Yuthavong, Y., and Leartsakulpanich, U. (2014) The structure of Plasmodium falciparum serine hydroxymethyltransferase reveals a novel redox switch that regulates its activities. *Acta Crystallogr., Sect. D: Biol. Crystallogr. 70*, 1517−1527.

DOI: 10.1021/acs.biochem.8b00625
Biochemistry 2018, 57, 6336−6348

(75) Coleman, C. S., Stanley, B. A., and Pegg, A. E. (1993) Effect of mutations at active site residues on the activity of ornithine decarboxylase and its inhibition by active site-directed irreversible inhibitors. *J. Biol. Chem. 268*, 24572−24579.
(76) Hasse, D., Andersson, E., Carlsson, G., Masloboy, A., Hagemann, M., Bauwe, H., and Andersson, I. (2013) Structure of the homodimeric glycine decarboxylase P-protein from Synechocystis sp. PCC 6803 suggests a mechanism for redox regulation. *J. Biol. Chem. 288*, 35333−35345.
(77) Schinagl, A., Kerschbaumer, R. J., Sabarth, N., Douillard, P., Scholz, P., Voelkel, D., Hollerweger, J. C., Goettig, P., Brandstetter, H., Scheiflinger, F., and Thiele, M. (2018) Role of the Cysteine 81 Residue of Macrophage Migration Inhibitory Factor as a Molecular Redox Switch. *Biochemistry 57*, 1523−1532.
(78) Xie, D., Wang, L., Xiao, Q., Wu, X., Zhang, L., Yang, Q., and Wang, L. (2018) New Insight into the Octamer of TYMS Stabilized by Intermolecular Cys43-Disulfide. *Int. J. Mol. Sci. 19*, 1393.

DOI: 10.1021/acs.biochem.8b00625
Biochemistry 2018, 57, 6336−6348